Sede Amministrativa: Università degli Studi di Padova

Dipartimento di Biologia

CORSO DI DOTTORATO DI RICERCA IN: BIOSCIENZE E BIOTECNOLOGIE

CURRICOLO: GENETICA E BIOLOGIA MOLECOLARE DELLO SVILUPPO

CICLO: XXIX

Modeling human mitochondrial diseases related to *MPV17* and *APOPT1* in *Drosophila melanogaster*

Coordinatore: Ch.mo Prof. Paolo Bernardi
Supervisore: Ch.mo Prof. Rodolfo Costa
Co-Supervisore: Dr. Cristiano De Pittà

Dottoranda: Samantha Corra'

Table of contents

dMpv17

Introduction, dMpv17

Results, dMpv17

Materials and methods

Abbreviations

AAA(+)	ATPases Associated with diverse cellular Activities
ABC	ATP-binding cassette
ACAD9	Acyl-CoA dehydrogenase family member 9
adPEO	Autosomal dominant progressive external ophthalmoplegia
AGT	Alanine/glyoxylate aminotransferase 1
AHS	Alpers-Huttenlocher syndrome
AIF	Apoptosis inducing factor
ANT	adenine nucleotide translocator
APOPT1	Apoptogenic 1
ATP	adenosine triphosphate
ATP5F1	ATP synthase subunit b
ATP5H	ATP synthase subunit d
ATP7B	ATPase copper transporting beta polypeptide
Bak	Bcl-2 homologous antagonist/killer
Bap31	B-cell receptor-associated protein 31
Bax	bcl-2-like protein 4
BCS1L	Mitochondrial chaperone BCS1
BER	mtDNA base excision repair
C20ORF7	NADH:ubiquinone oxidoreductase complex assembly factor 5
Cas9	CRISPR associated protein 9)
CI-V	Complex I-V
CJs	cristae junctions
COQ2	Para-hydroxybenzoate—polyprenyltransferase
COX	prostaglandin-endoperoxide synthase (PTGS) or Cyclooxygenase
CPEO	chronic progressive external ophthalmoplegia
CRISPR	Clustered Regularly Interspaced Short Palindromic Repeats
CypD	Chyclophilin D
dAMP	deoxyadenosine monophosphate
DGK	deoxyguanosine kinase
DGK	deoxyguanosine kinase
dGMP	deoxyguanosine monophosphate
DGUOK	Deoxyguanosine kinase
DNAJC19	Mitochondrial import inner membrane translocase subunit TIM14
DNC	deoxynucleotide carrier
dNDP	deoxyribonucleoside diphosphates
dNTP	deoxynucleoside triphosphate
dNTP	deoxyribonucleoside triphosphates
Drp1	Dynamine-1-like protein
EM	Electron microscopy
ERV1	Mitochondrial FAD-linked sulfhydryl oxidase ERV1
FA	Friedreich ataxia
FBSN	familial bilateral striatal necrosis
FEN1	DNA 5’ flap endonuclease
Fis1	Fission 1
FOXRED1	FAD-dependent oxidoreductase domain-containing protein 1
FSGS	focal segmental glomerulosclerosis

Fzo	Fuzzy onions
GFER	Growth factor, augmenter of liver regeneration
GFP	Green Fluorescent Protein
GGT	gamma-glutamyl transpeptidase
Gpx1	cellular glutathione peroxidase
Gpx3	plasma glutathione peroxidase
GTPases	guanosine triphosphatases
H2AX	H2A histone family member X
HD	Huntington's disease
HIF	Hypoxia-inducible factors
HSF	heat shock factor
HtrA2	Serine protease HTRA2
IGF-1	Insulin-like growth factor 1
IMM, IM	inner mitochondrial membrane
IMS	mitochondrial intermembrane space
IOSCA	infatile-onset spinocerebellar ataxia
KD	Knock-down
kdn	Knockdown
LETM1/Mdm38p	leucine zipper and EF-hand containing transmembrane protein 1
LHON	Leber's hereditary optic neuropathy
LS	Leigh syndrome
LYRM7	LYR Motif-Containing Protein 7
MDs	Mitochondrial diseases
MDS	Mitochondrial DNA depletion syndromes
Mff	Mitochondria fission factor
MFN	Mitofusin
MGME1	mitochondrial genome maintenance exonuclease 1
MIA	mitochondrial import and assembly
MIB	intermembrane space bridging complex
MICOS	mitochondrial contact site and cristae organizing system
MID	mitochondrial dynamics protein
MILS	Maternally inherited Leigh's syndrome
Miro	Mitochondrial Rho
MLS	microphthalmia characterized by linear skin lesions
MM	mitochondrial matrix
MNGIE	mitochondrial neurogastrointestinal encephalomyopathy
MPP	mitochondrial processing peptidase
MMP	Matrix metalloproteinase
MPV17	MPV17, mitochondrial inner membrane protein
MPV17L	MPV17-like protein
MPV17L2	MPV17-like 2 protein
MRC	mitochondrial respiratory chain
MRI	Magnetic resonance imaging
mtDNA	Mitochondrial DNA
mtRNAP	mitochondrial RNA polymerase
MTS	mitochondrial targeting sequence

mtSSB	mitochondrial single-stranded DNA-binding protein
NADH	Nicotinammide adenina dinucleotide
NARP	Neuropathy, ataxia, retinitis pigmentosa
ncDNA	Nuclear DNA
ND2	NADH dehydrogenase subunit 2
NDPK	nucleotide diphosphate kinase
NDUFA10	NADH:ubiquinone oxidoreductase subunit A10
NDUFAF1	NADH:ubiquinone oxidoreductase complex assembly factor 1
NDUFAF6	NADH:ubiquinone oxidoreductase complex assembly factor 6
NDUFB1	NADH:ubiquinone oxidoreductase subunit B1
NDUFC2	NADH:ubiquinone oxidoreductase subunit C2
NDUFS	NADH dehydrogenase [ubiquinone] iron-sulfur protein 7
NDUFS1	NADH:ubiquinone oxidoreductase core subunit S1
NDUFS2	NADH:ubiquinone oxidoreductase core subunit S2
NDUFS3	NADH:ubiquinone oxidoreductase core subunit S3
NDUFS7	NADH:ubiquinone oxidoreductase core subunit S7
NDUFV	NADH dehydrogenase [ubiquinone] iron-sulfur protein 7
NMPK	nucleotide monophosphate kinase
NNH	Navajo neurohepatopathy
NUBPL	nucleotide binding protein like
ODC1	ornithine decarboxylase 1
OMA1	mitochondrial inner membrane protease
OMM, OM	outer mitochondrial membrane
OPA1	Optic atrophy 1
OXPHOS	oxidative phosphorylation
PAM	pre-sequence translocase-associated import motor
PARL	presenilin-associated rhomboid-like protein
PD	Parkinson's disease
PDH	pyruvate dehydrogenase
PDSS1-2	decaprenyl diphosphate synthase subunit 1-2
PEO	progressive external ophthalmoplegia
PH1	primary hyperoxaluria type 1
PHB	Prohibitin
PI3K	Phosphatidylinositol-4,5-bisphosphate 3-kinase
PINK1	PTEN-induced putative kinase 1
PNC	pyrimidine nucleotide carrier
Pnp4a	purine nucleoside phosphorylase 4a
POLG	DNA polymerase γ
PTP	permeability transition pore
PXMP2	peroxisomal membrane protein 2
QH2	Coenzyme Q_{10}, also known as ubiquinone
R1-p53R2	p53-inducible R2 subunit of RNR
RHG	ring-h2 finger protein
Rhit	regulator of heat-induced transcription
RNR	ribonucleotide reductase
ROS	Reactive Oxygen Species

RPS14	ribosomal protein S14
RPS3	ribosomal protein S3
RRM2B	ribonucleotide reductase regulatory TP53 inducible subunit M2B
rRNA	Ribosomal RNA
SAM	sorting and assembly machinery
SCO(1-2)	SCO1, cytochrome c oxidase assembly protein
SDHAF1	SDH assembly factor 1
SDHAF3	succinate dehydrogenase complex assembly factor 3
SDHAF4	succinate dehydrogenase complex assembly factor 4
SDHB	succinate dehydrogenase complex iron sulfur subunit B
sesB	stress sensitive B
SOD2	mitochondrial manganese superoxide dismutase
SUCLA2	succinyl CoA ligase A2
SUCLG1	succinyl CoA ligase G1
surf-1	Surfeit locus protein 1
Surf-1	surfeit gene 1
SYM1	Stress-inducible yeast Mpv17
TAZ	Tafazzin
TCA	tricarboxylic acid
TCMK-1	Transformed C3H Mouse Kidney-1
TFAM	mitochondrial transcription factor A
TIM	Translocases of the IMM
TIMM8A DDP1	Mitochondrial import inner membrane translocase subunit Tim8 A
TK2	thymidine kinase 2
tko	technical knockout
TMEM	human TransMEMbrane protein
TOM	translocases of the OMM
TP	thymidine phosphorylase
tra	Transparent
tRNA	Transfer RNA
TS	thymidylate synthase
TTC19	tetratricopeptide repeat domain 19
TYMP	thymidine phosphorylase
UQ	Ubiquinone
UQCR10	Ubiquinol-Cytochrome C Reductase, Complex III Subunit X
UQCRB-Q-C-	Ubiquinol-cytochrome c reductase ubiquinone-binding protein
UQH2	Ubiquinol
YMC1	organic acid transporter

Abstracts

Modeling human mitochondrial diseases related to *MPV17* and *APOPT1* in *Drosophila melanogaster*

Mitochondrial diseases are a clinically heterogeneous group of inherited disorders associated with defects in the oxidative phosphorylation system, with an estimated incidence in between 1:5,000 and 1:10,000 live births. Mitochondrial respiratory chain function depends on the coordinated expression of both mitochondrial and nuclear genomes. Thus, also mutations affecting nuclear-encoded mitochondrial proteins are responsible for mitochondrial disease onset. During the last decades, an increasing number of novel nuclear disease genes have been identified. Among those genes, human *MPV17* and *APOPT1* have already been linked to mitochondrial diseases but their role in mitochondrial physiology and disease remains still puzzling. Mutations in the human *MPV17* nuclear gene, encoding a small hydrophobic mitochondrial inner membrane protein, are a prominent cause of a pediatric hepatocerebral form of mitochondrial DNA depletion syndrome. *APOPT1* mutations are responsible for an infantile or childhood mitochondrial encephalopathy hallmarked by profound deficiencies in both COX activity and amount.

In order to dissect out the role of these two genes, in this PhD project we focused our attention on the functional and molecular characterization of *Drosophila melanogaster* orthologs of *MPV17* and *APOPT1.*

We found that *dMpv17* down-regulation in flies causes a profound mitochondrial DNA depletion in the fat bodies (a Drosophila organ analogous to human liver). Depletion is also detected, albeit moderate, in *dMpv17* KD cells. Our results reveal that dMpv17 can form a channel when inserted in an artificial planar lipid bilayer. Moreover, we also show that the Drosophila protein could interact with dMic19, a component of the MICOS complex, as well as dMrp4, that could play a role in dMpv17 gating regulation. The analysis of mitochondrial morphology in *dMpv17* down-regulated cells together with the interaction with Mic19 suggest a possible role for dMpv17 in the maintenance of the structural and functional stability of the inner mitochondrial membrane.

Further, we confirmed that Drosophila is a reliable model for studying human mitochondrial disease also in the case of *APOPT1*. Indeed, our preliminary data show that *dApopt1* down-regulation in flies causes motor impairment and COX deficiency, characteristic features of the human disease. Not only COX activity but also *coxI* transcript is decreased in *dApopt1* down-regulated flies. Finally, we show that H_2O_2 treatment and, in turn, oxidative stress induce an increase in *dApopt1* transcript.

Finally, our data shed new light on the possible role of dMpv17 and dApopt1 in physiological and pathological conditions.

Modello di malattie mitocondriali da mutazioni ai geni *MPV17* e *APOPT1* in *Drosophila melanogaster*

Le malattie mitocondriali sono un gruppo ampio e eterogeneo di disordini ereditari causati da difetti del metabolismo energetico mitocondriale attribuibili a un malfunzionamento della catena respiratoria mitocondriale. La loro incidenza è stata stimata tra 1:1500 e 1:10000 nati vivi. Queste sindromi sono il risultato di un gran numero di mutazioni rilevabili sia nel genoma nucleare sia in quello mitocondriale. Negli ultimi decenni, il numero di geni scoperti essere responsabili dell'insorgenza di malattie mitocondriali è enormemente aumentato. Mutazioni nella proteina MPV17, localizzata nella membrana mitocondriale interna, sono state associate ad una particolare forma di sindrome da deplezione di DNA mitocondriale che colpisce primariamente il fegato e il sistema nervoso in età pediatrica. Invece, mutazioni in APOPT1 sono state identificate in pazienti caratterizzati da sintomi neurologici di vari entità associati a perdita della parola e della capacità motoria e accompagnati da un significativo deficit di citocromo C ossidasi a livello muscolare.

Dal momento che la funzione di queste due proteine risulta essere ancora sconosciuta, abbiamo cercato di determinare il loro ruolo a livello mitocondriale e nello sviluppo di queste malattie studiando i geni ortologhi in Drosophila, *dMpv17* e *dApopt1*. Abbiamo dimostrato che la *down-regolazione* dell'espressione di *dMpv17 in vivo* comporta una diminuzione significativa nel numero di copie di DNA mitocondriale nei *fat bodies*, un analogo funzionale del fegato dei mammiferi. Inoltre, alcuni risultati ottenuti molto recentemente suggeriscono che dMPV17 sarebbe in grado di formare un canale in un *planar lipid bilayer*. Infine, abbiamo identificato come suoi possibili interattori un componente del complesso MICOS e dMrp4, una proteina facente parte della famiglia dei trasportatori ABC che potrebbe regolare la sua attività di canale. L'interazione con il complesso MICOS e i risultati della microscopia elettronica sulla morfologia dei mitocondri nelle cellule silenziate per *dMpv17*, che hanno evidenziato una diminuzione nel numero e nella lunghezza delle creste, fanno ipotizzare un possibile ruolo nel mantenimento della struttura e, quindi, della funzionalità della membrana mitocondriale interna.

Studiando l'ortologo di APOPT1, *dApopt1,* abbiamo osservato che la sua down-regolazione *in vivo* comporta un marcato difetto locomotorio accompagnato da una significativa riduzione dell'attività della citocromo C ossidasi, sintomi descritti anche nella patologia umana. Infine, poiché la proteina umana sembra avere un ruolo nella risposta allo stress ossidativo, abbiamo dimostrato che l'espressione di *dApopt1* è indotta dal trattamento con H_2O_2. I risultati relativi alla caratterizzazione di dMpv17 e quelli preliminari riguardanti dApopt1 contribuiscono a fare luce sul ruolo di queste proteine sia a livello fisiologico che patologico, e confermano la validità di Drosophila come organismo modello per lo studio delle malattie genetiche umane.

General assumptions

1.1 *Drosophila melanogaster*: modeling human diseases in the fruit fly

The fruit fly, *Drosophila melanogaster*, is probably one of the best known and most employed model organism to date. Since it was introduced by Thomas Morgan for studies on inheritance at the beginning of the 20th century, Drosophila has played a critical role in the development of modern Biology, especially in Genetics. Drosophila was the model used in the discovery of sex-linked heredity and gene linkage (Morgan, 1910), homologous recombination (Bridges and Anderson, 1925), x-ray induced mutations (Muller, 1928) and the first tumor suppressor gene (Schneidermann and Gateff, 1967), to name just a few examples. Nowadays, with over a hundred years of genetic studies and a multitude of laboratories scattered worldwide, many tools have been created to manipulate Drosophila's gene expression and investigate its function.

The strength of Drosophila as a model organism resides first of all in its biology: rapid life cycle, high reproductive rate, small size, easy maintenance under laboratory conditions and a lower genetic redundancy compared to vertebrates (Bernards *et al.*, 2001). Secondly, the wealth of genetic tools repertoire as well as the variety of behavioural tests available enable to assess gene function, genetic interaction and environmental influences of almost all genes contained in the Drosophila genome. Forward mutagenesis, imprecise P-element excision or homologous recombination strategies can be exploited to create classic genetic mutants. Recently, more advanced methods for genome editing such as CRISPR/Cas9 have been established in Drosophila to create fly lines with single point mutations (Gratz *et al*., 2013; Bassett *et al*., 2013). Moreover, the system developed by Brand and Perrimon in 1993, the UAS-Gal4 system, allows to modulate gene expression in a spatially and temporally controlled manner, bypassing problems due to lethality in knockout strains.

In addition to the contribution in basic research, in the last years Drosophila has been established as a model organism for elucidating the molecular mechanisms underlying human diseases. Regardless of the evolutionary distance between humans and flies, a substantial conservation in genes, regulatory networks and physiological processes have been observed (Bier, 2005). The adult fly has structures functionally analogous to human organs and tissues: a heart, muscles, a tubular system similar to lungs, a complex nervous system (which is protected by a sort of blood-brain barrier), the fat body that plays a role similar to the liver and the white adipose tissue, and an excretory apparatus similar to kidneys (**Fig. 1**). Furthermore, Drosophila and vertebrates share many similarities in metabolic, energy-sensing and endocrine signalling pathways (Owusu and Perrimon, 2014). The fly genome, completely sequenced in 2000, encodes about 14.000 genes on four chromosomes. 75% of all human disease genes have a functional ortholog in Drosophila (Bier, 2005). Flies have been used to study pathophysiological mechanisms causing muscle degeneration disorders (Duchenne muscular dystrophy or spinal muscular atrophy) (Plantié *et al*., 2015), neuronal diseases (Parkinson's disease) (Feany *et al*., 2000; Withworth, 2011), cancer (flies harbour oncogenes and tumor suppressor genes which are similar to humans) (Rudrapatna *et al*., 2012; Gonzales,

2013; Miles *et al*., 2011), stem cells and metabolic disorders (Graham and Pick, 2017; Daenzer and Fridovich-Keil, 2017). Moreover, a substantial wealth of information about the immune system comes from Drosophila (Hoffman, 2003; Buchon *et al*., 2014). Another area of fly research that turned out fruitful to model human condition is sleep research, an area inflated in the last decades with the discovery of genes impacting fly circadian rhythms and sleep activity (Sehgal *et al*., 2007; Cavanaugh *et al*., 2016).

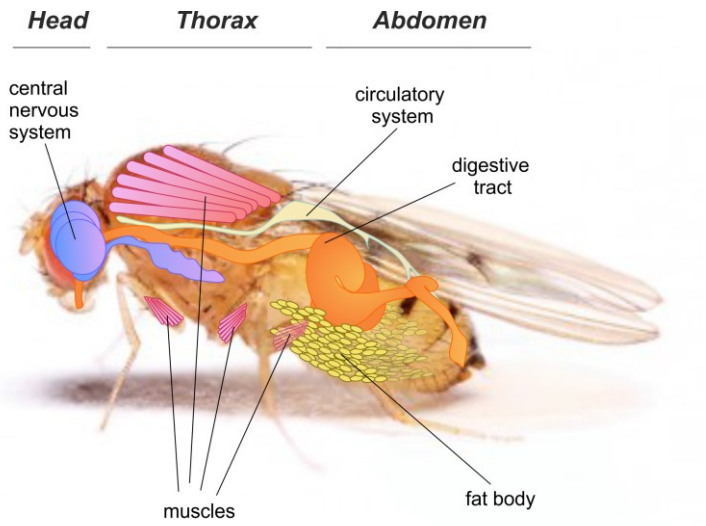

Fig. 1 *Drosophila melanogaster* tissues and organs.

1.2 Drosophila as a model for mitochondrial disorders

The power of a disease model resides in its capability to recapitulate clinical manifestations and molecular aspects of a specific human pathology. Mitochondrial diseases are often characterized by neurodegenerative features, including blindness, deafness, movement disorders, ataxia, and encephalopathy (DiMauro, 2004; Goldstein *et al*., 2013). Moreover, mitochondrial defects are also associated with muscular weakness, cardiac failure, diabetes, renal and hepatic dysfunction (McInnes, 2013; Tuppen *et al*., 2010). Given that human tissues/organs, which are frequently found affected in mitochondrial diseases have counterparts in Drosophila (although with simpler organizations than the human ones), disease-associated symptoms, tissue degeneration and molecular mechanisms can be investigated in this organism. Clinical features like seizures and brain degeneration are easily mimicked in Drosophila (Pandey and Nichols, 2011; Sen and Cox, 2017). Importantly, genes encoding the mitochondrial respiratory chain complexes are highly conserved from Drosophila to human, together with genes encoding enzymes involved in oxidative phosphorylation-related processes such as ROS scavenging (Angeles *et al.*, 2014). Likewise, the homologous of nuclear-encoded genes required for mitochondrial function are conserved (Caggese *et al*., 1999). This, together with the features mentioned above, strengthens the

relevance of Drosophila as a model for mitochondrial disorders and more specifically for OXPHOS deficiencies.

The first mutants for nuclear-encoded mitochondrial genes were discovered in the 1960s and 1970s through classical forward genetic screens to isolate flies that exhibited abnormal behaviours or responses to environmental stress. For instance, *stress sensitive B* (*sesB*), *knockdown (kdn)* and *technical knockout* (*tko*) were identified as bang sensitive flies (mutants exhibiting temporary paralysis after a mechanical stress) (Homyk and Sheppard, 1977; Ganetzky and Wu, 1982). Subsequently, the role of these genes in mitochondrial disease onset was elucidated. *tko* encodes the S12 subunit of the mitochondrial ribosome (MRPS12) involved in protein synthesis (Royden *et al.*, 1987), providing a model of mitochondrial syndromes due to perturbations of the protein translation machinery. *tko* mutant flies exhibit aberrant responses to auditory stimulation (deafness is common in patients), and impaired fertility (Toivonen *et al.*, 2001). *sesB* was identified as the fly's ortholog of the mitochondrial adenine nucleotide translocator (ANT) (Vartiainen *et al*., 2014), mutations of which have been associated with autosomal dominant progressive external ophthalmoplegia (Kaukonen *et al.*, 2000) and autosomal recessive hypertrophic cardiomyopathy, myopathy, and lactic acidosis (Palmieri *et al.*, 2005) in humans. Flies with mutation in this locus were characterized by abnormalities in synaptic vesicle recycling (Rikhy *et al.*, 2007) and defects in Malpighian tubules (Terhzaz *et al.*, 2010). Finally, *kdn* was proved to encode the Krebs' cycle enzyme citrate synthase (Fergestad *et al.,* 2006). Biochemically, these mutants were characterized by decrease in OXPHOS capacity, with reduced activity of CI, CIII, and CIV, and impaired ATP synthesis, which are key molecular features in patients suffering from mutation in the mitochondrial protein synthesis apparatus (Jacobs *et al*., 2004).

Since then, mutations causing human mitochondrial disease have been extensively reviewed, and in parallel, the number of Drosophila models for mitochondrial disorders has increased (Sen and Cox, 2017). Below, I summarize some of the most relevant findings exploiting Drosophila as a model organism for mitochondrial disease research.

Drosophila models for OXPHOS complexes deficiencies exhibit phenotypic features which are commonly observed in patients (Kemppainen *et al*., 2014). Mutants are often characterized by shortened lifespan or lethality, developmental delay, muscle weakness, neuronal dysfunction and degeneration, seizures, and a decreased activity of the specific targeted complex, although the degree of severity is variable. The existing fly's models for OXPHOS deficiencies are listed in **Table 1**.

Tab. 1 *D. melanogaster* models for OXPHOS proteins (adapted from Foriel *et al*., 2015).

OXPHOS complex	Drosophila gene	Human gene
Complex I	*ND-75 (CG2286)*	*NDUFS1*
	ND-49 (CG1970)	*NDUFS2*
	ND-B14.5B (CG12400)	*NDUFC2*
	ND-20 (CG9172)	*NDUFS7*
	ND-30 (CG12079)	*NDUFS3*
	ND-MNLL (CG18624)	*NDUFB1*
	mt:ND2 (CG34063)	*MT-ND2*
	CIA30 (CG7598)	*NDUFAF1*
	sicily (CG15738)	*NDUFAF6*
	ND-42 (CG6343)	*NDUFA10*
Complex II	*SdhB (CG3283)*	*SDHB*
	Sdhaf3 (CG14898)	*SDHAF3*
	Sirup (CG7224)	*SDHAF4*
Coenzyme Q	*qless (CG31005)*	*PDSS1*
Complex III	*Ttc19 (CG15173)*	*TTC19*

OXPHOS Complex	Drosophila gene	Human gene
	Oxen/QCR9 (CG8764)	*UQCR10*
Complex IV	*COX4 (CG10664)*	*COX4I2*
	COX5A (CG14724)	*COX5A*
	COX5B (CG11015)	*COX5B*
	levy (CG17280)	*COX6A*
	COX6B (CG14235)	*COX6B*
	cype (CG14028)	*COX6C*
	COX7A (CG9603)	*COX7A*
	Surf1 (CG9943)	*SURF1*
	Scox (CG8885)	*SCO1/SCO2*
	Cep89 (CG8214)	*CEP8*
Complex V	*Mt-ATPase6 (CG34073)*	*MT-ATP6*
	ATPsynb (CG8189)	*ATP5F1*
	ATPsynD (CG6030)	*ATP5H*

The main cause of Leigh syndrome (LS), the most common infantile mitochondrial encephalopathy, is mutations in the *surf-1* gene encoding a protein of the inner mitochondrial membrane (Tiranti *et al*., 1998; Zhu *et al.,* 1998). In our lab, Da Rè and colleagues (2014) demonstrated that ubiquitous *dsurf-1* knock-down (KD) in Drosophila causes a severe impairment in development. Larvae are characterized by defects in spontaneous and light-induced locomotor behaviour and always die before entering pupariation. Because both development and metamorphosis are highly energy-requiring processes, defects in respiration and ATP synthesis were thought to be responsible for the observed phenotypes. In fact, larvae display defects in all complexes of the mitochondrial respiratory chain and in the F-ATP synthase, while head-restricted adults have a COX-selective impairment. The Drosophila model has strengthened the hypothesis that Surf-1 is involved in COX assembly and provides a new tool that may help clarify the pathogenic mechanisms of LS.

Moreover, useful Drosophila models are also available for mitochondrial diseases not directly correlated with OXPHOS complexes. For instance, another disease extensively studied in Drosophila is Friedreich ataxia (FA), an inherited recessive neurodegenerative disorder due to a genetic insufficiency of frataxin, a mitochondrial iron chaperone (Kondapalli *et al*., 2008; Navarro *et al*., 2011; Anderson *et al*., 2008). Most FA patients are homozygous for a GAA triplet repeat expansion in the first intron of the gene, harbouring between 90 and 1.000 repeats (instead of standard 40) (Patel and Isaya, 2001). The resulting insufficient

frataxin levels cause iron accumulation in mitochondria and impaired activity of iron-sulfur containing enzymes. The set-up of an RNAi strategy in Drosophila provided a useful tool to mimic the genetics of FA, which determines a decrease rather than a complete loss of the protein (Anderson *et al*., 2005). Ubiquitous downregulation of *frataxin* led to long-living larvae that were unable to initiate metamorphosis due to a diminished iron cofactor-dependent enzyme activity, and an increased susceptibility to iron toxicity (Anderson *et al*., 2005). This long-living phenotype known to be typical of Drosophila mutants with defect in mtDNA maintenance prompted the hypothesis that FA depletion could promote mtDNA damage. Moreover, it was proved that over-expression of H_2O_2-scavenging enzymes in this fly model could effectively ameliorate the phenotype, suggesting that oxidative stress is an important pathogenic cause (Anderson *et al.*, 2008).

Mutations in mtDNA have been associated with multiple severe maternally inherited mitochondrial diseases, but the technical inability to create animal models for these syndromes has limited their study. Celotto *et al.* (2006) identified the first pathogenic mutation in the Drosophila mitochondrial ATP6 gene, a G–A transition in an evolutionarily conserved amino acid residue. The ATP6 protein is a component of the mitochondrial F_1F_0-ATP synthase that functions as a hydrogen ion channel, coupling ion transport with ATP synthesis. Point mutations in the human gene cause neuropathy, ataxia, retinitis pigmentosa (NARP) and maternally inherited Leigh's syndrome (MILS) (DiMauro and Schon, 2003). Drosophila mutants displayed a short lifespan, locomotion impairment, progressive myodegeneration and a neurodegenerative phenotype (Celotto *et al.,* 2006). In addition, ultrastructural defects in the mitochondrial inner membrane and marked reduction in ATP synthase activity were also found in association with the mutation. It was demonstrated that impaired ATP synthase function due to ATP6 dysfunction can cause severe encephalomyopathy in spite of the absence of defects in respiration rate *in vivo*. This Drosophila mutant, which shows features similar to those found in humans, has been used to study the pathogenesis of neuromuscular impairment resulting from altered OXPHOS (Palladino, 2010).

Currently, other two fly models harbouring a deleterious mutation in their mtDNA are available. Using a mitochondrial targeted restriction endonuclease to generate a single site cleavage in the mtDNA, Drosophila lines carrying a mutation in cytochrome c oxidase subunit I, or a small insertion/deletion in *ND2* were created. Adults homoplasmic for *mt:CoI*^{R301S} are characterized by 50% reduction of CoI levels, age related decrease in ATP levels and neurological as well as muscle defects. These features are consistent with human mitochondrial disease (Sen and Cox, 2017). The deletion in ND2 gene results in the loss of three amino acids in position 186-188. Patients with mutations in this gene are affected by Leigh syndrome, Leber's hereditary optic neuropathy, and exercise intolerance. ND2 mutant flies exhibit behavioural phenotypes including stress-induced seizures, progressive neurodegeneration (neurodegenerative vacuoles are present in aged fly brain) and shortened lifespan that parallel symptoms of complex I deficiency in humans. Biochemical characterization of Drosophila ND2 mutants revealed decreased level and activity of

complex I, as well as reduced ATP production and membrane potential, consistent with a role of ND2 subunit in the proton pumping activity of complex I (Burman *et al*., 2014). This was the first demonstration of the ND2 role in a eukaryote.

A relatively recently classified group of mitochondrial diseases involve perturbation of mitochondrial dynamics and/or morphology. The imbalance in mitochondrial fission and fusion has been found to significantly impact neuronal functions and the clearer evidence in this context comes from studies on Parkinson's disease (PD) (Su *et al*., 2010). Recently, it has become evident that mitochondrial dysfunction provides a prominent pathogenic contribution to numerous neurological and neurodegenerative diseases, including Parkinson's disease (PD) (Exner *et al*., 2012) and Huntington's disease (HD) (Johri and Beal, 2012). Drosophila led to major advances in this field, contributing significantly to the understanding of the pathological mechanisms of familial PD. Drosophila mutants of several identified PD-associated genes recapitulate features seen in patients, such as loss of DA neurons and locomotor defects (Muñoz-Soriano and Paricio, 2011; Guo, 2012). Drosophila has been fundamental in establishing that PINK1 and Parkin, two different PD-associated proteins, take part in the same signalling pathway protecting mitochondrial integrity and function, with Parkin acting downstream of PINK1 (Lu and Vogel, 2009). In particular, using fly genetic analyses, it was shown that the PINK1-Parkin pathway regulates mitochondrial morphology, including mitochondrial fusion and fission events (Park *et al.*, 2009).

Altogether, these and other examples confirm the great potential of Drosophila as an alternative organism to model human mitochondrial diseases.

2.1 Mitochondria: function and structure

Mitochondria were identified by Richard Altmann in 1890 who hypothesized that these ubiquitous cellular structures were "elementary organisms" living within cells. Nowadays, mitochondria are universally recognized as eukaryotic intracellular endosymbionts arisen 2 billion years ago from once free-living α-proteobacteria (endosymbiotic theory) (Zimorsky *et al.*, 2014; Archibald, 2015). Over time, mitochondrial genome has shortened and most of the genomic material of the α-proteobacterium progenitor has been transferred to the nuclear genome (Ku *et al.*, 2015). Mitochondria harbour only a remnant of their ancestor's DNA, but they have retained most of their prokaryotic biochemistry, acquiring also diverse additional functions in the cell. Mitochondria are the powerhouse of eukaryotic cells, i.e. the cellular organelles responsible for most of the cell's supply of adenosine triphosphate (ATP) through oxidative phosphorylation (OXPHOS) (Lehninger and Kennedy, 1948). Yet, several other metabolic pathways take place in this organelle. Indeed, mitochondria are also required for heme, steroids, as well as nucleotide biosynthesis (Sen and Cox, 2017). Moreover, in the last few years, it has become evident that mitochondria are intimately involved in complex cellular processes like cell differentiation, aging and apoptosis (Seo *et al*., 2010; Wang and Youle, 2009; Xu *et al*., 2013) (**Fig. 2**).

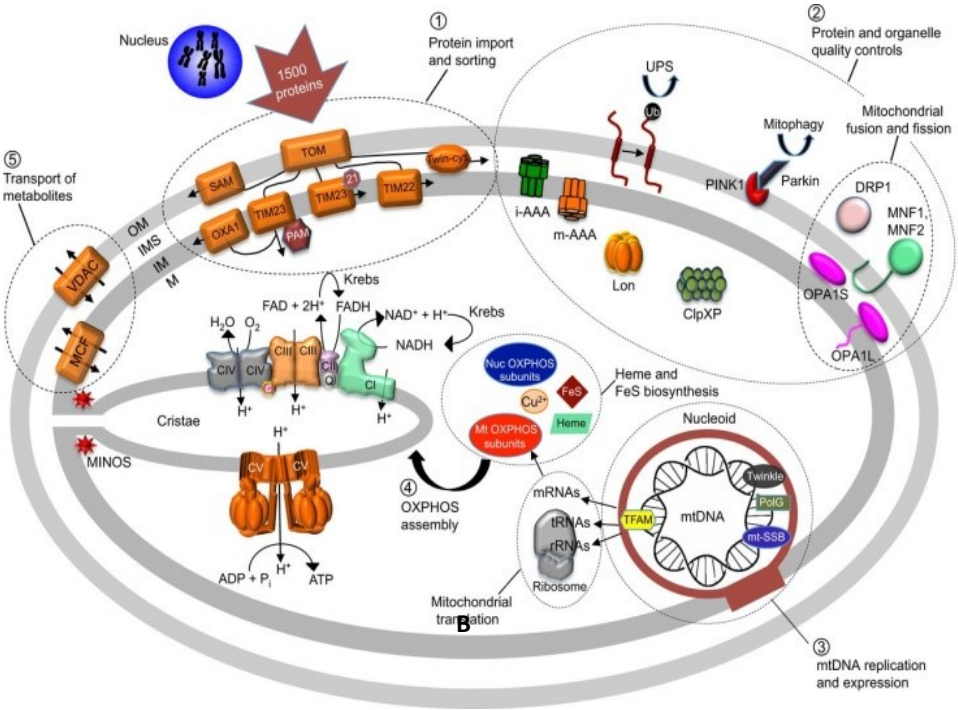

Fig. 2 Mitochondrial pathways., Mitochondrial pathways discussed in this introduction (from Lasserre *et al*., 2015).

Mitochondria possess a double membrane system, which appears to have arisen by mitochondria entering eukaryotic cells via endocytosis. The double phospholipidic membrane organization of mitochondria, composed of an outer mitochondrial membrane (OMM) and an inner mitochondrial membrane (IMM),

create and delimit two internal compartments, the mitochondrial intermembrane space (IMS), and the mitochondrial matrix (MM) (Tarasenko *et al*., 2017). The invaginations of the inner membrane, which increases its surface area, form the cristae.

The popular idea that depicted mitochondria as isolated sausage-shaped organelles in the cytoplasm was profoundly changed almost 30 years ago when, thanks to technological advances it became easier to track mitochondria movement. Mitochondria are highly dynamic, and mitochondrial morphology, which varies from small, individual organelles to highly interconnected networks, is determined by the balance between fission and fusion events (Rafelski *et al.*, 2013). Trafficking mechanisms through cytoskeleton networks drive mitochondria where they are needed.

Mitochondria are the only location of extra-chromosomal DNA within the animal eukaryotic cell, being under the dual genetic control of both nuclear DNA (ncDNA) and mitochondrial genomes (mtDNA). Mitochondrial proteome is composed by more than 1.000 proteins, and entails a mixture of eukaryotic-derived proteins and bacterial-like proteins (Friedman and Nunnari, 2014; Gabaldón and Huynen, 2004). Mitochondria are present in hundreds/thousands copies in every cell, and the number depends on the cell type and the bioenergetics requested from a specific tissue. Moreover, every mitochondrion can have multiple copies of mtDNA (up to ten) packed in nucleoids (Alexeyev *et al*., 2013).

2.2 Mitochondrial DNA replication

During evolution, mitochondria lost much of their genome, transferring most of their genes to the nucleus. Despite this, the paradigm that mtDNA encoded a small number of OXPHOS and ATP synthase subunits, ribosomal RNA (rRNA) and transfer RNA (tRNA) components (Anderson *et al.*, 1981) was revised in 1998, in a study that focused on mtDNA from non-animal species (Gray *et al.*, 1998). Indeed, in some non animal taxa, other proteins are encoded in mtDNA, such as proteins involved in translation, transcription, RNA processing, protein import and maturation. However, mammalian mtDNA is a circular, double-stranded molecule that shows highly variability in size (16.6 kb in human), coding capacity, and mode of expression among eukaryotes. Mammalian mtDNAs have retained only 13 polypeptide-encoding genes, which encode components of the respiratory chain, 2 rRNA genes and 22 tRNA genes required for protein synthesis. The remaining part (the vast majority) of mitochondrial proteins (including the remaining OXPHOS proteins, the metabolic enzymes, the DNA and RNA polymerases, the ribosomal proteins and the mtDNA regulatory factors) are encoded by nuclear genes (Wallace *et al*., 1999). Despite differences in mtDNA organization (in terms of gene order and distribution), the gene content within *D. melanogaster* mtDNA is the same as that found in vertebrates (Wolff *et al.*, 2016).

mtDNA has a highly compact organization where introns are not present. The only non-coding region (in vertebrates and likely also in invertebrates) contains the promoters for mtDNA transcription and the

replication origin and is named control region. The two DNA strands are named heavy (H) and light strands (L), based on their buoyancy densities (Garesse and Kaguni, 2005).

mtDNA replication occurs independently from nuclear DNA replication. mtDNA is synthesized and repaired by a specific DNA polymerase γ (POLG) in conjunction with several additional proteins forming the mtDNA replisome. Human POLG is a heterotrimeric complex composed of a catalytic subunit encoded by *POLG* and two asymmetrically bound accessory proteins encoded by *POLG2*, forming a homodimeric processing subunit. The proximal of these two proteins increases the binding affinity to mtDNA, the distal one accelerates the rate of nucleotide incorporation. Moreover, the mtDNA replisome includes the 5'-3' DNA helicase Twinkle, mitochondrial topoisomerase I, mitochondrial RNA polymerase (mtRNAP) required for RNA primer formation to initiate replication, RNase H1 and mitochondrial genome maintenance exonuclease 1 (MGME1), mitochondrial single-stranded DNA-binding protein (mtSSB), and mitochondrial DNA ligase III. Other factors involved in mitochondrial genome maintenance are: the multifunctional mitochondrial transcription factor A (TFAM) involved in mtDNA replication and packaging, the RNA and DNA 5' flap endonuclease (FEN1), and the helicase/nuclease DNA2 which has been demonstrated to co-localize with Twinkle in nucleoids suggesting a possible involvement in the replisome. Moreover, MGME1, FEN1, and DNA2 play a role in mtDNA base excision repair (BER) pathways.

Over 20 years ago, the mechanism of mammalian mtDNA replication was unveiled. According to this standard model, mtDNA replication consists of continuous and asynchronous DNA synthesis on both parental strand templates, starting with replication of the heavy strand from the control region. Replication begins at heavy strand (O_H) origin displacing the parental strands in what is known as the displacement loop (D-loop). To initiate the synthesis of the H-strand DNA polymerase γ adds nucleotides to the 3'-end of an already existing RNA primer thanks to the activity of mtRNAP, which has primase activity. When the two-thirds of the mtDNA is copied, the H-strand synthesis reaches the light strand (O_L) and the displacement exposes the site where light strand replication can start, in the opposite direction. The template H-strand O_L sequence adopts a stem-loop structure that is recognized by mtRNAP. The mtSSB protein covers the displaced H-strand to stabilize the single strand. Before the replication of the daughter strands terminates, the Top2β gyrase acts to segregate the two mtDNA, thus avoiding catenation. Once the replication is terminated, RNA primers are displaced by DNA polymerase γ and removed by RNase H1. The last two ribonucleotides at the RNA-DNA junction are eliminated by nucleases DNA2, FEN1 and MGME1. Finally, DNA ligase III seals the nick.

Some experimental work suggests the existence of another mechanism of mtDNA replication, at least in vertebrates, involving a symmetric and semi-discontinuous synthesis of leading and lagging strands. These two mechanisms might be used depending on the physiological conditions (Holt *et al.*, 2000).

In Drosophila, little is known about mtDNA replication, and only one origin in the A+T region was identified in the mitochondrial genome. DNA polymerase γ, mitochondrial single-stranded DNA binding protein and a

mitochondrial DNA helicase were established to be important for mtDNA replication in Drosophila. Mutants for these genes are lethal and characterized by loss of mtDNA and respiratory function.

2.3 Mitochondrial dNTP synthesis

A carefully balanced pool of deoxynucleoside triphosphates (dNTPs) needs to be present for both nuclear and mitochondrial DNA replication (and repair) to occur. Two different pathways work in cells to maintain dNTP pools, the *de novo* and the salvage pathways.

de novo process is cytosolic and cell-cycle regulated, i.e. it is active only in S-phase cells (Lane and Fan, 2015). Starting from small molecules such as amino acids and CO_2, nucleoside monophosphates are produced. The end product of the *de novo* pathway are ribonucleotides then reduced to deoxyribonucleotides diphosphate by ribonucleotide reductase (RNR). Finally, nucleoside diphosphate kinases (NDPKs) phosphorylate these deoxynucleotides to the corresponding dNTPs. In addition, the methylation of dUMP to dTMP is mediated by thymidylate synthase (TS), then thymidine monophosphate kinase (TMPK) and NDPK are required for the phosphorylation to dTTP. In quiescent cell, the RNR small subunit (R2) is down-regulated and substitutes by a p53 inducible subunit able to form an active RNR complex which is fundamental to sustain dNTP synthesis for DNA repair. The salvage pathway, in which dNTPs are produced from pre-existing nucleosides, operates both in the cytosol and in mitochondria. Four deoxynucleoside kinases work in mammalian cells (thymidine kinase 1, TK1, and deoxycytidine kinase, dCK, in the cytosol; thymidine kinase 2, TK2, and deoxyguanosine kinase, dGK, in the mitochondria) to produce deoxynucleoside monophosphates (dNMPs) which are further phosphorylated to dNTPs.

In proliferating cells, the mitochondrial dNTPs are mainly imported by the mitochondrial nucleotide transporters from the cytosol (Wang, 2016) (**Fig. 2A**). 53 genes encoding members of the solute carrier proteins (SLC) are present in the human genome, including the mitochondrial carrier proteins and transporters. Adenine dinucleotide translocator (ANT) is a channel in the inner mitochondrial membrane that transports ADP in the mitochondrial matrix and ATP outside (Klingenberg, 2008). Three different isoforms exist which are expressed solely in post-mitotic tissue (ANT1, encoded by *SLC25A4*), only in proliferating cells (ANT2, encoded by *SLC25A5*), or ubiquitously (ANT3, encoded by *SLC25A6*) (Stepien *et al*., 1992; Chevrollier *et al.*, 2011). Except from its important role in cell bioenergetics, it has been suggested that ANT plays an important role in dNTPs maintenance importing ADP that can be converted to dADP and dATP (Klingenberg, 2008). Recently, it has been demonstrated that *SLC25A33* and *SLC25A36* code for mitochondrial pyrimidine nucleotide carriers (PNC) (Di Noia *et al*., 2014). SLC25A33 transports across the mitochondrial membrane ribose and deoxyribose di- and tri-phosphate of cytidine, uridine, and thymidine. Instead, SLC25A36 is responsible for the transport of cytidine-, uridine-, deoxycytidine-, and deoxyuridine mono-, di-, and tri-phosphates.

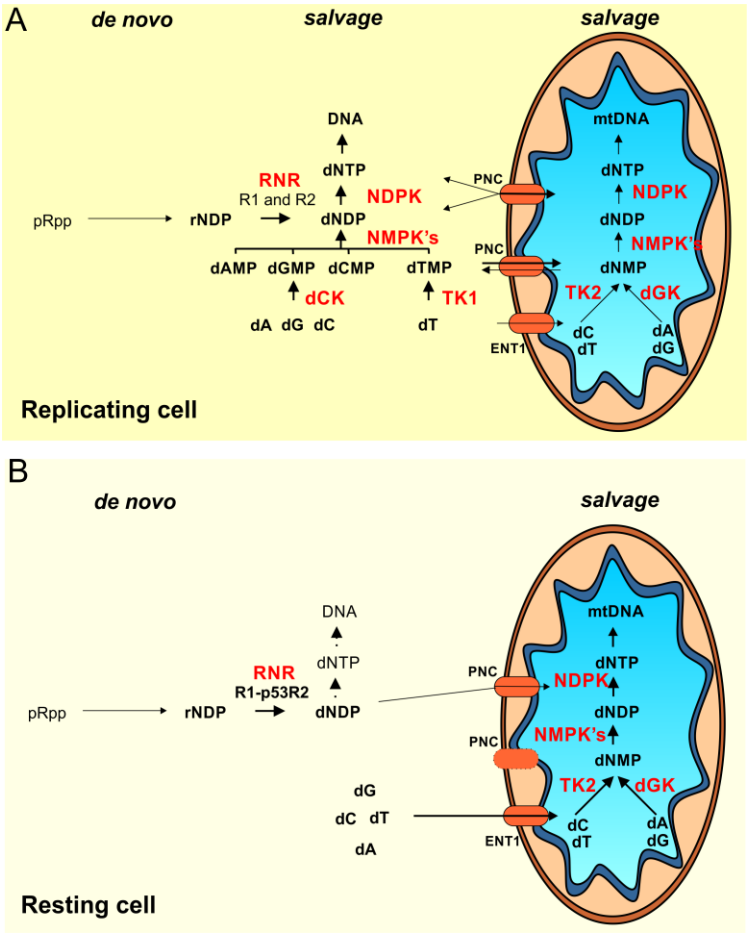

Fig. 3 Mitochondrial dNTP pools. **A**, in proliferating cells, the mitochondrial dNTPs are mainly imported by the mitochondrial nucleotide transporters from the cytosol where they are produced either by *de novo* and *salvage* pathway. **B**, dNTP pools in resting cells are mostly dependent on the mitochondrial enzymes, but also on the cytosolic p53-inducible R2 subunit.

Since mtDNA replication is independent of S-phase, mitochondrial pools cannot rely exclusively on nucleotide production in the cytosol (Ferraro *et al.*, 2006). The salvage enzymes thymidine kinase 2 (TK2) and deoxyguanosine kinase (dGK) together with nucleotide monophosphate kinase (NMPK) and nucleotide diphosphate kinase (NDPK) are involved in the mitochondrial nucleotide salvage pathway. TK2 participates in pyrimidine nucleotides synthesis mediating the first and rate-limiting step in the phosphorylation of pyrimidine deoxynucleosides deoxycytidine and thymidine into the corresponding nucleotides, deoxycytidine monophosphate and thymidine monophosphate. Likewise, DGK converts purine nucleosides deoxyguanosine and deoxyadenosine into deoxyguanosine monophosphate (dGMP) and deoxyadenosine monophosphate (dAMP). Deoxyribonucleoside monophosphates (dNMP) are subsequently phosphorylated and converted to deoxyribonucleoside diphosphates (dNDP) by NMPK and, finally, to deoxyribonucleoside triphosphates (dNTP) by NDPK (Fig. 2A). However, it has been demonstrated dNTP pools in quiescent cells are not only dependent on the mitochondrial enzymes, but also on the cytosolic p53-inducible R2 subunit of RNR (R1-p53R2) of the *de novo* pathway (Rampazzo *et al.*, 2007) (**Fig. 3B**).

In Drosophila, evidence regarding either the synthesis or the transport of dNTPs into mitochondria is scarce. Recently, our group identified the gene drim2 (CG18317) of Drosophila as the homolog of Rim2 from yeast, encoding a pyrimidine deoxynucleotide transporter (Da Rè *et al*., 2014). Similar to its counterpart in yeast, also dRIM2 localized to mitochondria, and its downregulation in Drosophila cells caused a marked reduction in both purine and pyrimidine mitochondrial dNTP pools. The Drosophila *drim2*$^{-/-}$ mutant died at the third larval instar. Moreover, mutants were characterized by impaired locomotor behaviour, drop in oxygen consumption and mtDNA depletion. Taken together, these data provided the first insights into mitochondrial dNTP pool maintenance in Drosophila and suggest dRIM2 as a mitochondrial carrier for both types of deoxynucleotides.

2.4 Mitochondrial protein import

Proteins that are encoded by the nuclear genome and synthesized as precursors on cytosolic ribosomes are targeted to mitochondria, translocated through mitochondrial membranes and sorted to the different sub-mitochondrial compartments (Neupert, 1997). Several cytosolic chaperones are involved in driving pre-proteins toward mitochondrial surface where translocases in the OMM (TOM complex) and in the IMM (TIM complex) transport these pre-proteins across the two membranes (Wiedemann *et al*., 2004). Many cytosolic factors bind to and stabilize these proteins in a translocation competent form, driving them to receptors localized on the OMM. The Hsp90/p23 and Hsc70/Hsp40 are the best characterized chaperone systems (Young *et al*., 2003). Notwithstanding, Luk and colleagues (2005) demonstrated that some precursor proteins are imported co-translationally in mitochondria *in vivo*. In line with this, one-half of mRNAs encoding for mitochondrial proteins are targeted to mitochondria and localize to the mitochondrial surface (Marc *et al.,* 2002), especially by Puf3, a member of the Pumilio/FBF family of RNA binding proteins (Garcia-Rodriguez *et al.,* 2007).

Specific sequences recognized by specific receptors on the OMM surface determine the final destination of mitochondrial-targeted proteins. Pre-proteins that are directed to the matrix and some of the proteins of the IMM and IMS possess an N-terminal mitochondrial targeting sequence (MTS) that is cleaved on import by the mitochondrial processing peptidase (MPP). Conversely, OMM proteins and many IMS and IMM proteins carry internal targeting signals (Gakh *et al*., 2002).

Independently from the type of targeting signal, the general translocase of the OMM for all nuclear encoded proteins is the TOM complex, which is composed of several receptors and a common insertion pore (Hill *et al*., 1998; Diekert *et al*., 1999). After this step, precursor proteins into the IMS are transferred to specialized protein sorting machineries. Pre-proteins can follow three different pathways (**Fig. 4**).

1) Pre-proteins with a cleavable MTS are transferred to the translocase of the inner membrane (TIM23) in a Δψ-dependent manner without involvement of a soluble stage (Kutik *et al*., 2007). The matrix chaperone mtHsp70, member of the pre-sequence translocase-associated import motor (PAM),

through an ATP-dependent mechanism induces the completion of the translocation into the matrix. Here, specific metalloproteases (MMP) remove the cleavable targeting sequence and the correct folding of the protein occurs by chaperones (i.e. mtHsp60) (Baker *et al*., 2014).

2) The vast majority of hydrophobic proteins (metabolite carriers and few others integral membranes proteins) are inserted into the IMM by the translocase of the inner membrane 22 (TIM22). The insertion process is Δψ-dependent (Becker *et al*., 2012).
3) OMM proteins are integrated into the outer membrane by the sorting and assembly machinery (SAM complex) (Stojanovski *et al*., 2012).

Furthermore, IMS protein that are small in size and contain conserved cysteine residues in Cx3C orCx9C conformation are imported by the mitochondrial import and assembly (MIA) machinery (Becker *et al*., 2012).

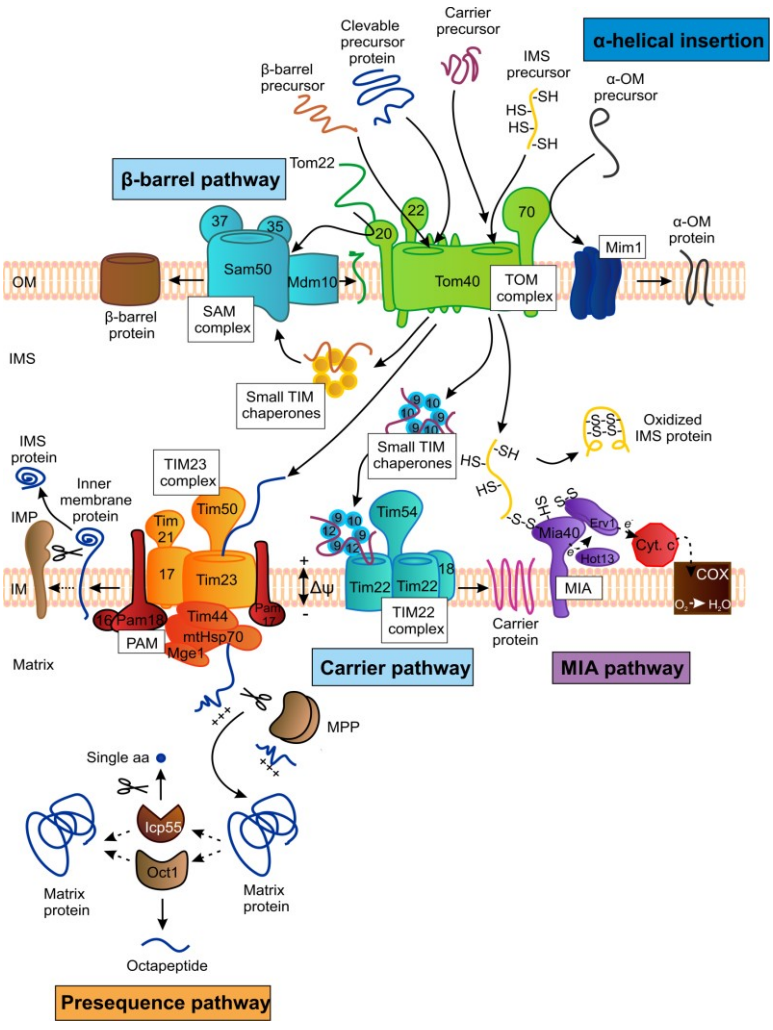

Fig. 4 Protein import pathways. The pre-sequence pathway imports pre-proteins with charged amino-terminal pre-sequence that are recognized by Tom20 and Tom22 pathway. The pre-proteins are transferred to the TIM23 complex that drives their translocation across the IMM. Then, the pre-sequences are cleaved off by the mitochondrial processing peptidase (MPP). The carrier pathway transports proteins with an internal targeting sequence that are recognized by Tim70 and translocated by Tom40. The β-barrel pathway transports the precursor of β-barrel proteins translocated through the OMM by the TOM complex; then, the SAM complex mediates their insertion in the OM. The MIA pathway is used by cysteine-rich IMS protein.

In Drosophila, genes encoding Tom20 and Tom40 are represented by two differentially expressed homologues each, as a result of gene duplication events. Interestingly, although *dtom20* and *dtom40* are ubiquitously expressed, their paralogues (called *tomboy20* and *tomboy40)* mRNAs were detected only in the male germ-line (Hwa *et al*., 2004). Another study in Drosophila shed light also on how proteins cope with the hydrophilic (cytosolic)/lipophilic (membrane) environmental transition before and during mitochondrial import. Zhang and colleagues (2013) demonstrated that cytosolic chaperones are involved in ND42 transport towards mitochondria. The protein encoded by the gene *sicily*, homolog of the human C8orf38 (the loss of which causes Leigh syndrome) was showed to interact with a cytosolic Hsp90 to chaperone the CI subunit ND42, before mitochondrial import. The loss of this gene determined CI deficiency and neurodegeneration.

2.5 Mitochondrial dynamics, mitophagy and apoptosis

2.5.1 Fission and fusion

Mitochondria are known to be very dynamic organelles that continuously change shape through the combined actions of fusion and fission. In some cells they form a single closed network fusing together, in other cells or under certain circumstances they fragment into smaller units. Mitochondria undergo fusion and fission to accommodate cell growth, cell division, mitochondria distribution during differentiation and ensure cell survival (van der Bliek *et al*., 2013).Fission and fusion rates are determined by mitochondrial metabolic and pathogenic conditions and cellular environment (van der Bliek *et al*., 2013). In more recent years, the discovery of numerous mutations affecting fission and fusion proteins and leading to human diseases have shed light on the connections between this phenomenon and apoptosis and mitophagy (van der Bliek *et al*., 2013). Fission and fusion events become fundamental in maintaining functional mitochondria when cells experience metabolic and environmental stresses. Fusion mitigates stress by mixing the contents of partially damaged mitochondria. Fission enables the removal of damaged

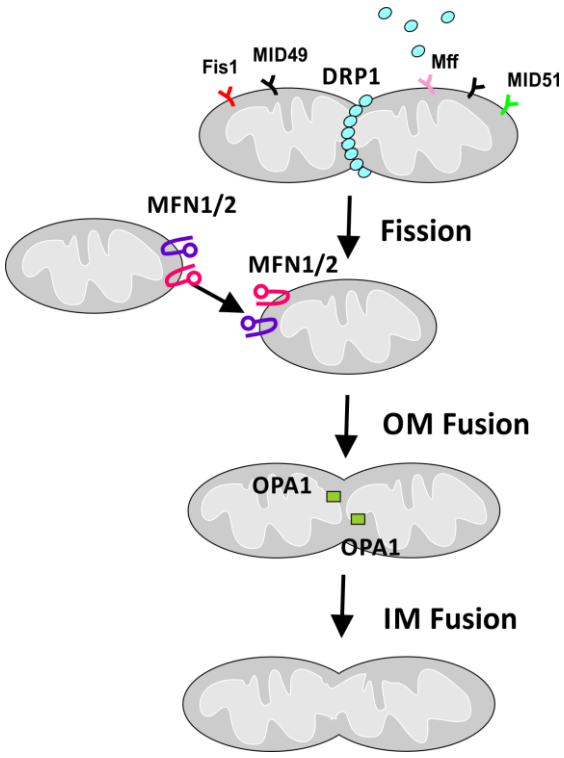

Fig. 5 Fission and Fusion mechanism. DRP1 proteins cycle to the outer membrane. They form large complexes at scission sites surrounded the organelle in spirals, which then constrict until fission occurs. Fusion required the coordinated fusion of both mitochondrial membranes and is mediated by MFN1/2 and OPA1, respectively.

mitochondria (Youle and van der Bliek, 2012).

The main mitochondrial fission and fusion proteins are guanosine triphosphatases (GTPases) members of the Dynamin family that are well conserved between yeast, flies, and mammals (Youle and van der Bliek, 2012).

Fusion implies the coordinated merge of both the outer and the inner mitochondrial membranes (**Fig. 5**). However, mutations or loss of membrane potential can block inner membrane fusion whereas outer membrane fusion can still occur. Three large GTPases are known to be important in these processes. Fusion of mitochondria outer membrane is mediated by mitofusin 1 (MFN1, encoded by *MFN1*) and mitofusin 2 (MFN2, encoded by *MFN2*) (Schrepfer and Scorrano, 2016). Interestingly, the homolog of Mfn1/2 was first discovered in Drosophila sperm cells and named fuzzy onions (Fzo) (Hales and Fuller, 2003). A second outer membrane fusion protein called Marf was shown to mediate fusion in other Drosophila cell types (Dorn *et al*., 2011). Two transmembrane domains tether the proteins to the outer mitochondrial membrane, with the remaining part of the protein facing the cytosol. The cytosolic portion contains the GTPase domain. Two coiled-coil protein-interacting domains mediate binding of Fzo/Mfn proteins located on adjacent mitochondria (Scott and Youle, 2010). Optic atrophy 1 (OPA1 encoded by *OPA1*) is instead essential for inner membrane fusion. First discovered in yeast, it was called Mgm1 because mutations were able to cause a maintenance defect of the mitochondrial genome (Jones and Fangman, 1992), which was later demonstrated to be a consequence of impaired fusion of the inner mitochondrial membrane (Wong *et al*., 2000). Mutations in OPA1 cause dominant optic atrophy, a hereditary autosomal disease which results in progressive vision loss (van der Bliek *et al*., 2013). There are eight variants of OPA1 in human cells as the result of alternative splicing. These peptides inside mitochondria undergo proteolytic processing that generates long and short OPA1 isoforms (Olichon *et al*., 2007). In yeast, this combination of short and long isoforms seems to be necessary for mitochondrial fusion (Song *et al*., 2007). In Drosophila, mutated dOPA1 has been demonstrated to increase ROS production leading to damage and death of eye cells (Yarosh *et al*., 2008), whereas heterozygous mutations have been reported to shorten lifespan (Tang *et al*., 2009). This phenotype was associated to irregular and dysmorphic mitochondria, impairment in CII and CIII activities, increased ROS production, and a consequent enhanced susceptibility to oxidative stress. Interestingly, heart-specific knock-down of *dOPA1* in flies has been demonstrated to induce mitochondrial morphological heterogeneity, heart tube dilatation and contractile impairment (Dorn *et al.*, 2011). Similar phenotypic effects observed in Marf-RNAi flies were rescued by expressing superoxide dismutase 1, underscoring the important relationship between dOPA1 and oxidative stress.

Different proteins are involved in OPA1 processing including the presenilin-associated rhomboid-like protein PARL, an AAA-metalloprotease found in the intermembrane space Yme1, and paraplegin, another AAA protease located in the IMM (Hill and Pellegrini, 2010). OPA1 plays also an important role in regulating mitochondrial cristae morphology (van der Bliek *et al*., 2013).

Low levels of impaired mitochondria can be corrected by complementation through mitochondrial fusion. Vertebrates have evolved a mechanism that relies on the requirement of the mitochondrial inner membrane potential for fusion to happen (Meeusen *et al*., 2006). This provides a defence mechanism to avoid heavily damaged mitochondria from re-joining mitochondrial network. The mitochondrial inner membrane protease OMA1 is rapidly activated by low membrane potential and mediates the proteolysis of OPA1 (Ehses *et al*., 2009; Head *et al*., 2009).

Conversely, unlike the fusion machinery, higher eukaryotes and yeast seem to possess a single Dynamin-related member involved in mitochondrial fission (**Fig. 5**) (van der Bliek *et al*., 2013). The mammalian protein is most commonly named Drp1. It is a cytosolic protein that can move on and off from the mitochondrial membrane. During fission events, dynamins move to the outer membrane forming large homomultimeric complexes at scission sites that surround the organelle in spirals, which then shrinks until fission occurs (van der Bliek *et al*., 2013). Adaptor proteins recruit dynamin to the outer membrane. Drp1 interacts with four mitochondrial receptor proteins: fission 1 (Fis1) interaction seems to play a minor role in this process, whereas interactions with mitochondria fission factor (Mff), mitochondrial dynamics protein of 49 kDa (MID49) and MID51 are fundamental for fission (van der Bliek *et al*., 2013). Interestingly, Drp1 localizes at endoplasmic reticulum-mitochondria contact sites, which suggest a possible involvement of the endoplasmic reticulum in the process.

2.5.2 Regulators of cristae shape

Numerous diseases in humans are characterized by alterations of mitochondrial architecture, often accompanied by inclusions or aggregates in the mitochondrial matrix. Some examples are Barth syndrome, Alzheimer's disease, and amyotrophic lateral sclerosis (Zick *et al*., 2009). In all these conditions mitochondrial morphology appears altered in such a way that cristae are disrupted, inclusions within mitochondria are present and varying types of inner membrane arrangements including concentric and parallel stacks of cristae membranes have been observed. Mitochondrial ultrastructure depends on the tissue, the physiological and developmental stage (Elmore, 2007). Cristae size and number can also change in response to metabolic requirements, thus, optimizing distribution of metabolites and proteins (Westermann, 2012). Furthermore, cristae remodelling occurs during apoptosis to allow the complete release of cytochrome *c* (Arnould *et al*., 2005). Many factors are involved in the process of cristae remodelling. Cristae are connected to the inner boundary membrane by small tubular structures, called cristae junctions (CJs), which play a crucial role in establishing IMM topology and matrix configuration (Kühlbrandt, 2015). Prohibitin-1 (PHB1) and the closely related protein Prohibitin-2 (PHB2), which were originally linked to cell-cycle progression, are known to regulate cristae structure. These proteins are assembled into large ring complexes in the IMM and act as protein and lipid scaffolds (Peng *et al*., 2015).

Prohibitins take also part in apoptosis regulating the processing of OPA1 (Merkwirth *et al*., 2008). Besides its role in proton conduction, cardiolipin, the main component of the mitochondrial inner membrane, has also been implicated in contributing to the shape of the IMM by maintaining its fluidity and osmotic stability (Koshkin and Greenberg, 2002; Zecycki *et al*., 2014). In addition, in the last years, strong evidence supporting a role of mitochondrial F_1F_O-ATP synthase in the regulation of cristae structure and positive curvature, emerged (Habersetzer *et al*., 2013; Seelert and Dencher, 2011; Wittig and Schagger, 2009; Zick *et al*., 2009). In **tab. 2**, proteins known to be involved in the regulation of cristae morphology are listed.

Tab. 2 Proteins involved in cristae morphology (modified from Zick *et al*., 2009)

Protein (organism)	**Function**	**Mitochondrial ultrastructure**
Atp21p/Tim11p	Components of the F_1F_0-ATP synthase	Onion-like, elongated cristae
ATP6/ATP6p (***H. sapiens*, *C. elegans*, *D. melanogaster***)	Proton channel of F_1F_0-ATP synthase	Aberrant mitochondrial morphology, IM vesicles, septa
PINK1 (***H. sapiens*, *C. elegans*, *D. melanogaster***)	Serine/threonine kinase	Swollen mitochondria, cristae fragmentation
Tafazzin (***H. sapiens***)	Acyltransferase-biosynthesis of phospholipids	Mitochondria fragmentation, reduced cristae surface
DICE1/DIC-1 (***H. sapiens*, *C. elegans***)	Tumor suppressor protein	IM vesiculations
AIF (***M. musculus***)	Induction of apoptosis	Aberrant IM topology
Mdm33p (***S. cerevisiae***)	IMM fission	Over-expression leads to cristae loss
LETM1/Mdm38p (***H. sapiens*, *D. melanogaster*, *C. elegans*, *S. cerevisiae***)	K+/H+ exchange; chaperone	Mitochondrial fragmentation, loss of membrane potential, osmotic swelling
OPA1/Mgm1p (***H. sapiens*, *M. musculus*, *S. cerevisiae***)	IMM fusion; remodelling of crista	Cristae remodelling during apoptosis, septa
Prohibitins (***H. sapiens*, *M. musculus*, *S. cerevisiae***)	Regulation of OPA1 processing; other functions	Cristae loss and vesiculation oh the IMM
Mitofilin (***H. sapiens***)	Organization of cristae and crista junctions	Absence of crista junctions, IMM disorganization

The IMM contains a large multiprotein complex, which is called the mitochondrial contact site and cristae organizing system (MICOS), required for architecture maintenance of the IMM and involved in multiple contact sites between IMM and OMM (Harner *et al.*, 2011). Seven subunits have been described in yeast (Mic10, Mic12, Mic19, Mic25, Mic26, Mic27, Mic60), six of which with identified human orthologs (MIC10/MINOS1, MIC19/CHCHD3, MIC25/CHCHD6, MIC27/APOOL, MIC26/APOO and MIC60/Mitofilin) (Huynen *et al*., 2016). All proteins are located on the inner membrane, and exposed to the IMS. Mic10 and Mic60 mediate the attachment of the cristae membranes to the inner boundary membrane. In yeast, they form two different and independent MICOS-organizing complexes connected by Mic19. The complex composed of Mic27, Mic10, and Mic12 controls cristae shape together with complex III and IV, and is cardiolipin dependent; on the contrary, the Mic60 complex is OXPHOS and cardiolipin independent,

suggesting a role for nascent cristae. Mic12, Mic26, and Mic27 contribute to complex integrity and cristae folding.

Mic19 resides in the inner membrane facing the intermembrane space and interacts with Mic60 and OPA1 and with Sam50 in the outer membrane. Mic19 is not only important for the presence of CJ, but also for the formation of intact cristae. Indeed, its depletion leads to the appearance of branched cristae. MICOS forms contact sites with the OMM, to allow the import of proteins, metabolite channelling, lipid transport, and membrane dynamics (Kozjak-Pavlovic, 2017).

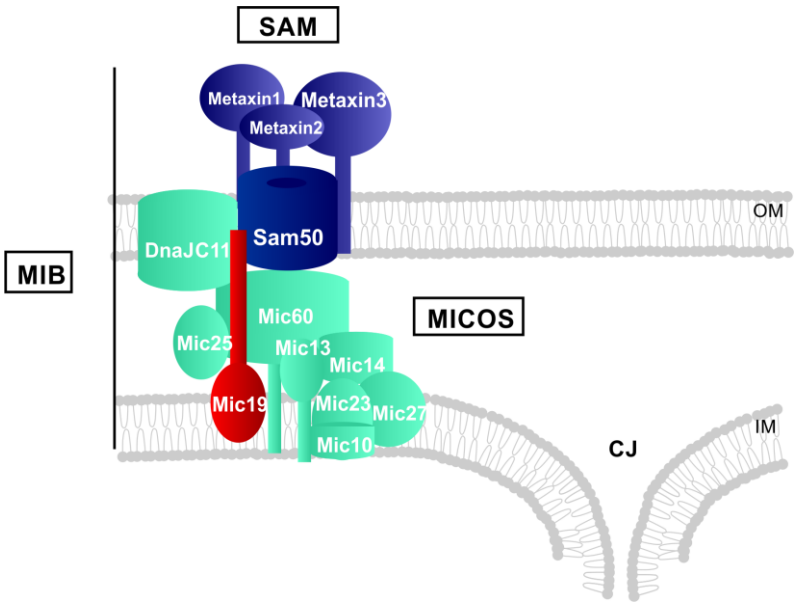

Fig. 6 MIB complex components. Mitochondrial contact site and cristae organizing system (MICOS) and sorting and assembly machinery (MIA) complex form the mitochondrial intermembrane space bridging complex (MIB)(redrawn from Pavlovic, 2017).

Recently, a new MICOS complex component has been identified, QIL1 (C19orf70) (Guarani *et al.,* 2015). The loss of QIL1 results in MICOS disassembly and CJs disruption in cultured human cells, and in Drosophila muscles causes impaired respiration and increased mitochondrial fragmentation (Guarani *et al*., 2015). In addition, the human MICOS complex strongly interacts with SAM forming a larger complex that spans both membranes named mitochondrial intermembrane space bridging complex (MIB) (Ott *et al.*, 2012) (**Tab 3**, **Fig 6**).

Tab. 3 MICOS and MIB complex components in human (from Kozjak-Pavlovic, 2017).

Name	Alternative name(s)	Localization	Molecular weight	Yeast homolog
		MIB		
		MICOS		
Mic60	Mitofilin, IMMT	IMM	88 kDa, 90 kDa	Mic60/Fcj1
Mic10	MINOS1, C1orf151	IMM	8.8 kDa	Mic10/YCL057C

Mic19	CHCHD3	IMM	26.2 kDa	Mic19/Aim13
Mic25	CHCHD6, CHCM1	IMM, associated	26.5 kDa	Mic19/Aim13
Mic23	Mic26, ApoO	IMM	22.3 kDa	Mic26/YGR235C Mic27/Aim37
Mic27	ApoOL, FAM121A	IMM	29.2 kDa	Mic26/YGR235C Mic27/Aim37
Mic13	Qil1, C19orf70	IMM	13 kDa	Mic12/Aim5
Mic14	CHCHD10, C22orf16	IMM, associated	14.1 kDa	–
MICOS and SAM interacting proteins				
DnaJC11	–	OMM/IMM	63.3 kDa 57.2 kDa 35 kDa	–
SAM				
Sam50	Samm50, CGI-51	OMM	51.8 kDa	Sam50
Metaxin 1	–	OMM	35.8 kDa	Sam37, Sam35
Metaxin 2	–	OMM	30 kDa	Sam37, Sam35
Metaxin 3	–	OMM	35 kDa	Sam37, Sam35

Cristae were first discovered in rat cells by George Palade in 1953, and the involvement of the mitochondrial contact site proteins with cristae was described in 2005. Despite this, only very recently evidences of the presence of the MICOS complex has been found in other organisms, such as Drosophila. In 2015, Guarani and co-workers identified the Drosophila ortholog of the human QIL1 (CG7603) and observed an increase in abnormal mitochondria containing IM swirls in larval muscles and in neurons upon *QIL1* down-regulation. A detailed mapping of the MIB proteins present across species (including Drosophila) is reported in **Fig.7**.

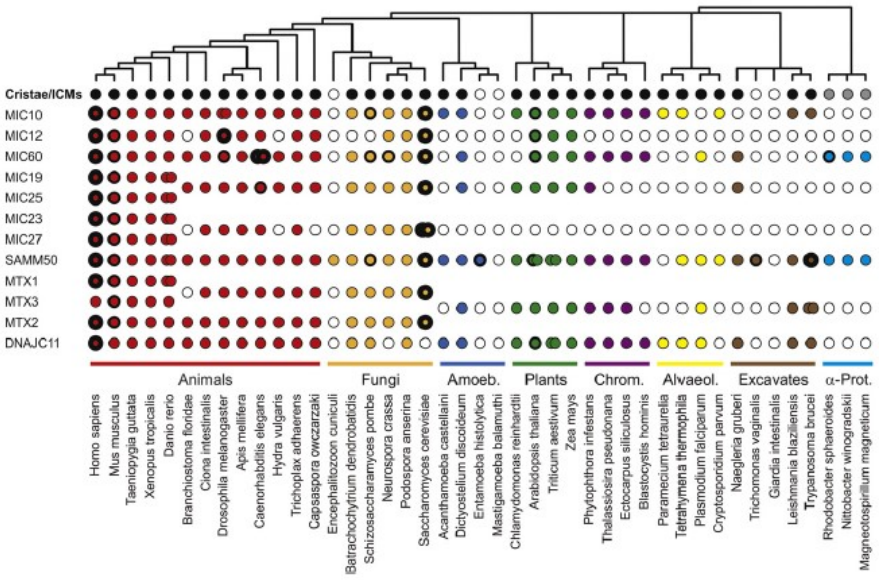

Fig. 7 The phylogenetic distribution of MICOS and MIB subunits. The phylogenetic distribution was determined among eukaryotes with and without cristae (black), and among α-proteobacteria with intracellular cytoplasmic membranes (ICM, gray). Empty circles indicate the absence of an ortholog; coloured circles with a thin rim, the presence of an orthologous gene; medium rims denote the

presence of the protein in a mitochondrial or ICM fraction; thick rim indicates experimental evidence that the protein functions in mitochondria; double circles underlined the presence of two or more genes that are the result of duplication (from Huynen *et al*., 2016).

2.5.3 Mitochondrial fission and fusion and mitophagy

Defective mitochondria can produce excessive amounts of Reactive Oxygen Species (ROS), consume ATP through reversal of ATP synthase, and interfere with a lot of metabolic processes, with effects ultimately resulting highly toxic for cells (Zorov *et al*., 2014). By mixing proteins content, the fusion process allows mitochondria to mitigate stress, compensating for one another's defects. However, when a certain threshold of damage is reached, mitochondria are eliminated by autophagy (Youle and van der Bliek, 2012). Mitophagy, the autophagic elimination of damaged mitochondria, seems to be linked to mitochondrial fission and fusion processes. Fission segregates the most seriously damaged mitochondria to preserve the functionality of the network (Youle and van der Bliek, 2012; Ashrafi and Schwartz, 2013).

Recent work on two proteins found mutated in patients affected by familial Parkinson's disease, PINK1 and Parkin, shed new light on the mechanism of quality control via mitophagy (Fig. 7). Patients with either Parkin or PINK1 mutations show similar clinical manifestations, suggesting that PINK1 and Parkin could act in the same pathway (Narendra *et al*., 2012). In Drosophila, deletions of one of these two genes determine muscle degeneration, loss of dopaminergic neurons and disrupted spermatogenesis (Guo, 2012).

PINK1 is a nuclear-encoded serine/threonine kinase targeted to mitochondria (Narendra *et al*., 2012). It possesses a mitochondrial targeting sequence and, like others mitochondrial proteins, it requires the electrochemical gradient of the inner mitochondrial membrane for its import via the TOM/TIM complexes (Narendra *et al*., 2012).

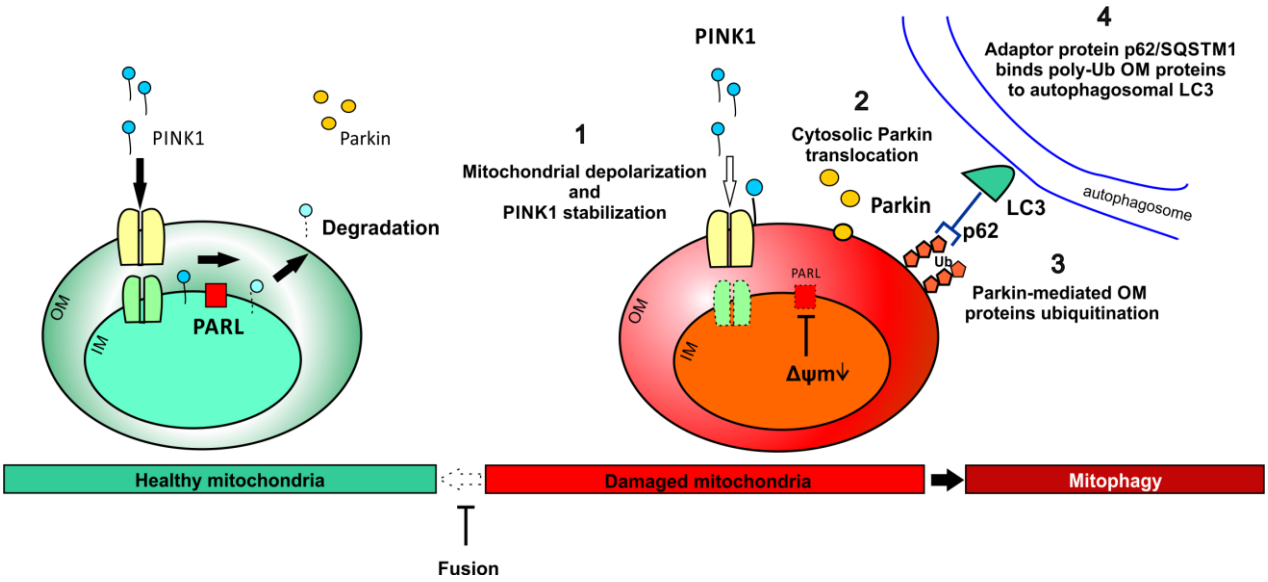

Fig. 8 The PINK1/Parkin pathway of mitophagy. In healthy mitochondria, PINK1 is continuously cleaved by PARL. In unhealthy mitochondria, PINK1 is no more cleaved and accumulates on the cytosolic face recruiting Parkin from the cytosol.

In healthy mitochondria, PINK1 is present at very low level, being continuously cleaved by the rhomboid protease PARL (Narendra *et al*., 2012). PINK1 has a second weaker MTS that drives the protein to the OMM if the TOM/TIM complex is blocked by a collapse of the membrane potential (Zhou *et al*., 2008). Thus, unhealthy mitochondria accumulate PINK1 on their cytosolic face. It has been shown that PINK1 associates with TOM complex, probably to facilitate a rapid re-import (and subsequently degradation) of the protein when the membrane potential is restored (Lazarou *et al.*, 2012). On damaged mitochondria, PINK1 recruits the E3 ubiquitin ligase Parkin from the cytosol, where it resides in an inactive form. Once there, Parkin ubiquitinates outer mitochondrial membrane proteins and induces autophagic elimination of the mitochondrion (Narendra *et al*., 2012). Ubiquitin-binding adaptor proteins, as sequestosome 1 (p62), are recruited on mitochondria following Parkin activation (Lee *et al.*, 2010). p62 mediates the recruitment of unfolded protein aggregates to autophagosome, thus connecting ubiquitinated mitochondria with the autophagy machinery (Kirkin *et al*., 2009; Narendra *et al*., 2012) (**Fig. 8**).

PINK1 and Parkin have been demonstrated to regulate mitofusins and Miro, to isolate and immobilize damaged mitochondria, respectively (Narendra *et al*., 2012). In Drosophila, Parkin depletion leads to a decrease in mitofusin ubiquitination, thus increasing indirectly mitofusin levels, which finally induces mitochondrial network hyperfusion (Poole *et al*., 2010; Ziviani *et al*., 2010). Miro1 and Miro2, together with Milton and kinesin, form a complex responsible for the transport of mitochondria along microtubules (Stowers *et al*., 2002; Guo *et al*., 2005). Interestingly, PINK1 has been found to interact with both Miro1 and Milton (Weihofen *et al.*, 2009). Moreover, Miro1 is degraded when Parkin is activated (Wang *et al*., 2011; Liu *et al*., 2012). This degradation is also considered to promote mitophagy of damaged mitochondria (Liu *et al*., 2012).

2.5.5 Apoptosis

Mitochondrial morphology is tightly linked to apoptosis. High levels of cell stress that lead to apoptosis induce the recruitment of Drp1 on mitochondria, which prompts the organelles inside the dying cell to rapidly undergo fragmentation (Martinou and Youle, 2011). This happens concomitantly with the translocation from the cytosol to the mitochondria of the pro-apoptotic protein Bax (a member, like Bak, of the Bcl-2 protein family) as well as cytochrome c release (Martinou and Youle, 2011). Bax accumulation co-localizes with Drp1 at mitochondrial fission sites (Karbowski *et al*., 2002). It has been demonstrated that RNAi knock-down of the two fission proteins Drp1 and Fis1 protects cell from apoptosis preventing fragmentation and cytochrome c release, even if Bax translocation occurs (Lee *et al*., 2004). Moreover, Bcl-2 family proteins are able to regulate mitochondrial morphology in healthy cells. In mouse cells lacking both Bax and Bak, mitochondria are fragmented under normal conditions (Karbowski *et al*., 2006). Bax seems also to have a role in controlling Mfn2 distribution on the OMM, thus influencing mitochondrial fusion

(Karbowski *et al*., 2006). Conversely, over-expression of OPA1 maintains tight mitochondrial cristae junctions, which inhibit the movement of cytochrome *c* and prevent its release (Scott and Youle, 2010).
The importance of mitochondria in the regulation of cell apoptosis in non-mammalian species has been considered limited, primarily because in these organisms cytochrome c does not play a key role in caspase activation. These cysteine-dependent aspartate-driven proteases play a fundamental role in apoptosis cleaving proteins involved in the dismantle of the dying cells (Parrish *et al*., 2013). However, recent studies indicate mitochondria as a central component of caspase activation and apoptosis in Drosophila. Indeed, key actors in the regulation of Drosophila cell death, like RHG proteins (Reaper, Hid, and Grim) and members of the Bcl-2 family, constitutively or transiently localize to mitochondria. These proteins can contribute in triggering apoptosis through different mechanisms, such as promoting Diap1 degradation, increasing ROS production, or activating fission processes (Abdelwahid *et al*., 2011; Clavier *et al*., 2016).

2.6 Mitochondrial respiratory chain and oxidative phosphorylation

The mitochondrial respiratory chain (MRC) is composed of five multiheteromeric complexes embedded in the inner mitochondrial membrane (Complex I, II, III, IV, and V) (Fig. 8). Except for complex II, the remaining four MRC complexes contain subunits encoded by both genomes, and then synthesized *in situ* by the mitochondrial specific translation machinery (Ghezzi and Zeviani, 2012). Chaperones and assembly factors, some of which are specific to each complex, are involved in the incorporation of protein subunits and prosthetic groups, including metal-containing reactive centres. Complexes I-IV mediate the two linked events of electron transfer and proton pumping. Electrons move from an electron donor (NADH or QH2) to a terminal electron acceptor (O_2) through a series of redox reactions. These reactions are coupled to the generation of a proton gradient across the inner membrane. The resulting transmembrane proton gradient is used by complex V or ATP synthase which carries out the phosphorylation of ADP into ATP. Aerobic glucose oxidation starts in the cytoplasm with glycolysis which yields two NADH, two ATP and two molecules of pyruvate. The pyruvates are imported into the mitochondrial matrix, where pyruvate dehydrogenase transfers their acetyl groups to CoA forming two NADH molecules. The acetyl groups of the two acetyl-CoA products enter the tricarboxylic acid (TCA) cycle where they are oxidized to CO_2, yielding six NADH and two GTP. The NADH together with succinate, an intermediate of the TCA cycle, are electron-rich substrates that are oxidized by the respiratory chain complexes I and II, respectively. At the level of Complex I (also called NADH dehydrogenase or NADH: ubiquinone oxidoreductase) two electrons are removed from NADH and transferred to ubiquinone, a small, lipid-soluble organic molecule that can freely diffuse within and across the IMM. In this step the first four protons are translocated across the inner membrane towards the intermembrane space. The reduced UQ [UQH2 (ubiquinol)] diffuses to complex III where it is reoxidized. Complex III (or cytochrome bc1 complex) removes two electrons from QH_2 at the QO

site, which are sequentially transferred to two molecules of cytochrome c located on the inner-membrane. The other two electrons pass through the protein towards the Qi site, where the quinone of ubiquinone molecules is reduced to quinol. Complex III maintains the electrochemical gradient by an asymmetric mechanism of absorption/release of protons (Edward *et al*., 2001). In total, six protons are translocated: two protons reduce quinone to quinol and four protons are released from two ubiquinol molecules. Complex IV (or cytochrome c oxidase) is involved in the removal of four electrons from four molecules of cytochrome c and their transfer to molecular oxygen, producing two molecules of water. In this way, four additional protons are translocated across the membrane, contributing to the proton gradient. The electrochemical gradient created with the efflux of protons from the mitochondrial matrix is used by the Complex V or F_OF_1 ATP synthase to generate ATP. The F_O component of ATP synthase acts as an ion channel that provides a proton flux back into the mitochondrial matrix. The free energy is used to drive ATP synthesis, catalysed by the F1 component of the complex (**Fig. 9**).

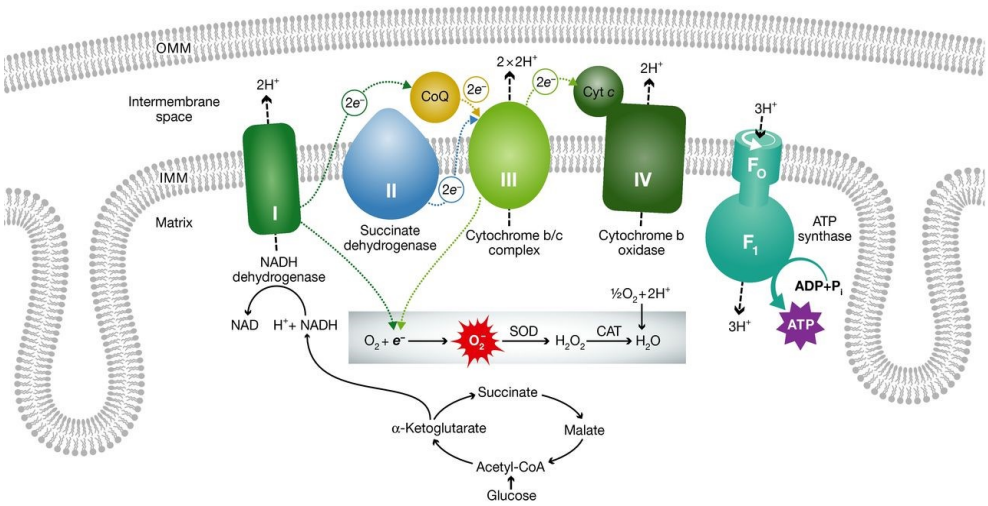

Fig. 9 The oxidative phosphorylation process. The respiratory chain complexes are localized in the cristae membranes. Complexes I, III and IV pump protons from the matrix to the IMS, creating an electrochemical gradient that is used by complex V for ATP production. The subunits that are encoded by the mtDNA are listed under each respiratory chain complex (Dorn, 2015).

In **tab. 4** the identified *Drosophila melanogaster* orthologs of the nuclear genes encoding mitochondrial proteins involved in oxidative phosphorylation are reported.

Tab. 4 OXPHOS proteins in *Drosophila melanogaster* genome (Tripoli *et al*., 2005)**.**

Complex (subunit)	Protein name	*D. melanogaster* gene name
Complex I: NADH:ubiquinone oxidoreductase		
NUMM	13 kDa A subunit	CG8680
NUFM	13 kDa B subunit	CG6463
NIPM	15 kDa subunit	CG11455

NUYM	18 kDa subunit	CG12203
NUPM	19 kDa subunit	CG3683
NUKM	20 kDa subunit	CG9172
NUIM	23 kDa subunit	ND23
NUHM	24 kDa subunit	CG5703
NUGM	30 kDa subunit	CG12079
NUEM	39 kDa subunit	CG6020
NUDM	42 kDa subunit	ND42
NUCM	49 kDa subunit	CG1970
NUBM	51 kDa subunit	CG9140
NUAM	75 kDa subunit	ND75
NI8M	B8 subunit	CG15434
NB2M	B12 subunit	CG10320
NB4M	B14 subunit	CG7712
N4AM	B14.5A subunit	CG3621
N4BM	B14.5B subunit	CG12400
NB5M	B15 subunit	CG12859
NB6M	B16.6 subunit	CG3446
NB7M	B17 subunit	l(2)35Di
N7BM	B17.2 subunit	CG3214
NB8M	B18 subunit	CG5548
NI2M	B22 subunit	CG9306
ACPM	Acyl carrier	mtacp1
NIAM	ASHI subunit	CG3192
NUML	MLRQ subunit	CG32230
NINM	MNLL subunit	CG18624
NIDM	PDSW subunit	Pdsw
NISM	SGDH subunit	l(3)neo18
NIGM	AGGG subunit	CG40002
Complex II: Succinate dehydrogenase		
DHSA	Flavoprotein subunit	Scs-fp
DHSB	Iron-sulfur protein	SdhB
C560	Cytochrome B560 subunit	CG6666
DHSD	Cytochrome b small subunit	CG10219
Complex III: Ubiquinol-cytochrome c reductase		
UCRY	6.4 kDa protein	CG14482
UCRX	7.2 kDa protein	ox
UCRH	11 kDa protein	Ucrh
UCR6	14 kDa protein	CG3560
UCRI	Iron-sulfur subunit	RFeSP
CY1	Cytochrome c1, heme protein	CG4769
UCR1	Core protein 1	CG3731
UCR2	Core protein 2	CG4169
UCRQ	Ubiquinone-binding protein QP-	CG7580
Complex IV: Cytochrome c oxidase		

CX41	Polypeptide IV	CG10664
COXA	Polypeptide Va	CoVa
COXB	Polypeptide Vb	CG11015
COXD	Polypeptide Via	CG17280
COXG	Polypeptide VIb	CG18809
COXH	Polypeptide Vic	cype
COXK	Polypeptide VIIa	CG9603
COXO	Polypeptide VIIc	CG2249
Complex V: ATP synthase		
ATPA	Alpha chain	blw
ATPB	Beta chain	ATPsyn-beta
ATPG	Gamma chain	ATPsyn-gamma
ATPD	Delta chain	CG2968
ATPE	Epsilon chain	sun
ATPF	B chain	ATPsyn-b
ATPQ	D chain	ATPsyn-d
ATPJ	E chain	CG3321
ATPK	F chain	CG4692
ATPN	G chain	l(2)06225
ATPR	Coupling factor 6	ATPsyn-Cf6
AT91	Lipid-binding protein P1	CG1746
ATPO	OSCP	Oscp
Others		
ATPW	ATP synthase coupling factor B	CG10731
CI30	Complex I intermediate-associate protein 30	CG7598
CYC	Cytochrome C	Cyt-c-p
COXZ	Complex IV assembly protein COX11	CG6922
COXS	Complex IV copper chaperone	CG9065
OXA1	Biogenesis protein OXA1	CG6404
ETFA	Electron transfer flavoprotein alpha subunit	wal
ETFB	Electron transfer flavoprotein beta subunit	CG7834
ETFD	Electron transfer flavoprotein-ubiquinone oxidoreductase	CG12140
COXX	Protoheme IX farnesyltransferase	CG5037
SCO1	Sco1 protein homolog	CG8885
SUR1	Surfeit locus protein 1	Surf1

3.1 Mitochondrial diseases

Mitochondrial diseases (MDs) are a clinically heterogeneous group of inherited disorders caused by dysfunction of the mitochondrial respiratory chain. Altogether, they are the most common inborn errors of metabolism in humans, with an estimated prevalence of between 1:5,000 and 1:10,000 live births (Nogueira *et al.*, 2014).

As aforementioned, MRC function depends on the coordinated expression of both mitochondrial and nuclear genomes. Since the majority of proteins involved in mitochondrial metabolism and in mtDNA maintenance are encoded by nuclear genes, mitochondrial diseases can also arise from genetic defects in nuclear genes. An impaired cross-talk is known to give rise to nuclear-mitochondrial intergenomic communication disorders, which result in depletion or instability of the mtDNA and defective maintenance of qualitative and quantitative mtDNA integrity (Nogueira *et al.*, 2014).

The age of onset and the phenotypic variability of mitochondrial diseases are determined by diverse factors, including threshold effect, tissue dependent segregation of heteroplasmy, nuclear background, age, sex, and environment. Only some deleterious mtDNA mutations are homoplasmic. In the presence of heteroplasmy, the ratio of wild-type to mutant mtDNA determines the onset of clinical symptoms. The offset of a threshold value, which is the minimum critical proportion of mutated mtDNAs, is necessary for biochemical defects and tissue dysfunction to appear. This level is lower in tissues highly dependent on OXPHOS metabolism than in tissues that can rely on anaerobic glycolysis. However, other factors mentioned above, often contribute to the disease process. Thus, a wide range of phenotypes can derive from the same mutation. Furthermore, different mtDNA mutations can cause the same phenotype, probably mirroring a common pathway of impaired OXPHOS in a particular set of tissues. OXPHOS represents the main source of cellular energy, so any organ or tissue may be involved in mitochondrial diseases but generally tissues with higher energy demand, such as brain, skeletal and cardiac muscle, kidney and endocrine systems are the most frequently affected. Clinical features range from lesions in single tissues, such as the optic nerve in Leber's hereditary optic neuropathy (LHON), to complex multisystem syndromes. In general, childhood presentations of mitochondrial diseases are more severe than those with adult onset and frequently involve many different organ systems. In **Tab. 5** the main clinical manifestations associated with pediatric and adult onset mitochondrial diseases are summarized.

Tab. 5 Mitochondrial diseases associated manifestations.

	Pediatric	Adult
Neurological	Epilepsy, myopathy, psychomotor retardation, ataxia, spasticity, dystonia, sensorineural deafness	Epilepsy, dementia, myopathy, peripheral neuopathy, ataxia
Gastrointestinal	Vomiting, failure to thrive, dysphagia	Constipation, irritable bowel, dysphagia
Cardiac	Cardiomyopathy, rhythm abnormalities	Heart failure, heart block, cardiomyopathy

Respiratory	Central hypoventilation, apnoea	Respiratory failure
Endocrinal	Diabetes, adrenal failure	Diabetes, thyroid disease, parathyroid disease, ovarian failure
Ophthalmological	Optic atrophy	Optic atrophy, cataract, ophthalmoplegia, ptosis
Renal	Renal tubular defects	
Liver	Hepatic failure	

The genetic classification of mitochondrial diseases distinguishes disorders caused by defects in mtDNA, which are maternally inherited, from those due to defects in ncDNA, which are transmitted by Mendelian inheritance (autosomal dominant, autosomal recessive and X-linked).

3.2 Mutations in mtDNA genes

Despite the small size of human mtDNA, mutations in mitochondrial genome are an important cause of inherited diseases. Most mtDNA alterations are neutral polymorphisms that have proved to be very useful in tracking human migrations. The first pathogenic mtDNA mutation was identified in 1988 when Wallace and colleagues found a point mutation in the gene encoding subunit ND4 of Complex I in a family with Leber's hereditary optic neuropathy (LHON) (Wallace *et al*., 1988). Since then, over 250 pathogenic point mutations and rearrangements in mitochondrial genome have been characterized, which cause a wide spectrum of heterogeneous phenotypes with variable age of onset (**Fig. 10**).

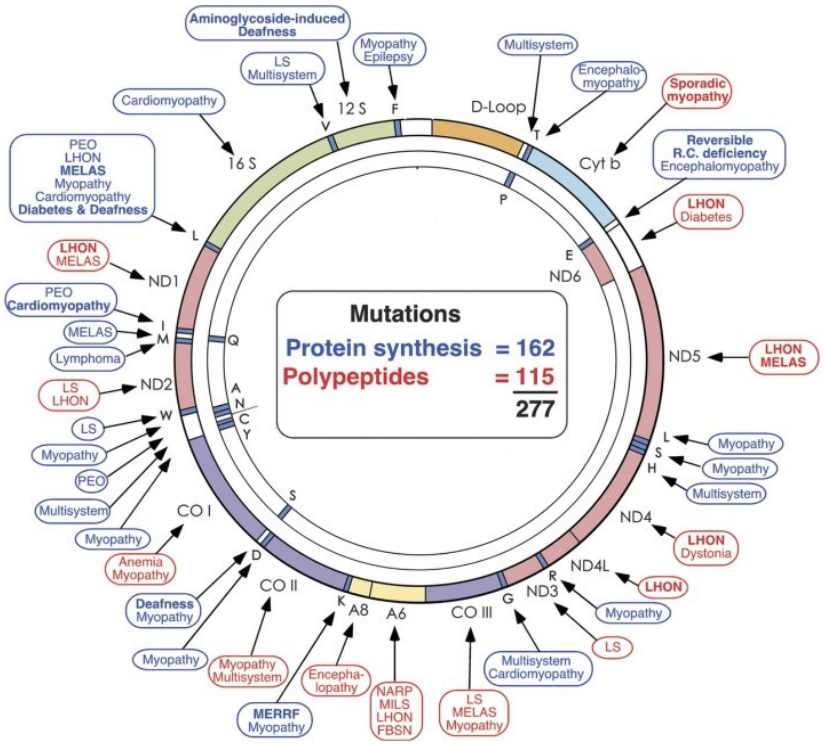

Fig. 10 Localization of known point mtDNA mutations and related diseases Human mitochondrial DNA map showing mutations and relative diseases (from DiMauro, 2013).

These alterations are distributed throughout the mitochondrial genome and account for 10-20% of all mitochondrial diseases. Although defective OXPHOS is a common feature, clinical variability is often remarkable. Different phenotypes can arise depending on mutations intrinsic severity, targeted gene, and heteroplasmy levels (Chen *et al.*, 2015). Common hallmarks of several mtDNA mutations are defective OXPHOS, and massive mitochondrial proliferation in muscle (resulting in ragged-red fibers) (Schon *et al*., 2012). Mitochondrial mutations entail point mutations and large-scale rearrangements (both deletions and duplications).

Point mutations may affect within protein, tRNA, or rRNA genes, and are usually maternally inherited. These mutations are usually heteroplasmic, and characterized by clinical heterogeneity (Tuppen *et al*., 2010). Remarkably, more than a half of disease-related point mutations are located within mt-tRNA genes, although tRNAs account for only the 10% of the mitochondrial genome. Mutations in tRNA genes seem to be 'tolerated' over a broader range of mutant loads compared to mutations in polypeptide-coding genes (Schon *et al*., 2012). Conversely, only one mutation in 16S rRNA has been found associated with a primary mitochondrial disease. Furthermore, none of the five mutations in the 12S rRNA gene, responsible for non-syndromic deafness, are lethal (Raimundo *et al.*, 2012). Finally, m.8993T→G mutation in the ATP synthase 6 gene causes maternally inherited Leigh's syndrome (MILS), a fatal encephalopathy, when mutation loads is above 90%, whereas at mutation loads in the range of 70–90% patients present neuropathy, ataxia and retinitis pigmentosa (Holt *et al*., 1990).

Heteroplasmic mtDNA deletions were associated with human diseases in 1988 (Holt *et al*., 1988). The corresponding syndromes are sporadic and heteroplasmic, and characterized by a wide range of clinical manifestations and spectrum of severity. The prevalence of single deletion disorders is estimated at 1-2:100000 cases (Gorman *et al*., 2015). Deletions can span several genes, varying in size from 1.3 Kb to 8 Kb. Interestingly, they are always localized in the major arc between the two replication origins. Rearranged mtDNAs have been found in human oocytes (Chen et al, 1995) supporting the hypothesis that pathogenic deletions can arise in the female germ line. Thus, single mtDNA deletions can occur sporadically early in development as the result of clonal amplification of a single mutational event. Macrodeletions have been associated with particular phenotypes, including chronic progressive external ophthalmoplegia (CPEO), Kearns-Sayre syndrome, and Pearson's bone marrow-pancreas syndrome (DiMauro and Hirano, 2011). Small mtDNA deletions have been described within the genes encoding subunits of cytochrome oxidase, cytochrome b and complex I, and are associated with a wide range of clinical manifestations.

Mutations in nuclear genes involved in mtDNA maintenance and replication, as well as mitochondrial nucleotide metabolism, may determine the occurrence of multiple mtDNA deletions in affected tissue. In aged post-mitotic tissues and in individuals with neurodegenerative diseases an exponential accumulation of multiple mtDNA deletions was also reported (Tuppen *et al*., 2010).

3.3 Mutations in nuclear genes

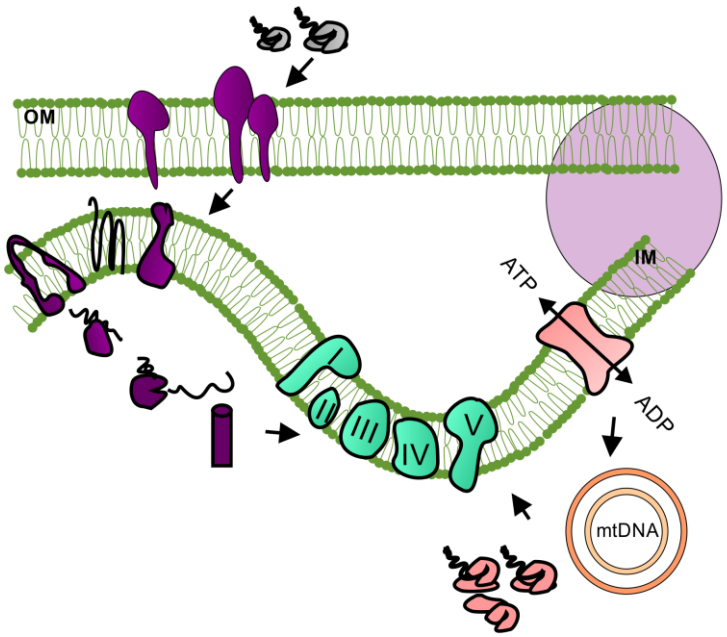

OXPHOS subunits	Biosynthesis of lipids and co-factors	mtDNA expression/ maintenance	OXPHOS biogenesis/regulation	Protein import and membrane dynamics
ncDNA **I**: NDUFV1, NDUFV2, NDUFA1, NDUFA2,NDUFA10, NDUFA11, NDUFS1, NDUFS2, NDUFS3, NDUFS4, NDUFS6, NDUFS7, NDUFS8 **II**: SDHA, SDHB, SDHC, SDHD **III**: UQCRB,UQCRQ, CYCS **IV**: COX6B1, COX4I2 **mtDNA** **I**: ND1, ND2, ND3, ND4, ND4L, ND5, ND6 **III**:CYTB **IV**: COX1, COX2, COX3 **V**: ATP6, ATP8	**Coenzyme Q10 biogenesis** COQ2, COQ4, COQ9, PDSS1, PDSS2,CABC 1 **Iron homeostasis** FRDA, ABCB7, ISCU, NFU1, BOLA3, GLRX5 **Others** TAZ	**mtDNA maintenace** POLG, POLG2, C10orf2, MPV17, SLC25A4, SLC25A3, TYMP, DGUOK, TK2, SUCLA2, SUCLG1, RRM2B **Protein synthesis** EGF1, YARS2, SARS2, DARS2, RARS2, MRPS16, MRPS22, TSFM, TUFM, TMRU, PUS1, GFMI, **mtDNA transcription** LRPPRC	**I:** NDUFAF1, NDUFAF2, NDUFAF3, NDUFAF4, C8orf38, C20orf7, NUBPL, FOXRED1, ACAD9 **II**: SDHAF1, SDHAF2 **III:** BCS1L, LYRM7 **IV:** SURF1, SCO1, SCO2, COX10, COX15, TACO1, ETHE1, FASTKD2, LRPPRC **V**: ATPAF2, TMEM70	**Protein import** TIMM8A, DNAJC19, GFER, AGT **Chaperone function** SPG7, HSPD1 **Dynamics** OPA1, MFN

Fig. 11 Biological pathways underlying respiratory chain diseases. The panel below lists protein that have been shown to cause mitochondrial diseases according to their function (redrawn from Calvo *et al.*, 2010).

Mitochondrial proteome consists of approximately 1.500 gene products. Except for 13 essential polypeptides of OXPHOS encoded by the mitochondrial genome, all other structural subunits and assembly factors are nuclear-encoded and imported into mitochondria (Ruiz-Pesini *et al.*, 2007). Mitochondrial diseases-associated nDNA mutations can affect: a) genes encoding structural components of the OXPHOS

complexes; b) genes encoding factors involved in the biosynthesis of lipids and cofactors; c) genes encoding proteins involved in mitochondrial protein import and dynamics; d) genes encoding assembly factors of the OXPHOS complexes; e) genes encoding factors affecting mtDNA maintenance and replication (**Fig. 11**).

a) Mutations in genes encoding structural components of the OXPHOS complexes

Although nuclear DNA encodes most of the subunits of the OXPHOS system, mutations have only rarely been described. Such mutations are probably highly deleterious and perhaps lethal in early embryonic stages. Consistently, mutations are associated with neonatal or early-onset. Complex I is the most frequent target in these pathologies, counting for up to 30% of cases in childhood. Complex I deficiency results from mutation in nuclear genes including *NADH:ubiquinone oxidoreductase core subunit V1* (*NDUFV1*), *NADH:ubiquinone oxidoreductase core subunit S2* (*NDUFS2*), *NADH:ubiquinone oxidoreductase core subunit S1* (*NDUFS1*), *NADH:ubiquinone oxidoreductase core subunit S3* (*NDUFS3*), *NADH:ubiquinone oxidoreductase subunit S4* (*NDUFS4*), *NADH:ubiquinone oxidoreductase subunit S6* (*NDUFS6)*, *NADH:ubiquinone oxidoreductase core subunit S7* (*NDUFS7*), *NADH:ubiquinone oxidoreductase core subunit S8* (*NDUFS8*), *NADH:ubiquinone oxidoreductase subunit A2* (*NDUFA2*), *NADH:ubiquinone oxidoreductase subunit A11* (*NDUFA11*), *NADH:ubiquinone oxidoreductase subunit A13* (*NDUFA13*). Patients are affected by neurological disorder, often Leigh syndrome, sometimes complicated by cardiomyopathy, or multisystem involvement (Fassone and Rahman, 2012). Mitochondrial diseases associated with complex II deficiency are extremely rare, and predicted to cover only 2% of respiratory chain defects (Brière *et al*., 2005). Few cases with CII deficiency associated with mitochondrial disorders were found to carry mutations in *succinate dehydrogenase complex flavoprotein subunit A* (*SDHA*). In these cases, infantile Leigh syndrome is the most common associated clinical manifestation. Moreover, mutations in *succinate dehydrogenase complex subunit D* (*SDHD*), *succinate dehydrogenase complex subunit C* (*SDHC*), *succinate dehydrogenase complex iron sulfur subunit B* (*SDHB*), and in an assembly factor of SDH, *succinate dehydrogenase complex assembly factor 2* (*SDHAF2*), have been linked to inherited paragangliomas, phaeochromocytomas or glomus tumours (Kanabus *et al*., 2014). The pathogenesis of tumors induced by mutations in complex II subunits is still unclear. Disorders related to mitochondrial complex III deficiency are mostly caused by mutations in the mtDNA-encoded cytochrome b subunit. Additional mutations include a homozygous deletion of *ubiquinol-cytochrome c reductase binding protein* (*UQCRB*) associated with severe CIII deficiency in the liver and metabolic crises during fasting. *Ubiquinol-cytochrome c reductase complex III subunit VII* (*UQCRQ*), *ubiquinol-cytochrome c reductase complex III subunit VII* (*UQCRC*), and *cytochrome c1* (*CYC1*) mutant patients present severe neuromuscular syndrome, mental retardation, lactic acidosis and metabolic imbalance (Barel *et al*., 2008; Miyake *et al*., 2013; Gaignard *et al*., 2013). Although different mutations in mitochondrial encoded subunits of complex IV are known, few cases of mutations in nDNA-encoded subunits have been described. *cytochrome c oxidase subunit 6B1* (*COX6B-1*) mutations are associated with

leukodystrophic encephalopathy, myopathy and growth retardation; mutations in *cytochrome c oxidase subunit 4I2* (*COX4-2*) with congenital exocrine pancreatic insufficiency; whereas those affecting *cytochrome c oxidase subunit 7B* (*COX7-B*) are associated with microphthalmia characterized by linear skin lesions (MLS) (Indrieri *et al*., 2012). So far, mitochondrial diseases due to impairment in the ATP synthase activity have been shown to result from mutations in mtDNA-encoded subunits *ATP synthase 6* (*ATP6*) and *ATP synthase 8* (*ATP8*), nuclear genes encoding the structural subunits α (*ATP5A1*) and ε (*ATP5E*) (Ackerman and Tzagoloff, 1990; Houstek *et al*., 2009). These mutations share a similar biochemical phenotype characterized by a profound decrease in the content of fully assembled and functional ATP synthase, but the pathogenesis and the clinical manifestations differ substantially (Hejzlarová *et al.*, 2014). Recently, a homozygous mutation in the ε subunit encoded by the nuclear gene *ATP5E* has been found in a patient with lactic acidosis, 3-methylglutaconic aciduria, mild mental retardation and peripheral neuropathy (Mayr *et al*., 2010).

b) Mutations in genes encoding factors involved in the biosynthesis of lipids and cofactors

Mutations in ubiquinone (CoQ-10) biosynthetic genes *coenzyme Q2, polyprenyltransferase (COQ2)*, *decaprenyl diphosphate synthase subunit 1* (*PDSS1),* and *decaprenyl diphosphate synthase subunit 2 (PDSS2)* were associated with severe infantile mitochondrial syndromes and tissue CoQ-10 deficiency. CoQ-10 is a lipophilic component of the electron transport chain, which also plays a role as antioxidant and membrane stabilizer (Zeviani and Carelli, 2007; Duncan *et al*., 2009). The OXPHOS complex needs also to be equipped with cofactors such as Cu and Fe-S clusters for their activity. Thus, enzymes, assembly factors and chaperones, involved in their synthesis or incorporation, are necessary for the correct functioning of the complexes. In particular, mutations in frataxin cause Friedreich's ataxia, while defects in ABC7, an iron mitochondrial exporter, lead to X-linked sideroblastic ataxia and anemia (Bekri *et al*., 2014). Wilson's disease is due to a defect in copper internalization caused by mutations in ATPase copper transporting beta polypeptide (ATP7B). Mutations in TAZ, an X-linked gene encoding an acyl–coenzyme A synthetase (Tafazzin) that plays an important role in cardiolipin synthesis, causes Barth syndrome, characterized by mitochondrial myopathy, cardiomyopathy, growth retardation, and leukopenia (McKenzie *et al*., 2006).

c) Mutations in genes encoding proteins involved in mitochondrial protein import and dynamics

This group includes proteins with a role in mitochondrial metabolic pathways that are not directly correlated with the mitochondrial energy pathway. However, impairment in the respiratory chain activity can contribute to the development of the clinical phenotype. Only two known mitochondrial diseases are clearly attributable to defects in protein import, probably because they are generally incompatible with life. The deafness–dystonia syndrome (Mohr–Tranebjaerg syndrome), an X-linked recessive disorder characterized by progressive neurosensory deafness, dystonia, cortical blindness, and psychiatric

symptoms, is due to mutations in translocase of inner mitochondrial membrane 8A (TIMM8A), a protein belonging to a family of evolutionarily conserved polypeptides organized in heterooligomeric complexes in the IMS (Tranebjaerg *et al.,* 1995). This protein is responsible for the import and insertion of hydrophobic membrane proteins into the mitochondrial inner membrane. Mutations in GFER (growth factor, the homologue of ERV1) were found in four patients showing cataracts, hypotonia, developmental delay, sensorineural hearing loss, progressive myopathy and partial combined respiratory-chain deficiency (Di Fonzo *et al.,* 2009). Erv1 is a sulfhydryl oxidase that, together with the redox-regulated import receptor Mia40, allows the import of cysteine-rich proteins into the IMS, through an oxidative folding mechanism (Hell, 2008). Recently, DNAJC19, encoding a putative mitochondrial import protein similar to yeast TIM14, has been linked to dilated cardiomyopathy with ataxia (Davey *et al*., 2006). This novel autosomal recessive condition identified in the Canadian Dariusleut Hutterite population is characterized by cardiomyopathy, non-progressive cerebral ataxia, growth failure, testicular dysgenesis and 3-methylglutaconic aciduria. The mutation results in a protein lacking the DNAJ domain required in the fungal protein to stimulate the ATPase activity of mtHsp70. Moreover, it has been demonstrated that DNAJC19 forms a complex with prohibitins to regulate cardiolipin remodelling (Richter-Dennerlein *et al.,* 2014).

Mutations in mitochondrial targeting signal sequence have also been reported. The first defect in a mitochondrial targeting signal described a mutation in the N-MTS of one of the subunits of the mitochondrial matrix enzyme pyruvate dehydrogenase (PDH), which led to PDH deficiency (Takakubo *et al.,* 1995).

Alanine/glyoxylate aminotransferase 1 (AGT) catalyzes the conversion of glyoxylate to glycine in the peroxisomes of hepatocytes. Although most cases of primary hyperoxaluria type 1 (PH1) are due to the lack of active AGT, in one-third of patients AGT deficiency is caused by its mis-targeting to mitochondria (Danpure *et al*., 1989).

Pathogenic mutations in regulators of mitochondrial dynamics were found in patients affected by mitochondrial diseases. Mutations in the human *OPA1* gene lead to autosomal dominant optic atrophy (OPA1) characterized by the loss of retinal ganglion cells, causing decreased visual acuity, colour vision deficits, and optic nerve pallor. Rarely, mutations in OPA1 GTPase domain have been associated with autosomal dominant progressive external ophthalmoplegia (adPEO) and accumulation of multiple mtDNA deletions. Notably, *MFN2* gene is responsible for an axonal variant of the most frequent inherited peripheral neuropathy in humans, Charcot–Marie–Tooth neuropathy (type 2A), (Zuchner *et al.*, 2004).

d) Mutations in genes encoding assembly factors of the OXPHOS complexes

Given the complexity of the respiratory chain complexes, a large number of nuclear genes encode proteins likely involved in their biogenesis. Mutations affecting the assembly of complex I were reported for a number of complex I specific assembly factors, including *NADH:ubiquinone oxidoreductase complex*

assembly factor 2 (*NDUFAF2*), *NADH:ubiquinone oxidoreductase complex assembly factor 3* (*NDUFAF3*), *NADH:ubiquinone oxidoreductase complex assembly factor 4* (*NDUFAF4*), *NADH:ubiquinone oxidoreductase complex assembly factor 5* (*C20orf7*), *NADH:ubiquinone oxidoreductase complex assembly factor 6* (*C8orf38*), *nucleotide binding protein like* (*NUBPL*), *FAD dependent oxidoreductase domain containing 1* (*FOXRED1*) and *acyl-CoA dehydrogenase family member 9* (*ACAD9*) (Haack *et al*., 2010; Nouws *et al*., 2010). More than a half of patients suffering of CI deficiency showed no mutations in either known CI subunits or assembly factors, suggesting that additional genes necessary for the assembly or stability of CI are still unidentified. These mutations are responsible for a wide range of disorders, from lethal neonatal disease to adult-onset neurodegeneration, including micro- or macro-cephalic encephalopathy, progressive leucodystrophy, cardiomyopathy, myopathy and liver disease (Fernández-Vizarra *et al*., 2009). Mutations in SDH assembly factor 1 (*SDHAF1*), responsible for the insertion or retention of the Fe-S centers within the subunit SDHB of complex II, cause infantile leukoencephalopathy (Ghezzi *et al*., 2009). Several mutations in the CIII assembly factor *BCS1 homolog, ubiquinol-cytochrome c reductase complex chaperon (BCS1L)*, a member of the AAA+ family of proteins, were associated with a wide variety of clinical presentation: multivisceral GRACILE syndrome, congenital metabolic acidosis, neonatal proximal tubulopathy, liver failure, and encephalopathy (Fernández-Vizarra *et al*., 2009).

A single case of mutation in LYR motif containing 7 (LYRM7), a stabilizing chaperone of the Rieske protein in CIII, was described in a child, with symptoms including progressive weakness associated with anemia. Subsequently, the disease developed into a severe encephalopathy and metabolic acidosis leading to death for respiratory failure (Invernizzi *et al.*, 2013). More than 40 mutations in *SURF-1*, an early CIV assembly factor, causing the accumulation of specific subassemblies, have been found. As already reported, mutations in *SURF-1* are the most common cause of Leigh syndrome. Conversely, mutations in SCO1 and SCO2, two genes implicated in copper delivery to COX, cellular copper homeostasis and redox signalling, have been associated with neonatal hepatopathy and ketoacidotic coma (SCO1) or infantile cardiomyopathy (SCO2), both characterized by profound COX deficiency (Fernández-Vizarra *et al*., 2009).

Mutations in *COX10* and *COX15* were both found linked to profound COX activity deficiency. COX10 and COX15 are enzymes involved in the biosynthesis of the COX-specific haem A, which is incorporated early in the assembly of CIV. Mutations in *COX10* gene are associated with Leigh syndrome, progressive mitochondrial encephalopathy with proximal renal tubulopathy, metabolic acidosis, hypotonia and hypertrophic cardiomyopathy. Mutations of *COX15* cause fatal infantile hypertrophic cardiomyopathy and rapidly progressive or protracted Leigh syndrome. A few cases of complex V deficiency were attributed to mutations in the two biogenetic factors ATP synthase mitochondrial F1 complex assembly factor 2 (ATP12) and transmembrane protein 70 (TMEM70). In those cases, lactic acidosis was present immediately after birth, with dysmorphic features, and methyl-glutaconic aciduria (Zeng *et al*., 2007).

e) Mutations in genes encoding factors affecting mtDNA maintenance and replication

A large group of mitochondrial disorders alters the stability and the integrity of mtDNA. Mutations in genes encoding proteins involved in mtDNA replication, transcription, translation, repair, and maintenance can induce multiple mtDNA deletions or mtDNA depletion. Typically, defects of the DNA-processive enzymes cause qualitative alterations of mtDNA with accumulation of multiple mtDNA deletions (Copeland, 2014). On the contrary, mutations in genes important for dNTP pools maintenance cause quantitative alterations of mtDNA, the so-called mtDNA depletion syndrome (MDS). Given that my thesis focuses on a gene belonging to this class, I will describe in detail these syndromes in the next chapter.

During the last decade, an increasing number of nuclear disease genes associated with mtDNA deletions and depletion have been identified (**Tab. 6**). The list includes: a) genes encoding proteins that are directly involved in mtDNA replication as part of the replication machinery *(POLG* and *2*, *C10orf2, DNA2,* and *MGME1*); b) genes involved in mitochondrial nucleotides pool maintenance (*TK2, DGK*, *SUCLG1*, *SUCLA2*, *RRM2B*, *TYMP,* and *MPV17*) (El-Hattab and Scaglia, 2013). Recently, OPA1 and MFN2, which are part of the mitochondrial fusion machinery, and paraplegin and AFG3L2, which are involved in mitochondrial quality control, have been tied to mtDNA deletions syndromes (Viscomi and Zeviani, 2017).

Tab. 6 Genes affecting mtDNA stability and relative syndromes (adapted from Viscomi and Zeviani, 2017).

Gene	mtDNA alteration	Main clinical phenotype
SLC25A4	Multiple deletions (AD)	ad/arCPEO
	Multiple deletions (AR)	Myophaty and cardiomyophathy
	Depletion (AR)	Myophaty and cardiomyophathy
TWNK	Multiple deletions (AD)	adCPEO
	Multiple deletions (AR)	IOSCA
	Depletion (AR)	Alpers-like
POLG	Multiple deletions (AD)	adCPEO
	Multiple deletions (AR)	arCPEO
	Depletion (AR)	Alpers-Huntenlocher
	Multiple deletions (AR)	SANDO/SCAE
POLG2	Multiple deletions (AD)	adCPEO
TFAM	Depletion (AR)	Hepatocerebral syndrome
MGME1	Multiple deletions (AR)	arCPEO
DNA2	Multiple deletions (AD)	adCPEO
RNASEH1	Multiple deletions (AR)	arCPEO
RRM2B	Multiple deletions (AD)	adCPEO
	Depletion (AR)	Myopathy and tubulophathy
TK2	Multiple deletions (AR)	arCPEO
	Depletion (AR)	Myopathy
DGUOK	Multiple deletions (AR)	Lower motr neuron syndrome
	Multiple deletions (AR)	Myopathy with or w/o CPEO
	Depletion (AR)	Hepatocerebral syndrome
MPV17	Multiple deletions (AR)	arCPEO, leukoencephalopathy, parkinsonism
	Depletion (AR)	Hepatocerebral syndrome
OPA1	Multiple deletions (AD)	DOA
	Multiple deletions (AD)	DOA plus
MFN2	Multiple deletions (AD)	DOA plus

SPG7	Multiple deletions (AR)	arCPEO and ataxia
AFG3L2	Multiple deletions (AD)	arCPEO and ataxia
TYMP	Multiple deletions and depletion (AD)	MNGIE
SUCLA2	Depletion (AR)	Hepatocerebral syndrome
SUCLG1	Depletion (AR)	Hepatocerebral syndrome
ABAT	Multiple deletions (AR)	Encephalomyopathy
FBXL4	Depletion (AR)	Encephalomyopathy
GFER	Multiple deletions (AR)	Myopathy

Genes underlined are responsible for mtDNA depletion syndromes and will be discussed in the next chapter. AR: autosomal recessive; AD: autosomal dominant; CPEO: chronic progressive external ophthalmoplegia; IOSCA:infantile onset spinocerebellar ataxia; SANDO: sensory-ataxia neuropathy, dysarthria and ophthalmoplegia; SCAE: spinocerebellar ataxia-epilepsy; DOA: dominant optic atrophy; MNGIE: mitochondrial neurogastrointestinal encephalomyopathy.

The most common diseases associated with the presence of deleted mtDNA species are autosomal dominant or recessive progressive external ophthalmoplegia (PEO) and autosomal recessive neurogastrointestinal encephalomyopathy (MNGIE) (Copeland, 2012). PEO is characterized by progressive muscle weakness, with skeletal muscle showing ragged-red fibres and a mild reduction in the activities of respiratory chain enzymes. Ataxia, depression, hypogonadism, hearing loss, peripheral neuropathy and cataract can also be present. PEO has been linked to mutations in *Twinkle, POLG1* and *POLG2,* but also in other genes like *ANT1*, *TFAM*, and *OPA1* (Lamperti and Zeviani, 2009). MNGIE is an autosomal recessive juvenile disorder, characterized by progressive external ophthalmoplegia, cachexia, peripheral neuropathy, leucoencephalopathy, gastrointestinal dismotility and histologically abnormal mitochondria in muscle (Lamperti and Zeviani, 2009). The analysis performed on postmortem tissues of MNGIE patients revealed also strong mtDNA depletion specifically in the external layer of the muscolaris propria of the small intestine associated with marked atrophy (Viscomi and Zeviani, 2017).

POLG encodes the catalytic subunit of DNA polymerase γ. Pathogenic mutations in this gene result in a reduction of DNA polymerase γ activity, leading to stalling at the replication fork (Copeland, 2014). The Twinkle DNA helicase, encoded by *C10orf2*, is also required for DNA replication. Therefore, mutations in these genes result in insufficient mtDNA synthesis, which can not further sustain mtDNA turnover and segregation during cell divisions (Copeland, 2014). So far, over 100 mutations have been reported in the *POLG* gene. Besides PEO, other clinical phenotypes associated with these mutations are juvenile spinocerebellar ataxia, epilepsy with or without dysarthria, Alpers-Huttenlocher syndrome (AHS), and MNGIE, characterized by mtDNA depletion in affected tissues (Copeland, 2014; Viscomi and Zeviani, 2017). Biallelic mutations in *C10orf2* can result in infantile-onset spinocerebellar ataxia (IOSCA), a severe and progressive neurodegenerative disorder, or hepatocerebral MDS (Pierce *et al*., 2016). Clinical presentations associated with Twinkle mutations include CPEO with proximal muscle and facial weakness, dysphagia and dysphonia, ataxia and peripheral neuropathy (Pierce *et al*., 2016). Besides the main components of the mitochondrial replisome, mutations in other genes encoding proteins involved in maturation of the newly

synthesized strands or in mtDNA repair have been identified in patients suffering from PEO and accumulation of mtDNA deletions. *MGME1* and *RNASEH1* mutations are recessive, while mutations in *DNA2* seem to be inherited as a recessive trait (Viscomi and Zeviani, 2017).

In addition, as aforementioned, impaired mitochondrial fusion may lead to mtDNA instability and depletion. In particular, mutations in *OPA1* are responsible for non-syndromic autosomal dominant optic atrophy (DOA) and few missense mutations in the GTPase domain for a DOA plus syndrome characterized by a combination of DOA with CPEO, ataxia, deafness, and peripheral neuropathy. A *MFN2* heterozygous missense mutation has been identified in a family with DOA plus without CPEO.

Finally, mutations in m-AAA protease components, an IMM proteolytic complex, have been associated with multiple mtDNA depletion through a still unknown mechanism. *paraplegin matrix AAA peptidase subunit* (*SPG7*) mutations have been found in patients affecting by adult onset CPEO/ptosis and spastic ataxia. Mutations in *AFG3 like matrix AAA peptidase subunit 2* (*AFG3L2*) have been found associated with indolent ataxia and CPEO.

4.1 Mitochondrial DNA depletion syndromes

Mitochondrial DNA depletion syndromes (MDSs) form a heterogeneous group of mitochondrial diseases inherited as an autosomal recessive traits characterized by profound reduction in mtDNA copy number. Pathogenic mutations in gene products involved in either nucleotide pools maintenance (*TK2, SUCLA2, SUCLG1, RRM2B, DGUOK, TYMP*, and *MPV17*) or mtDNA replication (*POLG, C10orf2*) result in impaired mtDNA synthesis leading to quantitative (mtDNA depletion) defects (El-Hattab and Scaglia, 2013) (**Fig. 12**). Indeed, an adequate amount of mtDNA is necessary for the synthesis of the mitochondrial-encoded subunits of respiratory chain complexes, and ultimately for energy production. Thus, a decrease in mtDNA copy number results in organ dysfunction (El-Hattab and Scaglia, 2013). The remaining mtDNA does not harbour any rearrangements or mutations.

Although the number of genes linked to MDS onset is rapidly increasing, MDS is considered rare, with an estimated prevalence of 1:100000 (Cohen and Naviaux, 2010). mtDNA depletion can affect a specific tissue (muscle or liver and brain) or multiple organs (kidney, heart, and brain). Consistent with the different phenotype, MDSs are classified in 4 categories: myopathic, encephalomyopathic, hepatocerebral, and neurogastrointestinal form.

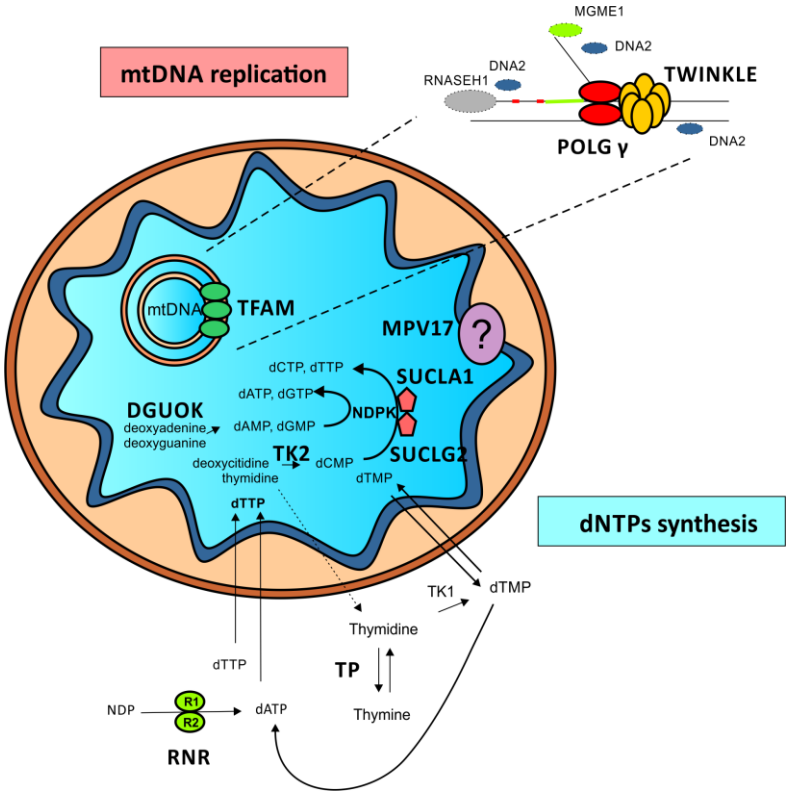

Fig. 12 Proteins involved in mitochondrial dNTP pools maintenance and mtDNA replication. TK2, thymidine kinase 2; dGK, deoxyguanosine kinase; SUCL, succinyl CoA ligase (the alpha subunit is encoded by *SUCLG1* and the beta subunit by either *SUCLA2* or *SUCLG2*); POLG, DNA polymerase gamma; TP, thymidine phosphorylase (encoded by TYMP); RNR, ribonucleotide reductase (*RRM2B* encodes the p53-inducible small subunit (p53R2) of the RNR). The Twinkle protein is encoded by *C10orf2* and the MPV17 by the *MPV17* gene (redrawn from Viscomi and Zeviani, 2017) .

Myopathic form. The disease usually presents in the first year of life (after an uncomplicated pregnancy) with feeding difficulty, weakness, hypotonia, and sometimes progressive external ophthalmoplegia. All muscle fibers in early onset patients are characterized by profound mtDNA depletion and cytochrome c oxidase-deficiency. Instead, in late-onset patients the situation appears less severe with normal fibers and other lacking both mtDNA and COX activity. Elevated serum creatinine kinase levels are found in patients.

Encephalomyopathic forms. Two different forms have been described both characterized by methylmalonic aciduria due to impaired conversion into succinyl-CoA of propionyl-CoA derived from the beta oxidation. Mutations in *succinate-CoA ligase ADP-forming beta subunit* (*SUCLA2*) encoding the ATP-dependent succinyl-CoA synthase activity (SCS) are responsible for a mild clinically presentation with high lactate in blood, psychomotor retardation, muscle hypotonia, and moderate mtDNA depletion in skeletal muscle. The second severe form is caused by mutations in *succinate-CoA ligase alpha subunit* (*SUCLG1*) encoding the GTP-dependent isoform SUCLG1 and is characterized by muscle and liver mtDNA depletion, dysmorphic features, and connatal lactic acidosis. Death occurs in the first days of life (Ostergaard *et al*., 2007). Recently, mutations in the *ABAT* gene, codifying another component of the SCS, have been associated with mtDNA depletion, psychomotor retardation, seizures, and hypotonia (Besse *et al*., 2015).

Hepatocerebral form. Typically disease onset is between birth and six months and death occurs within 1 year of age. Persistent vomiting, failure to thrive, hypotonia, and hypoglycemia are the most common symptoms. In the liver of few patients a generalized decrease in the mitochondrial respiratory chain enzymes activities has been measured. Changes in liver architecture have been found including fatty degeneration, fibrosis, bile duct proliferation, and disruption of lobular organization.

4.2 Defects in mitochondrial dNTP pools maintenance

TK2, *DGUOK*, *SUCLA2*, *SUCLG1*, *ribonucleotide reductase regulatory TP53 inducible subunit M2B (RRM2B)*, and *thymidine phosphorylase* (*TYMP)* encode proteins involved in mitochondrial dNTP pools maintenance; therefore, mutations in any of these genes result in an imbalance of mitochondrial nucleotides leading to mtDNA depletion. Mutations in *RRM2B*, *TK2*, and *DGUOK* have been also linked with adult onset disorders associated with mtDNA deletions (El-Hattab and Scaglia, 2013).

RRM2B and TYMP are the two cytosolic enzymes controlling the *de novo* synthesis of deoxynucleotide. *TYMP* encodes thymidine phosphorylase (TP), which is a cytosolic enzyme involved in the catabolism of pyrimidines mediating the phosphorolysis of thymidine into thymine and deoxyribosephosphate. Mutations in this gene cause MNGIE (El-Hattab and Scaglia, 2013). Low TP activity results in an imbalance of cytosolic dNTP pools due to the accumulation of its substrates, thymidine and deoxyuridine, with impairment in mitochondrial dNTP pools and mtDNA synthesis (El-Hattab and Scaglia, 2013). The p53-inducible small

subunit (p53R2) of the ribonucleotide reductase, encoded by *RRM2B*, is a cytosolic enzyme that catalyzes the reduction of ribonucleoside diphosphates to their corresponding deoxyribonucleoside diphosphates, providing deoxynucleotides for both nuclear and mtDNA replication. Expressed in post-mitotic cells, this enzyme plays a key role in the maintenance of mitochondrial dNTP pools (Pontarin *et al*., 2008). Recessive mutations are found in infantile cases of myophatic MDS with renal proximal tubulopathy. Bulbar dysfunction, fatigue, sensorineural hearing loss are other prominent symptoms (Pitceathly *et al.*, 2012). On the contrary, heterozygous mutations are associated with adCPEO (Viscomi and Zeviani, 2017).

As mitochondrial DNA replicates in all tissues during the entire lifetime of the organism, independently from the cell cycle, the salvage pathway becomes fundamental for mtDNA maintenance. TK2 mediates the first step in the phosphorylation of pyrimidine nucleosides in the mitochondrial matrix (Johansson and Karlsson, 1997); likewise, mitochondrial deoxyguanosine kinase (DGUOK) is essential for the purine nucleoside salvage pathway of mitochondria, as it mediates the first step in the phosphorylation of purine nucleosides (Johansson *et al.,* 1996). Mutations in both genes result in impaired synthesis of mitochondrial dNTPs leading to decreased mtDNA amount (El-Hattab and Scaglia, 2013). *TK2*-related myopathic MDS is an autosomal recessive disorder which, to date, has been reported in 60 individuals associated with mtDNA depletion. Onset is typically in childhood and affected individuals exhibit no prenatal or perinatal symptoms and a normal initial development. During the first two years hypotonia, delay or arrest of motor milestones, and muscle atrophy appear; muscle weakness can lead to respiratory failure (El-Hattab and Scaglia, 2013). Mutations in *TK2* have also been associated with CPEO with mtDNA multiple deletions (Saada *et al*., 2003). Progressive weakness and respiratory failure has also been reported in adult myopathic adults (Viscomi and Zeviani, 2017). DGK deficiency can occur as early-onset severe hepatocerebral MDS associated with feeding difficulties, hypotonia, nystagmus, and psychomotor retardation, or as adult-onset myopathy with or without CPEO associated with multiple mtDNA deletions. Hepatic manifestations appear within weeks of birth. Depletion of mtDNA has been documented mainly in liver and muscles combined with a reduction in complexes I, III and IV (El-Hattab *et al*., 2017).

SUCLA2 and *SUCLG1* encode two subunits of succinyl CoA ligase (SUCL), a mitochondrial Krebs cycle enzyme that catalyzes the conversion of succinyl-CoA and ADP (or GDP) to succinate and adenosine triphosphate (or guanosine triphosphate). The alpha subunit, encoded by *SUCLG1*, forms a heterodimer with a beta subunit, which can be codified by either *SUCLA2* or *SUCLG2*, resulting in an ADP-forming SUCL or a GDP-forming SUCL, respectively (El-Hattab and Scaglia, 2013). SUCL interacts also with the mitochondrial nucleoside diphosphate kinase: the lack of this complex formation has been proved to disturb the kinase function with the consequent decrease in mtDNA synthesis (Kowluru *et al*., 2002) (*see paragraph 4.1, "Encephalomyopathic form" clinical features).*

4.3 Human *MPV17*

The human *MPV17* is located on chromosome 2p23-21 and encodes a mitochondrial inner membrane protein of 176 amino acids involved in mtDNA maintenance, although its function remains unknown (Karasawa *et al*., 1993). Mutations in this gene were first described in 2006 causing a peculiar form of infantile hepatocerebral mtDNA depletion syndrome inherited as an autosomal recessive disease (Spinazzola *et al*., 2006). Since then, more than 20 different *MPV17* mutations have been associated with mitochondrial diseases (**Tab. 7**). Nonsense, missense, deletion and insertion mutations occur in the coding region of the gene, and splicing mutations were also found (El-Hattab *et al.*, 2010). Patients can be homozygous or compound heterozygous for these mutations. *MPV17* mutations have been also reported in patients with mtDNA multiple deletions affected by adult onset mitochondrial myopathy with CPEO, parkinsonism and leukoencephalopathy (Blakely *et al*., 2010; Garone *et al*., 2012).

Tab. 7 *MPV17* pathogenic mutations found in patients (from El-Hattab *et al*.,2010).

Type of mutation	Nucleotide change	Amino acids change
Missense	c.70G>T	p.Gly24Trp
	c.148C>T	p.Arg50Trp
	c.149G>A	p.Arg50Gln
	c.262A>G	p.Lys88Glu
	c.280G>C	pGly94Arg
	c.293C>T	p.Pro98Leu
	c.485C>A	p.Ala162Asp
	c.498C>A	p.Asn166Lys
	c.509C>T	p.Ser170Phe
Nonsense	c.206G>A	p.Trp69Ter
	c.359G>A	p.Trp120Ter
In-frame deletion	c.234_242del9	p.Gly79_Thr81del
	c.263_265del3	p.Lys88del
	c.271_273del3	p.Leu98del
Frame shift deletion	c.116_141del26	p.Arg41Profster63
Insertion	c.22_23insC	p.Gln8ProfsTer24
	c.451_452insC	p.Leu151ProfsTer39
Splicing site	c.70+5G>A	
	c.186+2T>C	
Large deletion	1.57kb deletion exon 8	

MPV17 is a remarkable cause of hepatocerebral MDS, accounting for about 50% of the cases. Generally, disease-onset occurs between birth and childhood and hepatic and neurologic manifestations appear to be the main characteristic symptoms (El-Hattab *et al*., 2012). In 90% of affected individuals, liver impairment deteriorates to liver failure during infancy or early childhood, and represents the main cause of death. Hepatic symptoms comprise severe hypolglycemic crisis, cholestasis, jaundice, elevated transaminases and gamma-glutamyl transpeptidase (GGT), hyperbilirubinemia, and coagulopathy. Progression into cirrhosis and sometimes hepatocellular carcinoma was also reported associated with *MPV17* mutations (Karadimas

et al., 2006). Most of patients exhibit neurological signs, including developmental delay, hypotonia, and muscle weakness, but motor- and sensory- peripheral neuropathy and leukoencephalopathy were also described. Psychomotor delay appears early during infancy. In general, in contrast to other mtDNA depletion syndromes, neurologic involvement in *MPV17*-related mtDNA depletion syndrome is generally mild at disease onset. For one third of the affected individuals, brain MRI abnormalities were described, with white matter abnormalities being the most frequent sign. Less frequent manifestations include renal tubulopathy, hypoparathyroidism, and gastrointestinal dysmotility. Metabolic disorders occur with lactic acidosis characterized by mild or moderate elevation of lactate and early-onset hypoglycemia, typically during the first six months of life associated with lethargy, apnea, and/or seizures (El-Hattab *et al*., 2012).

Navajo neurohepatopathy (NNH), a disease that has been known for decades to afflict the Navajo people of South-western USA, have been attributed to a mutation in the MPV17 protein, the p.R50Q (Karadimas *et al*., 2006). NNH syndrome includes liver derangement, sensory motor neuropathy with ataxia, leukoencephalopathy, corneal ulcerations, acral mutilation, reduced weight gain, short stature, sexual infantilism, and serious systemic infections.

Although no cure is currently available, disease progression slowdown has been achieved through liver transplantation or frequent meals of cornstarch-based diet which seem to be effective in preventing hypoglycemic crises. Importantly, it has been shown that expression of the human gene by adeno-associated virus(AAA)-mediated gene replacement in *Mpv17* knock-out mice restores liver mtDNA copy number and OXPHOS activity, opening a new therapeutic possibility for the treatment of *MPV17*-related MDS (Bottani *et al*., 2013).

The cellular content of mtDNA is highly variable in different tissues of the patients. More severe mtDNA depletions were observed in liver, where mean mtDNA copy number was 16% with respect to age-matched controls. In muscle tissue, mtDNA copy number ranged between 10 and 100% of controls (Uusimaa *et al*., 2014).

MPV17 was previously believed to localized in peroxisomes, but in 2006 Spinazzola and co-workers demonstrated that this protein was imported into mitochondria through the $\Delta\Psi$-dependent TOM-TIM import machinery. This relatively small (19.5 kDa) and ubiquitously expressed protein is localized in the inner membrane anchored by four (or five) transmembrane domains. Moreover, *MPV17*-specific *in vitro* translation product showed the same electrophoretic mobility before and after internalization into mitochondria, indicating that MPV17 is not cleaved after its import.

4.3.1 The *Mpv17* mutant mouse model

The *Mpv17* gene was first identified in 1990 by random insertion of a retroviral construct in the genome of mouse embryonic stem cells. The insertions produced a loss of function mutation leading to a renal phenotype in homozygous mutants, which developed focal segmental glomerulosclerosis (FSGS) leading to

nephrotic syndrome (Weiher *et al*., 1990). Mice developed renal disease in early adulthood (6-8 weeks of age) with abnormal serum, blood, and urine parameters, hallmarking renal failure associated with nephrotic syndrome. High blood cholesterol, urea, and creatinine levels were accompanied by proteinuria. At 2–3 months of age, many animals started to loose weight, became inactive and developed pallor. It was observed that the coat of *Mpv17*$^{-/-}$ mice invariably turned grey 5–6 months after birth; the phenotype includes severe atrophy of the skin layers (Viscomi *et al*., 2009).

In combination with the renal phenotype, *Mpv17*$^{-/-}$mice displayed degeneration of the inner ear structures. Deterioration of the organ of Corti, loss of inner and outer hair cells, as well as spiral ganglion cells was observed, probably due to the over-expression of matrix metalloproteinase II (MMP-2), which catalyzes the breakdown of glomerular basement, found in mutant animals. Mice showed sensineural hearing loss progressing to deafness by 2 months of age (Meyer zum Gottesberge *et al.,* 2012).

Mitochondrial DNA copy number depletion is profound in liver (as low as 4% of mtDNA copy number with respect to controls) and in muscle, while kidney and brain contains 60% of mtDNA compared to controls. Viscomi *et al.* demonstrated that at birth mtDNA contents in liver and skeletal muscle of *Mpv17*$^{-/-}$ and wild-type cells were similar, but unlike wild-type, no increase was seen after birth (Viscomi *et al*., 2009). Surprisingly, only mild morphological alterations of the liver cytoarchitecture were detected, whereas, at the ultrastructural level, mitochondria of *Mpv17*$^{-/-}$ hepatocytes were markedly altered. Despite this severe depletion, liver phenotypes have hardly been described, suggesting a possible feedback mechanism which might up-regulate mtDNA gene expression in mtDNA depletion background (Viscomi *et al*., 2009). Consistently, 40% reduction was found in the transcript level of *Mterf1*, a transcriptional termination factor. However, it was shown that the knockout mouse model for *Mpv17* fed with a high-fat ketogenic diet (KD) rapidly developed liver cirrhosis and failure (Bottani *et al*., 2013).

Thus, the clinical phenotype associated with *Mpv17* mutations consisted of focal segmental glomerulosclerosis (FSGS), followed by hyaline degeneration and loss, degenerative changes of the tubular system, and fibrosis. As a consequence of the leakiness of the glomerular filtering system, mice developed massive proteinuria and, starting from 18 months after birth, they showed progressive downhill of their health conditions with lifespan reduction (Viscomi *et al*., 2009). Strikingly, after few generations, this phenotype was no longer detected. It has been described that renal pathology still occurs in *Mpv17*$^{-/-}$ mice but onset of disease is delayed by 12-18 months (Viscomi *et al*., 2009). The reason for this age-dependent time shift of disease onset is unknown, but it seems to be dependent on a modification of the genetic background of the mice.

4.3.2 The yeast ortholog *SYM1*

A functional ortholog of *MPV17* in the yeast *Saccharomyces cerevisiae* was identified in 2004 (Trott *et al*., 2004). Stress-inducible yeast Mpv17 (Sym1) is a stress-induced mitochondrial inner membrane protein

associated with oxidative growth at high temperature (37°C), also involved in ethanol metabolism and tolerance (Trott *et al*., 2004). The *sym1Δ* mutant strain fails to grow on 2% ethanol at 37°C, whereas growth is normal at 28°C (Dallabona *et al*., 2010). At high temperature, the *sym1Δ* mutant displays variably impaired OXPHOS, defective glycogen storage, altered mitochondrial morphology and high mtDNA instability. Accordingly, binding sites for transcription factors involved in stress response were found in the *SYM1* promoter region. The morphology of *sym1Δ* mutant mitochondria was found deeply altered, with organelle ballooning, flattening of *cristae* and accumulation of electron-dense material. Succinate dehydrogenase activity was reduced by 60%, whereas only mild reduction of enzymatic activities of complex III, IV and V was measured (Dallabona *et al*., 2010).

It was demonstrated that the expression of the wild-type human protein was able to complement *sym1Δ* phenotype, while mutated variants did not, confirming the functional equivalence between the two proteins (Spinazzola *et al*., 2006). Supplementation with glutamate, aspartate, glutamine or asparagine partially restored aerobic oxidative growth. Likewise, over-expression of YMC1, a mitochondrial carrier protein involved in metabolites trafficking between peroxisomes and mitochondria, was sufficient to suppress defective OXPHOS growth phenotype and mtDNA instability (Dallabona *et al*., 2010). Also the over-expression of ODC1, another protein involved in anaplerotic reactions (which fuel TCA cycle with intermediates from the cytosol into mitochondria, i.e. 2-oxoadipate and 2-oxoglutarate) restored the growth phenotype. Thus, Dallabona and co-workers hypothesized a possible involvement of Sym1 in the transport of TCA cycle intermediates. Accordingly, yeast glycogen storage was found diminished in these mutants. Notably, gluconeogenesis is well known to rely on the flux of TCA cycle intermediates to the cytosol. A defective exchange of TCA cycle intermediates between the cytosol and mitochondria could then affect metabolic reactions (which would no longer be fuelled) and in turn the oxidative growth phenotype (**Fig. 13**).

In 2012, Reinhold *et al.* demonstrated that Sym1 forms a channel with a pore size of about 1.6 nm, capable of transporting large molecules, such as metabolites, across the inner mitochondrial membrane. Data suggested that Sym1 is close at physiological membrane potential (Reinhold *et al.,* 2012), but its role in physiological conditions and the nature of the cargo remain still unknown.

Moreover, data provided by two different studies independently demonstrated that Sym1 takes part in a high molecular–weight complex (Dallabona *et al.*, 2010; Reinhold *et al.,* 2012).

4.3.3 The zebrafish *MPV17* homolog *tra*

The gene *transparent* (*tra*) encodes the zebrafish homolog of human *MPV17*, which is ubiquitously expressed, and localizes on the inner mitochondrial membrane (Krauss *et al*., 2013). Human and fish Mpv17 proteins show 69% of sequence identity, and conserved transmembrane domains (Krauss *et al.,* 2013). A small deletion in the *mpv17* gene causing a frameshift in the open reading frame (which results in an early

truncation of the protein) is responsible for a tissue specific phenotype characterized by strong reduction in iridophores pigmentation. Reflective iridophores, together with black melanophores and yellow xanthophores, are responsible for the regular pattern of horizontal dark blue stripes coating the body sides of the adult fish. Within iridophores, cytoplasmic organelles called iridosomes are present, and inside these structures guanine is arranged into crystal-like reflective stacks. Krauss and co-workers demonstrated that iridophores specification and initial differentiation occur normally in *tra* mutants. Indeed, in young adults, silvery pigmentation is still visible in the first and dorsal interstripe regions, albeit reduced, but it is completely lost during further maturation (Krauss *et al.,* 2013). However, in this study they failed to prove that the loss of iridophores was caused by apoptosis.

Unlike the human counterpart, *tra* mutants are viable, and show no depletion in mitochondrial DNA content in liver, muscle and brain. In Krauss *et al.* paper, they suggested that a possible explanation for this might be gene redundancy. Indeed, zebrafish genome possesses four genes encoding proteins with high similarity to *tra*, and this could explain the non-lethal phenotype observed in *tra* mutant fish. However, also human *MPV17* gene family comprises four protein members.

As above mentioned, iridophores accumulate high amounts of guanine in iridosomes. This deposit shifts the equilibrium of the reaction catalyzed by purine nucleoside phosphorylase 4a (Pnp4a, found upregulated in iridophores), which metabolizes guanosine to guanine, towards guanine. In this scenario, dGTP required for mitochondrial DNA replication may become limiting, requiring a mechanism of active import of its precursors or dGTP itself. Despite no difference in mtDNA copy number was measured in mutant fish, researchers speculated that the absence of tra function may reduce the transport of nucleotides and precursors, coming from guanine stacks, into mitochondria of iridophores (**Fig. 13**).

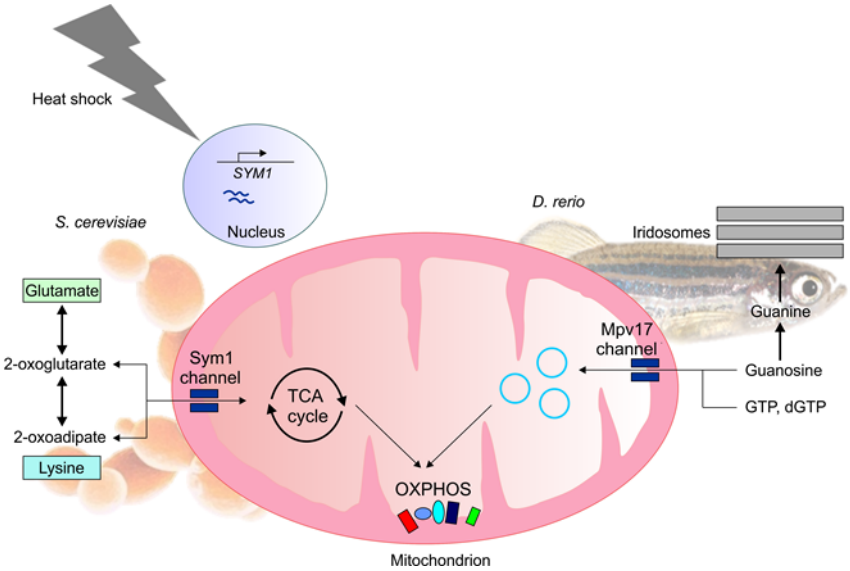

Fig. 13 The two proposed model for MPV17 orthologs function. Sym1 is a heat-shock protein probably involved in the transport of TCA cycle intermediates. tra might transport nucleotides and precursors, coming from guanine stacks in iridosomes, into mitochondria of iridophores (redrawn from Löllgen and Weiher, 2015).

4.3.4 Mpv17-like proteins in human and mouse

In mammals, other three proteins with high homology to MPV17 are present: MPV17-like protein (MPV17L), MPV17-like 2 protein (MPV17L2 or FKSG24) and peroxisomal membrane protein 2 (PXMP2) (Dalla Rosa *et al*., 2014).

A peroxisomal localization for PXMP2 was first suggested by experimental data provided by Brosius *et al*. (2002). Moreover, in 2009 PXMP2 was proposed to form a constitutively open and voltage-independent pore in the peroxisomal membrane, displaying weak cationic selectivity (Rokka *et al*., 2009).

MPV17L2, an MPV17 paralogue that acquired a new function after gene duplication, was found to localize only in the IMM (Dalla Rosa *et al*., 2014). MPV17L2 seems to have a role in mitochondrial protein synthesis. This protein was found to associate with the mitoribosome, (specifically forming interactions with the large subunit of the mitochondrial ribosomes and the monosome), suggesting an involvement in the assembly and stability of mitochondrial ribosomes. Indeed, *MPV17L2* RNAi caused the disruption of ribosomes and consequently impaired translation, in line with a potential role of MPV17L2 in ribosomal biogenesis (Dalla Rosa *et al*., 2014).

The mouse *M-LP* gene is composed of five exons and is expressed as two distinct splicing transcripts, generated by the alternative usage of two distinct promoters (M-LP_L and M-LP_S), localized upstream of exon 1 and exon 2, respectively. The two M-LP isoforms show different expression patterns and activities, suggesting an involvement in different functions. Despite this, both isoforms have been suggested to play a role in ROS metabolism (Iida *et al*., 2003; 2005). Indeed, transfection with M-LP_L upregulated the expression of mitochondrial manganese superoxide dismutase (*SOD2*) gene, whereas transfection with M-LP_S upregulated the expression of *SOD2*, downregulating cellular glutathione peroxidase (*Gpx1*) and plasma glutathione peroxidase (*Gpx3*) (Iida *et al.,* 2003). Krick *et al.* (2008) demonstrated also that M-LP interacts with serine protease HtrA2, a proapoptotic protein, preventing its translocation into the cytosol. Moreover, in the mouse kidney cell line TCMK-1, M-LP_S was found transcriptionally regulated by regulator of heat-induced transcription (Rhit) and heat shock factor (HSF), with Rhit being responsible for M-LP_S age-dependent expression (Iida *et al*., 2010).

The human M-LP (M-LPH) gene is composed of four exons and is expressed as two alternatively spliced variants, M-LPH1 and M-LPH2, with only the first isoform detected at the protein level and linked to ROS metabolism (Iida *et al*., 2006). M-LPH is localized predominantly in the nucleus, to some extent in a subset of mitochondria (probably in close proximity to mitochondrial nucleoids), and marginally in the cytosol (Iida *et al.*, 2015). In 2012, Iida and co-workers demonstrated that Rhit was also a transcriptional repressor of human *M-LP*. Moreover, the human protein was found to interact with other four proteins: H2A histone family member X (H2AX), ribosomal protein S14 (RPS14), ribosomal protein S3 (RPS3) and B-cell receptor-associated protein 31 (Bap31) (Iida *et al*., 2015). Knock-down of *M-LPH* increased mtDNA damage and

reduced the expression of mtDNA-encoded genes. Antimycin treatment (inducing ROS production) raised the number and size of the mitochondrial M-LPH foci that were found to co-localize with two proteins involved in mtDNA repair, DNA polymerase γ and DNA ligase III. Furthermore, *M-LPH* knock-down was demonstrated to hamper the mitochondrial localization of these enzymes. M-LPH could be involved in the maintenance of mitochondrial functions by preventing mtDNA damage, together with mtDNA repair enzymes.

Summary

In the table below, I summarize all the phenotypes related to MPV17 mutations that have been observed in humans and in different model organisms and MPV17 hypothesized function in yeast and zebrafish.

Tab. 8 MPV17-related phenotypes summary.

ORGANISM	PHENOTYPE	MECHANISM
Homo sapiens - Chromosome 2; - 1051 bp; - 176 aa - 7 exons	MDS (hepatocerebral form) - Tissue-specific mtDNA depletion; - Hepatic disfunction and failure; - coagulopathy; - psychomotor delay; - muscular hypotony.	?
Saccharomyces cerevisiae - Chromosome 12; - 594 bp; - 1 exon; - 197 aa; - Identity: 29,55%.	- Impair growth and gluconeogenesis on ethanol at 37°C; - Mutations and deletions in mtDNA.	**Heat-shock protein.** **Transport of Krebs cycle intermediates into mitochondria.**
Mus musculus - Chromosome 5; - 903 bp; - 7 exons; - 178 aa; - Identity: 92,05%	- Tissue-specific mtDNA depletion; - Glomerulosclerosis; - Premature aging; - Deafness; - dNTP pools alteration.	?
Danio rerio - Chromosome 20; - 875 bp; - 7 exons; - 177 aa; - Identity: 68,75%	- Normal mtDNA levels; - Non-pathologic phenotype; - Iridophores loss (transparent phenotype).	**dGTP transport into iridophores mitochondria**

5.1 *CG11077* (*dMpv17*) is the ortholog of the human *MPV17* in *D. melanogaster*

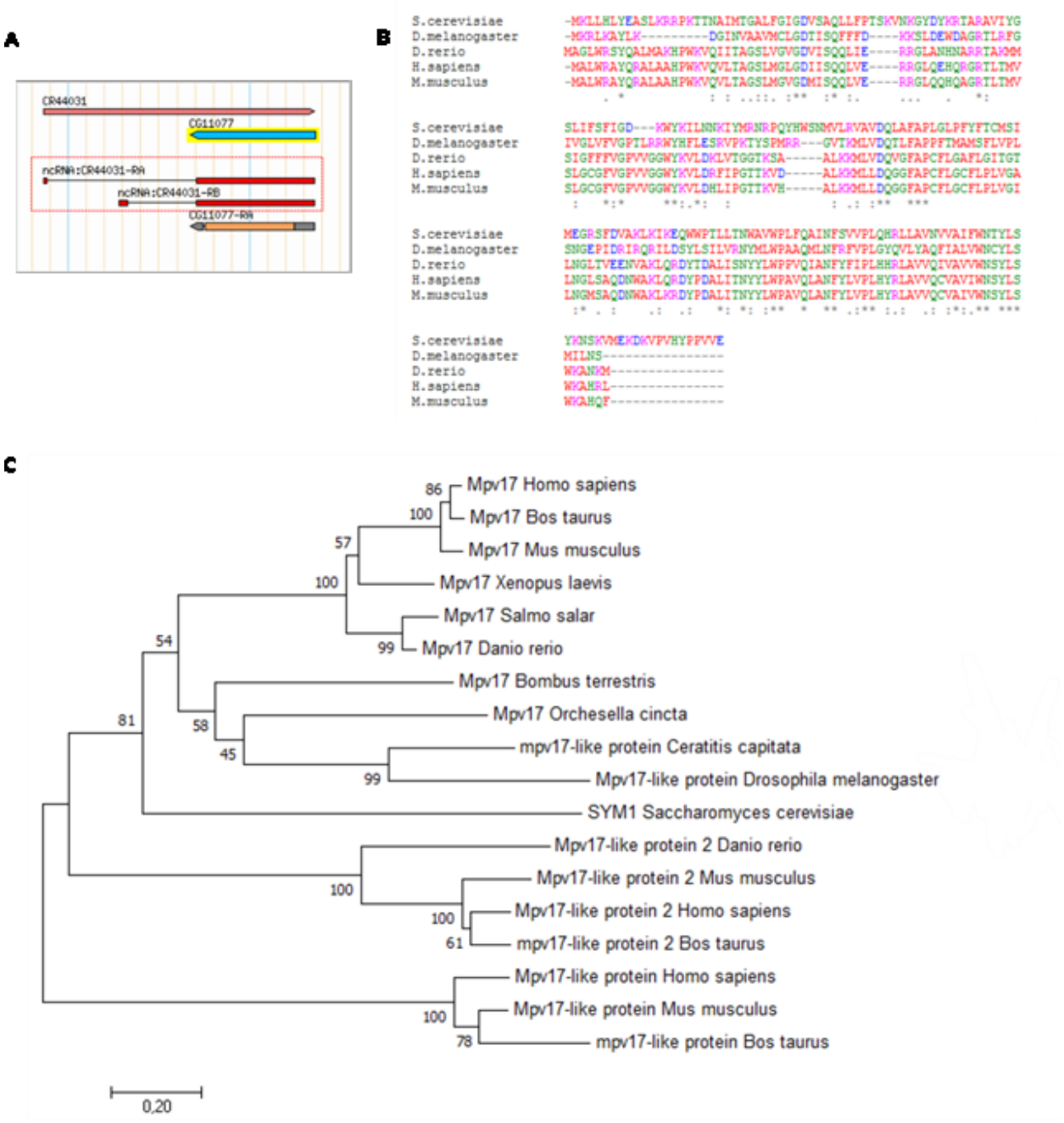

Fig. 14 Analysis of homology, genomic localization and evolution of Drosophila Mpv17 protein. **A**, Sequence alignment of human MPV17 protein with its orthologs from different species was performed by using ClustalW software. *Saccharomyces cerevisiae*, *Homo sapiens*, *Mus musculus*, *Danio rerio,* and *Drosophila melanogaster* sequences of MPV17 were included in this analysis. The alignment highlights identical amino acidic residues (*) and similar ones (. and :). **B**, The genomic localization of *dMpv17* showed that two ncRNAs (CR44031) are overlapping this nucleotide sequence (picture adapted from Genome Browser, https://genome.ucsc.edu). **C**, Phylogenesis was performed using Mega7 program with Jones-Taylor-Thornton (JTT) model (pairwise deletion, n° Bootstrap replications 1000). Sequences from *Homo sapiens*, *Bos taurus*, *Mus musculus*, *Xenopus laevis*, *Salmo salar*, *Danio rerio*, *Bombus terrestris*, *Orchesella cincta*, *Ceratitis capitate*, *Drosophila melanogaster*, and *Saccharomyces cerevisiae* were used.

Our bioinformatics analysis identified a putative *MPV17* ortholog in the *Drosophila melanogaster* genome, the uncharacterized CG11077, named hereafter *dMpv17*. The gene, localized on the small fourth chromosome, encodes a 687 bp transcript (NM_143687.4) translated into a 168 amino acids protein (NP_002428.1). We found that two non-coding RNAs (which are not presented in the human genome), expressed only in embryonic tissues, completely overlap *dMpv17* sequence but they (**Fig. 14, A**). In order to evaluate the degree of protein conservation, we performed an alignment using ClustalW with yeast, human, mouse, zebrafish and fruit fly amino acidic sequences. The alignment revealed a 38% identity between Drosophila homolog and the human protein. As expected the Drosophila protein was closer to mammalian MPV17 than the yeast Sym1 (28% identity) (**Fig. 14, B**). Finally, we reconstructed the MPV17 phylogenesis to investigate the origin of the Drosophila ortholog and its relationship with homologs from other species. The phylogenetic tree shows that Drosophila Mpv17 groups with MPV17 family and it is more similar to MPV17 than to the MPV17-like proteins (**Fig. 14, C**). According with the low percentage of sequence similarity found with the human protein, Mpv17 proteins from insects species form a separate subgroup.

5.2 dMpv17 is an inner mitochondrial membrane protein

In contrast with early data, that assigned a peroxisomal localization to the Mpv17 protein (Zwacka *et al*., 1994), Viscomi and co-workers clearly demonstrated that this polypeptide is exclusively present in the inner mitochondrial membrane, tightly anchored to this membrane by four transmembrane domains. Previously, also the yeast ortholog was shown to be targeted to and reside in the inner mitochondrial membrane (Trott and Morano, 2004). Furthermore, MitoCarta2.0, a database of human and mouse genes encoding proteins with high probability to be localized in mitochondria, assigned MPV17 to mitochondria (Calvo *et al*., 2016; Pagliarini *et al*., 2008).

To test experimentally the hypothesis that Drosophila dMpv17 is a mitochondrial protein, we transiently transfected Drosophila S2R+ cells with a construct expressing dMpv17 tagged, on the C-terminus, with the hemagglutinin (HA) epitope of the influenza virus. The immunofluorescence pattern specific to dMpv17-HA, detected with an α-HA antibody, overlapped with the fluorescent signal of the mitochondrial specific dye MitoTracker Red (**Fig.15, A**). This evidence clearly confirms the mitochondrial localization of Mpv17 in Drosophila. Moreover, the analysis performed with TMpred on dMpv17 sequence identified four potential transmembrane domains (**Fig.15, B**), thus resembling the structure of the human and murine proteins. Transmembrane domains were predicted from amino acidic positions 12-21, 41-61, 82-101, and 144-166, with the N-terminal of the protein facing the matrix compartment. The sequence similarity between MPV17 and other members of the family, including Pxmp2, led to the hypothesis that this protein could form transmembrane channels in the inner membrane. Indeed, five α-helical regions were identified in the

human protein sequence. Five α-helical regions in the Drosophila protein, sufficiently long to penetrate membrane lipid bilayer (minimum 18 amino acids, **Fig.15, B**), were also identified by using Jpred4.

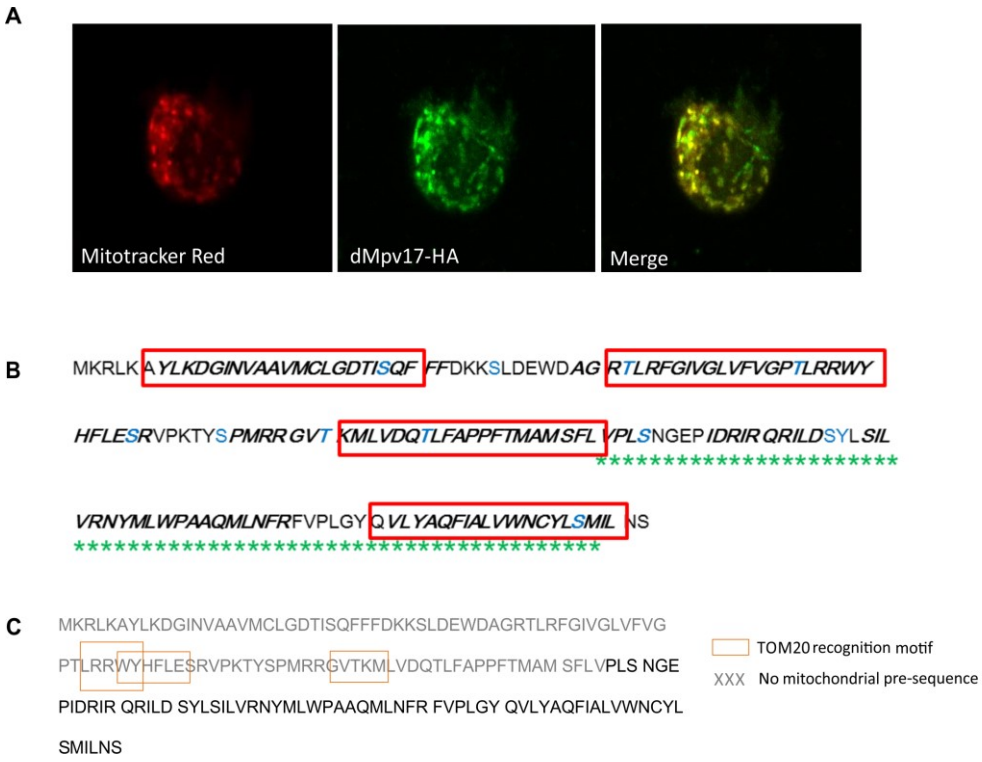

Fig.15 Immunolocalization and *in silico* analysis of dMpv17. A, Drosophila cells were transiently transfected with pACT-dMpv17 HA tagged, incubated with MitoTracker Red dye (red), and then immunolabeled with the anti-HA antibody (green). Overlay of images confirms the mitochondrial localization of dMpv17. **B**, *in silico* analysis of dMpv17. Boxes showed the putative membrane-spanning domains predicted by using TMpred software. The α-helices, predicted by Jpred4, are marked in boldface italic type. The putative phosphorylation sites are shown in blue. Mpv17_PMP22 domain is underlined (asterisks). **C,** dMpv17 sequence analysis using MitoFates. TOM20 recognition motifs are shown in boxes. Specific sequences for mitochondrial localization have been not predicted.

Human MPV17 is imported into mitochondria through the Δψ-dependent TOM-TIM import machinery, which targets proteins to either the IMM or the mitochondrial matrix. Unlike other IMM or mitochondrial matrix proteins, MPV17 does not possess an N-terminal cleavable pre-sequence, which is proteolysed after the import process is completed (Spinazzola *et al.*, 2006). To further characterize the Drosophila ortholog, we analyzed the protein sequence using MitoFates. Different TOM20 recognition motifs were identified in the fly's ortholog, whereas an N-terminal mitochondrial targeting signal was not present as in the human counterpart (**Fig.15, C**).

5.3 *dMpv17* down-regulation causes mtDNA depletion *in vivo*

In humans, *MPV17* mutations are responsible for a severe form of mitochondrial DNA depletion syndrome, mainly affecting the liver and the nervous system, with early onset in infancy. In mice, as in humans, the ablation of *Mpv17* determines a marked reduction in mtDNA content in liver and, to a lesser extent, in skeletal muscle, but neither in brain nor in kidney (Viscomi *et al*., 2009). In order to verify if *dMpv17* knock-

down (KD) could result in depletion of mtDNA copy number, we measured mtDNA copy number using two different Drosophila RNA interference (RNAi) lines (104377/KK and 31101/GD). The RNAi transgenes consist of short gene fragments cloned as inverted repeats and expressed via the binary GAL4/UAS system. First, we used *act5C*- and *da-Gal4* drivers to ubiquitously down-regulate *dMpv17* mRNA. *dMpv17* expression was strongly down-regulated using both RNAi lines and with both drivers (31101/GD: 40% of down-regulation with both drivers; 104377/KK: 65% and 60% with *da-Gal4* and *act5C-Gal4*, respectively) (Fig. 13, A). Moreover, we found a mild but statistically significant decrease in mtDNA copy number in adult flies (31101/GD: 25% of mtDNA depletion with both drivers; 104377/KK: 27% of mtDNA depletion with both drivers) (Fig. 13, B). In contrast with the early onset in patients, no differences in mtDNA amount were measured during third larval stage (data not shown).

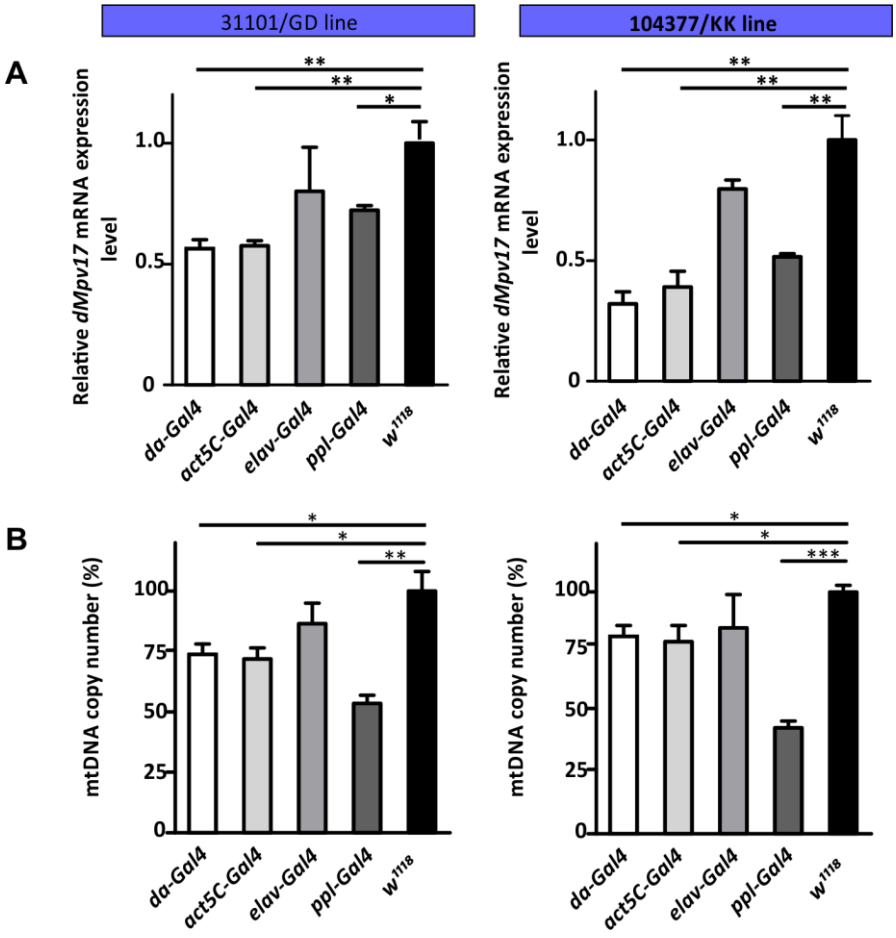

Fig.16 Quantification of *dMpv17* expression level and mtDNA copy number analysis in Drosophila RNAi lines. A, *dMpv17* expression level in two different UAS-*dMpv17*-RNAI Drosophila lines (31101/GD and 104377/KK) with different Gal4 drivers was quantified. *da-* and *act5C-Gal4* drives the ubiquitous expression of the RNAi construct; *elav-* and *ppl-Gal4* drives the expression of the RNAi construct in the nervous system and in fly's fat bodies, respectively. Data plotted are means ± SEM. The Drosophila line 104377/KK (marked in boldface), showing a higher down-regulation levels of *dMpv17* expression, was used for further *in vivo* analysis. 31101/GD down-regulation levels: 40% with *da-Gal4*, 40% with *act5C-Gal4*, 20% with *elav-Gal4*, and 30% with *ppl-Gal4*. 104377/KK down-regulation levels: 60% with *da-Gal4*, 65% with *act5C-Gal4*, 25% with *elav-Gal4*, and 50% with *ppl-Gal4*. **B**, mtDNA copy number, measured by qRT-PCR, upon different Gal4 drivers was performed. Data are ratios of mtDNA to genomic DNA. Values are expressed as a mean of three independent experiments, and *error bars* represent the SEM of the mtDNA/nDNA ratio among the replicates. 31101/GD mtDNA depletion levels: 25% with *da-Gal4*, 25% with *act5C-Gal4*, 20% with *elav-Gal4*, and 50% with *ppl-Gal4*. 104377/KK down-regulation levels: 25% with *da-Gal4*, 25% with *act5C-Gal4*, 20% with *elav-Gal4*, and 60% with *ppl-Gal4*.Strong mtDNA depletion was observed in fly's fat bodies (Student's *t* test * $p < 0.05$, ** $p < 0.01$, *** $p < 0.001$).

Furthermore, to specifically mimic human conditions we attempted to knock-down *dMpv17* only in those tissues which are markedly affected in patients (i. e., liver and nervous system). *ppl*- and *elav-Gal4* drivers were used to drive *dMpv17* down-regulation in Drosophila fat bodies (an analogous of human liver and white adipose tissue) and nervous system, respectively (**Fig. 16, A**). Tissue-specific mtDNA levels were measured after tissues dissection. Interestingly, a strong decrease in mtDNA copy number (50% with respect to controls) was observed in fat bodies. No difference was observed in mtDNA amount in heads (**Fig.16, B**).

To further address whether *dMpv17* KD (*UAS-RNAI-dMpv17/da-Gal4*) and mtDNA depletion could affect Drosophila phenotype, we tested flies for their locomotor activity and seizure sensitivity (Bang test). Neither the spontaneous locomotor activity nor the post-mechanical shock recovery time showed any difference with respect to controls flies (*UAS-RNAi-dMpv17/+* and *da-Gal4/+*) (**Fig.17**). No reduction in median lifespan compared to controls was found in *dMpv17* KD flies (Fig.14), in contrast with the dramatic decrease observed in humans, where most of the patients die during infancy/early childhood.

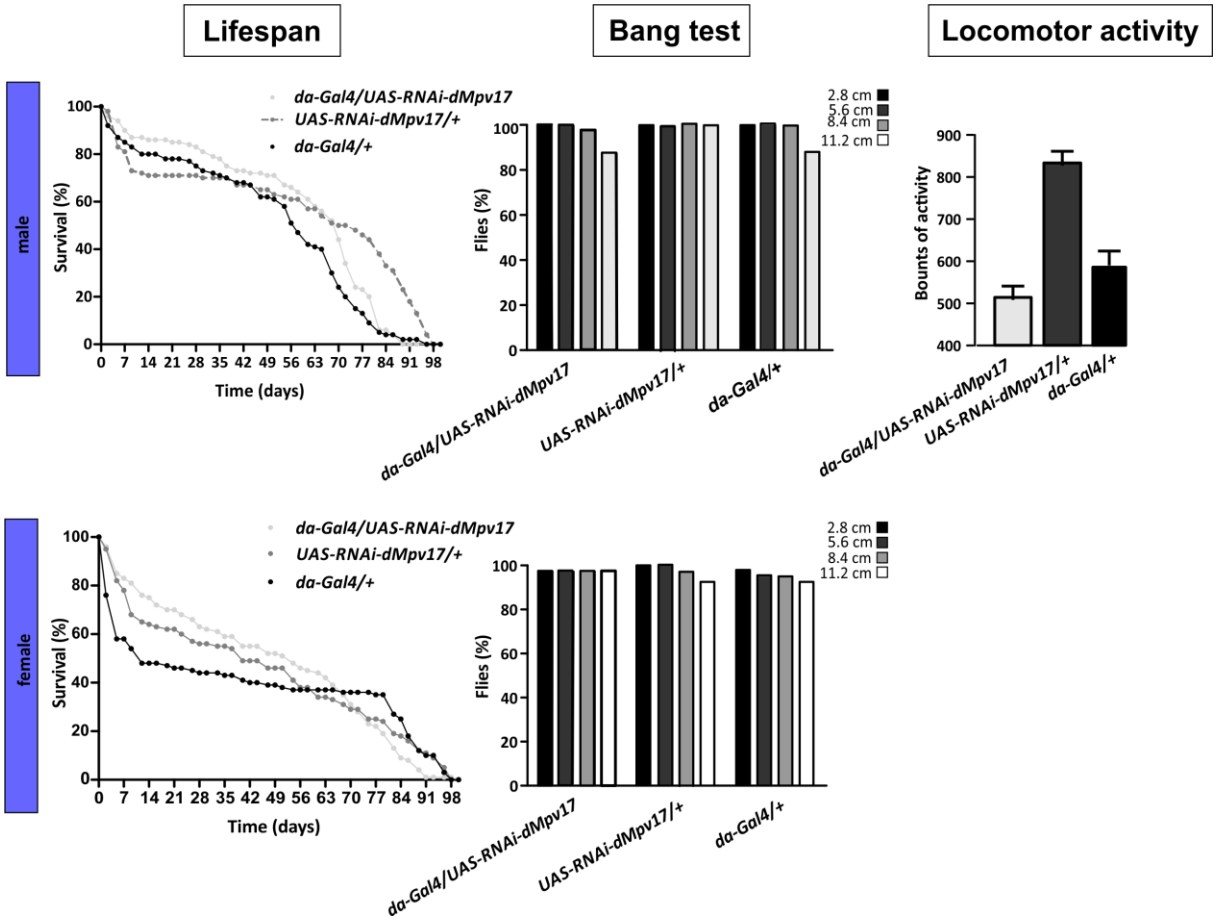

Fig.17 Behavioural analyses of *dMpv17* KD flies. Lifespan, bang test and locomotor activity were assayed separately in male and female. Experiments were performed in *dMpv17* RNAi flies (*da-Gal4/UAS-RNAi-dMpv17*) and in the two parental controls (*UAS-RNAi-dMpv17/+* and *da-Gal4/+*). Flies survival was quantified by counting dead flies three times per week. The ability of flies to recover from the mechanical shock was scored as the percentage of flies able to climb to four selected distance markers corresponding to 2.8, 5.6, 8.4 and 11.2 cm from the bottom of the tube. Locomotor activity was monitored for three days in 12:12 light:dark cycle in male flies. No significant differences were observed between *dMpv17*-RNAi and control flies.

In response to mitochondrial DNA depletion, a mechanism of transcriptional compensation has been described for heterozygous *Tfam* knockout mice and in humans affected by *TK2* mutations (Larsson *et al.*, 1998; Barthelemy *et al.*, 2001). A similar mechanism is activated also in *Mpv17*$^{-/-}$ mice liver, as it was demonstrated by Viscomi and co-workers. Mitochondria in the hepatic tissue of Mpv17$^{-/-}$ mice showed a ratio between mtDNA transcripts and mtDNA content several fold higher than *Mpv17*$^{+/+}$ littermates (Viscomi *et al.*, 2009). To test the hypothesis of a transcriptional compensation mechanism in *dMpv17* KD flies, we evaluated the expression levels of some mtDNA genes. We found that the expression levels of both *ND1* and *ND5* transcripts were significantly decreased in *dMpv17* KD adult flies (**Fig.18**).

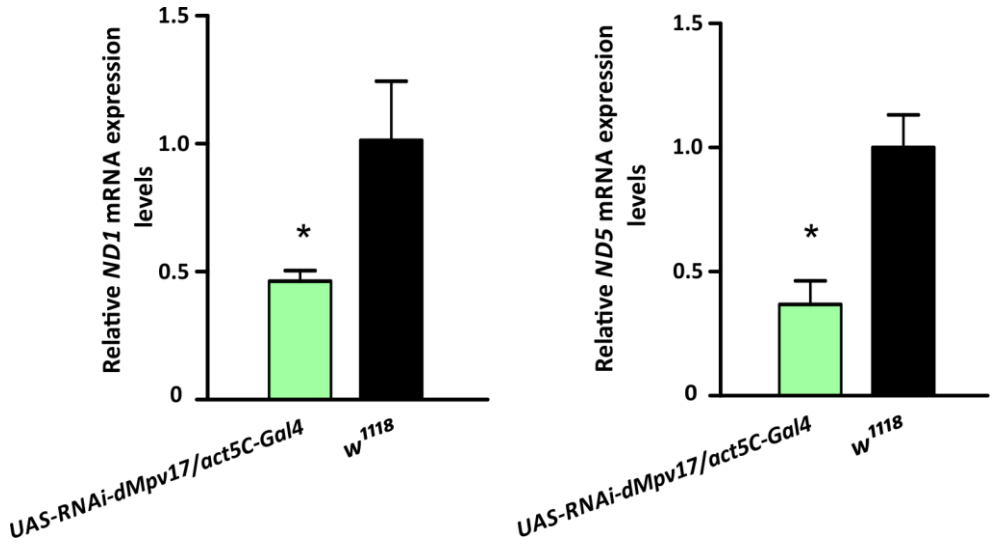

Fig.18 Analysis of mitochondrial transcription activity in *dMpv17* KD flies. *ND1* and *ND5* expression levels were measured by quantitative real time-PCR in *dMPv17* KD flies (*UAS-RNAi-dMpv17/act5C-Gal4*) and w^{1118} control strain. Data are presented as the mean ± SEM from three biological replicates (Student's *t* test * p < 0.05, ** p <0.01, *** *p* < 0.001).

5.4 Effects of *dMpv17* silencing on the deoxynucleotide pool contents of S2R+

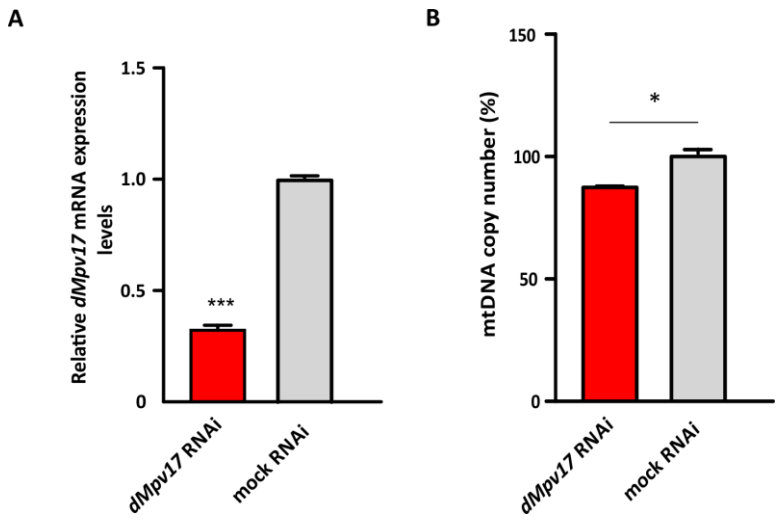

Fig.19 Effects of *dMpv17* silencing on mtDNA copy number in S2R^{+}. A, Quantification of *dMpv17* expression levels in S2R+ silenced cells (*dMpv17* RNAi) with respect to control (mock RNAi). **B**, mtDNA copy number analysis in S2R+ silenced cells (*dMpv17* RNAi) with respect to control (mock RNAi). Data are shown as the mean ± SEM from three biological replicates (Student's *t* test * p < 0.05, ** p <0.01, *** *p* < 0.001).

RNAi in Drosophila cells can be achieved by addition, directly in the culture medium, of long double-stranded RNA molecules complementary to the target gene. RNAi molecules caused 70-75% reduction in *dMpv17* expression levels after three days of treatment (**Fig.19, A**). Unlike adult flies, mtDNA copy number in proliferating cells was only slightly affected by the RNAi (**Fig.19, B**). In agreement with this evidence, proliferating cells from patients with MDS often have normal mtDNA levels (Dalla Rosa *et al.*, 2016).

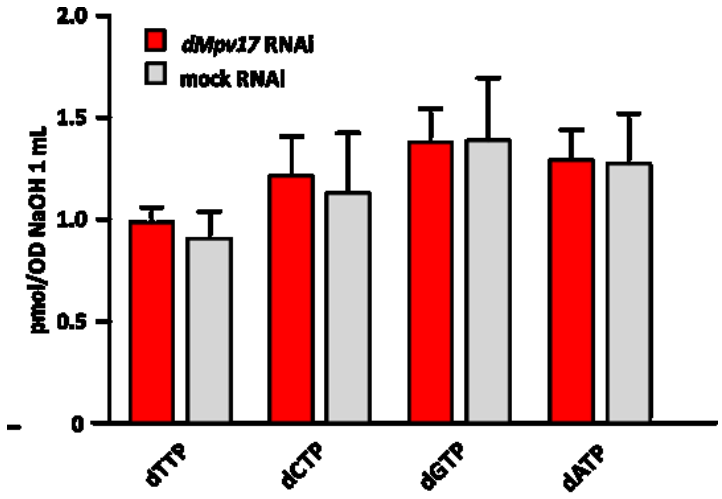

Fig. 20 Effects of *dMpv17* silencing on the deoxynucleotides pool contents in S2R$^+$. Pyrimidine and purine dNTP pool sizes in mitochondria of *dMpv17* silenced S2R$^+$ cells and mock control. Pool sizes are expressed as picomoles of dNTP/OD NaOH 1ml. Values are means ± S.D. from four independent experiments (Student's *t* test * $p < 0.05$, ** $p < 0.01$, *** $p < 0.001$).

Although the molecular role of MPV17 remains still unknown, it has been widely documented that absence of this protein impairs a dynamic control on mtDNA copy number in human and in mouse, probably in a tissue-specific manner. Many genes involved in MDS encode enzymes, which play an important role in dNTP pools maintenance in mitochondria. Indeed, the limited availability of nucleotide precursors for DNA synthesis is a primary cause of mitochondrial genomic instability and mtDNA depletion. The provision of dNTPs for the mitochondrial replisome is maintained either by *in organello* recycling or by the import from the cytosol of dNTPs. If dMpv17 was a nucleotide transporter, as it was hypothesized, its down-regulation should affect dNTP pools. To shed light on this aspect, we evaluated the amount of mitochondrial dNTP pools in d*Mpv17* KD cells after 72 hr of incubation with dsRNA (70% of silencing). We isolated mitochondrial and cytosolic dNTP pools from mock control and *dMpv17* KD cells. Since dNTP pools amount is strongly affect by the cell cycle, we analysed the percentage of S-phase in mock control and silenced cells in order to exclude the influence of cell-cycle phase. No difference in the proportion of cells in S-phase (12-15%) between the two conditions was observed. However, cytosolic (data not shown) and mitochondrial pools were not significantly different between the two samples (**Fig.20**).

5.5 dMpv17 forms a channel in a planar lipid bilayer

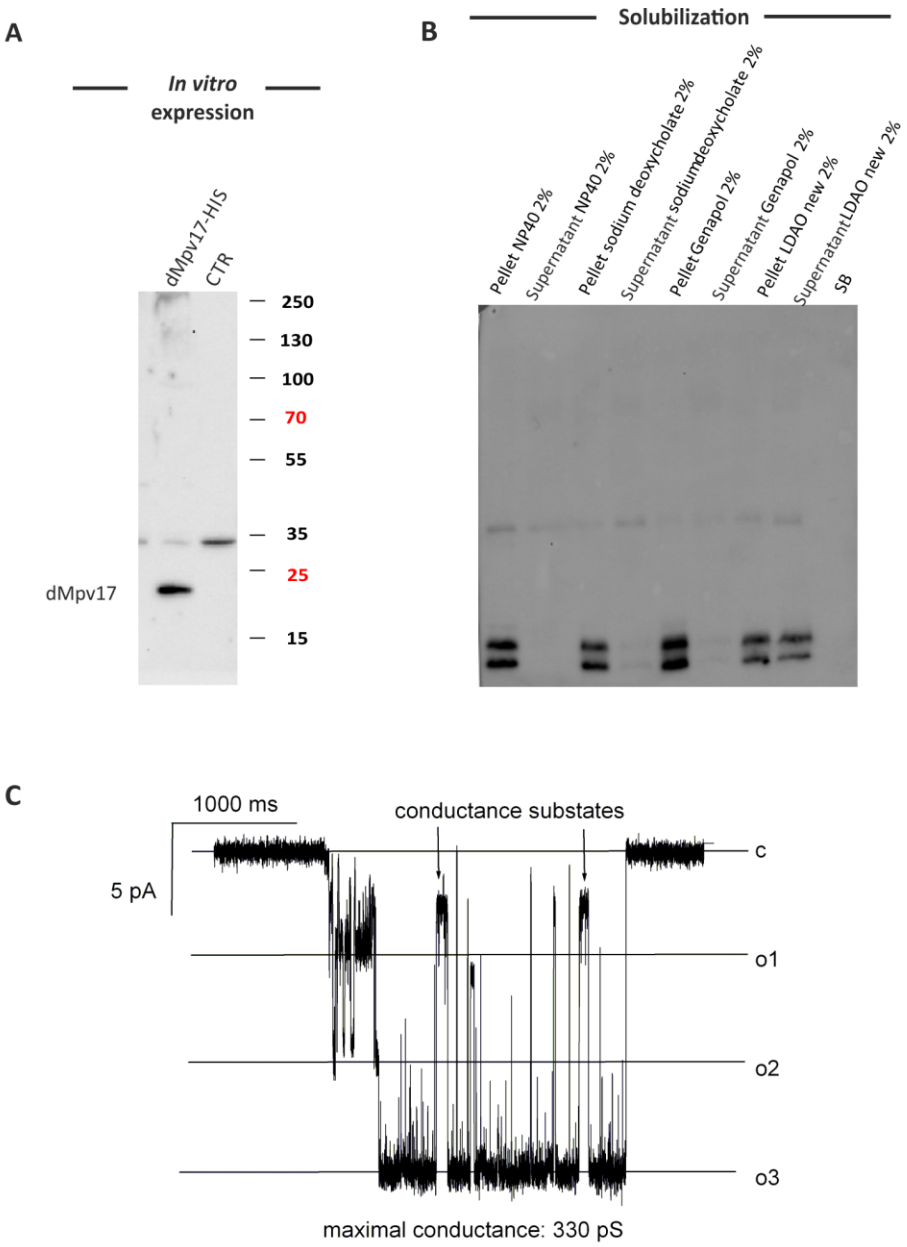

Fig.18 The dMpv17 protein exhibits channel activity in lipid bilayers. A, dMpv17 expression. Western blot analysis after *in vitro* transcription and translation reaction to verify protein expression. **B,** solubilisation was performed with different detergents, but only LDAO was found effective in solubilized dMpv17 protein (the protein is present in the supernatant only with LDAO). **C**, electrophysiological recordings of MPV17 produced *in vitro* and reconstituted in planar lipid bilayers. MPV17 traces in 50 mM KCl, 10 mM HEPES pH 7.4 at - 60 mV applied voltage. In particular, in this traces three channels are opened. The arrows indicates the presence of conductance substates.

In 2009, the Pxmp2 protein was demonstrated to form a relatively wide channel in the mammalian peroxisomal membrane (Rokka *et al.*, 2009). Afterwards, also Sym1 was found to form a channel after reconstitution into planar lipid bilayers (Reinhold *et al.*, 2012). Finally, very recently, Antonenkov and co-workers (2015) determined that human MPV17 showed pore-forming activity in an artificial membrane. To

gain insight into these aspects, and considering the predicted secondary structure of the fly's ortholog, we cloned the Drosophila *Mpv17* open reading frame, followed by a His-tag, in a pIVEX1.3 vector that allows cell free expression. *In vitro* expression was performed by using a RTS100 Wheat Germ CECF Kit and the success of the reaction as well as the apparent molecular weight of the dMpv17 protein was verified by western blot using an anti-His tag antibody (**Fig. 21, A**). Prior to electrophysiology experiments, the reaction mix was solubilized with different detergents (NP40, sodium deoxycholate, genapol, LDAO) and the solubilisation was verified by SDS-PAGE and Western blot. Only the treatment with 2% LDAO for 90 min at 30 °C was effective (**Fig. 21, B**). Preliminary electrophysiology experiments were performed in 150 mM KCl, 10 mM HEPES pH 7.4 (physiological conditions). We observed that the expressed protein works as a channel with a maximal conductance of 330 pS (**Fig. 21, C**).

5.6 *dMpv17* is involved in shaping cristae morphology

Many human disorders due to mutations in gene important for mitochondrial function are often associated with altered mitochondrial morphology. The analysis of *sym1Δ* mutant mitochondria revealed a profound alteration in organelle morphology, characterized by mitochondrial ballooning, flattening of *cristae* and accumulation of electron-dense material (Dallabona *et al.*, 2010). Mitochondrial ballooning and disappearance of the cristae were also observed in mitochondria from *Mpv17*$^{-/-}$ mouse liver, accompanied by a proliferation of membranes surrounding the altered organelles (Viscomi *et al.*, 2009). We examined mitochondrial cristae morphology in *dMpv17* KD cells by using transmission electron microscopy (EM). The down-regulation of *dMpv17* in S2R+ cells resulted in smaller mitochondria (**Fig. 22, A-B**) with reduced number of cristae (cristae length was measured and found also reduced) compared to mock controls (**Fig. 22, A-C**). Electron dense material was also observed in the mitochondrial matrix of *dMpv17*- silenced cells (**Fig. 22, D**).

Furthermore, we observed that *dMpv17* over-expression led to severe defects in mitochondrial morphology. S2R+ cells were transfected with a pAc5-STABLE2-neo vector in order to over-express dMpv17 tagged with GFP. Since the transfection efficiency of S2R+ cells is very low (10%), we decided to perform a correlative EM analysis to define mitochondrial morphology. Firstly, we scored GFP transfection positive cells and, then, we investigated mitochondrial morphology in these cells by using EM. In *dMpv17* over-expressing cells, mitochondrial morphology appeared profoundly altered with mitochondria mostly devoid of cristae. In mitochondria where cristae were still present, they tended to form vesicles. In some cases, mitochondria lost their characteristic double membrane system being surrounded by one membrane (**Fig.22, E**).

Mitochondrial morphology is directly linked to mitochondrial function. Cristae membranes, in particular, contain the electron transport chain and the ATP synthase, being the sites where oxidative phosphorylation takes place. In turn, disruption of mitochondrial morphology directly impacts cellular and organismal

metabolism. Thus, we measured oxygen consumption rate (OCR) at basal condition and after glucose, oligomycin, FCCP and antimycin A injections (as indicated by arrows in **Fig. 22, F**) in *dMpv17* KD and mock

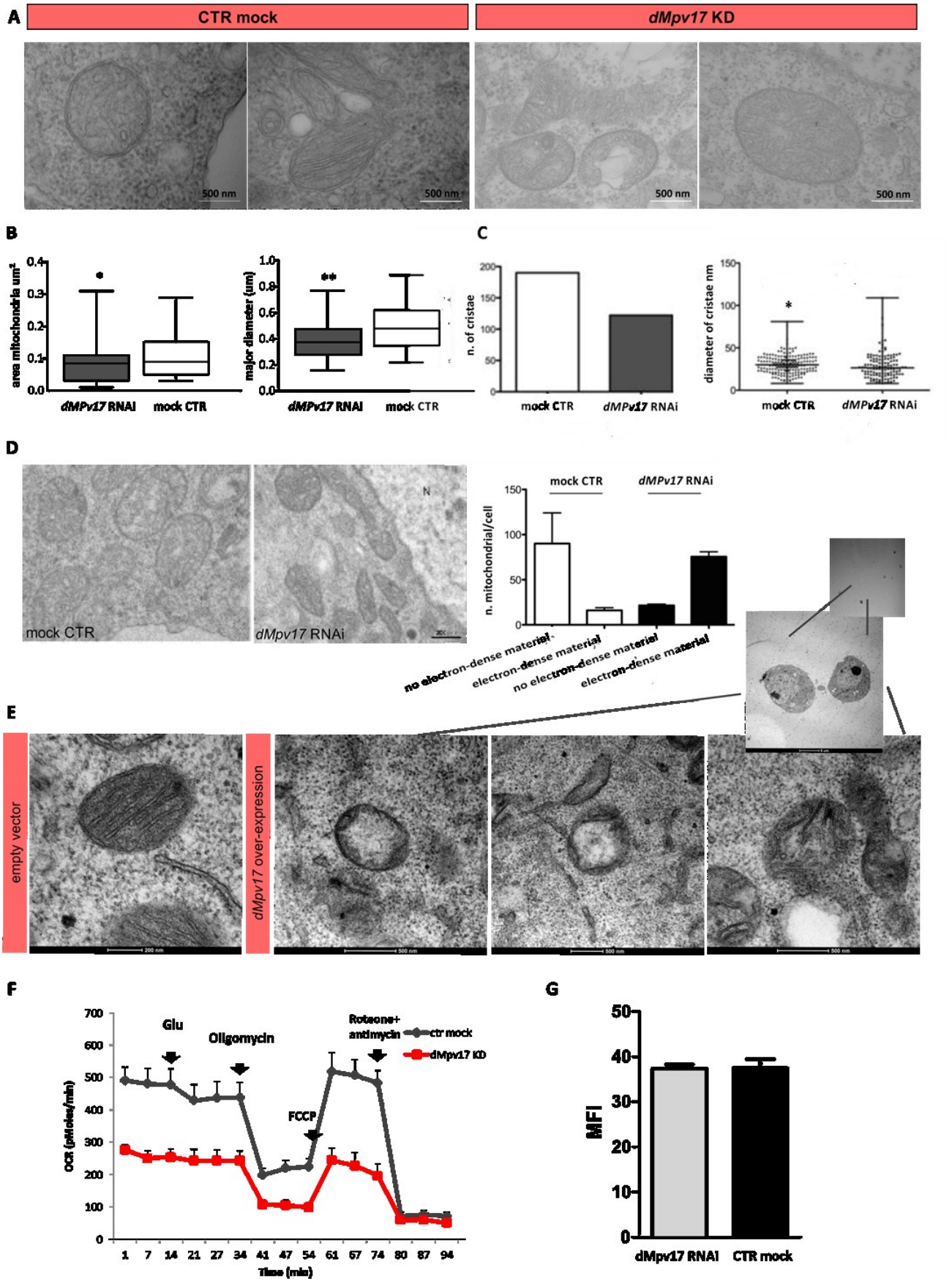

Fig. 22 Electron microscopy analysis on *dMpv17* KD and over-expressing S2R+ cells. A, cross-sectional ultrastructure of mock control and *dMpv17* KD S2R+ cells illustrating the morphology of mitochondria. **B**, morphometric analyses of mitochondrial dimensions in terms of major diameter and area, both expressed in nanometres and presented as box plots. **C**, morphometric analyses of mitochondrial cristae in terms of number and diameter, expressed in nanometres and presented as box plots. **D**, quantification of mitochondria containing electron-dense material. **E**, cross-sectional ultrastructure of mock control and over-expressing *dMpv17* S2R+ cells illustrating the morphology of mitochondria. **F**, oxygen consumption rate (pmoles/min) in mock control (black vehicles) and *dMpv17* KD (red vehicles) S2R+ cells. 10 mM glucose (Glu), 1 µM FCCP, and 5 µM rotenone plus 5 µM antimycin A were added at the times marked by arrows. **G**, mitochondrial mass in mock control and *dMpv17* KD S2R+ cells measured with Mitotracker Green dye. (Student's *t* test * p < 0.05, ** p <0.01, *** *p* < 0.001)

control S2R+ cells. Depletion of *dMpv17* resulted in a substantial reduction in respiration measured with Seahorse Analyzer (**Fig. 22, F**). To demonstrate that this respiration impairment was not due to a decrease in mitochondrial number, we evaluated mitochondrial mass in S2R+ cells through cytofluorometry of cells stained with Mitotracker Green. No difference in mitochondrial mass was observed in *dMpv17* KD cells with respect to mock control (**Fig. 22, G**). Thus, the observed reduction in oxygen consumption could be due to the presence of damaged mitochondria, rather than lower number of organelles.

5.7 *dMpv17* affects the mitochondrial network

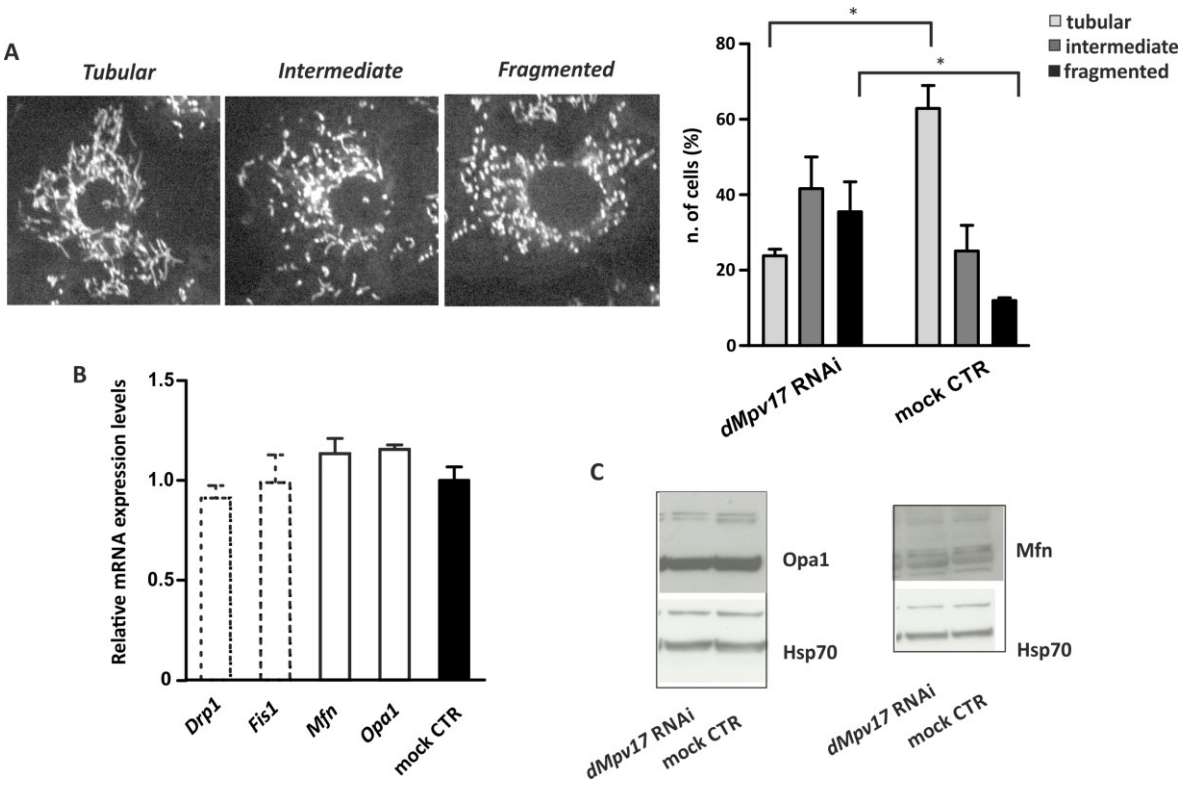

Fig. 23 *dMpv17* KD causes an alteration in mitochondrial network morphology. A, mitochondrial network morphology of S2R+ cells treated with *dMpv17* dsRNA for three days (dMpv17 KD) and control (mock CTR) was obtained by using Mitotracker Green. Cells were classified into three groups on the basis of mitochondrial network morphology (tubular, intermediate and fragmented) and the percentage of cells for each group was plotted. The bar graphs represent the mean + SEM for three independent experiments (Student's *t* test * p < 0.05, ** p <0.01, *** *p* < 0.001). **B**, Drosophila *Drp1*, *Fis1*, *Mfn*, *Opa1* mRNA levels, expressed as relative quantity of template in the sample, were determined by qRT-PCR in untreated cells (black column) and in *dMpv17* silenced cells (open column). Data plotted are means ± S.E.M. of three biological replicates. **C**, the Opa1 and Mfn protein levels were assessed by Western Blot in *dMpv17* KD and control (mock CTR) cells. Three independent experiments were performed.

Balanced fusion and fission events shape mitochondria to meet metabolic demands and to ensure removal of damaged organelles. Mitochondrial fragmentation occurs in response to nutrient excess and cellular dysfunction and it has been observed in response to different disorders and diseases. Single treatment of cells with H_2O_2 resulted in fragmentation of mitochondria that was more severe in *Mpv17*$^{-/-}$ fibroblasts (Antonenkov *et al.*, 2015). Thus, we investigated mitochondrial network morphology in *dMpv17* KD Drosophila cells. Since the fixation process significantly alters mitochondrial morphology, cells were imaged live by using the selective mitochondrial dye Mitotracker Green FM. An increase in mitochondrial fragmentation was observed in silenced cells with respect to mock control (**Fig. 23, A**). mRNA expression levels of the key mitochondrial morphology modulators (*Drp1*, *Fis1*, *Opa1*, and *Mfn*) were found unchanged by *dMpv17* KD, indicating that the morphology changes were not due to a transcriptional response altering the level of fission and/or fusion genes (**Fig. 23, B**). Also, Western blot showed no differences in OPA1 and Marf (Mfn) protein levels in *dMpv17* KD cells with respect to control (**Fig. 23, C**).

5.8 *dMpv17* could impair mitochondrial autophagy

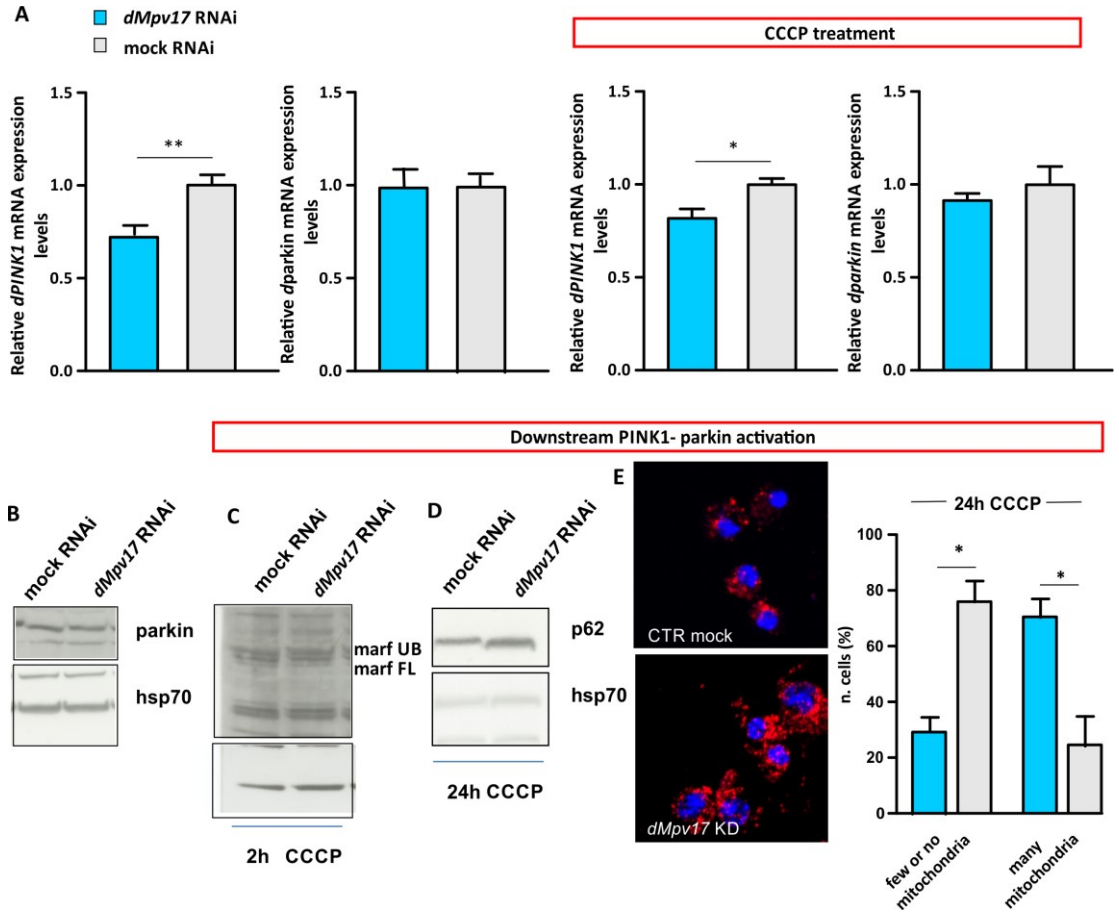

Fig. 24 *dMpv17* KD seems to slow-down the mitophagy process. A, *dPINK1* and *dparkin* mRNA levels were determined by qRT-PCR in untreated cells (grey column, mock RNAi) and cells silenced for the *dMpv17* expression (blue column, *dMpv17* RNAi). **B**, dparkin protein level was assessed by Western blot in *dMpv17* KD and mock control cells. **C**, mfn is ubiquitinated in a parkin-dependent manner. mfn protein ubiquitinated levels upon 2h of CCCP treatment. **D**, p62 protein level, upon 24h of CCCP treatment, was measured by Western blot. **E**, Representative pictures of *dMpv17* KD and control (CTR mock) S2R+ cells treated for 24h with CCCP and then stained with DAPI that marks nuclei in blue and with anti-Complex Va that labels mitochondria in red. Cells were scored

for the presence or absence of mitochondria such as represented in bar graphs (blue: dMpv17 KD; grey: mock RNAi). Three independent experiments were performed. Data are plotted as mean ± SEM (Student's *t* test * p < 0.05, ** p <0.01, *** *p* < 0.001).

To further characterize damaged mitochondria and fragmentation of the mitochondrial network (mitochondrial fragmentation seems to promote mitophagy) observed in our *dMpv17* KD cells, we sought to determine whether *dMpv17* KD impairs mitochondrial autophagy. We focused on PINK1 and Parkin, which are two key components of the mitophagy machinery. *dPink1* expression levels in *dMpv17* KD S2R+ cells showed a significant down-regulation both after or without the treatment with the mitochondrial uncoupling agent carbonyl cyanide m-chlorophenyl hydrazone (CCCP) (**Fig. 24, A**). By contrast, difference in parkin mRNA and protein levels between silenced and control cells were not detected (**Fig. 24, A and B**). Interestingly, Antonenkov and colleagues (2015) demonstrated that the unprocessed form of PINK1 was higher in *Mpv17*$^{-/-}$ mouse fibroblasts when compare to wild-type cells both in normal condition and after H_2O_2 treatment.

The induction of mitophagy has been found to correlate with the ubiquitination of different mitochondrial proteins including mitofusins (Gegg *et al.*, 2010). These post-translational modifications are reduced with the silencing of PINK1 or Parkin and are accompanied by an accumulation of the nonubiquitinated full-length form of Mfn (Ziviani *et al.*, 2010). No difference in *dMpv17* KD cells compared to control were found in Mitofusin (also known as Marf, the Drosophila homolog of MFN1-2) ubiquitinated levels after CCCP treatment (**Fig. 24, C**).

In the mitophagic process, sequestosome-1 (p62) binds ubiquitinated proteins and targets them for degradation by the proteasome. However, p62 also directly binds LC3 in order to deliver ubiquitinated proteins for degradation. During this process, p62 itself is degraded. In the Drosophila genome there is an ortholog of p62, named *refractory to sigma P* (*Ref(2)P*). The inhibition of autophagy leads to the accumulation of this protein, which can be used as a marker of autophagic flux. We found that p62 (alias Ref(2)P), which acts downstream the activation of PINK1 and Parkin and has been shown to be recruited to mitochondria ubiquitinated by Parkin, was present in higher amount in *dMpv17* KD cells with respect to control (**Fig. 24, D**).

In addition, we found that upon 24h of CCCP treatment, the silencing of *dMpv17* seemed to slow down the clearance of damaged mitochondria. Indeed, a higher percentage of cells with intact mitochondrial mass were detected in *dMpv17* KD sample with respect to control cells (**Fig. 24, E**).

5.9 Membrane potential and ROS amount in *dMpv17* KD cells

Earlier reports suggested that podocyte lesions of *Mpv17*$^{-/-}$ mice were associated with increased ROS production, and administration of ROS scavengers proved to be effective in preventing, or ameliorating

the proteinuria and focal nephrosclerosis in these mice (Binder *et al.*, 1999). Accumulation of tetramethylrhodamine ethyl ester (TMRE) in mitochondria is a $\Delta\psi_m$-dependent process, and Mito-SOX has

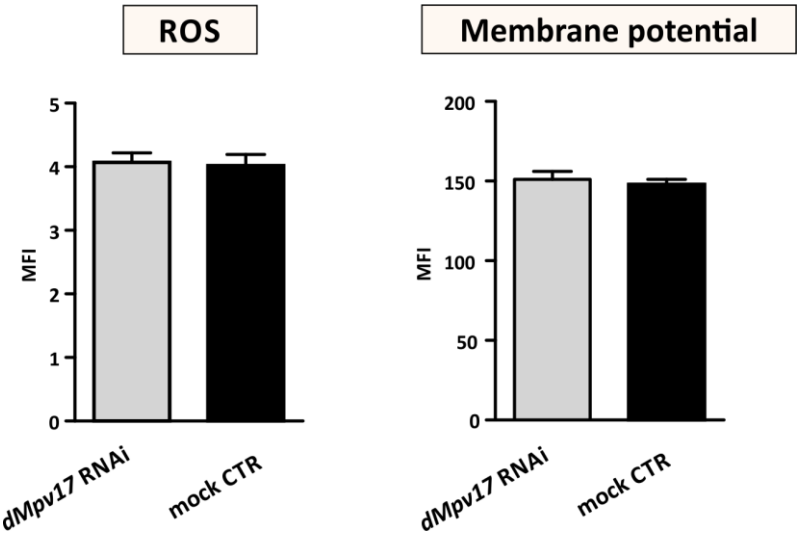

Fig. 25 ROS production and mitochondrial membrane potential are not affected by *dMpv17* KD. A, ROS amount and **B**, membrane potential measured in dMpv17 KD and mock control S2R+ cells by cytofluorimetry by using MitoSOX and TMRE dye, respectively. Data are expressed as median fluorescence intensity (MFI) ± SEM of three independent experiments.

been demonstrated to reliably detect ROS amount. We measured these parameters by using a cytofluorimeter. Interestingly, neither an increase in TMRE fluorescence nor an increase in ROS production was measured in *dMpv17* KD cells (**Fig. 25**). Thus, ROS production and mitochondrial membrane potential are not affected by *dMpv17* KD in Drosophila cells.

5.10 dMpv17 is part of a high molecular weight complex

Both HA-tagged Sym1 (Dallabona *et al*., 2009) and mouse Mpv17 (Bottani *et al.*, 2013) has been shown to participate in a high molecular–weight complex (>600 kDa) necessary for its function. In fact, variants that are not incorporated in this complex are not able to rescue mtDNA depletion and liver phenotype of *Mpv17*$^{-/-}$ mice (Bottani *et al.*, 2017).

To investigate the physical status of dMpv17 *in vivo* we analyzed mitochondria isolated from a fly strain ubiquitously expressing an HA-tagged form of the protein (under Act5C-*Gal4* control) and the two parental controls (*Act5C-Gal4/+* and *UAs-dMpv17-HA/+*) by 2-dimensional blue native gel electrophoresis (2D-BNGE) immunoblot. Given the lack of antibodies against the Drosophila protein, we used an antibody against HA tag. We identified dMpv17-HA crossreacting material (*) in the mitochondria of flies expressing the tagged form of the protein (*UAS-dMpv17-HA/Act5C-Gal4*), but not in controls flies (**Fig. 26, A**). Most of the protein was present in a spot corresponding to a complex of molecular weight between complex II and IV (**Fig. 26, B**).

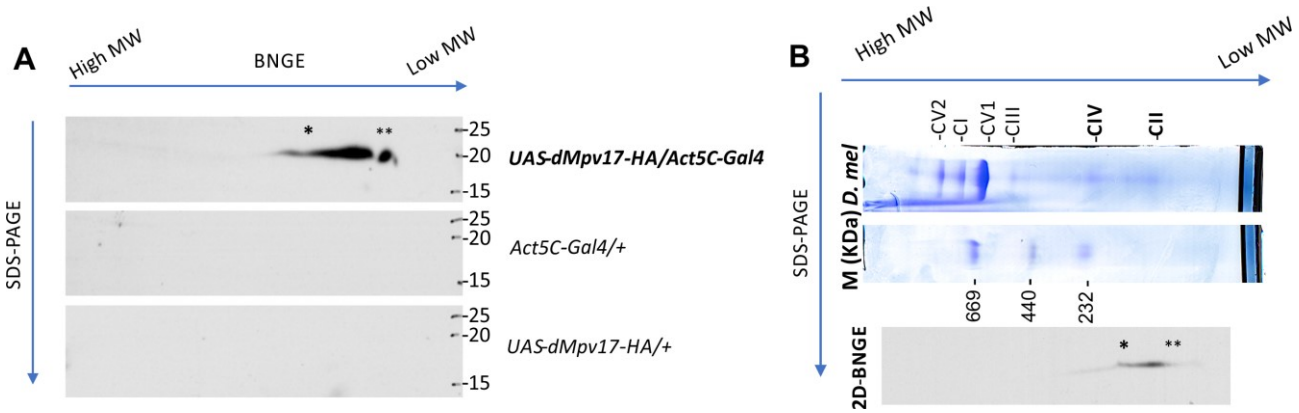

Fig. 26 Blue native gel electrophoresis on Drosophila mitochondria. A, mitochondria from UAS-dMpv17-HA/Act5C-Gal4 and parental controls were analyzed by 2D BNGE. The * underlines dMpv17-HA specific spot (the ** marks unspecific spot due to protein not correctly assembled in the complex). B, molecular weight of dMpv17-HA comprising complex. The protein was present in a spot corresponding to a complex of molecular weight between complex II and IV.

5.11 dMpv17 putative interactors

To gain insight into the molecular role of dMpv17, we decided to study its interactome *in vivo*. In order to identify proteins which could be part of the Mpv17-containing complex, mitochondrial protein content of flies ubiquitously expressing dMpv17 terminally tagged with an HA-epitope (*UAS-dMpv17-HA/Act5C-Gal4*) and the two parental controls (*Act5C-Gal4/+* and *UAs-dMpv17-HA/+*) were analysed by co-immunoprecipitation followed by mass spectrometry. Isolated mitochondria were solubilized using 0.5% TritonX-100, allowing detecting only strong interactions. Lysates were incubated with an anti-HA resin overnight at 4°C and, after three washes, SDS loading buffer was added and the samples were boiled for 10 minutes. Samples were separated on a SDS-PAGE gel and the gel was stained with Coomassie prior to proteomic analysis. Mass spectrometry data were ordered on Gal4 control, and proteins over-expressed in dMpv17-HA over-expressing flies with respect to both controls, were considered promising partners of dMpv17. Overall, after this filtering, the interaction network of dMpv17 was composed of 7 proteins, which were present in our over-expressing flies (*UAS-dMpv17-pUAST/act5C-Gal4*) and absent in both control strains (*act5C-Gal4/+* and *UAS-dMpv17-pUAST/+*). Mass spectrometry data are summarized in **Tab.9**.

Tab.9 The most significant partners of dMpv17 identified by mass spectrometry.

Protein ID (Uniprot)	Drosophila ID	Protein function	Gal4/ratio (log2)	UAS/ratio (log2)	MitoProt
Q9VSG0	CG13678	Uncharacterized protein	8871721.747	8871721.747	0.849
Q9V492	**CG11077**	**Drosophila dMpv17 ortholog**	**2033533.253**	**2033533.253**	
Q9VGM1	**CG14709**	**Drosophila multidrug resistance protein ortholog**	**346022.2581**	**16.495**	**0.0058**
Q9VA18	**CG1715**	**Drosophila Mic19 ortholog**	**261675.158**	**8.164**	**0.5856**
Q8T019; Q9VM97	CG11326	Thrombospondin (A)	240226.577	240226.577	0.0495
Q9VA93	CG15531	Uncharacterized protein	230306.299	230306.299	0.1293
Q9VHW0	CG7910	Putative cell-cycle regulators	126328.924	126328.924	0.6598

Interestingly, among these hits, we found the Drosophila ortholog of human coiled-coil-helix-coiled-coil-helix domain containing 3 (*CHCHD3*, alias *MIC19*). MIC19 is part of the MICOS complex, which is involved in mitochondrial cristae organization. Surprisingly, mass spectrometry analysis identified also the fly's ortholog of the human multidrug resistance protein 4 (*MRP4*), encoded a member of the ABC transporter family subtype C. MRP4 resides in the plasma membrane and it has never been shown to localize in mitochondria. In addition, we identified two uncharacterized proteins (CG13678 and CG15531) with the first one (Q9VSG0-CG13678) that shows high probability of export to mitochondria, as predicted by the MitoProt software. We found also a member of thrombospondins. They are a family of extracellular matrix proteins (ECM) that mediate cell-cell and cell-matrix interactions (Adams, 2001; Lawler, 2000). In particular we found the isoform A of Drosophila thrombospondin (TspA) that is the closest in structure to vertebrate Tsp-5/COMP. Tsp-5/COMP is expressed mainly in cartilage and certain other connective tissues and it has a role in chondrocyte attachment, differentiation and cartilage ECM assembly (Adams *et al.*, 2003). Finally, we identified the CG7910 protein that was firstly discovered through a large-scale RNAi-based screen investigating cell-cycle regulators (Guest *et al.*, 2011). All protein sequences were analysed by using Mitofates, but none of these proteins showed an N-terminal targeting pre-sequence.

5.12 *dMpv17* KO flies

Since RNAi only partially down-regulates the expression level of a specific gene, sometimes some effects can be hidden. Thus, we planned to generate a Drosophila *dMpv17* KO model that can better resemble human disease by using CRISPR/Cas9 technology. CRISPR&Cas9 mediated genome editing by homology-dependent repair (HDR) employed one guide RNA (gRNA) and a dsDNA plasmid donor. The CRISPR/Cas9 system has been widely used in Drosophila to disrupt, delete, replace, tag and edit multiple genes. Briefly, gRNAs (designed as 20-nt complementary to the target sequence) interact with Cas9 nuclease and guide it to the DNA sequence. Upon binding its target, Cas9 utilizes its two nuclease domains to generate a double-strand break. Homology-directed repair (HDR) pathway is used to fix the break by providing donor repair templates containing exogenous sequence flanked by homology-sequences (commonly referred to as homology arms).

To disrupt *CG11077* (*dMpv17*) we decided to insert a stop codon near the first ATG and a PBac-DsRed to facilitate genetic screening after insertion. The choice to insert an AATT sequence as close as possible to the initial ATG of our gene instead of a simple deletion was designed in order to avoid issues given to the presence of two non-coding RNA sequences (that, as aforementioned, completely overlapped *dMpv17* sequence). A PBac-DsRed cassette was inserted at the 47th nucleotide from the ATG of CG11077 in a w^{1118} strain background. This cassette has a 3XP3-DsRed and can be excised by PBac transposase. After excision, TTAA sequence, encoded a premature stop codon at 16th amino acid of CG11077, was left.

To circumvent the lack of a balancer chromosome (which would be fundamental in the case this KO line was homozygous lethal) for the small fourth chromosome, we decided to employ a line carrying a dominant mutation in a gene located on the fourth chromosome, which is lethal in homozygosity (Bloomington line 638). However, KO flies proved to be viable in homozygosity.

PCR from genomic DNA and sequencing were used to verify if the knock-in cassette was correctly used as template for HDR and thus incorporated into guide RNA cutting site, as well as to check for the presence of the TTAA sequence in PBac excised line. We finally managed to obtain three different Drosophila lines carrying the AATT sequence in *dMpv17* coding sequence.

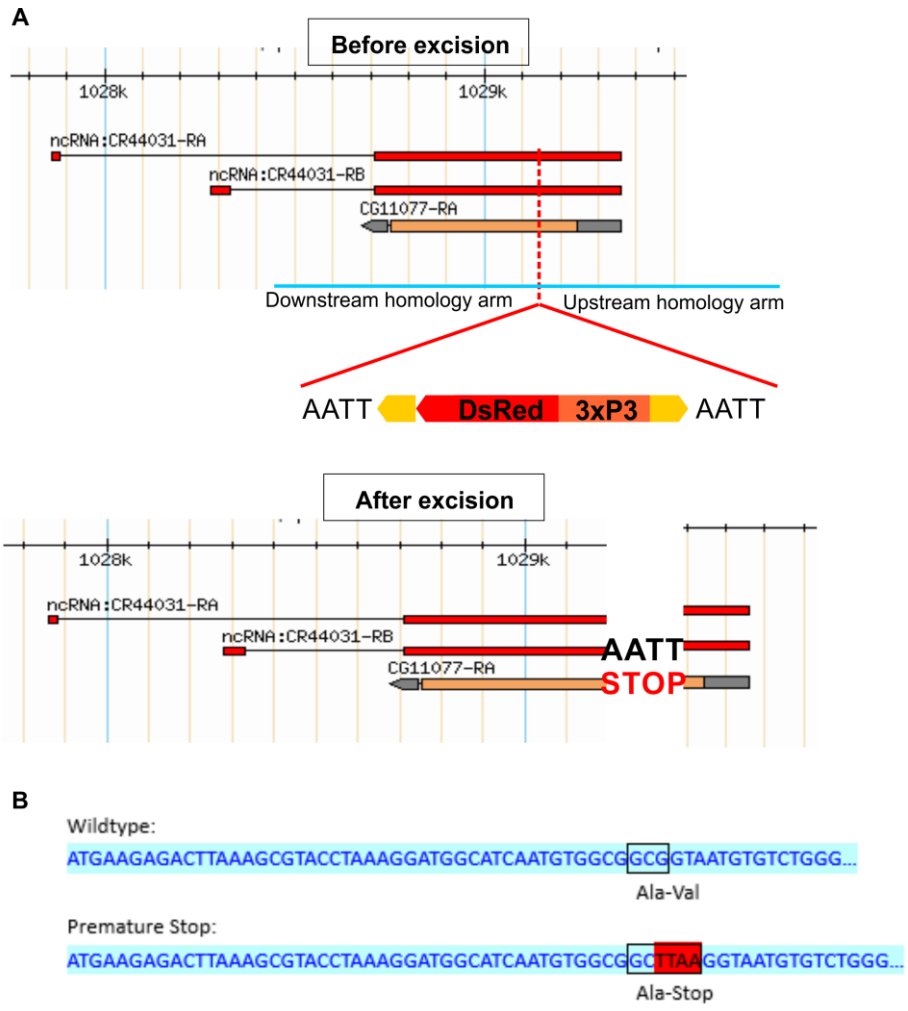

Fig. 27 *dMpv17* genome editing map. A, genome editing map before and after pBac excision. **B**, comparison between wildtype and mutated sequence showing the presence of the stop codon after Ala residue. DsRed: discosoma red fluorescent protein ; 3xP3: artificial promoter containing 3 Mmus\Pax6 homodimer binding sites ; Ala: alanine, Val: valine.

Mammalian mtDNA encodes only 13 proteins, which make up ~20% of the subunits of the oxidative phosphorylation system (Chinnery and Hudson, 2013). However, the mammalian mitochondrial proteome comprises 1.500 or more gene products (Calvo *et al.*, 2006). Most of these proteins are nuclear-encoded, synthesized in the cytosol and then imported into mitochondria. Nuclear-encoded proteins have been associated with the structure, assembly and maintenance of the respiratory chain, being structural components, factors involved in the biosynthesis of lipids and cofactors, proteins that mediate mitochondrial import and dynamics, and assembly factors. Another group of proteins plays a fundamental role in mtDNA expression and maintenance, either being part of the replication machinery or being involved in dNTP pools synthesis and transport. Despite this, the precise role of many mitochondrial proteins remains still unknown.

Mitochondrial diseases (MDs) are a clinically heterogeneous group of inherited disorders associated with defects in the oxidative phosphorylation system, with an estimated prevalence of between 1:5,000 and 1:10,000 live births (Noqueira *et al.*, 2014). Mitochondrial respiratory chain function strongly depends on the coordinated expression of both mitochondrial and nuclear genomes. Accordingly, mutations affecting nuclear-encoded mitochondrial proteins account for the onset of most mitochondrial diseases. During the last decades, an increasing number of novel nuclear disease genes have been identified. Among those genes, human *MPV17* was linked to mitochondrial disease in 2006 (Spinazzola *et al*., 2006), but its role in mitochondrial physiology and disease remains still puzzling. Mutations in the human *MPV17* nuclear gene, which encodes a small hydrophobic mitochondrial inner membrane protein, are responsible for a pediatric hepatocerebral form of mitochondrial DNA (mtDNA) depletion syndrome (MDS).

The fruit fly *Drosophila melanogaster* has been used successfully as a model organism in biomedical research for over a century and, recently, also in the field of mitochondrial diseases (Sánchez-Martínez *et al.*, 2006). Thus, to shed light into the functional role of MPV17, we decided to exploit Drosophila genetics and behavioral, biochemical and molecular tools in order to characterize the *Mpv17* fly ortholog and provide new information on its role in mtDNA maintenance.

MPV17 (and its yeast ortholog, Sym1) belongs to a family of proteins which is highly conserved from protozoans and yeast to higher eukaryotes. Indeed, members of this family were found within hydrogenosomes in *Nyctotherus ovalis* (an anaerobic ciliate) (Reinhold *et al*., 2012). *D. melanogaster* genome harbours a gene with significant similarity to human *MPV17*. This gene, denominated CG11077 (hereinafter indicated as *dMpv17)*, maps on the 4th chromosome and encodes a protein of 19 kDa showing 38% of sequence similarity with the human protein. Currently, there is no information about the function of *Mpv17* in flies. First, we demonstrated that Drosophila dMpv17 has a mitochondrial localization even without a cleavable mitochondrial targeting sequence, similar to its mammalian counterpart. Then, we reconstructed the MPV17 phylogenesis to investigate the origin of the Drosophila ortholog and its relationship with homologs from other species. Indeed, human MPV17 is part of the MPV17_PXMP2 family,

which in mammals includes at least three other members: MPV17-like protein, MPV17-like protein 2, and PXMP2. The phylogenetic tree showed that Drosophila Mpv17 groups with the MPV17 family and thus it is more similar to MPV17 than to the MPV17-like proteins. But, according to the low percentage of sequence similarity found in the alignment with the human protein, Mpv17 proteins from insect species form a separate subgroup.

Despite high levels of silencing, the ubiquitous knock-down of *dMpv17 in vivo,* obtained through the UAS-GAL4 system-driven RNAi, shows only a moderate, albeit significant, decrease in mtDNA copy number. Interestingly, the downregulation of the gene in the fat bodies (a functional analogous of human liver) determines a 50% of reduction in mtDNA copy number with respect to control flies, consistent with previous findings in human and mouse. However, we observe no effects associated with *dMpv17* down-regulation on fly's behaviour, neither in locomotor activity nor in bang sensitivity. Furthermore, in contrast with the dramatic decrease observed in patients, who die during infancy/early childhood, the lifespan in the fruit flies seems to be unaffected by *dMpv17* downregulation. These results suggest that a low residual mRNA level of *dMpv17* could be sufficient to maintain wild-type phenotypes in flies. As already described for mitochondrial DNA depletion diseases affecting humans, it is likely that mtDNA depletion has to fall below a critical threshold to become clinically relevant. This conclusion is also supported by the results obtained in the characterization of the Drosophila homolog of the yeast mitochondrial deoxynucleotides transporter *Rim2*. Despite high levels of silencing, d*rim2* KD flies were able to reach the adult stage (the Drosophila KO was then found to be lethal at larval stages) and lived longer than the controls (Da Re *et al.,* 2014). Alternatively, it has also been demonstrated that compensatory mechanisms (for instance, a shift to glycolysis and an increase in mitochondrial mass) are activated in flies in response to mtDNA maintenance defects (Adàn *et al.,* 2008).

Thus, in order to investigate molecular and phenotypic defects in a model that could better resemble human disease, we have already generated Drosophila *dMpv17* KO flies through the CRISPR&Cas9 technology.

Although the molecular role of MPV17 is still unknown, it has been widely documented that the absence of this protein impairs, probably in a tissue-specific manner, a dynamic control mechanism on mtDNA copy number in human, mouse and yeast. dNTP pools synthesis is fundamental for mtDNA maintenance, as it is underlined by the number of human syndromes caused by mutations in proteins involved in nucleotide metabolism and transport (Gandhi and Samuels, 2011). dNTPs supply for the mitochondrial replisome is maintained either by *in organello* recycling or by the import from the cytosol. Many genes involved in MDS onset encode enzymes which play an important role in dNTP pools maintenance and balance in mitochondria (*TK2, DGUOK*, *SUCLG1*, *SUCLA2*, *RRM2B,* and *TYMP*) (El-Hattab, 2013). MPV17 was first associated with mtDNA depletion diseases in 2006 (Spinazzola *et al.,* 2006) and a physiological role as a nucleotide transporter was hypothesized. This prompted us to evaluate the consequences of *dMpv17*

down-regulation on mitochondria dNTP pools in Drosophila cells. Albeit nucleotides and deoxynucleotides metabolism in Drosophila has been poorly investigated, the presence of the homologs of key enzymes for nucleotide *de novo* synthesis in the extra-mitochondrial compartment suggests that also in flies mitochondria receive their nucleic acid precursor from extra-mitochondrial sources. However, cytosolic and mitochondrial nucleotide pools appear not affected by *dMpv17* silencing in proliferating cells, as previously demonstrated in proliferating cells from patients with MDS (Dalla Rosa *et al.*, 2016). Conversely, Dalla Rosa and colleagues recently observed a significant decrease in dCTP and dGTP pool in differentiated cells.

By reconstitution into lipid bilayers, in 2009, it was demonstrated that Pxmp2 protein formed a relatively wide channel in the mammalian peroxisomal membrane, which showed features of a non-selective channel with respect to the chemical nature of solutes, whereas was highly selective relative to the size of the solutes (Rokka *et al.*, 2009). Sequence analysis performed on MPV17_PXMP2 family members predicted that all these multi-spanning membrane proteins possess four transmembrane domains. Moreover, the secondary structure (characterized by the presence of α-helical regions) and, consequently, the sequence similarity between MPV17 and the other members of the family led to the hypothesis that this family could form transmembrane channels either in the mitochondrial or in the peroxisomal membrane. Indeed, the presence of α-helix segments, which contain hydrophilic amino acids, in the secondary structure is necessary to fulfil specific requirements such as hydrophilic environment along the side facing the internal part of a channel (pore). Our *in silico* analysis performed on dMpv17 amino acidic sequence reveals four putative transmembrane domains. Moreover, five α-helix segments are predicted in the fly's protein, as in the human ortholog. In 2012, also Sym1 was found to form a channel (Reinhold *et al.*, 2012) with a conductance of ~450 pS (corresponding to a pore size of about 1.6 nm) considered sufficient to allow the transport of large molecules across the inner mitochondrial membrane. Closure occurred at physiological membrane potential to prevent ion leakage. Conceivably, specific proteins *in vivo* could regulate channel gating. Later, in 2015, Antonenkov and co-workers demonstrated that also the human MPV17 protein could form a channel in the IMM regulated by membrane potential, redox state, pH and protein phosphorylation (Antonenkov *et al.*, 2015). Again, the size of the human pore was found sufficient to allow the transfer of different metabolites. However, the physiological function of these channels and the nature of the cargo remain unknown. Thus, to gain insight into these aspects, given the secondary structure and sequence similarity of the fly's ortholog, we cloned the Drosophila Mpv17 open reading frame in a pIVEX1.3 vector that allowed cell free *in vitro* transcription and translation of the protein. In a preliminary study, we demonstrate that also the Drosophila protein inserted in an artificial planar lipid bilayer is able to form a channel in physiological conditions. We performed the experiment in 150 mM KCl, 10 mM HEPES pH 7.4 and determine that the conductance in this medium is 330 pS. Since experiments on the human protein were performed expressing the protein in the yeast *Pichia pastoris* cells, we cannot exclude the possibility that post-translational modifications are needed for the correct formation of the Drosophila channel. Thus,

we are currently considering the opportunity to repeat the experiment using an *in vivo* system for protein expression, or to purify the protein directly from mitochondria isolated from flies expressing a tagged form of dMpv17.

In order to determine in which way channel formation and activity could be perturbed by mutations, we decided to mutagenize the wild-type sequence. We looked for human disease mutations affecting amino acidic residues conserved in the Drosophila protein and we manage to introduce mutations in the fly sequence at residues corresponding to human S170F (509C>T), which is also one of the three predicted phosphorylation sites, and R50Q (149G>A) mutations. We plan to analyze the mutated protein channel-forming activity and perform electrophysiological measurements to determine if channel activity and properties are modified by these mutations, especially in the case of the phosphomimicking mutation.

We also show that *dMpv17* KD in Drosophila cells caused alterations in mitochondrial ultrastructure. Transmission electron microscopy reveals structural/morphological changes in mitochondria including decreased average diameter, cristae number and length. Moreover, we observe an accumulation of electron-dense structures in the matrix. Similar mitochondrial morphology was also described in mouse, yeast and *MPV17* mutant patients. We investigated also the effect of *dMpv17* up-regulation on mitochondrial morphology that appeared profoundly altered, with mitochondria mostly devoid of cristae. Where cristae were still present, they had the tendency to form vesicles. Taken together, these results suggest that Mpv17 could have a role in controlling/determining the shape of the cristae and the structure of the inner mitochondrial compartment.

Mitochondria are sensors of cellular metabolism and can modulate different pathways, triggering specific gene expression to change their morphology in order to respond to cellular needs. In particular, fission and fusion events are fundamental to maintain functional mitochondria when cells undergo diverse stress stimuli. We analyzed mitochondrial network morphology in S2R+ and found that *dMpv17* down-regulation causes an increase in the percentage of cells with a fragmented mitochondrial network (with a parallel decrease in tubular mitochondria). Next, we examined expression levels of key components of the mitochondrial fission ad fusion machinery, but we observed no changes at the transcriptional level in genes controlling fission and fusion (*Drp1*, *Fis1*, *Mfn*, and *Opa1*).

In turn, the disruption of mitochondrial morphology directly impacts cellular and organismal metabolism. In fact, mitochondrial morphology is intimately linked to mitochondrial functions. Since the formation of the cristae/convolutions of the inner mitochondrial membrane leads to an increase of the membrane surface, enhancing oxidative phosphorylation, we wondered whether S2R+ cells KD for *dMpv17* displayed impairment in oxygen consumption. Seahorse analysis reveals a decrease in respiration that is not caused by mitochondrial loss because mitochondrial mass is the same both in silenced and control cells. Thus, the reduction in respiration could be due to the presence of damaged/altered mitochondria in *dMpv17* KD

cells. Accordingly, Viscomi *et al*. (2009) observed that damaged mitochondria with low content of mtDNA were present in liver from *Mpv17* knock-out mice.

Regulation of mitochondrial fission and fusion is involved in sorting-out damaged mitochondria for degradation, enhancing mitochondrial quality control through mitophagy. Nevertheless, premature aging, which is a feature of *Mpv17*$^{-/-}$ mice, is characterized by a gradual storage of damaged mitochondria. PINK1 and Parkin have been demonstrated to play a major role in mitochondrial quality control. PINK1 is known to get stuck into the outer mitochondrial membrane of mitochondria after the loss of the mitochondrial membrane potential, inducing its autophosphorylation (Okatsu *et al.*, 2012) and in turn Parkin recruitment and activation (Narendra and Youle, 2011). Once migrated to damaged mitochondria, Parkin promotes mitophagy (Vives-Bauza *et al*., 2010). Antonenkov and co-workers demonstrated that the amount of PINK1 in its inactive form was higher in *Mpv17*$^{-/-}$ fibroblasts compared to wild-type cells in standard condition and after a single treatment with H_2O_2 (Antonenkov *et al.*, 2015). Likewise, a significant down-regulation of *dPink1* is observed in *dMpv17* KD cells with respect to control both in normal condition and upon CCCP treatment. Moreover, loss of PINK1 in Drosophila cells has been demonstrated to abrogate mitophagy (Ziviani *et al.*, 2010). To extend this observation we tried to understand whether Parkin, which acts downstream of PINK1, could be affected by *dMpv17* impairment. However, no difference in *dparkin* transcript and protein levels has been detected. The induction of mitophagy has been found to correlate with the ubiquitination of different mitochondrial proteins including mitofusins (Gegg *et al.*, 2010). These post-translational modifications are reduced with the silencing of PINK1 or Parkin (Ziviani *et al.*, 2010). Consistent with our previous data, no difference in *dMpv17* KD cells compared to control cells are found in Mitofusin (also known as Marf, the Drosophila homolog of MFN1-2) ubiquitination levels after CCCP treatment. Antonenkov and co-workers also observed a decrease in the content of autophagy-related LC3B protein in *Mpv17*$^{-/-}$ fibroblasts. This decrease is also characteristic of PINK1 silencing (Gegg *et al.*, 2010). Besides LC3, levels of other autophagy substrates can be used to monitor autophagic flux, and the best-studied example is sequestosome 1 (SQSTM1 also known as p62). p62 directly binds to LC3B and is selectively incorporated into autophagosomes and then degraded by autophagy (Mizushima *et al.*, 2010). Thus, the cellular expression level of p62 inversely correlates with autophagic activity. We observe an accumulation of p62 after CCCP treatment in *dMpv17* KD cells. Consistent with this, we find that prolonged exposure to CCCP (24h) led to a slowdown of mitochondrial clearance. Together, these findings suggest that the down-regulation of *dMpv17* might impact on mitochondria quality control pathway.

Importantly, we demonstrated that like the yeast ortholog Sym1 and the mouse protein, Drosophila Mpv17 participates in a high molecular–weight complex *in vivo*. We determined that the molecular weight of the complex is comprised between complex II and complex IV.

Although the formation of this complex is necessary for Mpv17 function (from the moment that variants that are not incorporated do not rescue the mtDNA depletion of *Mpv17*$^{-/-}$ mice), Mpv17/Sym1 putative

partners remain still unknown (Dallabona *et al.*, 2010; Reinhold *et al.*, 2012). Moreover, the analysis of MPV17 gating properties indicates that the channel is closed under conditions that correspond to healthy mitochondria, such as high membrane potential, high ATP/ADP ratio, and reducing environment. Indeed, the conclusion that MPV17 is a (non-selective) channel could be apparently counterintuitive, if we consider the necessity of keeping the inner mitochondrial membrane impermeable in order to maintain metabolic activity and membrane potential. Thus, this putative channel should be finely-tuned regulated. So, to identify dMpv17 molecular partners we performed Co-IP experiments on mitochondria isolated from flies over-expressing an HA-tagged form of dMpv17 following by mass spectrometry analysis. Subunit 19 of MICOS, MIC19 (Lethal in Drosophila), and multidrug resistance protein 4, MRP4 (Mrp4 in Drosophila), were identified as putative partners of dMpv17. Interestingly, MIC19 is a protein involved in cristae remodelling, which takes part in MICOS complex formation (Ott *et al.*, 2015), whereas MRP4 is a member of the ABC transporter family subtype C (Russell *et al.*, 2008).

Recently, modifications of cristae morphology have been demonstrated to be a response to cope with changes in physiological energetic states and oxygen availability (Zick *et al.*, 2009). Indeed, several mitochondrial disorders in humans are accompanied by alteration of mitochondrial ultrastructure (Zick *et al.*, 2009). However, only some mechanisms regulating this process have been well characterized. Recent studies in yeast and human cells identified MICOS as a large protein complex (700 kDa) important for mitochondrial membrane architecture, cristae junctions' formation (contact sites between the outer and inner membranes), as well as mitochondrial dynamics (Pfanner *et al.*, 2014; Zerbes *et al.*, 2012). MICOS complex entails at least seven components in mammals: MIC60, MIC27, MIC26, MIC25, MIC19, MIC10, and QIL1 (Guarani *et al.*, 2015; Pfanner *et al.*, 2014) and seems to be functionally organized into two sub-complexes, containing MIC10 and MIC60 as central components, respectively (Friedman *et al.*, 2015; Guarani *et al.*, 2015). Genetic removal of different MICOS subunits leads to mitochondrial fragmentation, reduced respiration, CJs loss and formation of concentric stacks of inner mitochondrial membrane disconnected from the inner boundary membrane (Zick *et al.*, 2009). Recently, Guarani *et al.* (2015) identified a new subunit of the MICOS complex, QIL1, and demonstrated its key role in CJs formation and MICOS complex maturation. QIL1 depletion in human cells disrupts CJs structure and impairs respiration. Moreover, they found an increase in mitochondrial fragmentation (and sphericity), as well as in the number of abnormal mitochondria (those containing IM swirls), also in Drosophila third instar larval muscles (upon QIL1 down-regulation through UAS/Gal4 system). Strikingly, these phenotypes resemble the abnormalities that we find in *dMpv17* KD cells. Indeed, transient depletion of *dMpv17* resulted in smaller mitochondria showing a reduction in number and length of cristae, as well as substantial decrease in respiration level.

In mammals, Mic19 resides in the inner membrane, facing the intermembrane space, and interacts with Mic60 and OPA1, and with Sam50 in the outer membrane (Zick *et al.*, 2009). Down-regulation of *MIC19* in HeLa cells resulted in fragmented mitochondria, reduction in OPA1 levels, and fewer and fragmented

cristae. Additionally, a reduction in subunits of complex IV (the activity of which was found reduced in patients with MPV17 mutations) has been measured, which led to a decrease in both coupled and uncoupled respiration. Mic19 has been found in two different redox forms (Sakowska *et al.*, 2015). Interestingly, in view of a possible role for MPV17 in membrane potential control (Antonenkov *et al.*, 2015), it was found that oxidized Mic19 was able to connect the two MICOS subcomplexes, whereas, in the reduced form, it caused defects in cristae. Finally, it was demonstrated that MIC60 down-regulation reduced PINK1 localization in depolarized mitochondria, thereby inhibiting Parkin recruitment to mitochondria (Rua *et al.*, 2016). To a lesser extent, also Mic19 down-regulation reduces Parkin recruitment (Akabane *et al.*, 2016). These results support our preliminary conclusion of a possible impairment in mitophagy in *dMpv17* knock-down cells.

Because of the lack of antibodies against Drosophila Mic19, in order to confirm the possible interaction between MIC19 and MPV17, currently we are cloning the human sequence His-tagged in a mammalian expression vector for human cells transfection. Our idea is to perform a new Co-IP experiment using MPV17-His as a bait to determine the presence of MIC19 in the Co-IP elute through western blot analysis.

As already mentioned, the second protein we identified through mass spectrometry analysis is a member of the ABC transporters family. ABC transporters are one of the most representative families of integral membrane proteins found in all three kingdoms of life. Members have a role in different cellular processes and mediate the active transport of a broad variety of solutes (e.g. amino acids, polysaccharides, peptides, lipids, drugs, antibiotics, toxins) across cellular membranes. In eukaryotes, ABC transporters are located in the plasma membrane as well as in intracellular membranes of the endoplasmic reticulum (ER), the *Golgi* apparatus, lysosomes, peroxisomes and mitochondria. Almost all eukaryotic ABC transporters function as exporters. In particular, ABC transporters localized in the inner mitochondrial membrane translocate molecules in the inner mitochondrial space. To date, four members of mitochondrial ABC system have been identified in mitochondria, all belonging to the subfamily B, which are involved in iron metabolism and transport of Fe/S protein precursors and in peptide export (Dean, 2002). Instead, no clear mitochondrial localization for MRP4, an ABC transporter of subtype C, has ever been demonstrated. However, it has been demonstrated that MRP4 membrane localization is cell-type-dependent. Basolateral localization was observed in glandular epithelial cells of the prostate and in hepatocytes, while it was also detected in the apical membrane of proximal tubule cells of the kidney. A possible reason for the different localization and function of MRP4 in several cell types is that MRP4 interacts with different adaptor proteins that regulate its intracellular trafficking. In agreement with our findings, MRP4 would not be the first ABC transporter belonging to the subfamily C possibly present in the inner mitochondrial membrane. Indeed, Roundhill and co-workers demonstrated that a glycosylated form of MRP-1 is present in the outer mitochondrial membrane of cancer cells (Roundhill *et al.*, 2016). MRP-1 does not have a MTS (as MRP4), but it is a client protein for the chaperone HSP90b, which together with other HSPs, is known to transport hydrophobic

proteins to the mitochondrial outer membrane (Roundhill *et al.*, 2016). Likewise, also ABCC6 has been found to localize to the mitochondria-associated membrane (MAM) rather than, as previously thought, to the basolateral plasma membrane of liver and kidney (Martin *et al.*, 2012). Importantly, a role as channel regulatory subunit has also been described for ABC transporters of subtype C. Indeed, SUR1 was demonstrated to be the regulatory subunit of the ATP-sensitive (KATP) channel (Aittoniemi *et al*., 2009).
To note, transporters and channels localized in the inner mitochondrial membrane depend on ATP for they activity. ABC transporters have an ATP binding site and they use the energy derived from ATP hydrolysis for their functioning. Taken together, these conclusions might support a possible role for MRP4 as regulator of dMpv17 channel activity.

In conclusion, we demonstrate that *dMpv17* down-regulation in flies causes a profound mitochondrial DNA depletion in fat bodies (an analogous of human liver). A milder depletion has been also measured in *dMpv17* KD cells. Our data on mitochondrial morphology suggest a possible role for dMpv17 in the maintenance of the structural and functional stability of the inner mitochondrial membrane, and in the quality control of these organelles. These effects could also impact on mitochondrial DNA stability. mtDNA is contained within a protein-DNA nucleoid complex physically associated with the mitochondrial inner membrane; thus, the disorganization of this membrane can lead to mtDNA defective replication. Furthermore, it has also been demonstrated that the absence of proteins normally located in the inner mitochondrial membrane, but not directly involved in mtDNA synthesis, can compromise the integrity of the mitochondrial genome (Contamine *et al.*, 2000). In addition, our results reveal that dMpv17 can form a channel when inserted in an artificial planar lipid bilayer. We also show that dMpv17 take part in a high molecular weight complex and could interact with dMic19 and thus be involved in cristae organization and with dMrp4 that could play a role in dMpv17 gating regulation. Further work is now necessary to confirm these interactions and to define a molecular/functional model for dMpv17.

dApopt1

7.1 Apopt-1 and its role in apoptosis

Dysregulation of apoptosis results in deficient (involved in carcinogenesis) or excessive (implicated in the pathogenesis of stroke, myocardial infarction, and heart failure) cell death and is implicated in many human diseases. *Apop*-encoding gene was originally identified in 2006, analyzing the differences in gene expression patterns in samples isolated from atherosclerotic plaque and non-plaque areas of the aorta in apolipoprotein E-deficient mice (Yasuda *et al*., 2006). Notably, it is known that atherosclerotic plaque tends to rupture at sites where the number of vascular smooth muscle cells is reduced due to apoptosis possibly induced by activated macrophages (Wang *et al*., 2001). The *Apop1* gene was identified as a novel transcript showing up-regulated levels in murine muscle cells cultured from atherosclerotic plaques.

There are two major pathways for the induction of apoptosis. Mitochondria play a crucial role in the intrinsic pathway, by releasing cytochrome *c* from the IMS into the cytoplasm after OMM permeabilization. Mitochondrial permeabilization can be initiated by opening the permeability transition pore (PTP) but it is also mediated by Bcl-2 family proteins which act directly on the OMM (and PT and the inner membrane do not play major roles in this case). Particularly, it was observed that *Apop-1* expression induced apoptosis in mice through the release of cytochrome c from mitochondria followed by caspase-9 and -3 activation (Yasuda *et al.*, 2006). Inhibition of cyclophilin D (CypD, a component of the permeability transition pore (PTP) by cyclosporine A determined a reduction in the Apop1-dependent release of cytochrome c. Conversely, inhibitors of Bax/Bak-dependent channels did not show significance effects. Consistently, CypD-deficiency prevented Apop-1-induced apoptosis in mouse cells, whereas *Apop-1* down-regulation arrested cell death in cells exposed to apoptosis-inducing drugs.

Further evidence uncovering Apop-1 regulation and networking was provided by Xin *et al.* (2008), demonstrating Apop-1 control by Akt signaling, the activation of which counteracted Apop-1-induced cell death (Sun *et al*., 2008). Moreover, Akt anti-apoptotic effects were due to the inhibition of the Apop1-induced cytochrome c release from mitochondria and caspase-9 activation. Akt was already shown to play an anti-apoptotic role, as its activation was known to inhibit pro-apoptotic proteins like Bad, caspase-9, while activating anti-apoptotic proteins such as NF-κB and cAMP-response element-binding protein (Tsujimoto and Shimizu, 2000; Borner, 2003; Willis *et al*., 2003; Puthalakath and Strasser, 2002; Wei *et a*l. 2001; Adams and Cory, 1998). Although Akt represents a key crossroad for a plethora of signaling pathways, this study also showed that the addition of IGF-1 to cell culture prevented Apop-1-induced cell death in a PI3K-dependent manner (Sun *et al*., 2008).

Mouse *Apop* encodes two transcripts, Apop-1 and Apop-2, found ubiquitously expressed but at different levels in all the organs analyzed. Apop-1 showed the highest expression in the brain while Apop-2 in the kindey. However, a role in apoptosis for Apop-2 has not been demonstrated. Moreover, this gene is highly conserved, with homologues identified in both Drosophila and *Caenorhabditis elegans*. In humans, the

gene (*APOPT1*) is located on chromosome 14, and encodes a mitochondrial protein with poorly understood functions. APOPT1 protein sequence comprises 194 amino acids, with the 160 N-terminal residues shared with APOPT2. The N-terminal region of this gene was predicted to function as a mitochondrial-targeting sequence.

7.2 *APOPT1* mutations and mitochondrial disease onset

Deleterious mutations in *Apoptogenic protein 1* (*APOPT1*) have been recently related with the onset of mitochondrial disorders (Melchionda *et al.*, 2013). Mutations in the *APOPT1* gene have been identified in patients affected by COX deficiency, with a peculiar brain MRI pattern showing early and rapid onset of cavitating white matter abnormalities in the posterior areas of the cerebral hemispheres and corpus callosum (Melchionda *et al*., 2013). Although the human gene contains two predicted ATG start codons, on the basis of phylogenetic comparisons, the authors suggested that the most likely human APOPT1 protein starts from the second ATG, the first one being present only in primates. The localization of APOPT1 in the mitochondrial matrix has been demonstrated in both human and murine cells (Yasuda *et al.,* 2006; Melchionda *et al.*, 2013).

Clinical manifestations associated with mutations in this gene varied from acute neurometabolic decompensation in infancy to subtle neurological signs in adolescence. Patients featuring encephalopathic episodes showed inability to walk or sit, loss of speech, somnolence, seizure and spastic tetraparesis. In all cases, this clinical scenario tended to stabilize, showing in some subjects also signs of recovery over time (Melchionda *et al.,* 2013).

A marked and diffuse reduction in histochemical COX reaction has been shown in muscle biopsies from 4 patients, and further EM studies showed enlarged mitochondria with osmiophilic inclusions as well as impaired cristae organization in at least one patient (Melchionda *et al.*, 2013). Moreover, the biochemical analysis of individual mitochondrial respiratory chain complex activities in muscle and fibroblasts revealed profound reduction in cIV activities and to a lesser extent in CII activity as well (muscle: residual activity 3-44% of controls; fibroblasts: 25-61%). A 3-fold increase in mtDNA content was also reported (Melchionda *et al*., 2013).

To date, *APOPT1* mutant alleles have been identified in six subjects belonging to five unrelated families, and mutations are predicted to result in the synthesis of severely damaged protein species. In particular, in two of these patients (two sisters), Sanger sequencing showed a c.235C>T substitution in the *APOPT1* gene which was predicted to introduce a premature stop codon resulting in a truncated protein. Another subject showed a nucleotide change (c.163-1G>A) within intron 1, a mutation which may affect mRNA splicing. In one patient, exon 3 was absent, suggesting a deletion in the region between exon 2 and 4. The lack of this sequence caused a change in the reading frame, leading to the introduction of a predicted premature stop codon. In another case, a homozygous c.353T>C change determined the substitution of a highly conserved

Phe118 to Ser, predicted as extremely deleterious for protein function. In the sixth affected individual, two heterozygous mutations have been identified: the already described c.235C>T change and a deletion of 3 nucleotides responsible for the loss of a highly conserved Glu residue.

APOPT1 precursor protein was suggested to be degraded by the proteasome in standard culture conditions. On the contrary, oxidative stress (H_2O_2 exposure) increased APOPT1-HA accumulation within mitochondria, whereas APOPT1-HA expression was sufficient to prevent ROS production also in H_2O_2 treated fibroblasts. Coherently, APOPT1-deficient fibroblasts were characterized by higher levels of ROS. Together, this evidence suggests that APOPT1 is involved in mitochondrial anti-ROS defense, whereas it must be eliminated by proteasome-mediated degradation in standard conditions (at least, in cultured cells), a similar scenario observed for PINK1 and HIF-1 (Narendra *et al*., 2011; Zheng *et al*., 2006). Importantly, no evidence supporting a role for APOPT1 as a proapoptotic factor was obtained in this work.

Further analysis on fibroblast from the first two patients showed also a marked reduction in the amount of both COX holocomplex and cIII2/cIV supercomplex, the amount of which was significantly increased in APOPT1-HA-expressing cells. As suggested by the authors, these results were consistent with a potential role of APOPT1 in cIV assembly and/or stability.

As aforementioned, COX deficiency represents a typical feature of APOPT1 mutant patients, yet no functional mechanisms has been unveiled about APOPT1 involvement in cIV assembly or stability. In spite of this lack of knowledge, a link between apoptosis and high ROS production has been suggested as a key component in the pathophysiology of mitochondrial diseases associated with COX deficiency (Di Giovanni *et al*., 2001; Kadenbach *et al*., 2004).

Although both *SURF*-deficient LS and *APOPT1*-associated encephalopathy are neurological conditions characterized by marked cIV impairment, the clinical course of the latter exhibits a notable variability in severity. Indeed, inside the cohort of APOPT1 mutant patients, cases showing severe neurological signs during early age have been observed, as well as others with rather intermediate phenotypes featuring severe motor impairment but mild or absent cognitive involvement.

In contrast with the rapid and often fatal decline of the other early-onset COX-defective encephalopathies, in all cases of APOPT1-associated encephalopathy both MRI lesions and the clinical progression stabilize, leading to a chronic and long-surviving clinical course. Interestingly, in some cases, vitamin and/or coQ10-based treatments were reported to coincide with clinical stabilization. Given that the stabilization of the clinical course was obtained spontaneously in the other three patients, the efficacy of these therapies remains to be validated.

Intriguingly, a recent RNA-sequencing study suggested APOPT1 as a potential schizophrenia risk-associated gene (Takata *et al*., 2017). Indeed, DNA regions encompassing *APOPT1* and other genes associated with various human diseases, and in particular schizophrenia, are enriched in splicing quantitative trait loci

(sQTLs). Thus, mutations in these hotspots for schizophrenia risk could contribute to disease onset by altering gene regulatory functions (Nicolae *et al*., 2010; Maurano *et al*., 2012).

8.1 *CG14806* (*dApopt1*) is the Drosophila ortholog of the human *APOPT1*

Analysis of the human APOPT1 sequence identified two putative start codons, encoding methionine at position 1 (APOPT1-M1) and 14 (APOPT1-M2). Both APOPT1 isoforms were experimentally localized in the mitochondrial matrix (Melchionda *et al*., 2014). However, M1 is present only in primates. However, it was demonstrated that the predicted mature form of the protein, starting from both methionines, was the same because the cleavage after mitochondrial import was predicted to occur between amino acids 39 and 40. A mitochondrial localization of APOPT1 was also demonstrated in mouse (Yasuda *et al*., 2006).

Drosophila genome harbors an *APOPT1* ortholog (*CG14806,* named *dApopt1*) that is localized on the X chromosomes. Two different isoforms of *dApopt1* but only one protein were found in flies. ClustalW alignment of the Drosophila protein showed 37% of sequence similarity with the human one (**Fig.28, A**). By using MitoFates, we found that the Drosophila protein sequence apparently lacked an N-terminal mitochondrial targeting signal, in contrast with the mammalian ortholog. However, we demonstrated that GFP-tagged recombinant Drosophila dApopt1 have mitochondrial localization when transiently expressed in cultured cells. Indeed, we showed that both the protein colocalize with a mitochondrial marker (Mitotracker red) when transiently transduced in Drosophila S2R+ cells (**Fig. 28, B**).

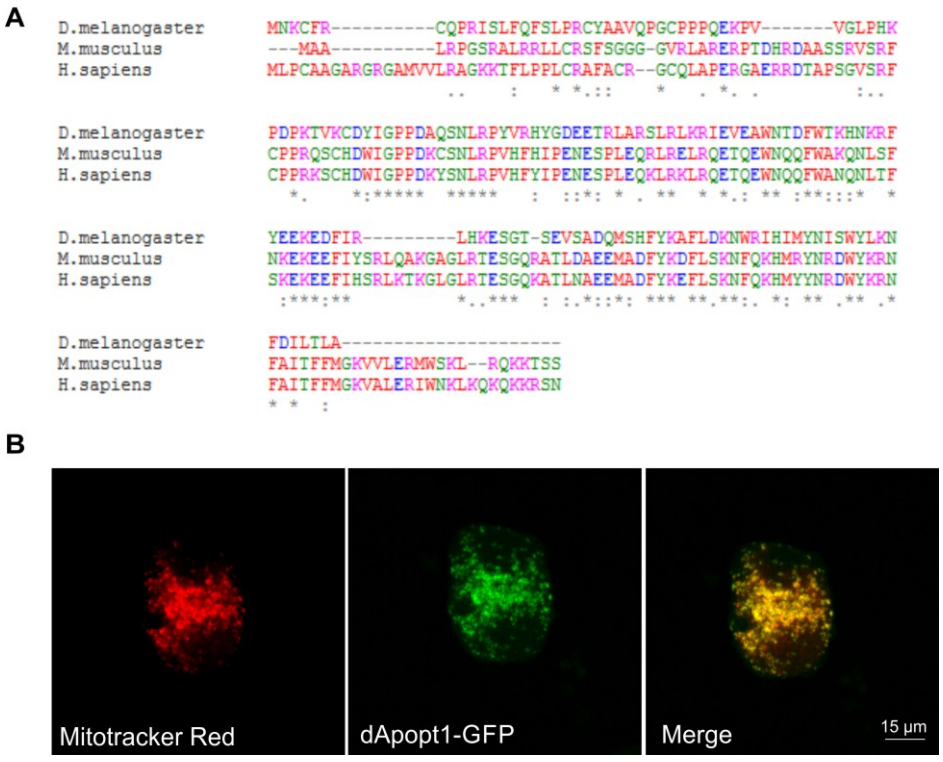

Fig.28 Analysis of homology and immunolocalization of Drosophila Apopt1 protein. **A**,_using Clustal W software we performed sequence alignment of human APOPT1 protein with its orthologs from *Mus musculus* and *Drosophila melanogaster*. The alignment highlights identical amino acid residues (*) and similar ones (. and :). **B**, Drosophila cells were transiently transfected with pAc5-STABLE2-neo-dApopt1 GFP tagged (green) and incubated with MitoTracker Red dye (red). Overlay of images confirms the mitochondrial localization of dApopt1.

8.2 *dApopt1* expression is induced by oxidative stress

The experiments performed in human fibroblasts showed that *APOPT1* was normally expressed but, the protein precursor seemed to be continuously degraded by the proteasome system. Conversely, exposure to H_2O_2 determined the accumulation of the mature intra-mitochondrial isoforms. To test a possible role also for dMpv17 in response to oxidative stress, we treated Oregon R adult flies (wild-type strain) with 1% of H_2O_2 dissolved in the food and we measured *dApopt1* expression levels after 10 hours of treatment. In agreement with previous findings (Melchionda *et al.*, 2014), *dApopt1* mRNA levels were increased in treated flies with respect to control flies (**Fig. 29**).

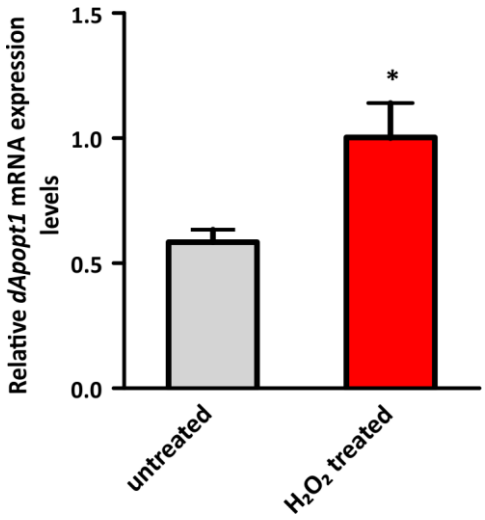

Fig. 29 *dApopt1* expression levels after oxidative stress. *dApopt1* expression levels in H_2O_2 treated and control flies were quantified. Data plotted are means ± SEM of three biological replicates (Student's *t* test was performed: * $p < 0.05$, ** $p < 0.01$, *** $p < 0.001$).

8.3 *dApopt1* knock-down flies show no effect on mtDNA amount

Since a 3-fold increase in muscle mtDNA amount was observed in one APOPT1 mutant patient (Melchionda *et al.*, 2014), we measured the mtDNA copy number in flies where the expression of *dApopt1* was down-regulated specifically in muscle (by using *24B-Gal4* driver) and in the nervous system (by using *elav-Gal4* driver). However, no mtDNA copy number variation was found both in muscle and in nervous system (**Fig. 30**).

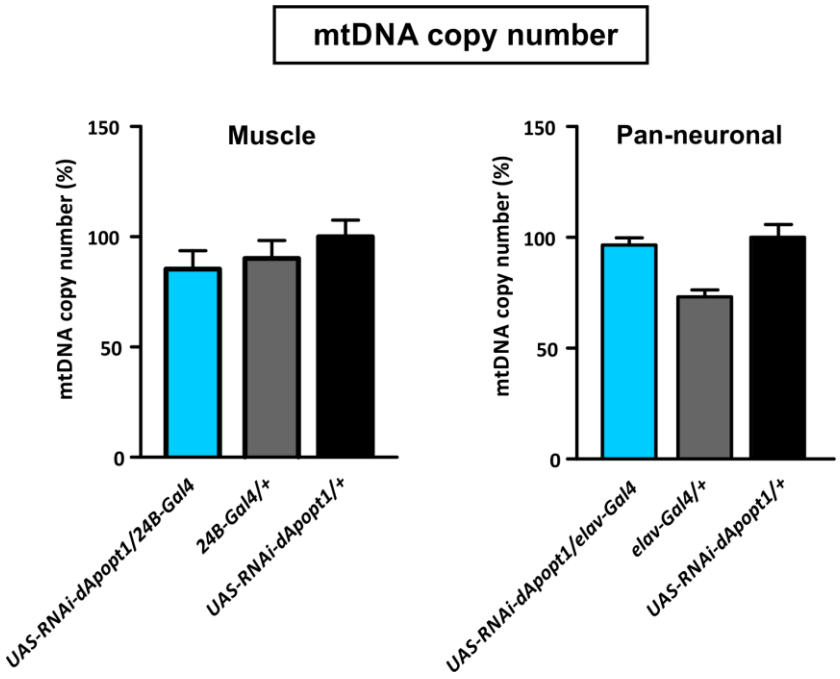

Fig. 30 mtDNA copy number analysis in *dApopt1* KD flies. mtDNA copy number, measured by qRT-PCR, was performed in *dApopt1* RNAi flies upon different Gal4 drivers (muscle, *24B-Gal4* and pan neuronal, *elav-Gal4*) and in the two parental controls (*24B-* and *elav-Gal4* and *UAS-RNAi-dApopt1*). Values are expressed as a mean of three independent experiments, and error bars represent the SEM of the mtDNA/nDNA ratio among the replicates. (Student's *t* test was performed: * $p < 0.05$, ** $p < 0.01$, *** $p < 0.001$).

8.4 *dApopt1* down-regulation impairs Drosophila locomotor activity

In contrast with neurological conditions that appeared highly variable in severity and in age of onset, all the patients showed severe motor impairment evolving into spastic quadriparesis (Melchionda *et al.,* 2014). In order to detect possible impairments in flies locomotor phenotype, we monitored locomotor activity for 48 hours in KD flies. *dApopt1* down-regulation was achieved ubiquitously (*act5C-Gal4*) or specifically in muscle (*24B-Gal4*) or in the nervous system (*elav-Gal4*) through the UAS-Gal4 system. Locomotor activity was quantified as total locomotion in groups of ten flies in 2 days recordings. Geotaxis behavior was measured as total movements at three different heights alongside the tube (at the bottom-near the food, intermediate and in the upper part of the tube; see materials and methods), in order to determine possible defects in fly negative geotaxis. *dApopt1* KD flies showed a strong impairment in locomotor phenotype when gene expression was ubiquitously downregulated (**Fig. 31, A**: *UAS-RNAi-dApopt1/act5C-Gal4*). A severe impairment in the negative geotaxis response was noted, particularly a low activity was measured in the upper part of the vials (**Fig. 31, A**, light blue columns) with respect to control flies (*act5C-Gal4/+* and *UAS-RNAi-dApot1/+*). We observed a significant reduction in locomotor activity also in muscle-specific (**Fig. 31, B**: *UAS-RNAi-dApopt1/24B-Gal4*) and in nervous system-specific (**Fig. 31, C**: *UAS-RNAi-dApopt1/elav-Gal4) dApopt1* KD flies with respect to control flies (respectively, *24B-Gal4/+* and *elav-Gal4/+*, and *UAS-RNAi-dApopt1)*. However, locomotor behavior especially referring to geotaxis response was found less

affected by tissue-specific down-regulation. So, the strong impairment measured after *dApopt1* ubiquitous down-regulation could be due to a combination of nervous and muscle system involvement.

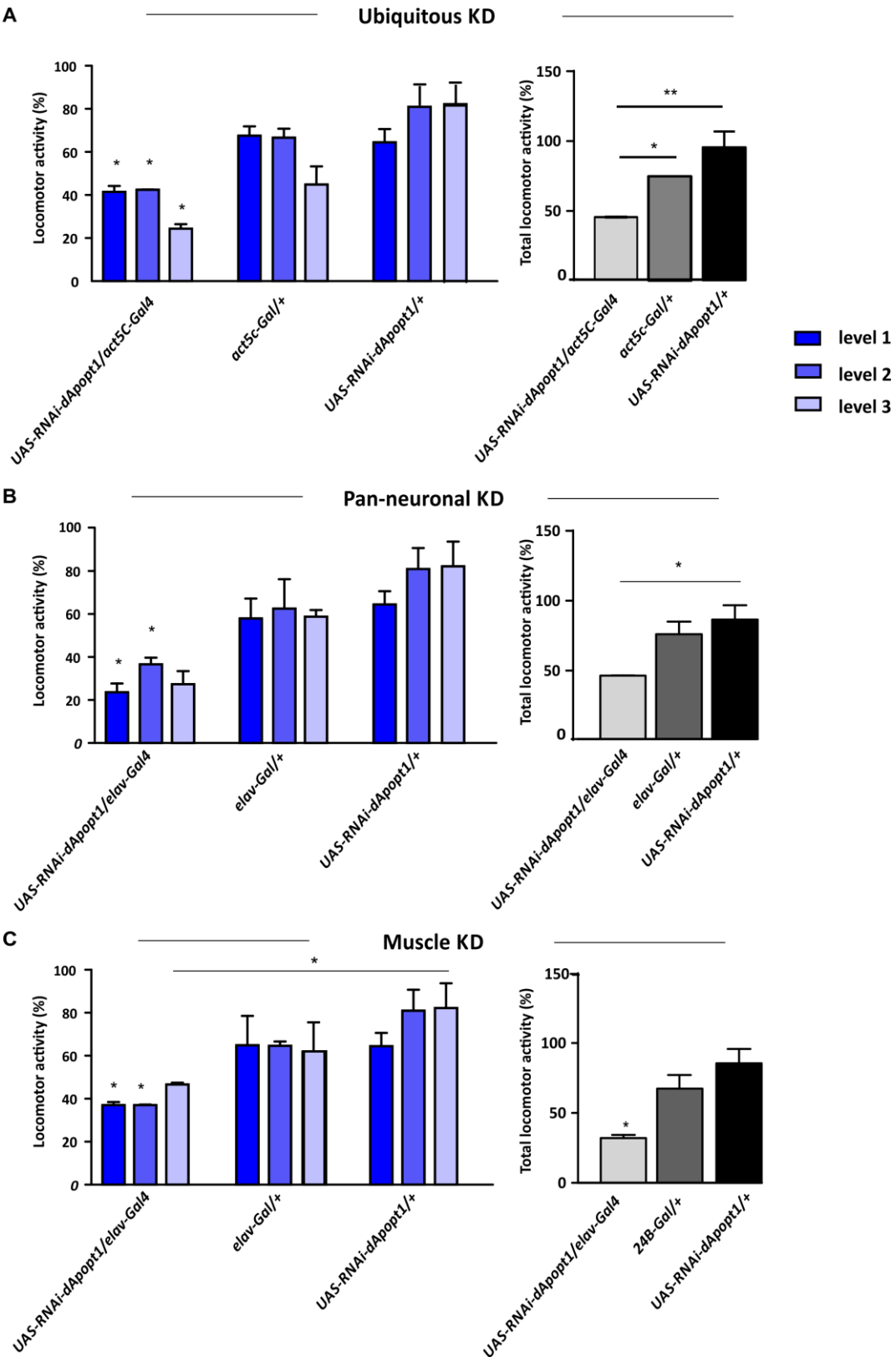

Fig.31 Locomotor activity in *dApopt1* KD flies. Locomotor activity was measured both as negative geotaxis response at three different heights alongside the vials (graphs on the right, blue bars) and as total locomotor activity in two days recording (graphs on the right, grey-black bars) by using three different drivers: **A**, *act5C-Gal4* (ubiquitous *dApopt1* silencing); **B**, *elav-Gal4* (pan-neuronal KD) and **C**, *24B-Gal4* (muscle KD). Data were normalized on the total locomotor activity of the common parental control between three different drivers (*UAS-RNAi-dApopt1*) that it was settled to 100%. Data plotted are means ± SEM of three different experiments (Student's *t* test was performed: * p < 0.05, ** p <0.01, *** *p* < 0.001).

8.5 *dApopt1* knock-down reduces *Cox1* expression and CIV activity

In all the analyzed patients, Melchionda and co-workers documented a profound decrease in COX activity associated with a marked reduction of cIV holocomplex and cIII+cIV supercomplex. Accordingly, we found that ubiquitous *dApopt1* down-regulation *in vivo* (*UAS-RNAI-dApopt1/act5c-Gal4*) caused a strong reduction in COX/CS activity with respect to controls (*act5C-gal4, UAS-RNAI-dApopt1* **Fig.31, A**). Interestingly, in these flies *coI* (*COXI*) transcript level, but not *coII* (*COX2*), were significantly reduced compare to control flies (**Fig. 32, B**).

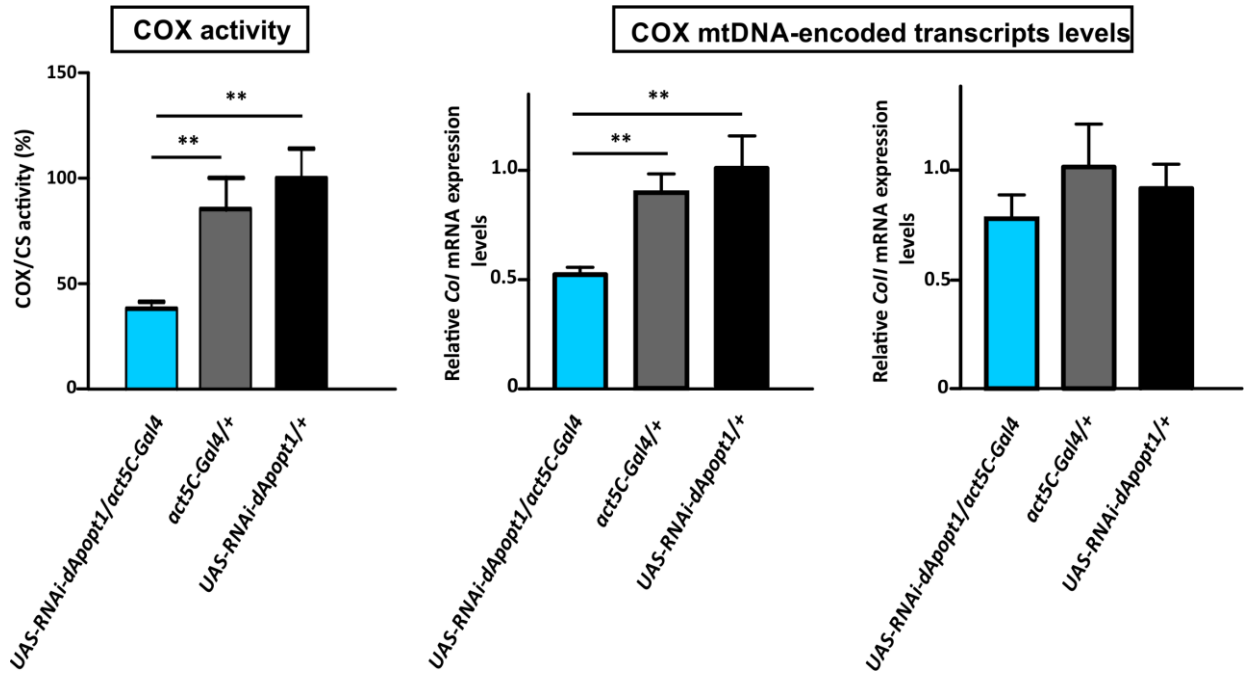

Fig. 32 COX enzymatic activity and mtDNA-encoded genes transcription levels (*coI* and *coII*) in ubiquitous *dApopt1* KD flies. A, COX activity was measured spectrophotometrically in *dApopt1* KD flies (*UAS-RNAi-dApopt1/act5C-Gal4*) and controls (*act5C-gal4* and *UAS-RNAI-dApopt1)*. Data were normalized to citrate synthase (CS) activity. Data plotted are means ± SEM of three biological replicates. **B,** *CoI* (*COX1*) and *CoII* (*COX2*) mRNA expression levels were measured by qRT-PCR in *dApopt1* KD flies (*UAS-RNAi-dApopt1/act5C-Gal4*) and parental controls (*act5C-Gal4* and *UAS-RNAi-dApopt1*). Data plotted are means ± SEM of three biological replicates. (Student's *t* test : * p < 0.05, ** p <0.01, *** *p* < 0.001)

The role of Apopt1 remains still elusive, in spite of some studies that provided insights about its function. Indeed, *Apopt1* over-expression has been shown to induce apoptosis in mouse cells, triggering the release of cytochrome c and caspase activation, whereas, on the contrary, *Apopt1* down-regulation prevented apoptosis (Yasuda *et al*., 2006).

COX deficiency is one of the most common biochemical phenotype associated with human mitochondrial diseases. However, about half of the syndromes characterized by reduced activity of the COX complex are genetically undefined. Furthermore, rare mutations in cytochrome oxidase subunits encoded either by mtDNA or ncDNA genes have been identified, suggesting embryonic lethality. Indeed, early-onset COX deficiencies are often due to mutations in its assembly factors, most of them affecting *SURF1.* Nevertheless, COX deficiency syndromes have been associated also with mutations in genes involved in mtDNA expression and translation. In 2014, for the first time, deleterious mutations in *APOPT1* have been associated to COX deficiency.

Mutations in the *APOPT1* gene have been identified in six patients and are responsible for the onset of a mitochondrial disease (MD) characterized by neurometabolic decompensation, and often encephalopathic episodes accompanied by inability to walk and sit, loss of speech, somnolence, seizure and spastic tetraparesis (Melchionda *et al.*, 2014). Strikingly, a marked increase in mtDNA levels has been observed in a tested patient (Melchionda *et al.*, 2014). At the cellular level, *APOPT 1*-induced mitochondrial disease is characterized by enlarged mitochondria, osmiophilic inclusions and cristae disorganization, whereas at the molecular level the main feature is the reduction in CIV activity (Melchionda *et al.*, 2014).

We exploited Drosophila as a model organism with the aim to shed light on the function of *APOPT1*, studying its fly ortholog, *dApopt1*. To verify whether d*Apopt1* KD could cause an increase in mtDNA amount, we measured mtDNA copy number in flies showing a tissue specific silencing. We used two different Gal4 lines to drive the silencing of *dApopt1* specifically in muscle (*24b-Gal4*) and in central nervous system (*elav-Gal4*). In contrast to humans, we did not observed an increase in mtDNA amount in *dApopt1-RNAi* flies.

Patients affected by mutations in the *APOPT1* and featuring encephalopathic episodes, showed also severe inability to walk (Melchionda *et al.*, 2014). For this reason we tested whether our fly model exhibit motor impairment as well. We analyzed the locomotor behavior of flies with either ubiquitous or tissue-specific *dApopt1* silencing. We found that locomotor activity was dramatically impaired in ubiquitous *dApopt1* KD adult flies. Although less severe, we observed a marked reduction in locomotor activity also in muscle (*24b-Gal4*) and in CNS (*elav-gal4*) *dApopt1* KD flies. These data provide phenotypic similarity between the clinical manifestations in human patients and our fly model.

Melchionda *et al.* (2014) also suggested that APOPT1 could play a role in response to oxidative stress. Indeed, treatment with H_2O_2 increases APOPT1 accumulation within mitochondria, whereas, its over-expression reduced ROS production under oxidative stress conditions. *Apopt1*-deficient fibroblast showed

increased levels of ROS production. Thus, APOPT1 could be involved in the control of ROS production and/or as ROS scavenger. To test whether also the fly ortholog is involved in homeostatic response to oxidative stress, we measured *dApopt1* expression levels in wild-type flies (Oregon R) exposed to 1% H_2O_2 for 10 h and in untreated controls. Interestingly, *dApopt1* expression increased under oxidative stress conditions suggesting a possible conserved molecular function of Drosophila and human protein.

COX deficiency represents a biochemical hallmark of mitochondrial disorders, and it has been reported also in patients affected by mutations in the *APOPT1* locus (Melchionda *et al*., 2014). Fibroblasts from patients with mutations in this gene showed a decreased amount of COX holocomplex with a strong reduction in cIV activity. (Melchionda *et al*., 2014). Notably, also CIV activity showed a marked decrease in *dApopt1*-KD flies, consistently with a potential role in cIV assembly/stability. We also measured transcript levels of *CoI* and *CoII* in ubiquitous *dApopt1* KD flies. A marked reduction in *CoI* but not *CoII* expression was observed.

Finally, we found that *dApopt1* KD flies showed features characteristic of the human disease, such as locomotor impairment and COX deficiency. Moreover, we demonstrated that d*Apopt1* expression is induced by oxidative stress. However, the link between dApopt1 (and APOPT1) and complex IV and how this protein is involved in the apoptosis process, remains still elusive. Thus, Drosophila could be a reliable model to clarify the functional role of this protein.

10.1 *In silico* analysis of dMpv17 sequence

Multiple protein sequences alignment was performed using the ClustalW program which calculates the best match for the selected sequences, and lines them underlined identities, similarities and differences (Larkin, 2007). The phylogenic tree was constructed exploiting the Mega 7 software (Kumar et al., 2016), suited for analyzing DNA and protein sequence data from species and populations. To analyze the secondary structure of dMpv17 we applied Jpred4 prediction program (Drozdetskiy *et al.*, 2015). The TMpred program, based on the statistical analysis of TMbase, a database of naturally occurring transmembrane proteins (Hofmann and Stoffel, 1993), was applied for prediction of membrane-spanning regions and their orientation. Pfam, a large collection of protein families, each represented by *multiple sequence alignments* and *hidden Markov models (HMMs)* (Finn *et al.*, 2016), was used to identify protein domains. Protein phosphorylation sites were predicted using the NetPhos 3.1 server which produces neural network predictions for serine, threonine and tyrosine phosphorylation sites in eukaryotic (Bloom *et al*., 1999). The probability of export to mitochondria was predicted using MitoProt (Claros *et al*., 1996). MitoFates was used to predict mitochondrial presequence, a cleavable localization signal located in N-terminal, and its cleaved position (Fukasawa *et al.*, 2015).

10.2 Fly stocks and breeding conditions

Drosophila lines were raised on standard cornmeal medium (1 litre: 50 g inactivated yeast powder, 8.5 g agar, 72 g cornmeal, 79.3 g sucrose, 13.5 ml Nipagin in 75% ethanol) and maintained at 23°C under a 12hr:12hr light:dark cycle. The *UAS-RNAi* fly's strains (*104377/KK*, *31101/GD*, *100605/KK*, and *45106/GD*) used to perform post-transcriptional silencing were obtained from the Vienna *Drosophila* RNAi Center (VDRC). w^{1118}, *Gal4* strains (*elav*-C155 BL458, *daughterless* BL8641, *Act5C* BL3954, *how24B* BL1767) and 638 line were obtained from the Bloomington Drosophila Stock Center. *ppl-Gal4* line was a gift from Michael Pankratz (Department of Molecular Brain Physiology and Behavior Life & Medical Sciences Institute (LIMES), University of Bonn).

10.3 Total RNA Isolation and quantitative Real Time PCR (qRT-PCR)

Total RNA was extracted in triplicate from ~10 larvae (3^{rd} instar)/adult flies (5 days old) or 2×10^6 cells (3 days after RNAi treatment or transfection) using TRIzol (Thermo Fisher) and further purified by precipitation with 8 M LiCl in order to reduce the contamination of carbohydrates. For each sample, 1 µg of total RNA was used for first strand cDNA synthesis, employing 1 µl of deoxynucleotides (dNTPs) 10 mM, 1 µl of random examers 300 ng/µl (Thermo Fisher) and 1 µl of SuperScript II [200U/µl] enzyme (Thermo Fisher)

following manufacturer's instructions. qRT-PCRs were performed in triplicate in a 7500 Real Time PCR system (Applied Biosystems, Thermo Fisher) using SYBR Green chemistry (Promega). The $2^{-\Delta\Delta Ct}$ (relative quantification) method implemented in the 7500 Real Time PCR system software was used to calculate the relative expression ratio (Livak and Schmittgen, 2001).

All oligonucleotides used were designed using the on-line Primer3 software (http://bioinfo.ut.ee/primer3/) and are listed in **tab. 10**.

Tab.10 Primer used in this work.

Primer	Sequence (5'-3')
dMpv17 F	GTTTCGGCATCGTTGGACTG
dMpv17 R	CAGCATTTTGGTAACGCCCC
Rp49 F	ATCGGTTACGGATCGAACAA
Rp49 R	GACAATCTCCTTGCGCTTCT
Drp1 F	ATCCACGTCGCCTCACTG
Drp1 R	AATACGATTTGATCAGGTGTTCG
Fis1 F	TGATCAAGTTCGCTCCCTAGA
Fis1 R	CGCCAAGTACTAAAGCTGCTC
Mfn (Marf) F	ACGAATTGCTTCTGCCAAGT
Mfn (Marf) R	CGCCAGTTGTTTGATGTTCA
Opa1 F	TGCACAGTCAGGTTCTCAAAA
Opa1 R	TATGAATTCCTGCTGCAACG
PINK1 F	GATATTGCGGCAAATGTGGT
PINK1 R	CGAAAGGAGCCACTGTAGGA
parkin F	GCCTGCACGGATGTGAGT
parkin R	AAACGGGAACGGCAATAAT
ND1 F	TGAAACTAATCGGAATCCTTTTG
ND1 R	AAGCCAAACCCCCTCTTCTA
ND5 F	TGCTATAACTAAAAGAGCTCAGATTCC
ND5 R	AAGAATGAACTAAAGCAGAAACAGG
dApopt1 F	CAATAAGCGCTTCTACGAGAA
dApopt1 R	CCAGTTCTTGTCGAGGAACG
CoI F	ATTGGCTGGAATACCTCGAC
CoI R	GCTGGTGGAGTATTTTGGTA
CoII F	AAAAAGAATCGGCCATCAAT
CoII R	TTTAATCGTCCAGGTGTACCG

10.4 Quantification of mtDNA copy number

DNA (genomic and mitochondrial) from larvae (3rd instar)/adult flies (5 days old) was extracted in triplicate using phenol/chloroform precipitation. The amount of mtDNA was assessed by the ratio of mtDNA with respect to nuclear DNA (nDNA) copy number determined by quantitative real time amplification of the mitochondrial *16S* gene and the nuclear *Rpl32* gene (**Tab. 11**). We generated two gene-specific calibration curves with six 10-fold serial dilutions (100–10.000.000) of plasmids containing the cloned target sequences. Concentration of plasmid stock solutions was assessed with an ND-1000 spectrophotometer (NanoDrop), and the plasmid copy number of dilutions was calculated using Avogadro's number. Reactions were performed in triplicate using SYBR Green chemistry (GoTaq qPCR Master Mix, Promega) in a 7500 Real Time PCR System instrument (Applied Biosystems, Thermo Fisher).

Tab. 11 Primer used for mtDNA copy number quantification.

Primer	Sequence (5'-3')
Rpl32 F	AGGCCCAAGATCGTGAAGAA
Rpl32 R	TGTGCACCAGGAACTTCTTGAA
16S F	AAAAAGATTGCGACCTCGAT
16S R	AAACCAACCTGGCTTACACC

10.5 Behavioral analysis: lifespan, locomotor activity and bang sensitivity

10.5.1 Lifespan of fruit flies

Lifespan was assayed as in Broughton *et al*. 2005. All flies were reared at standard low density, and virgins were collected in a five hours window. Adults of the same sex were kept at a density of 10 per vial (for a total of 100 individuals). Flies were transferred to fresh medium, without anaesthesia, three times per week and deaths were scored.

10.5.2 Analysis of locomotor activity

Single male flies were placed into small glass tubes containing a gel as a source of food and water. Groups of 32 such glass tubes were then loaded into Trikinetics® locomotor activity monitors in an incubator at T=25°C, light/dark cycles of 12 hours, for 3 days. Every time a fly crossed an infrared light beam cast across the glass tube, this was registered as a bout of activity. Bouts were collected in 30 min intervals (bins). Three independent replicates were performed.

For *dApopt1* KD flies locomotor activity analysis, groups of ten male flies were placed in standard glass Drosophila vial. A fly-food mixture was casted into the closed end. The vial was placed into a Drosophila population monitor (Trikinetics®). As the flies walked back and forward along the walls of the tube, they interrupted the infrared beam rings which cross in 3 places along its length. These beam interruptions were detected and registered as a bout of activity. The multiple beam rings provided measurements at 3 different positions relative to the food and tube ends, thus, it allowed flies negative geotaxis response analysis.

10.5.3 Bang test analysis

In order to assay sensitivity to mechanical stimulation (Glasscock and Tanouye, 2005), on the night before the experiment, groups of five CO_2-anesthesized flies of each sex (5 days old) were placed in clean plastic vials containing a strip of moistened tissue paper. The next day, the paper was removed and each vial was placed in a vortex at the maximum intensity for 10 seconds. The vial containing the vortexed flies was then placed upright into a graduated cylinder and videotapes were recorded for a 30 seconds. The number of individuals able to recover from the mechanical shock and climb the vial to reach each distance markings along the graduated cylinder was counted.

10.6 Isolation of mitochondria from fruit flies

200 larvae (3rd instar) or 200 adult flies (5 days old) were harvested and homogenized using a Dounce glass potter and loose fitting pestle. A mannitol-sucrose buffer (225 mM mannitol, 75 mM sucrose, 5mM Hepes pH 7.4) in 2% bovine serum albumin (BSA) was then added to a final volume of 25 ml. Samples were centrifuged at 1.500xg (Beckman Avanti J-25 Centrifuge, Beckman 2550 rotor) at 4°C for 6 minutes. The pellet was discarded by filtering the sample through a fine mesh, and the supernatant centrifuged at 7.000xg at 4°C for 6 minutes. The pellet was re-suspended in 20 ml of mannitol-sucrose buffer without BSA before being centrifuged at 7.000xg under the same conditions as above and re-suspended in 50 µl of buffer. All these steps were performed in a cold room at 4°C.

10.7 Cloning of *dMpv17*-HA and *dApopt1*-GFP in expression vectors and transfection

HA-tagged form of *dMpv17* was cloned into pACT (Promega) and pAc5-STABLE2-neo (pAc5-STABLE2-neo was a gift from Rosa Barrio & James Sutherland (Addgene plasmid # 32426)) (Gonzàlez *et al*., 2011) vectors for constitutive expression once transfected into Drosophila S2R+ cells. GFP-tagged *dApopt1* was cloned in pAc5-STABLE2-neo plasmid. Cloning was performed using In-Fusion® HD Cloning kit (Clontech) following the manufacturer's instruction. The enzyme mix contained in that system non-specifically recognizes the presence of identical sequences at the ends of a PCR fragment and a linearized plasmid vector and then

links both together in a 5–10-minute reaction. PCR primers were designed in such a way that they generate PCR products containing ends that were homologous to specific sequences of the vectors (**Tab. 12**). Cells were transfected using CellFectin II Reagent (Invitrogen) following manufacturer's instruction. Briefly, 800,000 cells were seeded on 24-wells plate on the day before transfection. Cells were then transfected with 10 µl of CellFectin II Reagent and 1 µg of vector in serum-free medium and incubated for 6 h. The medium was removed and replaced with complete Schneider's Drosophila medium (containing 10% heat-inactivated FBS). Cells were grown for two-three days before being used for the analysis.

UAS-dMpv17-HA line was constructed by cloning (using In-Fusion® HD Cloning kit, Tab.9) the entire Drosophila *dMpv17* coding sequence into pUAST vector (for constitutive expression of the construct *in vivo* under Gal4 control). The construct was injected into w^{1118} embryos for germline transformation (BestGene Inc., Chino Hills, California). Multiple isolated lines were obtained and assessed for *dMpv17*-HA expression by qRT-PCR and western blot.

Tab. 12 Primer used for *dMpv17* and *dApopt1* cloning.

Primer	Sequence (5'-3')
pUAST F	CAGATCTGCGGCCGCATGAAGAGACTTAAAGCGTA
pUAST R	AGAGGTACCCTCGAGTTAAGCGTAATCTGGAACATCGTATGGGTAGCTATTAAGTATCATGGA
pACT F	CAGAGACCCCGGATCCATGAAGAGACTTAAAGCGTA
pACT R	GATGAATTCGAGCTCTTAAGCGTAATCTGGAACATCGTATGGGTAGCTATTAAGTATCATGGA
pAc5-STABLE2-neo F (*dMpv17*)	TAGTCCAGTGTGGTGGAATTCATGAAGAGACTTAAAGCGTA
pAc5-STABLE2-neo R (*dMpv17*)	CACCATGGTGGCTCTAGAAGCGTAATCTGGAACATCGTATGGGTAGCTATTAAGTATCATGGA
pAc5-STABLE2-neo F (*dApopt1*)	TAGTCCAGTGTGGTG*GAATTC*ATGAACAAATGTTTTAGGTGC
pAc5-STABLE2-neo R (*dApopt1*)	CACCATGGTGGC*TCTAGA*AGATCTTCGCTTGGCC

In green: sequences homologous to the vector; in yellow: sequences specific to the target gene; in red: HA tag sequence).

10.8 Western Blot analysis

Flies homogenates, cell or mitochondrial pellets were lysed in 150 mM NaCl, 20 mM Tris, pH 7.4, 5 mM EDTA-Tris, 10% glycerol, 1% Triton X-100, supplemented with protease and phosphatase inhibitor cocktails (Sigma), and kept on ice for 30 minutes. Suspensions were then centrifuged at maximum speed for 15 minutes at 4°C. Proteins concentration was measured by Bradford assay. NuPAGE® LDS Sample Buffer 1X (Thermo Fisher Scientific) and DTT (to a final concentration of 200 µM) were added to 25 µg of protein extract. Samples were separated by SDS-PAGE and transferred electrophoretically to nitrocellulose membranes. The membrane was blocked for one hour at room temperature in 5% non-fat dry milk. Primary

antibodies (**Tab. 13**) were diluted in PBS containing 1% non-fat dry milk and incubated overnight at 4°C. For detection, secondary antibodies conjugated with HRP were used (1:5000), and immunoreactivity was visualized with ECL chemiluminescence.

Tab. 13 Antibodies used in this work.

Primary antibody	Secondary antibody
mouse α-HA (Sigma, cod. H9658), 1:1000	α-rabbit IgG (BioRad, cod. 170-6515)
mouse α-ATP5 (Abcam, cod. 14747), 1:1000	α-mouse IgG (Sigma, cod. A4416)
mouse α-HSP70 (Sigma, cod. HC147), 1:5000	
rabbit α-OPA1 (Abcam, cod. 42364), 1:500	
rabbit α-Marf (gift from E. Ziviani Lab), 1:1000	
mouse α-Parkin (gift from E. Ziviani Lab), 1:1000	
mouse α-Ref2p (p62) (gift from A. Brech Lab), 1:5000	

10.9 Cell Cultures

Drosophila S2R$^+$ cells derive from a primary culture of late stage (20–24 hours old) Drosophila embryos and were obtained from the Drosophila Genomics Resource Center (DGRC, Indiana University, Bloomington Campus, USA). S2R$^+$ cells were grown at 25°C in Schneider's Drosophila Medium (Thermo Fisher) with 10% heat-inactivated Fetal Bovine Serum (FBS) (Sigma). Cells presented as a loose semi-adherent monolayer, with a doubling time of about 48 hours. Where indicated, cells were treated with 10 µM **c**arbonyl cyanide m-chlorophenyl hydrazone CCCP for 2 hours or 24 hours.

10.10 dsRNA Production and RNAi transfection

Double-stranded RNAs (dsRNAs) were preparing employing the T7 MEGA script kit (Ambion). The oligonucleotide primers used to synthesize dsRNA starting from cDNA were *dMpv17*_T7 forward (F) and reverse (R) (**Tab. 14**) possessing a T7-promoter sequence overhang. These primers give two complementary 600 bp RNA products that anneal each other forming a final 600 bp dsRNA. About 3 × 10^6 cells were treated with 5 µg of dsRNA in serum-free medium and incubated at room temperature for 1 h. Subsequently, 1 volume of complete medium (2×) was added, and cells were grown in the presence of dsRNA for 3 days at 25 °C and then used for subsequent analysis. dsRNA of human *insulin like growth factor binding protein 2* (*IGFBP2)* gene was used as mock control.

Tab.14 Primers used for dsRNA synthesis.

Primer	Sequence (5'-3')
***dMpv17*_T7 F**	TTAATACGACTCACTATAGGGAGATGTAACACGAACAACAGCAAATCG
***dMpv17*_T7 R**	TTAATACGACTCACTATAGGGAGAATGGATGAACTGGGCGTAGAGCAC
***IGFBP2*_T7 F**	TTAATACGACTCACTATAGGGAGATGTAGACAATGGCGATGACCACTC
***IGFBP2*_T7 R**	TTAATACGACTCACTATAGGGAGAATGGTTTTCTGCCGGTGTTTGGAG

In yellow: T7 promoter sequence.

10.11 Immunocytochemistry

10.11.1 dMpv17 localization

48 hr after transfection, cells were washed once in PBS and incubated with 100 nM MitoTracker® Red CMXROS (Thermo Fisher) and 1 µg/ml cyclosporin H in Schneider's Drosophila Medium for 20 minutes. Cells were then washed once in PBS and fixed in 4% paraformaldehyde (PFA) for 20 minutes. Cells were washed again in PBS and permeabilized for 5 minutes with 50 mM NH_4Cl in PBS + 0.1% Triton X-100. Cells were then blocked for 1 hour in 3% goat serum in PBS, washed again, and incubated overnight in 1:100 monoclonal mouse α-HA antibody (Sigma, cod. H9658) at 4°C. Cells were washed other three times with PBS and then incubated with 1:500 Alexa Fluor®488 α-mouse IgG (Thermo Fisher) with 2% goat serum for 45 minutes at room temperature. After three final washes in PBS, the slides were mounted with Vectashield mounting medium (Vector laboratories, Inc). Images were taken with a Zeiss LSM700 confocal microscope (Dept. Biology, University of Padova) at 63X magnification and analyzed with Image J software.

10.11.2 Treatment with the protonophore carbonyl cyanide m-chlorophenyl hydrazone (CCCP)

Two days after appropriate RNAi probe treatment, S2R+ cells were treated with CCCP for 24 hours. After treatment the medium was removed and cells were fixed with 4% paraformaldehyde for 10 minutes at room temperature. Cells were permeabilized with 0.2% TritonX-100 (Sigma) in PBS for 10 minutes at room temperature and, then, incubated with blocking solution (2% goat serum, 0.2% Triton-100 in PBS) for 30 minutes. Cells were incubated for 1 hour at room temperature using specific primary antibody against ATP-5a (Abcam, cod. 14747). An appropriate secondary fluorochrome-conjugated antibody was added in blocking solution for 1 hour at room temperature (Alexa Fluor® 568 α-mouse, Thermo Fisher cod. A11031, 1:500). Images were acquired on a Zeiss LSM700 confocal microscope (Dept. Biology, University of Padova).

10.12 Measurements of Oxygen Consumption and respiratory chain complexes activity

Oxygen measurements were made using the XF24 Extracellular flux analyzer (Seahorse Bioscience). Measurements were performed in $S2R^{+}$ Drosophila cells. The instrument was maintained at 25 °C. Sensors of Seahorse XF Calibration Plate (Bioscience) were hydrated overnight in 1 mL XF calibrant (Bioscience). Cells were seeded onto XF-24-well plates at 20.000 cells/well and cultured for 48 hours. The day of the experiment, the culture medium was replaced with serum-free Schneider medium (Thermo Fisher). Basal oxygen consumption rates (OCR), reported in the unit of picomoles/minute, were measured three times before injecting the first drug that has to be tested. Thus, OCR was measured after stimulation with 10 mM glucose, 1 µM FCCP, and 5 µM rotenone plus 5 µM antimycin A.

The enzymatic activities of Complexes I–V and Citrate Synthase were measured as described in Spinazzi *et al.* 2012, "Assessment of mitochondrial respiratory chain enzymatic activities on tissues and cultured cells" (*Nature protocols*).

Complex I (CI, NADH:ubiquinone oxidoreductase)

For complex I activity measurement, isolated mitochondria were subjected to three cycles of freeze-thawing in hypotonic buffer in order to maximize the enzymatic rates. 5 µg of mitochondria were added to 100 µl of potassium phosphate buffer (0.5 M, pH 7.5), 60 µl of fatty acid–free BSA (50 mg/ml), 30 µl of KCN (10 mM) and 10 µl of NADH (10 mM) and the volume was adjusted to 994 µl with distilled water. In parallel, a separate cuvette containing the same quantity of reagents and sample but with the addition of 10 µl of 1 mM rotenone solution was prepared. After mixing, the baseline was read at 340 nm for 2 minutes. The reaction was started by adding 6 µl of ubiquinone (10 mM) and the decrease in absorbance was followed at 340 nm for 2 minutes.

Complex II (CII, succinate dehydrogenase)

50 µl of potassium phosphate buffer (0.5 M, pH 7.5), 20 µl of fatty acid–free BSA (50 mg/ml), 30 µl of KCN (10 mM), 50 µl of succinate (400 mM),5 µg of the sample, and 145 µl of DCPIP (0.015% (wt/vol)) were adjust to the volume of 996 µl with distilled water. After mixing, the cuvette was incubated at 37 °C for 10 minutes. The baseline activity was read at 600 nm for 2 minutes. Then, the reaction was started by adding 4 µl of 12.5 mM DUB and the decrease in absorbance was followed at 600 nm for 3 minutes. The specificity of complex II activity was determined by running the assay after the addition of 10 µl of either 1 M malonate or 50 mM TTFA before starting the reaction.

Complex III (CIII, decylubiquinol cytochrome *c* oxidoreductase)

50 µl of potassium phosphate buffer (0.5 M, pH 7.5), 75 µl of oxidized cytochrome *c*, 50 µl of KCN (10 mM), 20 µl of EDTA (5mM, pH 7.5), 10 µl of Tween-20 (2.5% (vol/vol)), and 5 µg of mitochondria were adjust to 990 µl with distilled water. In parallel, a separate cuvette containing the same quantity of reagents and sample but with the addition of 10 µl of 1 mg/ml antimycin A was prepared. The baseline was read at 550 nm for 2 minutes. The reaction was started by adding 10 µl of 10 mM decylubiquinol and observing the increase in absorbance at 550 nm for 1–2 minutes.

Complex IV (CIV, cytochrome *c* oxidase)

500 µl of potassium phosphate buffer (100 mM, pH 7.0) and 60 µl of reduced cytochrome *c* (1 mM) were added to 400 µl of distilled water and the baseline activity was read at 550 nm for 2 minutes. The volume was then adjusted to 995 µl with distilled water. The reaction was started by adding 5 µg of sample (diluted in homogenization buffer) and monitoring the decrease in absorbance at 550 nm for 3 minutes. To check the specificity of complex IV activity, 30 µl of 10 mM KCN was added in a separate reaction prepared as described.

Citrate synthase (CS)

300 µl of distilled water, 500 µl of Tris (200 mM, pH 8.0) with Triton X-100 (0.2% (vol/vol)), 100 µl of DTNB, 30 µl of Acetyl CoA (10 mM) and 10 µg of mitochondria were adjusted to 950 µl with distilled water. The baseline was read at 412 nm for 2 minutes. The reaction was started by adding 50 µl of 10 mM oxaloacetic acid and monitoring the increase in absorbance at 412 nm for 3 minutes.

10.13 ROS amount, mitochondrial mass and membrane potential measurement

Cells were transferred into suspension by using trypsin EDTA solution (GIBCO) and collected by centrifugation. The cell pellets were resuspended at 1 x 10^6 cells/ml in either complete medium or with Earle's modified buffered saline solution with equimolar replacement of NaCl with KCl (KBSS; 170 mM KCl, 1.82 $CaCl_2$, 0.83 mM $MgSO_4$, 1 mM NaH_2PO_4, 26.2 mM $NaHCO_3$, pH 7.6-7.8) supplemented with D-Glucose 5.55 mM. Cells were labeled in open tubes in complete medium with MitoSOX (Molecular Probes) at 5 mM for 20 min in a 37°C 5.0% CO2 humidified atmosphere, washed 3 times with complete medium at 37°C and analyzed by flow cytometry. Cells were labeled for 30 min in open tubes in Glucose supplemented KBSS with either Mitotracker green, or Tetramethyl Rhodamine Ester (TMRE), or JC1 at 25 nM, 0.2 µM, and 2µM, respectively, in a 37°C 5.0% CO2 humidified atmosphere. Cells labeled with Mitotracker green and TMRE were washed once with Glucose supplemented KBSS and further incubated at 37°C as described above for

30 min before flow cytometry analysis. Cells labeled with JC1 were washed twice before further incubation for 30 min at 37°C as described above before flow cytometry analysis. Stained samples were analyzed by using a CYAN flow cytometer and the Summit software (DAKO). For each cell type 3 replicates were performed and the median MitoSOX, Mitotracker green and TMRE fluorescence intensity (MFI) of each sample was determined. The percentage of cells displaying low red JC1 fluorescence was calculated for each sample. The analysis was performed in collaboration with dr. Patrizio Castagnola (A.O.U. San Martino - IST, Istituto Nazionale Ricerca sul Cancro, Genova).

10.14 dNTP Pools Extraction and Analysis

At the end of the treatment with dsRNA, about 10×10^6 $S2R^+$ cells were centrifuged in 15-ml tubes for 10 minutes at 400 × *g*, and the pellet was washed twice with ice-cold PBS. The cells were then re-suspended in 200 µl of extraction buffer (0.21 M mannitol, 0.07 M sucrose, 0.2 M ethyleneglycol-bis(2-aminoethylether)-N,N,N',N'-tetraacetic acid EGTA, 10 mM Tris-HCl, pH 7.5, 0.5% BSA), and a suspension of glass beads (0.1 mm diameter), corresponding to about half of the volume of the cellular pellet, was added. The cell/bead suspension was introduced in a Bullet Blender Storm homogenizer (Next Advance) and shaken for 2 minutes at speed 8, and then 400 µl of extraction buffer were added, and the glass beads were removed by a short centrifugation. Mitochondrial and cytosolic nucleotide pools were isolated from the whole cell homogenate by differential centrifugation and methanol extraction (Pontarin *et al*., 2003). All manipulations took place in a cold room. The pellet remaining after mitochondrial pool extraction was dissolved in 1 ml of 0.3 M NaOH. The $A_{260\ nm}$ of the NaOH fraction was used to normalize the number of cells from which the pools of the different samples were extracted. The sizes of the dNTP pools were determined with a DNA polymerase-based assay (Ferraro *et al*., 2010). The A_{260} nm of the NaOH fraction was used to normalize the number of cells from which the pools of the different samples were extracted. Two different aliquots of each pool extract were analysed, and pool sizes were expressed as pmol of dNTPs/million cells or pmol/OD NaOH. dNTPs pool extraction and analysis was performed in collaboration with Dr. Chiara Rampazzo (Dept. Biology, University of Padova).

10.15 Analysis of the mitochondrial network and morphology

10.15.1 Confocal microscopy

Cells were plated on imaging dishes reaching 70-80% of confluence the day of the experiment. For mitochondrial morphology analysis, live cells were incubated with Mitotracker green FM (Thermo Fisher) and imaged live in grown medium. Analysis of mitochondrial morphology was performed by using Image J software. Cells displayed an intact network of tubular mitochondria were classified as tubular. When this

network was disrupted and mitochondria appeared globular they were classified as fragmented. The mitochondria morphology of the cells was determined in a blinded manner in collaboration with dr. Joy Chakraborty (Dept. of Biology in the lab of Prof. Elena Ziviani, University of Padova). Quantification was based on 150 cells from three independent experiments.

10.15.2 Electron microscopy (EM)

Cells were fixed for 1 hour using a fixation solution containing 2.5% glutaraldehyde in sodium cacodylate buffer. Samples were washed in 0.1 M cacodylate buffer pH 7.4, and then post-fixed for 1 hour at room temperature with 1% OsO4 in 0.1 M sodium cacodylate buffer (pH 7.4). Cells were washed once with water and then incubated in 1% uranyl acetate in H2O for 1 hour at room temperature. Subsequently, cells were dehydrated through an ethanol gradient. Finally, the samples were embedded in Epon resin (Sigma) and polymerized at 60°C overnight. EM analysis was performed in collaboration with dr. Katia Cortese and dr. Cristina Gagliani (Dept. Experimental Medicine/Human Anatomy, University of Genova).

10.15.3 Correlative microscopy

Cells were transfected as in (7) with pAc5-STABLE2-neo vector expressing dMpv17-GFP and then transferred to glass bottom dishes provided with *gridded coverslips* (MatTek Corporation). After three days of transfection cells were fixed in 2.5% glutaraldehyde in sodium cacodylate buffer for one hour. Cells were imaged with a fluorescent microscope and the fields containing GFP positive cells were acquired. EM analysis was performed in GFP positive cells to determine mitochondria morphology.

10.16 Immunoprecipitation (IP) and proteomic analysis

Mitochondria isolated from flies over-expressing dMpv17-HA and parental controls were lysed in lysis buffer (150 mM NaCl, 5 mM EDTA, 50 mM HEPES (pH: 7.4), 0.5% Triton X-100 and protease inhibitors (Roche) for 30 minutes on ice to obtain whole cell extract. Lysates were cleared by centrifugation at 4°C for 15 minutes at maximum speed. About XX mg of mitochondrial lysate was used for IP. Lysates were incubated with XX of anti-HA resin (Sigma) overnight at 4°C. Beads were washed three times with lysis buffer (without detergent). After washing, 2X SDS loading buffer was added and the samples were boiled for 10 minutes. Samples were separated on a SDS-PAGE gel (Thermo Fisher) and the gel stained with Coomassie (DITTA???) prior to proteomic analysis. Proteomic analysis was performed by Proteomic core facility-EMBL (Heidelberg, Germany, https://www.embl.de/proteomics/proteomics_services/). Bands were excised from the gel and in-gel digested with trypsin followed by tandem mass tags (TMT) labelling. Isobarquant (Breitwieser and Colinge, 2013) and Mascot software (Perkins *et al*., 1999) were used for

protein identification. This analysis was performed by dr. Frank Stein (Computational Scientist, Proteomics Core Facility, EMBL, Heidelberg, Germany).

10.17 dMpv17 protein activity in lipid bilayer

10.17.1 *In vitro* expression and purification of dMpv17 protein

dMpv17 coding sequence was cloned into pIVEX 1.3 WG vector (Roche) by using In-Fusion® HD Cloning kit (Clontech) following the manufacturer's instructions. The generated expression vectors was sequenced to verify the correctness of the PCR-generated DNA fragment and cloning. *In vitro* expression was performed by using a RTS100 Wheat Germ CECF Kit (5'-PRIME, Fisher Scientific). After expression, the reaction mix was solubilized with 2% LDAO for 90 min at 30 °C under 1400 rpm shaking.

Tab.15 Primer used for *dMpv17* cloning.

Primer	Sequence (5'-3')
***D. melanogaster dMpv17* F**	CCACAACAGCTTGTCGAACCATGAAGAGACTTAAAGCGTA
***D. melanogaster dMpv17* R**	TGATGATGAGAACCCCCCCCCGCTATTAAGTATCATGGAGAG
Human *MPV17* F	CCACAACAGCTTGTCGAACCATGGCACTCTGGCGGGCA
Human *MPV17* F	TGATGATGAGAACCCCCCCCCGAGCCGATGTGCCTTCC

In green: sequences homologous to the vector.

10.17.2 Analysis of dMpv17 activity in lipid bilayer and electrophysiological recording

Electrophysiology experiments were carried out using a Warner Instruments Incorporated electrophysiological planar bilayer apparatus in collaboration with dr. Vanessa Checchetto (Lab of Prof. Ildiko Szabò, Dept. of Biology, University of Padova). Bilayers were prepared using L-α-Phosphatidylcholine in decane (Sigma-Aldrich) containing 1% chloroform (Sigma-Aldrich) across a 250 µM hole in a polystyrene cuvette (Warner Instruments). L-α-Phosphatidylcholine was partially purified by precipitation with cold acetone from a chloroform solution. The bilayer membrane was considered to be satisfactory for further experiment if it exhibited an approximately 150–200 picoFarad capacity. The lipid membrane divided the trans and the cis compartment. All reported voltages refer to the cis chamber, zero being assigned to the trans (grounded) side. The bilayer set up was connected to the external circuit through salt bridges (1 M KCl) with Ag/AgCl electrodes. Unitary currents were recorded using an Axon BC-525C patch clamp amplifier (Warner Instruments Incorporated). Recordings were filtered at 1 kHz, digitized at 300 KHz and analysed with pClamp 8.1 and ORIGIN 6.0 software. Experiments were performed in 150 KCl concentration media and the protein was added to the cis compartment. All measurements were made at room temperature.

10.18 Blue native gel electrophoresis (BNGE)

BNGE was performed in collaboration with dr. Emanuela Bottani (MRC, University of Cambridge) in isolated Drosophila mitochondria. 100 µg of sample were run through a 5–13% nondenaturating gradient (1D-BNGE). For denaturing two-dimensional BNGE electrophoresis, the one-dimensional BNGE lane was excised, treated for 1 hour at room temperature (20 °C) with 1% sodium dodecyl sulfate and 1% β-mercaptoethanol and then run through a 16.5% tricine-sodium dodecyl sulfate–polyacrylamide gel using a 10% spacer gel.

References

1. Abdelwahid E, Rolland S, Teng X, Conradt B, Hardwick JM, *et al.* Mitochondrial involvement in cell death of non-mammalian eukaryotes. *Biochim Biophys Acta*. 2011 Apr; 1813(4): 597–607. doi: 10.1016/j.bbamcr.2010.10.008

2. Ackerman SH, Tzagoloff A. Identification of two nuclear genes (ATP11, ATP12) required for assembly of the yeast F1-ATPase. *Proc Natl Acad Sci U S A*. 1990 Jul; 87(13):4986-4990.

3. Adams JM, Cory S. The Bcl-2 protein family: arbiters of cell survival. *Science*. 1998 Aug 28; 281(5381):1322-1326.

4. Adams JC. Thrombospondins: multifunctional regulators of cell interactions. *Annu Rev Cell Dev Biol*. 2001; 17:25-51. doi: 10.1146/annurev.cellbio.17.1.25

5. Adams JC, Monk R, Taylor AL, Ozbek S, Fascetti N, *et al.* Characterisation of Drosophila thrombospondin defines an early origin of pentameric thrombospondins. *J Mol Biol*. 2003 Apr 25; 328(2):479-494.

6. Adán C, Matsushima Y, Hernández-Sierra R, Marco-Ferreres R, Fernández-Moreno MA, *et al.* Mitochondrial transcription factor B2 is essential for metabolic function in Drosophila melanogaster development. *J Biol Chem*. 2008 May 2; 283(18):12333-12342. doi: 10.1074/jbc.M801342200

7. Aittoniemi J, Fotinou C, Craig TJ, de Wet H, Proks P, *et al.* SUR1: a unique ATP-binding cassette protein that functions as an ion channel regulator. *Philosophical Transactions of the Royal Society B: Biological Sciences*. 2009; 364(1514):257-267. doi:10.1098/rstb.2008.0142.

8. Akabane S, Uno M, Tani N, Shimazaki S, Ebara N, *et al.* PKA Regulates PINK1 Stability and Parkin Recruitment to Damaged Mitochondria through Phosphorylation of MIC60. *Mol Cell*. 2016 May 5; 62(3):371-384. doi: 10.1016/j.molcel.2016.03.037

9. Alexeyev M, Shokolenko I, Wilson G, LeDoux S. The maintenance of mitochondrial DNA integrity—critical analysis and update. *Cold Spring Harb Perspect Biol*. 2013 May; 5(5): a012641. doi: 10.1101/cshperspect.a012641

10. Altmann, R. (1890). Die Elementarorganismen Und Ihre Beziehungen Zu Den Zellen. *Leipzig: Veit & comp*., 145

11. Anderson PR, Kirby K, Hilliker AJ, Phillips JP. RNAi-mediated suppression of the mitochondrial iron chaperone, frataxin, in Drosophila. *Hum Mol Genet*. 2005 Nov 15; 14(22):3397-3405.

12. Anderson PR, Kirby K, Orr WC, Hilliker AJ, Phillips JP. Hydrogen peroxide scavenging rescues frataxin deficiency in a Drosophila model of Friedreich's ataxia. *Proc Natl Acad Sci U S A*. 2008; 105(2):611-616. doi:10.1073/pnas.0709691105.

13. Anderson S, Bankier AT, Barrell BG, de Bruijn MH, Coulson AR, *et al.* Sequence and organization of the human mitochondrial genome. *Nature*. 1981 Apr 9; 290(5806):457-465. doi:10.1038/290457a0

14. Angeles DC, Ho P, Chua LL, Wang C, Yap YW, *et al.* Thiol peroxidases ameliorate LRRK2 mutant-induced mitochondrial and dopaminergic neuronal degeneration in Drosophila. *Hum Mol Genet*. 2014 Jun 15; 23(12):3157-3165. doi: 10.1093/hmg/ddu026

15. Antonenkov VD, Isomursu A, Mennerich D, Vapola MH, Weiher H, *et al.* The Human Mitochondrial DNA Depletion Syndrome Gene MPV17 Encodes a Non-selective Channel That Modulates Membrane Potential. *J Biol Chem*. 2015 May 29; 290(22):13840-13861. doi: 10.1074/jbc.M114.608083

16. Archibald JM. Endosymbiosis and eukaryotic cell evolution. *Curr Biol*. 2015 Oct 5; 25(19):R911-921. doi: 10.1016/j.cub.2015.07.055

17. Arnoult D, Grodet A, Lee YJ, Estaquier J, Blackstone C. Release of OPA1 during apoptosis participates in the rapid and complete release of cytochrome c and subsequent mitochondrial fragmentation. *J Biol Chem*. 2005 Oct 21; 280(42):35742-35750. doi: 10.1074/jbc.M505970200

18. Ashrafi G, Schwarz TL. The pathways of mitophagy for quality control and clearance of mitochondria. *Cell Death Differ*. 2013 Jan; 20(1):31-42. doi: 10.1038/cdd.2012.81

19. Baker MJ, Palmer CS, Stojanovski D. Mitochondrial protein quality control in health and disease. *Br J Pharmacol*. 2014; 171(8):1870-1889. doi:10.1111/bph.12430

20. Barbot M, Jans DC, Schulz C, Denkert N, Kroppen B, *et al.* Mic10 oligomerizes to bend mitochondrial inner membranes at cristae junctions. *Cell Metab*. 2015 May 5; 21(5):756-763. doi: 10.1016/j.cmet.2015.04.006

21. Barel O, Shorer Z, Flusser H, Ofir R, Narkis G, *et al.* Mitochondrial complex III deficiency associated with a homozygous mutation in UQCRQ. *Am J Hum Genet*. 2008 May; 82(5):1211-1216. doi: 10.1016/j.ajhg.2008.03.020

22. Barthélémy C, Ogier de Baulny H, Diaz J, Cheval MA, *et al.* Late-onset mitochondrial DNA depletion: DNA copy number, multiple deletions, and compensation. *Ann Neurol*. 2001 May; 49(5):607-617.

23. Bassett AR, Tibbit C, Ponting CP, Liu JL. Highly efficient targeted mutagenesis of Drosophila with the CRISPR/Cas9 system. *Cell Rep*. 2013 Jul 11; 4(1):220-228. doi: 10.1016/j.celrep.2013.06.020

24. Becker T, Böttinger L, Pfanner N. Mitochondrial protein import: from transport pathways to an integrated network. *Trends Biochem Sci*. 2012 Mar; 37(3):85-91. doi: 10.1016/j.tibs.2011.11.004

25. Bekri S, D'Hooghe M, Vermeersch P. X-Linked Sideroblastic Anemia and Ataxia. In: Pagon RA, Adam MP, Ardinger HH, Wallace SE, Amemiya A, *et al.*, editors. *GeneReviews*. Seattle (WA): University of Washington, Seattle; 1993-2017. 2006 Mar 01 [updated 2014 Apr 03].

26. Bier E. Drosophila, the golden bug, emerges as a tool for human genetics. *Nat Rev Genet*. 2005 Jan; 6(1):9-23. doi:10.1038/nrg1503

27. Blakely EL, Butterworth A, Hadden RD, Bodi I, He L, *et al.* MPV17 mutation causes neuropathy and leukoencephalopathy with multiple mtDNA deletions in muscle. *Neuromuscul Disord*. 2012 Jul; 22(7):587-591. doi: 10.1016/j.nmd.2012.03.006

28. Blom N, Gammeltoft S, Brunak S. Sequence and structure-based prediction of eukaryotic protein phosphorylation sites. *J Mol Biol*. 1999 Dec 17; 294(5):1351-1362. doi: 10.1006/jmbi.1999.3310

29. Bohnert M, Zerbes RM, Davies KM, Mühleip AW, Rampelt H, *et al.* Central role of Mic10 in the mitochondrial contact site and cristae organizing system. *Cell Metab*. 2015 May 5; 21(5):747-755. doi: 10.1016/j.cmet.2015.04.007

30. Borner C. The Bcl-2 protein family: sensors and checkpoints for life-or-death decisions. *Mol Immunol.* 2003 Jan; 39(11):615-647.

31. Brand AH, Perrimon N. Targeted gene expression as a means of altering cell fates and generating dominant phenotypes. *Development*. 1993 Jun; 118(2):401-415.

32. Breitwieser FP, Colinge J. Isobar(PTM): a software tool for the quantitative analysis of post-translationally modified proteins. *J Proteomics*. 2013 Sep 2; 90:77-84. doi: 10.1016/j.jprot.2013.02.022

33. Bridges CB, Anderson EG. Crossing over in the X chromosomes of triploid females of Drosophila melanogaster. *Genetics*. 1925 Sep; 10(5):418-441.

34. Brière JJ, Favier J, El Ghouzzi V, Djouadi F, Bénit P, Gimenez AP, Rustin P. Succinate dehydrogenase deficiency in human. *Cell Mol Life Sci*. 2005 Oct; 62(19-20):2317-2324. doi: 10.1007/s00018-005-5237-6

35. Brosius U, Dehmel T, Gärtner J. Two different targeting signals direct human peroxisomal membrane protein 22 to peroxisomes. *J Biol Chem*. 2002 Jan 4; 277(1):774-784. doi: 10.1074/jbc.M108155200

36. Broughton SJ, Piper MD, Ikeya T, Bass TM, Jacobson J, *et al.* Longer lifespan, altered metabolism, and stress resistance in Drosophila from ablation of cells making insulin-like ligands. *Proc Natl Acad Sci U S A*. 2005 Feb 22; 102(8):3105-3110. doi: 10.1073/pnas.0405775102

37. Buchon N, Silverman N, Cherry S. Immunity in Drosophila melanogaster--from microbial recognition to whole-organism physiology. *Nat Rev Immunol*. 2014 Dec; 14(12):796-810. doi: 10.1038/nri3763

38. Burman JL, Itsara LS, Kayser EB, Suthammarak W, Wang AM, *et al.* A Drosophila model of mitochondrial disease caused by a complex I mutation that uncouples proton pumping from electron transfer. *Dis Model Mech*. 2014 Oct; 7(10):1165-1174. doi: 10.1242/dmm.015321

39. Caggese C, Ragone G, Perrini B, Moschetti R, De Pinto V, *et al.* Identification of nuclear genes encoding mitochondrial proteins: isolation of a collection of D. melanogaster cDNAs homologous to sequences in the Human Gene Index database. *Mol Gen Genet*. 1999 Feb; 261(1):64-70.

40. Calvo S, Jain M, Xie X, Sheth SA, Chang B, *et al.* Systematic identification of human mitochondrial disease genes through integrative genomics. *Nat Genet*. 2006 May; 38(5):576-582. doi: 10.1038/ng1776

41. Calvo SE, Clauser KR, Mootha VK. MitoCarta2.0: an updated inventory of mammalian mitochondrial proteins. *Nucleic Acids Res*. 2016 Jan 4; 44(D1):D1251-1257. doi: 10.1093/nar/gkv1003

42. Cavanaugh DJ, Vigderman AS, Dean T, Garbe DS, Sehgal A. The Drosophila circadian clock gates sleep through time-of-day dependent modulation of sleep-promoting neurons. *Sleep*. 2016 Feb 1; 39(2): 345–356. doi: 10.5665/sleep.5442

43. Celotto AM, Frank AC, McGrath SW, Fergestad T, Van Voorhies WA, *et al.* Mitochondrial encephalomyopathy in Drosophila. *J Neurosci*. 2006 Jan 18; 26(3):810-820. doi: 10.1523/JNEUROSCI.4162-05.2006

44. Chen C, Chen Y, Guan MX. A peep into mitochondrial disorder: multifaceted from mitochondrial DNA mutations to nuclear gene modulation. *Protein Cell*. 2015 Dec; 6(12): 862–870. doi: 10.1007/s13238-015-0175-z

45. Chen X, Prosser R, Simonetti S, Sadlock J, Jagiello G, Schon EA. Rearranged mitochondrial genomes are present in human oocytes. *Am J Hum Genet*. 1995 Aug; 57(2):239-247

46. Chevrollier A, Loiseau D, Reynier P, Stepien G. Adenine nucleotide translocase 2 is a key mitochondrial protein in cancer metabolism. *Biochim Biophys Acta*. 2011 Jun; 1807(6):562-567. doi: 10.1016/j.bbabio.2010.10.008

47. Chinnery PF, Hudson G. Mitochondrial genetics. *Br Med Bull*. 2013; 106:135-159. doi: 10.1093/bmb/ldt017

48. Claros MG, Vincens P. Computational method to predict mitochondrially imported proteins and their targeting sequences. *Eur J Biochem*. 1996 Nov 1; 241(3):779-786.

49. Clavier A, Rincheval-Arnold A, Colin J, Mignotte B, Guénal I. Apoptosis in Drosophila: which role for mitochondria? *Apoptosis*. 2016 Mar; 21(3):239-251. doi: 10.1007/s10495-015-1209-y

50. Contamine V, Picard M. Maintenance and integrity of the mitochondrial genome: a plethora of nuclear genes in the budding yeast. *Microbiol Mol Biol Rev*. 2000 Jun; 64(2):281-315.

51. Copeland WC. Defects in mitochondrial DNA replication and human disease. *Crit Rev Biochem Mol Biol*. 2012 Jan-Feb; 47(1):64-74. doi: 10.3109/10409238.2011.632763.

52. Copeland WC. Defects of mitochondrial DNA replication. *J Child Neurol*. 2014 Sep; 29(9): 1216–1224. doi: 10.1177/0883073814537380

53. Da Rè C, Franzolin E, Biscontin A, Piazzesi A, Pacchioni B, *et al.* Functional characterization of drim2, the Drosophila melanogaster homolog of the yeast mitochondrial deoxynucleotide transporter. *J Biol Chem*. 2014 Mar 14; 289(11):7448-7459. doi: 10.1074/jbc.M113.543926

54. Da Rè C, von Stockum S, Biscontin A, Millino C, Cisotto P, *et al.* Leigh syndrome in Drosophila melanogaster: morphological and biochemical characterization of Surf1 post-transcriptional silencing. *J Biol Chem*. 2014 Oct 17; 289(42):29235-29246. doi: 10.1074/jbc.M114.602938

55. Daenzer JM, Fridovich-Keil JL. Drosophila melanogaster models of galactosemia. *Curr Top Dev Biol*. 2017; 121:377-395. doi: 10.1016/bs.ctdb.2016.07.009

56. Dalla Rosa I, Durigon R, Pearce SF, Rorbach J, Hirst EM, *et al.* MPV17L2 is required for ribosome assembly in mitochondria. *Nucleic Acids Res*. 2014 Jul; 42(13):8500-8515. doi: 10.1093/nar/gku513

57. Dalla Rosa I, Cámara Y, Durigon R, Moss CF, Vidoni S, Akman G, Hunt L, Johnson MA, Grocott S, Wang L, Thorburn DR, Hirano M, Poulton J, Taylor RW, Elgar G, Martí R, Voshol P, Holt IJ, Spinazzola A. MPV17 Loss Causes Deoxynucleotide Insufficiency and Slow DNA Replication in Mitochondria. *PLoS Genet*. 2016 Jan 13; 12(1):e1005779. doi: 10.1371/journal.pgen.1005779

58. Dallabona C, Marsano RM, Arzuffi P, Ghezzi D, Mancini P, *et al.* Sym1, the yeast ortholog of the MPV17 human disease protein, is a stress-induced bioenergetic and morphogenetic mitochondrial modulator. *Hum Mol Genet*. 2010 Mar 15; 19(6):1098-1107. doi: 10.1093/hmg/ddp581

59. Danpure CJ, Cooper PJ, Wise PJ, Jennings PR. An enzyme trafficking defect in two patients with primary hyperoxaluria type 1: peroxisomal alanine/glyoxylate aminotransferase rerouted to mitochondria. *J Cell Biol*. 1989 Apr; 108(4):1345-1352.

60. Davey KM, Parboosingh JS, McLeod DR, Chan A, Casey R, *et al.* Mutation of DNAJC19, a human homologue of yeast inner mitochondrial membrane co-chaperones, causes DCMA syndrome, a novel autosomal recessive Barth syndrome-like condition. *J Med Genet*. 2006 May; 43(5):385-393. doi: 10.1136/jmg.2005.036657

61. Dean M. The Human ATP-Binding Cassette (ABC) Transporter Superfamily. *Bethesda (MD): National Center for Biotechnology Information* (US); 2002 Nov 18

62. Di Fonzo A, Ronchi D, Lodi T, Fassone E, Tigano M, *et al.* The mitochondrial disulfide relay system protein GFER is mutated in autosomal-recessive myopathy with cataract and combined respiratory-chain deficiency. *Am J Hum Genet*. 2009 May; 84(5):594-604. doi: 10.1016/j.ajhg.2009.04.004

63. Di Giovanni S, Mirabella M, Papacci M, Odoardi F, Silvestri G, *et al.* Apoptosis and ROS detoxification enzymes correlate with cytochrome c oxidase deficiency in mitochondrial encephalomyopathies. *Mol Cell Neurosci*. 2001 Apr; 17(4):696-705. doi: 10.1006/mcne.2001.0970

64. Diekert K, Kispal G, Guiard B, Lill R. An internal targeting signal directing proteins into the mitochondrial intermembrane space. *Proc Natl Acad Sci U S A*. 1999; 96(21):11752-11757.

65. DiMauro S, Hirano M. Mitochondrial DNA Deletion Syndromes. In: Pagon RA, Adam MP, Ardinger HH, Wallace SE, Amemiya A, et al, editors. *GeneReviews*. Seattle (WA): University of Washington, Seattle; 1993-2017. 2003 Dec 17 [updated 2011 May 3].

66. DiMauro S, Schon EA. Mitochondrial respiratory-chain diseases. *N Engl J Med*. 2003 Jun 26; 348(26):2656-2668. doi: 10.1056/NEJMra022567

67. DiMauro S. Mitochondrial diseases. *Biochim Biophys Acta*. 2004 Jul 23; 1658(1-2):80-88. doi: 10.1016/j.bbabio.2004.03.014

68. Dolce V, Fiermonte G, Runswick MJ, Palmieri F, Walker JE. The human mitochondrial deoxynucleotide carrier and its role in the toxicity of nucleoside antivirals. *Proc Natl Acad Sci U S A*. 2001 Feb 27; 98(5):2284-2288. doi:10.1073/pnas.031430998

69. Dorn GW, Clark CF, Eschenbacher WH, Kang MY, Engelhard JT, *et al.* MARF and Opa1 control mitochondrial and cardiac function in Drosophila. *Circ Res*. 2011 Jan 7; 108(1):12-7. doi: 10.1161/CIRCRESAHA.110.236745

70. Drozdetskiy A, Cole C, Procter J, Barton GJ. JPred4: a protein secondary structure prediction server. *Nucleic Acids Res*. 2015 Jul 1; 43(W1):W389-394. doi: 10.1093/nar/gkv332

71. Duncan AJ, Bitner-Glindzicz M, Meunier B, Costello H, Hargreaves IP, *et al.* A nonsense mutation in COQ9 causes autosomal-recessive neonatal-onset primary coenzyme Q10 deficiency: a potentially treatable form of mitochondrial disease. *Am J Hum Genet*. 2009 May; 84(5):558-566. doi: 10.1016/j.ajhg.2009.03.018

72. Ehses S, Raschke I, Mancuso G, Bernacchia A, Geimer S, *et al.* Regulation of OPA1 processing and mitochondrial fusion by m-AAA protease isoenzymes and OMA1. *J Cell Biol*. 2009 Dec 28; 187(7):1023-1036. doi: 10.1083/jcb.200906084

73. El-Hattab AW, Li FY, Schmitt E, Zhang S, Craigen WJ, *et al.* MPV17-associated hepatocerebral mitochondrial DNA depletion syndrome: new patients and novel mutations. *Mol Genet Metab*. 2010 Mar; 99(3):300-308. doi: 10.1016/j.ymgme.2009.10.003

74. El-Hattab AW, Scaglia F, Craigen WJ, Wong LJC. MPV17-Related Hepatocerebral Mitochondrial DNA Depletion Syndrome. In: Pagon RA, Adam MP, Ardinger HH, Wallace SE, Amemiya A, *et al*., editors. *GeneReviews*. Seattle (WA): University of Washington, Seattle; 1993-2017. 2012 May 17.

75. El-Hattab AW, Scaglia F. Mitochondrial DNA depletion syndromes: review and updates of genetic basis, manifestations, and therapeutic options. *Neurotherapeutics*. 2013 Apr; 10(2):186-198. doi: 10.1007/s13311-013-0177-6

76. Elmore S. Apoptosis: A review of programmed cell death. *Toxicol Pathol*. 2007; 35(4): 495–516. doi: 10.1080/01926230701320337

77. Exner N, Lutz AK, Haass C, Winklhofer KF. Mitochondrial dysfunction in Parkinson's disease: molecular mechanisms and pathophysiological consequences. *EMBO J*. 2012 Jun 26; 31(14):3038-3062. doi: 10.1038/emboj.2012.170

78. Fassone E, Rahman S. Complex I deficiency: clinical features, biochemistry and molecular genetics. *J Med Genet*. 2012 Sep; 49(9):578-590. doi: 10.1136/jmedgenet-2012-101159

79. Feany MB, Bender WW. A Drosophila model of Parkinson's disease. *Nature*. 2000 Mar 23; 404(6776):394-398. doi:10.1038/35006074

80. Fergestad T, Bostwick B, Ganetzky B. Metabolic disruption in Drosophila Bang-sensitive seizure mutants. *Genetics*. 2006 Jul 1; 173 (3):1357-1364. https://doi.org/10.1534/genetics.106.057463

81. Fernández-Vizarra E, Tiranti V, Zeviani M. Assembly of the oxidative phosphorylation system in humans: what we have learned by studying its defects. *Biochim Biophys Acta*. 2009 Jan; 1793(1):200-211. doi: 10.1016/j.bbamcr.2008.05.028

82. Ferraro P, Nicolosi L, Bernardi P, Reichard P, Bianchi V. Mitochondrial deoxynucleotide pool sizes in mouse liver and evidence for a transport mechanism for thymidine monophosphate. *Proc Natl Acad Sci U S A*. 2006 Dec 5; 103(49):18586-18591. doi:10.1073/pnas.0609020103

83. Ferraro P, Franzolin E, Pontarin G, Reichard P, Bianchi V. Quantitation of cellular deoxynucleoside triphosphates. *Nucleic Acids Res*. 2010 Apr; 38(6):e85. doi: 10.1093/nar/gkp1141

84. Finn RD, Coggill P, Eberhardt RY, Eddy SR, Mistry J, Mitchell AL, Potter SC, Punta M, Qureshi M, Sangrador-Vegas A, Salazar GA, Tate J, Bateman A. The Pfam protein families database: towards a more sustainable future. *Nucleic Acids Res*. 2016 Jan 4; 44(D1):D279-285. doi: 10.1093/nar/gkv1344

85. Foriel S, Willems P, Smeitink J, Schenck A, Beyrath J. Mitochondrial diseases: Drosophila melanogaster as a model to evaluate potential therapeutics. *Int J Biochem Cell Biol*. 2015 Jun; 63:60-65. doi: 10.1016/j.biocel.2015.01.024

86. Friedman JR, Nunnari J. Mitochondrial form and function. *Nature*. 2014 Jan 16; 505(7483):335-343. doi: 10.1038/nature12985

87. Friedman JR, Mourier A, Yamada J, McCaffery JM, Nunnari J. MICOS coordinates with respiratory complexes and lipids to establish mitochondrial inner membrane architecture. *Elife*. 2015 Apr 28; 4. doi: 10.7554/eLife.07739

88. Fukasawa Y, Tsuji J, Fu SC, Tomii K, Horton P, *et al.* MitoFates: improved prediction of mitochondrial targeting sequences and their cleavage sites. *Mol Cell Proteomics*. 2015 Apr; 14(4):1113-1126. doi: 10.1074/mcp.M114.043083

89. Gabaldón T, Huynen MA. Shaping the mitochondrial proteome. *Biochim Biophys Acta*. 2004 Dec 6; 1659(2-3):212-220. doi: 10.1016/j.bbabio.2004.07.011

90. Gaignard P, Menezes M, Schiff M, Bayot A, Rak M, *et al.* Mutations in CYC1, encoding cytochrome c1 subunit of respiratory chain complex III, cause insulin-responsive hyperglycemia. *Am J Hum Genet*. 2013 Aug 8; 93(2):384-389. doi: 10.1016/j.ajhg.2013.06.015

91. Gakh O, Cavadini P, Isaya G. Mitochondrial processing peptidases. *Biochim Biophys Acta*. 2002 Sep 2; 1592(1):63-77.

92. Galluzzi L, Kepp O, Trojel-Hansen C, Kroemer G. Mitochondrial control of cellular life, stress, and death. *Circ Res*. 2012 Oct 12; 111(9):1198-1207. doi: 10.1161/CIRCRESAHA.112.268946

93. Gandhi VV, Samuels DC. A review comparing deoxyribonucleoside triphosphate (dNTP) concentrations in the mitochondrial and cytoplasmic compartments of normal and transformed cells. *Nucleosides Nucleotides Nucleic Acids*. 2011 May; 30(5):317-339. doi: 10.1080/15257770.2011.586955

94. Ganetzky B, Wu CF. Indirect suppression involving behavioral mutants with altered nerve excitability in Drosophila melanogaster. *Genetics*. 1982 Apr; 100(4):597-614.

95. García-Rodríguez LJ, Gay AC, Pon LA. Puf3p, a Pumilio family RNA binding protein, localizes to mitochondria and regulates mitochondrial biogenesis and motility in budding yeast. *J Cell Biol*. 2007 Jan 15; 176(2):197-207. doi:10.1083/jcb.200606054

96. Garesse R, Kaguni LS. A Drosophila model of mitochondrial DNA replication: proteins, genes and regulation. *IUBMB Life*. 2005 Aug; 57(8):555-561.

97. Gegg ME, Cooper JM, Chau KY, Rojo M, Schapira AH, *et al.* Mitofusin 1 and mitofusin 2 are ubiquitinated in a PINK1/parkin-dependent manner upon induction of mitophagy. *Hum Mol Genet*. 2010 Dec 15; 19(24):4861-4870. doi: 10.1093/hmg/ddq419

98. Ghezzi D, Goffrini P, Uziel G, Horvath R, Klopstock T, *et al.* SDHAF1, encoding a LYR complex-II specific assembly factor, is mutated in SDH-defective infantile leukoencephalopathy. *Nat Genet*. 2009 Jun; 41(6):654-656. doi: 10.1038/ng.378

99. Ghezzi D, Zeviani M. Assembly factors of human mitochondrial respiratory chain complexes: physiology and pathophysiology. *Adv Exp Med Biol*. 2012; 748:65-106. doi: 10.1007/978-1-4614-3573-0_4

100. Glasscock E, Tanouye MA. Drosophila couch potato mutants exhibit complex neurological abnormalities including epilepsy phenotypes. *Genetics*. 2005 Apr; 169(4):2137-2149. doi: 10.1534/genetics.104.028357

101. Goldstein AC, Bhatia P, Vento JM. Mitochondrial disease in childhood: nuclear encoded. *Neurotherapeutics*. 2013 Apr; 10(2): 212–226. doi: 10.1007/s13311-013-0185-6

102. Gonzalez C. Drosophila melanogaster: a model and a tool to investigate malignancy and identify new therapeutics. *Nature Reviews Cancer*. 2013 Mar; 13, 172-183. doi:10.1038/nrc3461

103. González M, Martín-Ruíz I, Jiménez S, Pirone L, Barrio R, *et al.* Generation of stable Drosophila cell lines using multicistronic vectors. *Sci Rep*. 2011; 1:75. doi: 10.1038/srep00075

104. Gorman GS, Schaefer AM, Ng Y, Gomez N, Blakely EL, *et al.* Prevalence of nuclear and mitochondrial DNA mutations related to adult mitochondrial disease. *Ann Neurol*. 2015 May; 77(5):753-759. doi: 10.1002/ana.24362

105. Graham P, Pick L. Drosophila as a model for diabetes and diseases of insulin resistance. *Curr Top Dev Biol.* 2017; 121:397-419. doi: *10.101*6/bs.ctdb.2016.07.011

106. Gratz SJ, Cummings AM, Nguyen JN, Hamm DC, Donohue LK, *et al.* Genome Engineering of Drosophila with the CRISPR RNA-Guided Cas9 Nuclease. *Genetics*. 2013 Aug 1; 194(4):1029-1035. https://doi.org/10.1534/genetics.113.152710

107. Gray MW, Lang BF, Cedergren R, Golding GB, Lemieux C, *et al.* Genome structure and gene content in protist mitochondrial DNAs. *Nucleic Acids Res*. 1998 Feb 15; 26(4):865-78.

108. Guarani V, McNeill EM, Paulo JA, Huttlin EL, Fröhlich F, *et al.* QIL1 is a novel mitochondrial protein required for MICOS complex stability and cristae morphology. *Elife*. 2015 May 21;4. doi: 10.7554/eLife.06265

109. Guest ST, Yu J, Liu D, Hines JA, Kashat MA, *et al.* A protein network-guided screen for cell cycle regulators in Drosophila. *BMC Syst Biol*. 2011 May 6; 5:65. doi: 10.1186/1752-0509-5-65

110. Guo M. Drosophila as a model to study mitochondrial dysfunction in Parkinson's disease. *Cold Spring Harb Perspect Med*. 2012 Nov; 2(11): a009944. doi: 10.1101/cshperspect.a009944

111. Guo X, Macleod GT, Wellington A, Hu F, Panchumarthi S, *et al.* The GTPase dMiro is required for axonal transport of mitochondria to Drosophila synapses. *Neuron*. 2005 Aug 4; 47(3):379-393. doi: 10.1016/j.neuron.2005.06.027

112. Haack TB, Danhauser K, Haberberger B, Hoser J, Strecker V, *et al.* Exome sequencing identifies ACAD9 mutations as a cause of complex I deficiency. *Nat Genet*. 2010 Dec; 42(12):1131-1134. doi: 10.1038/ng.706

113. Habersetzer J, Ziani W, Larrieu I, Stines-Chaumeil C, Giraud MF, Brethes D, *et al.* ATP synthase oligomerization: from the enzyme models to the mitochondrial morphology. *Int J Biochem Cell Biol*. 2013; 45:99–105. doi: 10.1016/j.biocel.2012.05.017

114. Hales KG, Fuller MT. Developmentally regulated mitochondrial fusion mediated by a conserved, novel, predicted GTPase. *Cell*. 1997 Jul 11; 90(1):121-129.

115. Harner M, Körner C, Walther D, Mokranjac D, Kaesmacher J, *et al.* The mitochondrial contact site complex, a determinant of mitochondrial architecture. *EMBO J*. 2011 Oct 18; 30(21):4356-4370. doi: 10.1038/emboj.2011.379

116. Head B, Griparic L, Amiri M, Gandre-Babbe S, van der Bliek AM. Inducible proteolytic inactivation of OPA1 mediated by the OMA1 protease in mammalian cells. *J Cell Biol*. 2009 Dec 28; 187(7):959-966. doi: 10.1083/jcb.200906083

117. Hejzlarová K, Mráček T, Vrbacký M, Kaplanová V, Karbanová V, *et al.* Nuclear genetic defects of mitochondrial ATP synthase. *Physiol Res*. 2014; 63 Suppl 1:S57-71.

118. Hell K. The Erv1-Mia40 disulfide relay system in the intermembrane space of mitochondria. *Biochim Biophys Acta*. 2008 Apr; 1783(4):601-609. doi: 10.1016/j.bbamcr.2007.12.005

119. Hill K, Model K, Ryan MT, Dietmeier K, Martin F, *et al.* Tom40 forms the hydrophilic channel of the mitochondrial import pore for preproteins. *Nature*. 1998 Oct 1; 395(6701):516-521. doi:10.1038/26780

120. Hill RB, Pellegrini L. The PARL family of mitochondrial rhomboid proteases. *Semin Cell Dev Biol*. 2010 Aug; 21(6):582-592. doi: 10.1016/j.semcdb.2009.12.011

121. Hoffmann JA. The immune response of Drosophila. *Nature*. 2003 Nov 6; 426(6962):33-38. doi: 10.1038/nature02021

122. Hofmann K, Stoffel W. TMBASE - A database of membrane spanning protein segments. *Biol. Chem*. Hoppe-Seyler 374,166 (1993)

123. Holt IJ, Harding AE, Morgan-Hughes JA. Deletions of muscle mitochondrial DNA in patients with mitochondrial myopathies. *Nature* 331, 717-719 (25 February 1988); doi:10.1038/331717a0

124. Holt IJ, Lorimer HE, Jacobs HT. Coupled leading- and lagging-strand synthesis of mammalian mitochondrial DNA. *Cell*. 2000 Mar 3; 100(5):515-524. http://dx.doi.org/10.1016/S0092-8674(00)80688-1

125. Homyk T, Sheppard DE. Behavioral Mutants of Drosophila melanogaster. I. Isolation and mapping of mutations which decrease flight ability. *Genetics*. 1977 Sep; 87(1):95-104.

126. Houstek J, Kmoch S, Zeman J. TMEM70 protein - a novel ancillary factor of mammalian ATP synthase. *Biochim Biophys Acta*. 2009 May; 1787(5):529-532. doi: 10.1016/j.bbabio.2008.11.013

127. Huynen MA, Mühlmeister M, Gotthardt K, Guerrero-Castillo S, Brandt U. Evolution and structural organization of the mitochondrial contact site (MICOS) complex and the mitochondrial intermembrane space bridging (MIB) complex. *Biochim Biophys Acta*. 2016 Jan; 1863(1):91-101. doi: 10.1016/j.bbamcr.2015.10.009

128. Hwa JJ, Zhu AJ, Hiller MA, Kon CY, Fuller MT, *et al.* Germ-line specific variants of components of the mitochondrial outer membrane import machinery in Drosophila. *FEBS Lett*. 2004 Aug 13; 572(1-3):141-146. doi:10.1016/j.febslet.2004.07.025

129. Iida R, Yasuda T, Tsubota E, Takatsuka H, Masuyama M, *et al.* M-LP, Mpv17-like protein, has a peroxisomal membrane targeting signal comprising a transmembrane domain and a positively charged loop and up-regulates expression of the manganese superoxide dismutase gene. *J Biol Chem*. 2003 Feb 21; 278(8):6301-6306. doi: 10.1074/jbc.M210886200

130. Iida R, Yasuda T, Tsubota E, Takatsuka H, Masuyama M, *et al.* A novel alternative spliced Mpv17-like protein isoform localizes in cytosol and is expressed in a kidney- and adult-specific manner. *Exp Cell Res*. 2005 Jan 1; 302(1):22-30. doi: 10.1016/j.yexcr.2004.08.027

131. Iida R, Yasuda T, Tsubota E, Takatsuka H, Matsuki T, *et al.* Human Mpv17-like protein is localized in peroxisomes and regulates expression of antioxidant enzymes. *Biochem Biophys Res Commun*. 2006 Jun 9; 344(3):948-954. doi: 10.1016/j.bbrc.2006.04.008

132. Iida R, Ueki M, Yasuda T. A novel transcriptional repressor, Rhit, is involved in heat-inducible and age-dependent expression of Mpv17-like protein, a participant in reactive oxygen species metabolism. *Mol Cell Biol*. 2010 May; 30(10):2306-2315. doi: 10.1128/MCB.01025-09

133. Iida R, Ueki M, Yasuda T. Identification of Rhit as a novel transcriptional repressor of human Mpv17-like protein with a mitigating effect on mitochondrial dysfunction, and its transcriptional regulation by FOXD3 and GABP. *Free Radic Biol Med*. 2012 Apr 15; 52(8):1413-1422. doi: 10.1016/j.freeradbiomed.2012.01.003

134. Iida R, Ueki M, Yasuda T. Identification of interacting partners of Human Mpv17-like protein with a mitigating effect of mitochondrial dysfunction through mtDNA damage. *Free Radic Biol Med*. 2015 Oct; 87:336-345. doi: 10.1016/j.freeradbiomed.2015.07.008

135. Indrieri A, van Rahden VA, Tiranti V, Morleo M, Iaconis D, *et al.* Mutations in COX7B cause microphthalmia with linear skin lesions, an unconventional mitochondrial disease. *Am J Hum Genet*. 2012 Nov 2; 91(5):942-949. doi: 10.1016/j.ajhg.2012.09.016

136. Invernizzi F, Tigano M, Dallabona C, Donnini C, Ferrero I, *et al.* A homozygous mutation in LYRM7/MZM1L associated with early onset encephalopathy, lactic acidosis, and severe reduction of mitochondrial complex III activity. *Hum Mutat*. 2013 Dec; 34(12):1619-1622. doi: 10.1002/humu.22441

137. Jacobs HT, Fernández-Ayala DJ, Manjiry S, Kemppainen E, Toivonen JM, *et al.* Mitochondrial disease in flies. *Biochim Biophys Acta*. 2004 Dec 6; 1659(2-3):190-196. http://doi.org/10.1016/j.bbabio.2004.07.004

138. Johansson M, Bajalica-Lagercrantz S, Lagercrantz J, Karlsson A. Localization of the human deoxyguanosine kinase gene (DGUOK) to chromosome 2p13. *Genomics*. 1996 Dec 15; 38(3):450-451. doi: 10.1006/geno.1996.0654

139. Johansson M, Karlsson A. Cloning of the cDNA and chromosome localization of the gene for human thymidine kinase 2. J Biol Chem. 1997 Mar 28;272(13):8454-8458.

140. Johri A, Beal MF. Mitochondrial dysfunction in neurodegenerative diseases. *J Pharmacol Exp Ther*. 2012 Sep; 342(3): 619–630. doi: 10.1124/jpet.112.192138

141. Jones BA, Fangman WL. Mitochondrial DNA maintenance in yeast requires a protein containing a region related to the GTP-binding domain of dynamin. *Genes Dev*. 1992 Mar; 6(3):380-389.

142. Kadenbach B, Arnold S, Lee I, Hüttemann M. The possible role of cytochrome c oxidase in stress-induced apoptosis and degenerative diseases. *Biochim Biophys Acta*. 2004 Apr 12; 1655(1-3):400-408. doi: 10.1016/j.bbabio.2003.06.005

143. Kanabus M, Heales SJ, Rahman S. Development of pharmacological strategies for mitochondrial disorders. *Br J Pharmacol*. 2014 Apr; 171(8):1798-1817. doi: 10.1111/bph.12456

144. Karadimas CL, Vu TH, Holve SA, Chronopoulou P, Quinzii C, *et al.* Navajo neurohepatopathy is caused by a mutation in the MPV17 gene. *Am J Hum Genet*. 2006 Sep; 79(3):544-548. doi: 10.1086/506913

145. Karasawa M, Zwacka RM, Reuter A, Fink T, Hsieh CL, *et al.* The human homolog of the glomerulosclerosis gene Mpv17: structure and genomic organization. *Hum Mol Genet*. 1993 Nov; 2(11):1829-1834.

146. Karbowski M, Lee YJ, Gaume B, Jeong SY, Frank S, *et al.* Spatial and temporal association of Bax with mitochondrial fission sites, Drp1, and Mfn2 during apoptosis. *J Cell Biol*. 2002 Dec 23; 159(6):931-938 doi: 10.1083/jcb.200209124

147. Karbowski M, Norris KL, Cleland MM, Jeong SY, Youle RJ. Role of Bax and Bak in mitochondrial morphogenesis. *Nature*. 2006 Oct 12; 443(7112):658-662. doi: 10.1038/nature05111

148. Kaukonen J, Juselius JK, Tiranti V, Kyttälä A, Zeviani M, *et al.* Role of adenine nucleotide translocator 1 in mtDNA maintenance. *Science*. 2000 Aug 4; 289(5480):782-785. doi: 10.1126/science.289.5480.782

149. Kemppainen KK, Rinne J, Sriram A, Lakanmaa M, Zeb A, *et al.* Expression of alternative oxidase in Drosophila ameliorates diverse phenotypes due to cytochrome oxidase deficiency. *Hum Mol Genet*. 2014 Apr 15; 23(8): 2078–2093. doi: 10.1093/hmg/ddt601

150. Kirkin V, Lamark T, Sou YS, Bjørkøy G, Nunn JL, *et al.* A role for NBR1 in autophagosomal degradation of ubiquitinated substrates. *Mol Cell*. 2009 Feb 27; 33(4):505-516. doi: 10.1016/j.molcel.2009.01.020

151. Klingenberg M. The ADP and ATP transport in mitochondria and its carrier. *Biochim Biophys Acta*. 2008 Oct; 1778(10):1978-2021. doi: 10.1016/j.bbamem.2008.04.011

152. Kondapalli KC, Kok NM, Dancis A, Stemmler TL. Drosophila frataxin: an iron chaperone during cellular Fe–S cluster bioassembly. *Biochemistry*. 2008; 47(26):6917-6927. doi:10.1021/bi800366d

153. Koshkin V, Greenberg ML. Cardiolipin prevents rate-dependent uncoupling and provides osmotic stability in yeast mitochondria. *Biochem J*. 2002 May 15; 364(Pt 1): 317–322.

154. Kowluru A, Tannous M, Chen HQ. Localization and characterization of the mitochondrial isoform of the nucleoside diphosphate kinase in the pancreatic beta cell: evidence for its complexation with mitochondrial succinyl-CoA synthetase. *Arch Biochem Biophys*. 2002 Feb 15; 398(2):160-169. doi: 10.1006/abbi.2001.2710

155. Kozjak-Pavlovic V. The MICOS complex of human mitochondria. *Cell Tissue Res*. 2017 Jan; 367(1):83-93. doi: 10.1007/s00441-016-2433-7

156. Krauss J, Astrinides P, Frohnhöfer HG, Walderich B, Nüsslein-Volhard C. transparent, a gene affecting stripe formation in zebrafish, encodes the mitochondrial protein Mpv17 that is required for iridophore survival. *Biol Open*. 2013 Jul 15; 2(7): 703–710. doi: 10.1242/bio.20135132

157. Krick S, Shi S, Ju W, Faul C, Tsai SY, *et al.* Mpv17l protects against mitochondrial oxidative stress and apoptosis by activation of Omi/HtrA2 protease. *Proc Natl Acad Sci U S A*. 2008 Sep 16; 105(37):14106-14111. doi: 10.1073/pnas.0801146105

158. Ku C, Nelson-Sathi S, Roettger M, Garg S, Hazkani-Covo E, *et al.* Endosymbiotic gene transfer from prokaryotic pangenomes: inherited chimerism in eukaryotes. *Proc Natl Acad Sci U S A*. 2015 Aug 18; 112(33):10139-10146. doi: 10.1073/pnas.1421385112

159. Kühlbrandt W. Structure and function of mitochondrial membrane protein complexes. *BMC Biol*. 2015; 13: 89. doi: 10.1186/s12915-015-0201-x

160. Kumar S, Stecher G, Tamura K. MEGA7: Molecular Evolutionary Genetics Analysis Version 7.0 for Bigger Datasets. *Mol Biol Evol*. 2016 Jul; 33(7):1870-1874. doi: 10.1093/molbev/msw054

161. Kutik S, Guiard B, Meyer HE, Wiedemann N, Pfanner N. Cooperation of translocase complexes in mitochondrial protein import. *J Cell Biol*. 2007 Nov 19; 179(4): 585–591. doi: 10.1083/jcb.200708199

162. Lamperti C, Zeviani M. Encephalomyopathies caused by abnormal nuclear-mitochondrial intergenomic cross-talk. *Acta Myol*. 2009 Jul; 28(1): 2–11.

163. Lane AN, Fan TWM. Regulation of mammalian nucleotide metabolism and biosynthesis. *Nucleic Acids Res*. 2015 Feb 27; 43(4): 2466–2485. doi: 10.1093/nar/gkv047

164. Larkin MA, Blackshields G, Brown NP, Chenna R, McGettigan PA, *et al.* Clustal W and Clustal X version 2.0. *Bioinformatics*. 2007 Nov 1; 23(21):2947-2948. doi: 10.1093/bioinformatics/btm404

165. Larsson NG, Wang J, Wilhelmsson H, Oldfors A, Rustin P, *et al.* Mitochondrial transcription factor A is necessary for mtDNA maintenance and embryogenesis in mice. *Nat Genet*. 1998 Mar; 18(3):231-236. doi: 10.1038/ng0398-231

166. Lasserre JP, Dautant A, Aiyar RS, Kucharczyk R, Glatigny A, *et al.* Yeast as a system for modeling mitochondrial disease mechanisms and discovering therapies. *Dis Model Mech*. 2015 Jun; 8(6):509-526. doi: 10.1242/dmm.020438.

167. Lawler J.The functions of thrombospondin-1 and-2. Curr Opin Cell Biol. 2000 Oct; 12(5):634-640.

168. Lazarou M, Jin SM, Kane LA, Youle RJ. Role of PINK1 binding to the TOM complex and alternate intracellular membranes in recruitment and activation of the E3 ligase Parkin. *Dev Cell*. 2012 Feb 14; 22(2):320-333. doi:10.1016/j.devcel.2011.12.014

169. Lee JY, Nagano Y, Taylor JP, Lim KL, Yao TP. Disease-causing mutations in parkin impair mitochondrial ubiquitination, aggregation, and HDAC6-dependent mitophagy. *J Cell Biol*. 2010 May 17; 189(4):671-679. doi: 10.1083/jcb.201001039

170. Lee YJ, Jeong SY, Karbowski M, Smith CL, Youle RJ. Roles of the mammalian mitochondrial fission and fusion mediators Fis1, Drp1, and Opa1 in apoptosis. *Mol Biol Cell*. 2004 Nov; 15(11):5001-5011. doi: 10.1091/mbc.E04-04-0294

171. Lehninger AL, Kennedy EP. The requirements of the fatty acid oxidase complex of rat liver. *J Biol Chem*. 1948 Apr; 173(2):753-771.

172. Liu S, Sawada T, Lee S, Yu W, Silverio G, *et al.* Parkinson's disease-associated kinase PINK1 regulates Miro protein level and axonal transport of mitochondria. *PLoS Genet*. 2012; 8(3):e1002537. doi: 10.1371/journal.pgen.1002537

173. Livak KJ, Schmittgen TD. Analysis of relative gene expression data using real-time quantitative PCR and the 2(-Delta Delta C(T)) Method. *Methods*. 2001 Dec; 25(4):402-408. oi: 10.1006/meth.2001.1262

174. Löllgen S, Weiher H. The role of the Mpv17 protein mutations of which cause mitochondrial DNA depletion syndrome (MDDS): lessons from homologs in different species. *Biol Chem*. 2015 Jan; 396(1):13-25. doi: 10.1515/hsz-2014-0198

175. Lu B, Vogel H. Drosophila models of neurodegenerative diseases. *Annu Rev Pathol*. 2009; 4: 315–342. doi: 10.1146/annurev.pathol.3.121806.151529

176. Luk E, Yang M, Jensen LT, Bourbonnais Y, Culotta VC. Manganese activation of superoxide dismutase 2 in the mitochondria of Saccharomyces cerevisiae. *J Biol Chem*. 2005 Jun 17; 280(24):22715-22720. doi:10.1074/jbc.M504257200

177. Marc P, Margeot A, Devaux F, Blugeon C, Corral-Debrinski M, *et al.* Genome-wide analysis of mRNAs targeted to yeast mitochondria. *EMBO Rep*. 2002 Feb; 3(2):159-164. doi:10.1093/embo-reports/kvf025

178. Martin LJ, Lau E, Singh H, Vergnes L, Tarling EJ, *et al.* ABCC6 Localizes to the Mitochondria-Associated Membrane. *Circulation research*. 2012; 111(5):516-520. doi:10.1161/CIRCRESAHA.112.276667

179. Martinou JC, Youle RJ. Mitochondria in apoptosis: Bcl-2 family members and mitochondrial dynamics. *Dev Cell*. 2011 Jul 19; 21(1): 92–101. doi: 10.1016/j.devcel.2011.06.017

180. Maurano MT, Humbert R, Rynes E, Thurman RE, Haugen E, *et al.* Systematic localization of common disease-associated variation in regulatory DNA. *Science*. 2012 Sep 7; 337(6099):1190-1195. doi: 10.1126/science.1222794

181. Mayr JA, Havlícková V, Zimmermann F, Magler I, Kaplanová V, *et al.* Mitochondrial ATP synthase deficiency due to a mutation in the ATP5E gene for the F1 epsilon subunit. *Hum Mol Genet*. 2010 Sep 1; 19(17):3430-3439. doi: 10.1093/hmg/ddq254

182. McFarland R, Clark KM, Morris AA, Taylor RW, Macphail S, *et al.* Multiple neonatal deaths due to a homoplasmic mitochondrial DNA mutation. *Nat Genet*. 2002 Feb; 30(2):145-146. doi:10.1038/ng819

183. McInnes J. Mitochondrial-associated metabolic disorders: foundations, pathologies and recent progress. *Nutr Metab* (Lond). 2013; 10: 63. doi: 10.1186/1743-7075-10-63

184. McKenzie M, Lazarou M, Thorburn DR, Ryan MT. Mitochondrial respiratory chain supercomplexes are destabilized in Barth Syndrome patients. *J Mol Biol*. 2006 Aug 18; 361(3):462-469. doi: 10.1016/j.jmb.2006.06.057

185. Meeusen S, DeVay R, Block J, Cassidy-Stone A, Wayson S, *et al.* Mitochondrial inner-membrane fusion and crista maintenance requires the dynamin-related GTPase Mgm1. *Cell*. 2006 Oct 20; 127(2):383-95. doi:10.1016/j.cell.2006.09.021

186. Melchionda L, Haack TB, Hardy S, Abbink TE, Fernandez-Vizarra E, et al Mutations in APOPT1, encoding a mitochondrial protein, cause cavitating leukoencephalopathy with cytochrome c oxidase deficiency. *Am J Hum Genet*. 2014 Sep 4; 95(3):315-325. doi: 10.1016/j.ajhg.2014.08.003

187. Merkwirth C, Dargazanli S, Tatsuta T, Geimer S, Löwer B *et al.* Prohibitins control cell proliferation and apoptosis by regulating OPA1-dependent cristae morphogenesis in mitochondria. *Genes Dev*. 2008 Feb 15; 22(4): 476–488. doi: 10.1101/gad.460708

188. Meyer zum Gottesberge AM, Massing T, Hansen S. Missing mitochondrial Mpv17 gene function induces tissue-specific cell-death pathway in the degenerating inner ear. *Cell Tissue Res*. 2012 Feb; 347(2):343-356. doi: 10.1007/s00441-012-1326-7

189. Miles WO, Dyson NJ, Walker JA. Modeling tumor invasion and metastasis in Drosophila. *Dis Model Mech*. 2011 Nov; 4(6):753-761. doi: 10.1242/dmm.006908

190. Mishra P, Chan DC. Mitochondrial dynamics and inheritance during cell division, development and disease. *Nat Rev Mol Cell Biol*. 2014 Oct; 15(10):634-646. doi: 10.1038/nrm3877

191. Miyake N, Yano S, Sakai C, Hatakeyama H, Matsushima Y, *et al.* Mitochondrial complex III deficiency caused by a homozygous UQCRC2 mutation presenting with neonatal-onset recurrent metabolic decompensation. *Hum Mutat*. 2013 Mar; 34(3):446-452. doi: 10.1002/humu.22257

192. Mizushima N, Yoshimorim T, Levine B. Methods in mammalian autophagy research. *Cell*. 2010; 140(3):313-326. doi:10.1016/j.cell.2010.01.028.

193. Morgan TH. Sex limited inheritance in Drosophila. *Science*. 1910 Jul 22; 32(812):120-122. doi: 10.1126/science.32.812.120

194. Muller HJ. The production of mutations by x-rays. *Proc Nat Acad Sci*. 1928 Sep; 14(9):714–726.

195. Muñoz-Soriano V, Paricio N. Drosophila models of Parkinson's disease: discovering relevant pathways and novel therapeutic strategies. *Parkinsons Dis*. 2011; 2011: 520640. doi: 10.4061/2011/520640

196. Narendra DP, Youle RJ. Targeting mitochondrial dysfunction: role for PINK1 and Parkin in mitochondrial quality control. *Antioxid Redox Signal*. 2011 May 15; 14(10):1929-1938. doi: 10.1089/ars.2010.3799

197. Narendra D, Walker JE, Youle RJ. Mitochondrial quality control mediated by PINK1 and Parkin: links to Parkinsonism. Cold Spring Harb Perspect Biol. 2012 Nov; 4(11): a011338. doi: 10.1101/cshperspect.a011338

198. Navarro JA, Llorens JV, Soriano S, Botella JA, Schneuwly S, *et al.* Overexpression of human and fly frataxins in Drosophila provokes deleterious effects at biochemical, physiological and developmental levels. *PLoS ONE*. 2011; 6(7):e21017. doi:10.1371/journal.pone.0021017

199. Neupert W. Protein import into mitochondria. *Annu Rev Biochem*. 1997; 66:863-917. doi:10.1146/annurev.biochem.66.1.863

200. Nicolae DL, Gamazon E, Zhang W, Duan S, Dolan ME, *et al.* Trait-associated SNPs are more likely to be eQTLs: annotation to enhance discovery from GWAS. *PLoS Genet*. 2010 Apr 1;6(4):e1000888. doi: 10.1371/journal.pgen.1000888

201. Nogueira C, Almeida LS, Nesti C, Pezzini I, Videira A, *et al.* Syndromes associated with mitochondrial DNA depletion. *Ital J Pediatr*. 2014 Apr 3; 40:34. doi: 10.1186/1824-7288-40-34

202. Nouws J, Nijtmans L, Houten SM, van den Brand M, Huynen M, *et al.* Acyl-CoA dehydrogenase 9 is required for the biogenesis of oxidative phosphorylation complex I. *Cell Metab*. 2010 Sep 8; 12(3):283-294. doi: 10.1016/j.cmet.2010.08.002

203. Okatsu K, Oka T, Iguchi M, Imamura K, Kosako H, *et al.* PINK1 autophosphorylation upon membrane potential dissipation is essential for Parkin recruitment to damaged mitochondria. *Nat Commun*. 2012; 3:1016. doi: 10.1038/ncomms2016.

204. qOPA1 alternate splicing uncouples an evolutionary conserved function in mitochondrial fusion from a vertebrate restricted function in apoptosis. *Cell Death Differ*. 2007 Apr; 14(4):682-692. doi: 10.1038/sj.cdd.4402048

205. Ott C, Dorsch E, Fraunholz M, Straub S, Kozjak-Pavlovic V. Detailed analysis of the human mitochondrial contact site complex indicate a hierarchy of subunits. Cobine PA, ed. *PLoS ONE*. 2015; 10(3):e0120213. doi:10.1371/journal.pone.0120213.

206. Ott C, Ross K, Straub S, Thiede B, Götz M, *et al.* Sam50 functions in mitochondrial intermembrane space bridging and biogenesis of respiratory complexes. *Mol Cell Biol*. 2012 Mar; 32(6):1173-1188. doi: 10.1128/MCB.06388-11

207. Owusu-Ansah E, Perrimon N. Modeling metabolic homeostasis and nutrient sensing in Drosophila: implications for aging and metabolic diseases. *Dis Model Mech*. 2014 Mar; 7(3):343-350. doi: 10.1242/dmm.012989

208. Pagliarini DJ, Calvo SE, Chang B, Sheth SA, Vafai SB, *et al.* A mitochondrial protein compendium elucidates complex I disease biology. *Cell*. 2008 Jul 11; 134(1):112-123. doi: 10.1016/j.cell.2008.06.016

209. Palade GE. An electron microscope study of the mitochondrial structure. *J Histochem Cytochem*. 1953 Jul; 1(4):188-211. doi: 10.1177/1.4.188

210. Palladino MJ. Modeling mitochondrial encephalomyopathy in Drosophila. *Neurobiol Dis*. 2010 Oct; 40(1): 40–45. doi: 10.1016/j.nbd.2010.05.009

211. Palmieri L, Alberio S, Pisano I, Lodi T, Meznaric-Petrusa M, *et al.* Complete loss-of-function of the heart/muscle-specific adenine nucleotide translocator is associated with mitochondrial myopathy and cardiomyopathy. *Hum Mol Genet*. 2005 Oct 15; 14(20):3079-3088. https://doi.org/10.1093/hmg/ddi341

212. Pandey UB, Nichols CD. Human disease models in Drosophila melanogaster and the role of the fly in therapeutic drug discovery. *Pharmacol Rev*. 2011 Jun; 63(2): 411–436. doi: 10.1124/pr.110.003293

213. Park J, Lee G, Chung J. The PINK1-Parkin pathway is involved in the regulation of mitochondrial remodeling process. *Biochem Biophys Res Commun*. 2009 Jan 16; 378(3):518-523. doi: 10.1016/j.bbrc.2008.11.086

214. Patel PI, Isaya G.. Friedreich Ataxia: From GAA Triplet–Repeat Expansion to Frataxin Deficiency. *Am J Hum Genet*. 2001 Jul; 69(1): 15–24.

215. Peng YT, Chen P, Ouyang RY, Song L. Multifaceted role of prohibitin in cell survival and apoptosis. *Apoptosis*. 2015; 20(9): 1135–1149. doi: 10.1007/s10495-015-1143-z

216. Perkins DN, Pappin DJ, Creasy DM, Cottrell JS. Probability-based protein identification by searching sequence databases using mass spectrometry data. *Electrophoresis*. 1999 Dec; 20(18):3551-3567. doi: 10.1002/(SICI)1522-2683(19991201)20:18<3551::AID-ELPS3551>3.0.CO;2-2

217. Perkins G, Bossy-Wetzel E, Ellisman MH. New insights into mitochondrial structure during cell death . *Exp Neurol*. 2009 Aug; 218(2): 183–192. doi: 10.1016/j.expneurol.2009.05.021

218. Pfanner N, van der Laan M, Amati P, Capaldi RA, Caudy AA, *et al.* Uniform nomenclature for the mitochondrial contact site and cristae organizing system. *The Journal of Cell Biology*. 2014; 204(7):1083-1086. doi:10.1083/jcb.201401006.

219. Pierce SB, Gulsuner S, Stapleton GA, Walsh T, Lee MK, *et al.* Infantile onset spinocerebellar ataxia caused by compound heterozygosity for Twinkle mutations and modeling of Twinkle mutations causing recessive disease. *Cold Spring Harb Mol Case Stud*. 2016 Jul; 2(4):a001107. doi: 10.1101/mcs.a001107

220. Pitceathly RD, Smith C, Fratter C, Alston CL, He L, *et al.* Adults with RRM2B-related mitochondrial disease have distinct clinical and molecular characteristics. *Brain*. 2012 Nov; 135(Pt 11):3392-3403. doi: 10.1093/brain/aws231

221. Plantié E, Migocka-Patrzałek M, Daczewska M, Jagla K. Model organisms in the fight against muscular dystrophy: lessons from Drosophila and zebrafish. *Molecules*. 2015 Apr 9; 20(4):6237-6253. doi: 10.3390/molecules20046237

222. Pontarin G, Gallinaro L, Ferraro P, Reichard P, Bianchi V. Origins of mitochondrial thymidine triphosphate: dynamic relations to cytosolic pools. *Proc Natl Acad Sci U S A*. 2003 Oct 14; 100(21):12159-12164. doi: 10.1073/pnas.1635259100

223. Pontarin G, Fijolek A, Pizzo P, Ferraro P, Rampazzo C, *et al.* Ribonucleotide reduction is a cytosolic process in mammalian cells independently of DNA damage. *Proc Natl Acad Sci U S A*. 2008 Nov 18; 105(46):17801-17806. doi: 10.1073/pnas.0808198105

224. Poole AC, Thomas RE, Yu S, Vincow ES, Pallanck L. The mitochondrial fusion-promoting factor mitofusin is a substrate of the PINK1/parkin pathway. *PLoS One*. 2010 Apr 7; 5(4):e10054. doi: 10.1371/journal.pone.0010054.

225. Puthalakath H, Strasser A. Keeping killers on a tight leash: transcriptional and post-translational control of the pro-apoptotic activity of BH3-only proteins. *Cell Death Differ*. 2002 May; 9(5):505-512. doi: 10.1038/sj/cdd/4400998

226. Rafelski SM. Mitochondrial network morphology: building an integrative, geometrical view. *BMC Biol.* 2013 Jun 24; 11:71. doi: 10.1186/1741-7007-11-71

227. Raimundo N, Song L, Shutt TE, McKay SE, Cotney J, *et al.* Mitochondrial stress engages E2F1 apoptotic signaling to cause deafness. *Cell*. 2012 Feb 17; 148(4):716-726. doi: 10.1016/j.cell.2011.12.027

228. Rampazzo C, Fabris S, Franzolin E, Crovatto K, Frangini M, *et al.* Mitochondrial thymidine kinase and the enzymatic network regulating thymidine triphosphate pools in cultured human cells. *J Biol Chem*. 2007 Nov 30; 282(48):34758-34769. doi:10.1074/jbc.M705923200

229. Reinhold R, Krüger V, Meinecke M, Schulz C, Schmidt B, *et al.* The channel-forming Sym1 protein is transported by the TIM23 complex in a presequence-independent manner. *Mol Cell Biol*. 2012 Dec; 32(24):5009-5021. doi: 10.1128/MCB.00843-12

230. Richter-Dennerlein R, Korwitz A, Haag M, Tatsuta T, Dargazanli S, *et al.* DNAJC19, a mitochondrial cochaperone associated with cardiomyopathy, forms a complex with prohibitins to regulate cardiolipin remodeling. *Cell Metab*. 2014 Jul 1; 20(1):158-171. doi: 10.1016/j.cmet.2014.04.016

231. Rikhy R, Kamat S, Ramagiri S, Sriram V, Krishnan KS. Mutations in dynamin-related protein result in gross changes in mitochondrial morphology and affect synaptic vesicle recycling at the Drosophila neuromuscular junction. *Genes Brain Behav*. 2007 Feb; 6(1):42-53. doi: 10.1111/j.1601-183X.2006.00218.x

232. Rokka A, Antonenkov VD, Soininen R, Immonen HL, Pirilä PL, *et al.* Pxmp2 is a channel-forming protein in Mammalian peroxisomal membrane. *PLoS One*. 2009; 4(4):e5090. doi: 10.1371/journal.pone.0005090

233. Roundhill E, Turnbull D, Burchill S. Localization of MRP-1 to the outer mitochondrial membrane by the chaperone protein HSP90β. *FASEB J*. 2016 May; 30(5):1712-1723. doi: 10.1096/fj.15-283408

234. Royden CS, Pirrotta V, Jan LY. The tko locus, site of a behavioral mutation in D. melanogaster, codes for a protein homologous to prokaryotic ribosomal protein S12. Cell. 1987 Oct 23; 51(2):165-173. https://doi.org/10.1016/0092-8674(87)90144-9

235. Rudrapatna VA, Cagan RL, Das TK. Drosophila cancer models. *Dev Dyn*. 2012 Jan;241(1):107-118. doi: 10.1002/dvdy.22771

236. Ruiz-Pesini E, Lott MT, Procaccio V, Poole JC, Brandon MC, Mishmar D Yi C, Kreuziger J, Baldi P, Wallace DC. An enhanced MITOMAP with a global mtDNA mutational phylogeny. *Nucleic Acids Res*. 2007 Jan; 35. (Database issue): D823–D828. doi: 10.1093/nar/gkl927

237. Russel FG, Koenderink JB, Masereeuw R. Multidrug resistance protein 4 (MRP4/ABCC4): a versatile efflux transporter for drugs and signalling molecules. *Trends Pharmacol Sci*. 2008 Apr; 29(4):200-207. doi: 10.1016/j.tips.2008.01.006

238. Saada A, Shaag A, Elpeleg O. mtDNA depletion myopathy: elucidation of the tissue specificity in the mitochondrial thymidine kinase (TK2) deficiency. *Mol Genet Metab*. 2003 May; 79(1):1-5.

239. Saada A. Fishing in the (deoxyribonucleotide) pool. *Biochem J*. 2009 Aug 27; 422(3):e3-6. doi: 10.1042/BJ20091194

240. Sakowska P, Jans DC, Mohanraj K, Riedel D, Jakobs S, *et al.* The Oxidation Status of Mic19 Regulates MICOS Assembly. *Mol Cell Biol*. 2015 Dec; 35(24):4222-4237. doi: 10.1128/MCB.00578-15

241. Sánchez-Martínez A, Luo N, Clemente P, Adán C, Hernández-Sierra R, *et al.* Modeling human mitochondrial diseases in flies. *Biochim Biophys Acta*. 2006 Sep-Oct; 1757(9-10):1190-1198. doi: 10.1016/j.bbabio.2006.05.008

242. Schneiderman HA, Gateff E. Control systems in insect development. *Science*. 1967 Oct 27; 158(3800):534-535. doi: 10.1126/science.158.3800.534-c

243. Schon EA, DiMauro S, Hirano M. Human mitochondrial DNA: roles of inherited and somatic mutations. *Nat Rev Genet*. 2012 Dec; 13(12): 878–890. doi: 10.1038/nrg3275

244. Schrepfer E, Scorrano L. Mitofusins, from mitochondria to metabolism. *Mol Cell*. 2016 Mar 3; 61(5):683-694. doi: 10.1016/j.molcel.2016.02.022

245. Scott I, Youle RJ. Mitochondrial fission and fusion. *Essays Biochem*. 2010; 47: 85–98. doi: 10.1042/bse0470085

246. Seelert H, Dencher NA. ATP synthase superassemblies in animals and plants: two or more are better. *Biochim Biophys Acta*. 2011 Sep; 1807(9):1185-1197. doi: 10.1016/j.bbabio.2011.05.023

247. Sehgal A, Joiner W, Crocker A, Koh K, Sathyanarayanan S, *et al.* Molecular analysis of sleep: wake cycles in Drosophila. *Cold Spring Harb Symp Quant Biol*. 2007; 72:557-564. doi: 10.1101/sqb.2007.72.018

248. Sen A, Cox RT. Fly Models of Human Diseases: Drosophila as a Model for Understanding Human Mitochondrial Mutations and Disease. *Curr Top Dev Biol*. 2017; 121:1-27. doi: 10.1016/bs.ctdb.2016.07.001

249. Seo AY, Joseph AM, Dutta D, Hwang JCY, Aris JP, *et al.* New insights into the role of mitochondria in aging: mitochondrial dynamics and more. J Cell Sci. 2010 Aug 1; 123(15): 2533–2542. doi: 10.1242/jcs.070490

250. Song Z, Chen H, Fiket M, Alexander C, Chan DC.OPA1 processing controls mitochondrial fusion and is regulated by mRNA splicing, membrane potential, and Yme1L. *J Cell Biol*. 2007 Aug 27; 178(5): 749–755. doi: 10.1083/jcb.200704110

251. Spinazzi M, Casarin A, Pertegato V, Salviati L, Angelini C. Assessment of mitochondrial respiratory chain enzymatic activities on tissues and cultured cells. *Nat Protoc*. 2012 May 31; 7(6):1235-1246. doi: 10.1038/nprot.2012.058

252. Spinazzola A, Viscomi C, Fernandez-Vizarra E, Carrara F, D'Adamo P, *et al.* MPV17 encodes an inner mitochondrial membrane protein and is mutated in infantile hepatic mitochondrial DNA depletion. *Nat Genet.* 2006 May; 38(5):570-575. doi: 10.1038/ng1765

253. Stepien, A. Torroni, A.B. Chung, J.A. Hodge, D.C. Wallace, Differential expression of adenine nucleotide translocator isoforms in mammalian tissues and during muscle cell differentiation, *J. Biol. Chem*. 267 (1992) 14592–14597.

254. Stojanovski D, Bohnert M, Pfanner N, van der Laan M. Mechanisms of protein sorting in mitochondria. *Cold Spring Harb Perspect Biol*. 2012 Oct; 4(10): a011320. doi: 10.1101/cshperspect.a011320

255. Stowers RS, Megeath LJ, Górska-Andrzejak J, Meinertzhagen IA, Schwarz TL. Axonal transport of mitochondria to synapses depends on Milton, a novel Drosophila protein. *Neuron*. 2002 Dec 19; 36(6):1063-77.

256. Su B, Wang X, Zheng L, Perry G, Smith MA, *et al.* Abnormal mitochondrial dynamics and neurodegenerative diseases. *Biochim Biophys Acta*. 2010 Jan; 1802(1):135-142. doi: 10.1016/j.bbadis.2009.09.013

257. Sun X, Yasuda O, Takemura Y, Kawamoto H, Higuchi M, Baba Y, Katsuya T, Fukuo K, Ogihara T, Rakugi H. Akt activation prevents Apop-1-induced death of cells. *Biochem Biophys Res Commun*. 2008 Dec 26;377(4):1097-1101. doi: 10.1016/j.bbrc.2008.10.109

258. Takakubo F, Cartwright P, Hoogenraad N, Thorburn DR, Collins F, *et al.* An amino acid substitution in the pyruvate dehydrogenase E1 alpha gene, affecting mitochondrial import of the precursor protein. *Am J Hum Genet.* 1995 Oct; 57(4):772-780.

259. Takata A, Matsumoto N, Kato T. Genome-wide identification of splicing QTLs in the human brain and their enrichment among schizophrenia-associated loci. *Nat Commun*. 2017 Feb 27; 8:14519. doi: 10.1038/ncomms14519

260. Tang S, Khanh Le P, Tse S, Wallace DC, Huang T. Heterozygous mutation of Opa1 in Drosophila shortens lifespan mediated through increased reactive oxygen species production. *PLoS ONE*. 2009; 4(2): e4492. doi: 10.1371/journal.pone.0004492

261. Tarasenko D, Barbot M, Jans DC, Kroppen B, Sadowski B, *et al.* The MICOS component Mic60 displays a conserved membrane-bending activity that is necessary for normal cristae morphology. *J Cell Biol*. 2017 Apr 3; 216(4):889-899. doi: 10.1083/jcb.201609046

262. Terhzaz S, Cabrero P, Chintapalli VR, Davies SA, Dow JA. Mislocalization of mitochondria and compromised renal function and oxidative stress resistance in Drosophila SesB mutants. *Physiol Genomics*. 2010 Mar 3; 41(1):33-41. doi: 10.1152/physiolgenomics.00147.2009

263. Tiranti V, Hoertnagel K, Carrozzo R, Galimberti C, Munaro M, *et al.* Mutations of SURF-1 in Leigh disease associated with cytochrome c oxidase deficiency. *Am J Hum Genet*. 1998 Dec; 63(6):1609-1621. http://doi.org/10.1086/302150

264. Toivonen JM, O'Dell KM, Petit N, Irvine SC, Knight GK, *et al.* technical knockout, a Drosophila model of mitochondrial deafness. *Genetics*. 2001 Sep; 159(1):241-254.

265. Tranebjaerg L, Schwartz C, Eriksen H, Andreasson S, Ponjavic V, *et al.* A new X linked recessive deafness syndrome with blindness, dystonia, fractures, and mental deficiency is linked to Xq22. *J Med Genet*. 1995 Apr; 32(4):257-263.

266. Tripoli G, D'Elia D, Barsanti P, Caggese C. Comparison of the oxidative phosphorylation (OXPHOS) nuclear genes in the genomes of Drosophila melanogaster, Drosophila pseudoobscura and Anopheles gambiae. *Genome Biol*. 2005; 6(2):R11. doi: 10.1186/gb-2005-6-2-r11

267. Trott A, Morano KA. Sym1 is the stress-induced Saccharomyces cerevisiae ortholog of the mammalian kidney disease gene Mpv17 and is required for ethanol metabolism and tolerance during heat shock. *Eukaryot Cell*. 2004 Jun; 3(3):620-631. doi: 10.1128/EC.3.3.620-631.2004

268. Tsujimoto Y, Shimizu S. Bcl-2 family: life-or-death switch. *FEBS Lett*. 2000 Jan 21; 466(1):6-10.

269. Tuppen HA, Blakely EL, Turnbull DM, Taylor RW. Mitochondrial DNA mutations and human disease. *Biochim Biophys Acta*. 2010 Feb; 1797(2):113-128. doi: 10.1016/j.bbabio.2009.09.005

270. Uusimaa J, Evans J, Smith C, Butterworth A, Craig K, *et al.* Clinical, biochemical, cellular and molecular characterization of mitochondrial DNA depletion syndrome due to novel mutations in the MPV17 gene. *Eur J Hum Genet*. 2014 Feb; 22(2):184-191. doi: 10.1038/ejhg.2013.112

271. van der Bliek AM, Shen Q, Kawajiri S. Mechanisms of mitochondrial fission and fusion. *Cold Spring Harb Perspect Biol*. 2013 Jun; 5(6): a011072. doi: 10.1101/cshperspect.a011072

272. Vartiainen S, Chen S, George J, Tuomela T, Luoto KR, *et al.* Phenotypic rescue of a Drosophila model of mitochondrial ANT1 disease. *Dis Model Mech*. 2014 Jun; 7(6): 635–648. doi: 10.1242/dmm.016527

273. Viscomi C, Spinazzola A, Maggioni M, Fernandez-Vizarra E, Massa V, *et al.* Early-onset liver mtDNA depletion and late-onset proteinuric nephropathy in Mpv17 knockout mice. *Hum Mol Genet*. 2009 Jan 1; 18(1):12-26. doi: 10.1093/hmg/ddn309

274. Viscomi C, Zeviani M. MtDNA-maintenance defects: syndromes and genes. *J Inherit Metab Dis*. 2017 Mar 21. doi: 10.1007/s10545-017-0027-5

275. Vives-Bauza C, Zhou C, Huang Y, Cui M, de Vries RL, *et al.* PINK1-dependent recruitment of Parkin to mitochondria in mitophagy. *Proc Natl Acad Sci U S A*. 2010 Jan 5; 107(1):378-383. doi: 10.1073/pnas.0911187107

276. Wallace DC, Singh G, Lott MT, Hodge JA, Schurr TG, *et al.* Mitochondrial DNA mutation associated with Leber's hereditary optic neuropathy. *Science*. 1988 Dec 9; 242(4884):1427-1430. doi: 10.1126/science.3201231

277. Wallace DC, Chalkia D. Mitochondrial DNA genetics and the heteroplasmy conundrum in evolution and disease. *Cold Spring Harb Perspect Biol*. 2013 Nov 1; 5(11):a021220. doi: 10.1101/cshperspect.a021220

278. Wang C, Youle RJ. The role of mitochondria in apoptosis. *Annu Rev Genet*. 2009; 43: 95–118. doi: 10.1146/annurev-genet-102108-134850

279. Wang L. Mitochondrial purine and pyrimidine metabolism and beyond. *Nucleosides Nucleotides Nucleic Acids*. 2016 Dec; 35(10-12):578-594. doi:10.1080/15257770.2015.1125001

280. Wang X. The expanding role of mitochondria in apoptosis. *Genes Dev*. 2001 Nov 15; 15(22):2922-2933.

281. Wang X, Winter D, Ashrafi G, Schlehe J, Wong YL, *et al.* PINK1 and Parkin target Miro for phosphorylation and degradation to arrest mitochondrial motility. *Cell*. 2011 Nov 11; 147(4):893-906. doi: 10.1016/j.cell.2011.10.018

282. Wei MC, Zong WX, Cheng EH, Lindsten T, Panoutsakopoulou V, Ross AJ, Roth KA, MacGregor GR, Thompson CB, Korsmeyer SJ. Proapoptotic BAX and BAK: a requisite gateway to mitochondrial dysfunction and death. *Science*. 2001 Apr 27; 292(5517):727-730. doi: 10.1126/science.1059108

283. Weiher H, Noda T, Gray DA, Sharpe AH, Jaenisch R. Transgenic mouse model of kidney disease: insertional inactivation of ubiquitously expressed gene leads to nephrotic syndrome. *Cell*. 1990 Aug 10; 62(3):425-434.

284. Weihofen A, Thomas KJ, Ostaszewski BL, Cookson MR, Selkoe DJ. Pink1 forms a multiprotein complex with Miro and Milton, linking Pink1 function to mitochondrial trafficking. *Biochemistry*. 2009 Mar 10; 48(9):2045-52. doi: 10.1021/bi8019178

285. Westermann B. Bioenergetic role of mitochondrial fusion and fission. *Biochim Biophys Acta*. 2012 Oct; 1817(10):1833-8. doi: 10.1016/j.bbabio.2012.02.033

286. Whitworth AJ. Drosophila models of Parkinson's disease. *Adv Genet*. 2011; 73:1-50. doi: 10.1016/B978-0-12-380860-8.00001-X

287. Wiedemann N, Frazier AE, Pfanner N. The protein import machinery of mitochondria. *J Biol Chem*. 2004 Apr 9; 279(15):14473-14476. doi:10.1074/jbc.R400003200

288. Willis S, Day CL, Hinds MG, Huang DC. The Bcl-2-regulated apoptotic pathway. *J Cell Sci*. 2003 Oct 15; 116(Pt 20):4053-4056. doi: 10.1242/jcs.00754

289. Wittig I, Schagger H. Supramolecular organization of ATP synthase and respiratory chain in mitochondrial membranes. *Biochim Biophys Acta*. 2009; 1787:672–680. doi: 10.1016/j.bbabio.2008.12.016

290. Wolff JN, Camus MF, Clancy DJ, Dowling DK. Complete mitochondrial genome sequences of thirteen globally sourced strains of fruit fly (Drosophila melanogaster) form a powerful model for mitochondrial research. *Mitochondrial DNA A DNA Mapp Seq Anal*. 2016 Nov; 27(6):4672-4674. doi:10.3109/19401736.2015.1106496

291. Wong ED, Wagner JA, Gorsich SW, McCaffery JM, Shaw JM, *et al.* The dynamin-related GTPase, Mgm1p, is an intermembrane space protein required for maintenance of fusion competent mitochondria. *J Cell Biol*. 2000 Oct 16; 151(2):341-352

292. Xu X, Duan S, Yi F, Ocampo A, Liu GH, *et al.* Mitochondrial regulation in pluripotent stem cells. *Cell Metab*. 2013 Sep 3; 18(3):325-332. doi: 10.1016/j.cmet.2013.06.005

293. Yarosh W, Monserrate J, Tong JJ, Tse S, Le PK, *et al.* The molecular mechanisms of OPA1-mediated optic atrophy in Drosophila model and prospects for antioxidant treatment. *PLoS Genet*. 2008 Jan; 4(1):e6. doi: 10.1371/journal.pgen.0040006

294. Yasuda O, Fukuo K, Sun X, Nishitani M, Yotsui T, *et al.* Apop-1, a novel protein inducing cyclophilin D-dependent but Bax/Bak-related channel-independent apoptosis. *J Biol Chem*. 2006 Aug 18; 281(33):23899-23907. doi: 10.1074/jbc.M512610200

295. Youle RJ, van der Bliek AM. Mitochondrial fission, fusion, and stress. *Science*. 2012 Aug 31; 337(6098): 1062–1065. doi: 10.1126/science.1219855

296. Young JC, Hoogenraad NJ, Hartl FU. Molecular chaperones Hsp90 and Hsp70 deliver preproteins to the mitochondrial import receptor Tom70. *Cell*. 2003 Jan 10; 112(1):41-50. http://dx.doi.org/10.1016/S0092-8674(02)01250-3

297. Zeczycki TN, Whelan J, Hayden WT, Brown DA, Shaikh SR. Increasing levels of cardiolipin differentially influence packing of phospholipids found in the mitochondrial inner membrane. *Biochem Biophys Res Commun*. 2014 Jul 18; 450(1):366-371. doi: 10.1016/j.bbrc.2014.05.133

298. Zeng X, Neupert W, Tzagoloff A. The metalloprotease encoded by ATP23 has a dual function in processing and assembly of subunit 6 of mitochondrial ATPase. *Mol Biol Cell*. 2007 Feb; 18(2):617-626.

299. Zerbes R.M., Bohnert M., Stroud D.A., von der Malsburg K., Kram A., *et al.* Role of MINOS in mitochondrial membrane architecture: cristae morphology and outer membrane interactions differentially depend on mitofilin domains. *J. Mol. Biol*. 2012; 422:183–191 10.1016/j.jmb.2012.05.004

300. Zeviani M, Carelli V. Mitochondrial disorders. *Curr Opin Neurol*. 2007 Oct; 20(5):564-571. doi: 10.1097/WCO.0b013e3282ef58cd

301. Zhang K, Li Z, Jaiswal M, Bayat V, Xiong B, *et al.* The C8ORF38 homologue Sicily is a cytosolic chaperone for a mitochondrial complex I subunit. *J Cell Biol*. 2013 Mar 18; 200(6):807-820. doi: 10.1083/jcb.201208033

302. Zheng X, Ruas JL, Cao R, Salomons FA, Cao Y, *et al.* Cell-type-specific regulation of degradation of hypoxia-inducible factor 1 alpha: role of subcellular compartmentalization. *Mol Cell Biol*. 2006 Jun; 26(12):4628-4641.

303. Zhou C, Huang Y, Shao Y, May J, Prou D, *et al.* The kinase domain of mitochondrial PINK1 faces the cytoplasm. *Proc Natl Acad Sci U S A*. 2008 Aug 19; 105(33):12022-12027. doi: 10.1073/pnas.0802814105

304. Zhu Z, Yao J, Johns T, Fu K, De Bie I, *et al.* SURF1, encoding a factor involved in the biogenesis of cytochrome c oxidase, is mutated in Leigh syndrome. *Nat Genet*. 1998 Dec; 20(4):337-343. doi:10.1038/3804

305. Zick M, Rabl R, Reichert AS. Cristae formation-linking ultrastructure and function of mitochondria. *Biochim Biophys Acta*. 2009 Jan; 1793(1):5-19. doi: 10.1016/j.bbamcr.2008.06.013

306. Zimorski V, Ku C, Martin WF, Gould SB. Endosymbiotic theory for organelle origins. *Curr Opin Microbiol*. 2014 Dec; 22:38-48. doi: 10.1016/j.mib.2014.09.008

307. Ziviani E, Tao RN, Whitworth AJ. Drosophila parkin requires PINK1 for mitochondrial translocation and ubiquitinates mitofusin. *Proc Natl Acad Sci U S A*. 2010 Mar 16; 107(11):5018-5023. doi: 10.1073/pnas.0913485107

308. Zorov DB, Juhaszova M, Sollott SJ. Mitochondrial Reactive Oxygen Species (ROS) and ROS-induced ROS release. *Physiol Rev*. 2014 Jul; 94(3): 909–950. doi: 10.1152/physrev.00026.2013

309. Züchner S, Mersiyanova IV, Muglia M, Bissar-Tadmouri N, Rochelle J, *et al.* Mutations in the mitochondrial GTPase mitofusin 2 cause Charcot-Marie-Tooth neuropathy type 2A. *Nat Genet*. 2004 May; 36(5):449-451. doi: 10.1038/ng1341

310. Zwacka RM, Reuter A, Pfaff E, Moll J, Gorgas K, *et al.* The glomerulosclerosis gene Mpv17 encodes a peroxisomal protein producing reactive oxygen species. *EMBO J*. 1994 Nov 1; 13(21):5129-5134.

Appendix

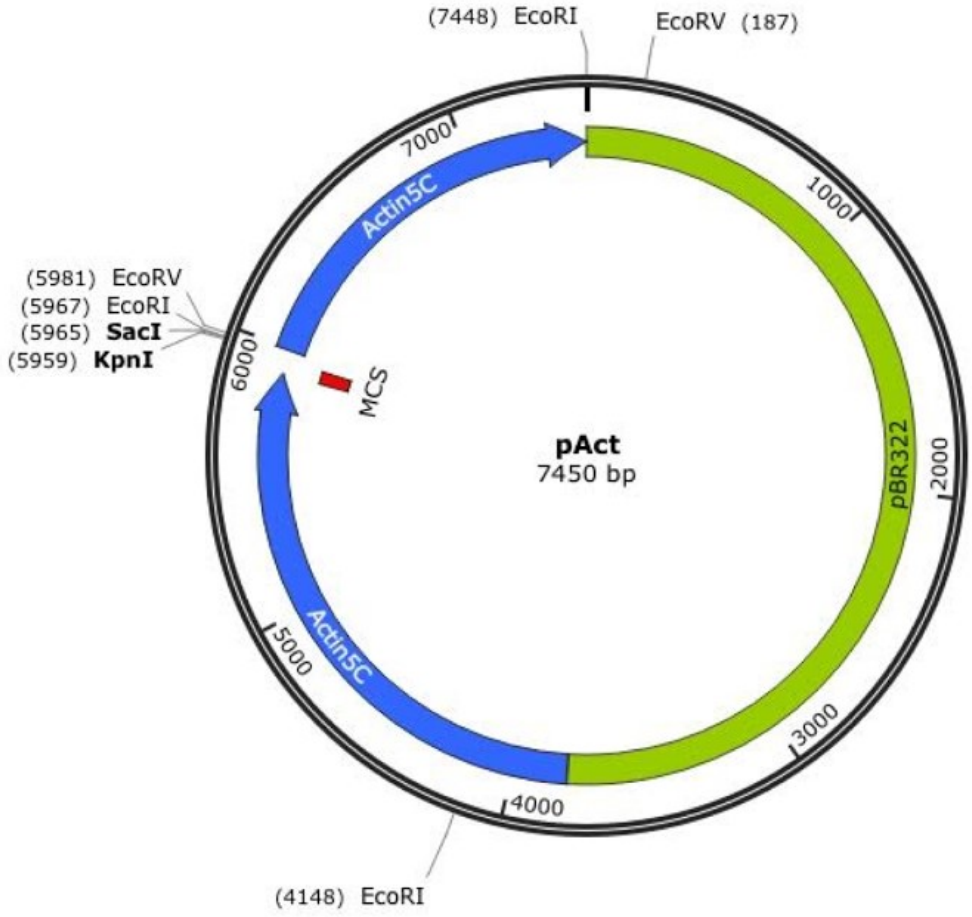

Fig.33 pAct plasmid map.

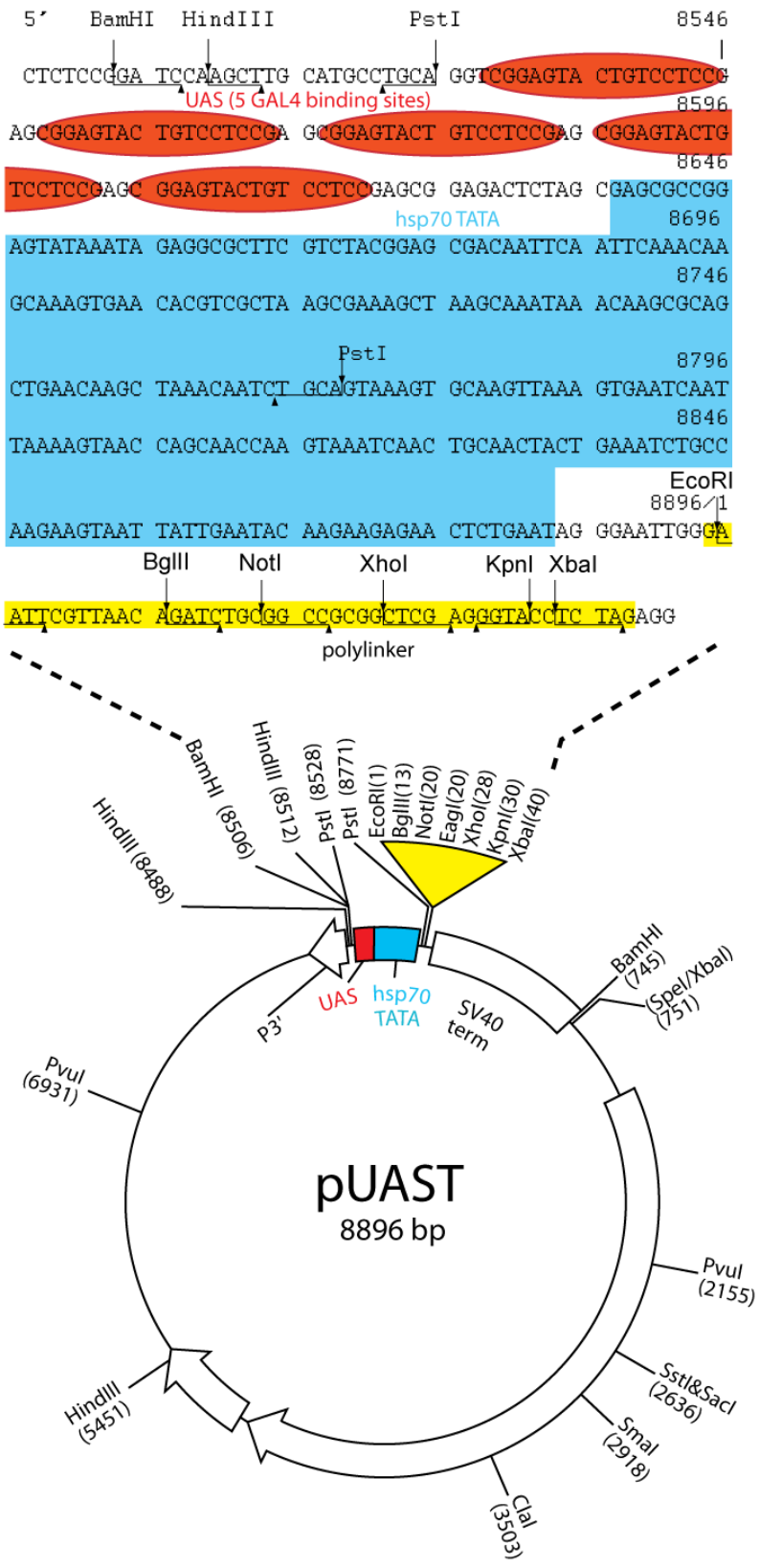

Fig. 34 pUAST plasmid map.

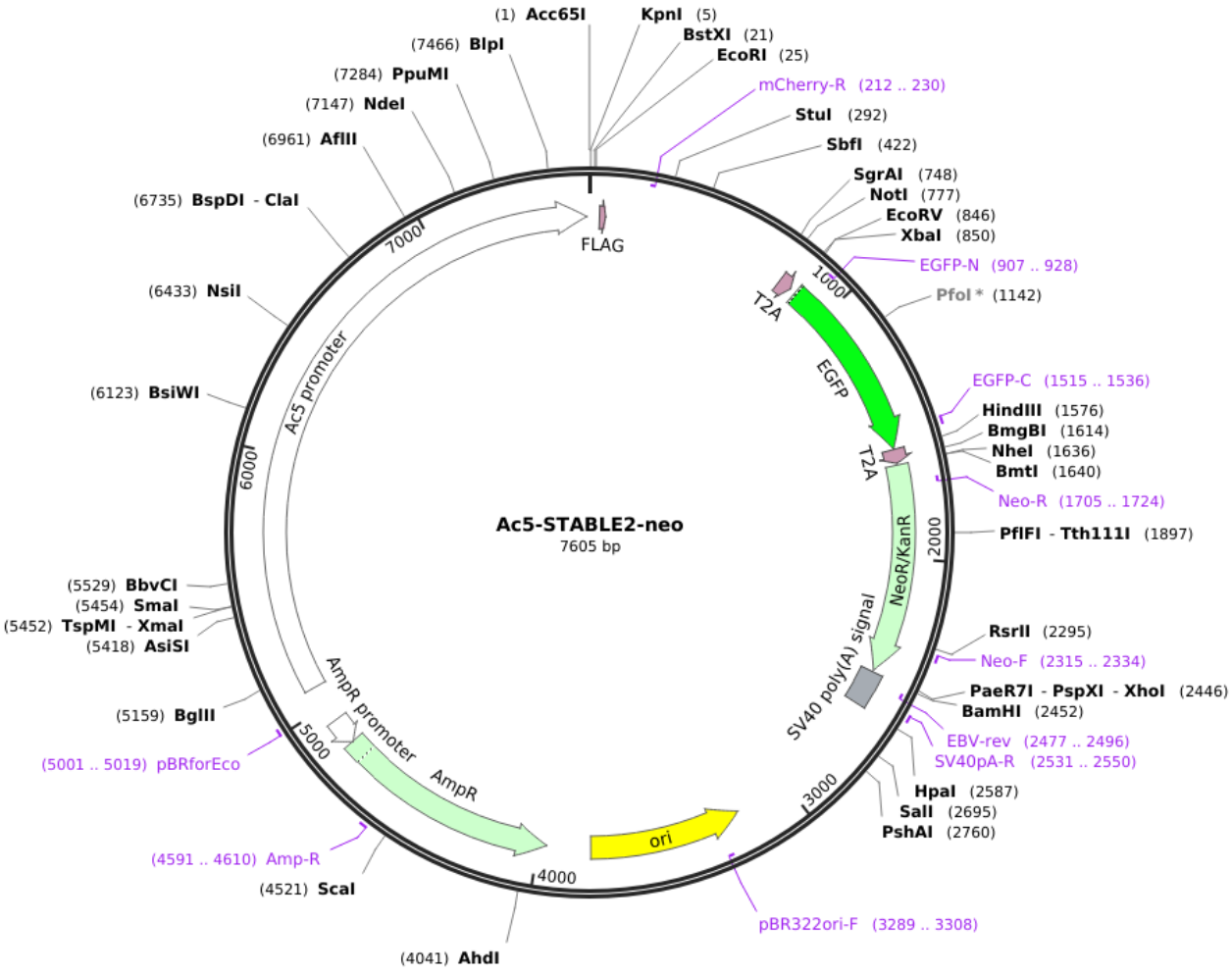

Fig. 35 Ac5-STABLE2-neo plasmid map.

Tab. 16 Mass spectrometry data.

full_dataset_V1

gene_names	Fasta.headers	Peptide.counts..unique.	Unique.sequence.co	iBAQ.Gal4	iBAQ.Overexpre	iBAQ.UAS	raw_Gal4	raw_Overexpres	raw_UAS	norm_Gal4	norm_Overexpr	norm_UAS	OE.Gal4.ratio	OE.UAS.ratio
CG13678	>tr|Q9VSG0|Q9VSG0	2	27.3	0	7172300	0	1	7172300	1	1	8871721.747	1	8871721.747	8871721.747
CG11077	>sp|Q9V492|	2	7.1	0	1644000	0	1	1644000	1	1	2033533.253	1	2033533.253	2033533.253
Mrp4	>tr|Q9VGM1|Q9VGM1	3	3	0	279740	12629	1	279740	12629	1	346022.2581	20976.75551	346022.2581	16.49550894
	>tr|Q9VA18|Q9VA18	2	19.3	0	211550	19295	1	211550	19295	1	261675.158	32048.97432	261675.158	8.164852809
Tsp	>tr|Q8T0I9|Q8T0I9	2;2	4.8	0	194210	0	1	194210	1	1	240226.5773	1	240226.5773	240226.5773
CG15531	>tr|Q9VA93|Q9VA93	2	3.6	0	186190	0	1	186190	1	1	230306.2995	1	230306.2995	230306.2995
CG7910	>tr|Q9VHW0|Q9VHW0	2	6.6	0	102130	0	1	102130	1	1	126328.9241	1	126328.9241	126328.9241
pgant4	>tr|B7Z006|B7Z006	3;3	5	0	98023	115480	1	98023	115480	1	121248.8018	191812.1556	121248.8018	0.632122617
Spat	>tr|Q9W3Z3|Q9W3Z3	3	11.2	0	52689	535760	1	52689	535760	1	65173.25646	889896.7823	65173.25646	0.073236872
CG6912	>tr|Q9VFD1|Q9VFD1	2	3	0	38936	8126.7	1	38936	8126.7	1	48161.58807	13498.44007	48161.58807	3.56793732
Ugt	>sp|Q09332|UGGG	4	3	0	35836	38933	1	35836	38933	1	44327.06673	64667.67114	44327.06673	0.685459457
Lsp1alpha	>sp|P11995|LSP1A	2	2.9	0	28322	44103	1	28322	44103	1	35032.68177	73255.03556	35032.68177	0.478228991
RhoGAPp190	>tr|M9PJQ3|M9PJQ3	2;2;2;2;2	1.4	0	24448	19096	1	24448	19096	1	30240.76704	31718.43553	30240.76704	0.953412945
Crys	>tr|Q9VKE2|Q9VKE2	11	35.2	247700	7315400	0	247700	7315400	1	120561.0971	9048728.2	1	75.05512487	9048728.2
dlg1	>tr|M9PJI4|M9PJI4	3;3;3;3;3;3;2	5.1	15616	262330	82403	15616	262330	82403	7600.654575	324487.0914	136871.2943	42.69199294	2.370746132
lectin-28C	>tr|Q9VLW1|Q9VLW1	2	4.5	28168	322040	39221	28168	322040	39221	13709.99203	398344.9202	65146.03883	29.05508036	6.114645302
mys	>tr|X2JE30|X2JE30	4;4;4	5.8	27928	178530	24946	27928	178530	24946	13593.1787	220831.321	41435.27922	16.24574545	5.329548277
wupA	>tr|M9PJQ5|M9PJQ5	7;7	27.2	4543900	20561000	2283800	4543900	20561000	2283800	2211617.151	25432772.03	3793389.337	11.49962687	6.704498213
CG8547	>tr|Q0E980|Q0E980	5	14.9	137560	604540	21662	137560	604540	21662	66953.51046	747781.1392	35980.55877	11.16866217	20.7829218
Cpr64Aa	>tr|Q9VZG2|Q9VZG2	3	38	358220	1528400	0	358220	1528400	1	174353.6382	1890542.715	1	10.84315036	1890542.715
Hml	>tr|M9PCE5|M9PCE5	15;15	5.2	59632	234090	13321	59632	234090	13321	29024.22035	289555.839	22126.16676	9.976352009	13.08657944
CG42235-RD;CG8951	>tr|Q9VBK1|Q9VBK1	2;1;1;1;1	3.9	70581	261750	158850	70581	261750	158850	34353.34207	323769.6649	263849.6788	9.424691904	1.227098954
Mip84B	>tr|A4V2J1|A4V2J1	13;13	41.4	3215700	11070000	715030	3215700	11070000	715030	1565152.682	13692952.01	1187664.059	8.748636582	11.52931413
dec-1	>tr|M9NEY9|M9NEY9	8;8;8;8;8;8	19.5	202600	590850	0	202600	590850	1	98609.92445	730847.3982	1	7.411499424	730847.3982
Tig	>tr|X2JDD7|X2JDD7	24;24	14.2	308050	864090	113640	308050	864090	113640	149934.7838	1068829.531	188755.9176	7.128629552	5.662495484
Piezo	>tr|M9PCC7|M9PCC7	7;7;7;7;7;6;6;6;6;6;6	3.3	53455	147900	16986	53455	147900	16986	26017.73712	182943.7763	28213.72781	7.031502218	6.484211427
Atg1	>tr|Q8MQJ7|Q8MQJ7	2;1	4.2	57412	144390	56038	57412	144390	56038	27943.69699	178602.1086	93079.05769	6.391498899	1.918821623
CG5432-RA	>tr|Q9VBF5|Q9VBF5	4	13.7	1000200	2408000	421450	1000200	2408000	421450	486819.5769	2978557.222	700027.9956	6.118400664	4.254911577
Cyp6d5	>sp|Q9VFP1|CP6D5	4	11.2	166530	354210	524870	166530	354210	524870	81053.85353	438137.3562	871808.5041	5.405509265	0.502561462
Srp68	>sp|Q9VSS2|SRP68	2	4.1	30632	64466	0	30632	64466	1	14909.27561	79740.72673	1	5.348397118	79740.72673
Cpr62Bb	>tr|Q9W078|Q9W078	4;1	29.9	1702100	3537300	74686	1702100	3537300	74686	828449.9117	4375436.239	124053.3656	5.281473481	35.2705968
CG31195-RA	>tr|Q8IN49|Q8IN49	7	9.8	93754	188480	134880	93754	188480	134880	45632.15636	233138.8976	224035.5347	5.109092276	1.040633567
norpA	>tr|X2JCI4|X2JCI4	2;2;2	2.1	37146	71155	21515	37146	71155	21515	18079.78423	88014.63423	35736.39192	4.868124148	2.462885297
prc	>tr|Q9VTR6|Q9VTR6	6	8.5	2570900	4803300	896130	2570900	4803300	896130	1251314.187	5941405.277	1488470.964	4.748132274	3.991616512
825-Oak;CG32213	>tr|Q8IQU7|Q8IQU7	3;2;1	36.4	11451000	21234000	8292800	11451000	21234000	8292800	5573456.282	26265234.24	13774331.86	4.712557687	1.906824557
CG45076;fau	>tr|A0A0B4LGZ7|A0A0B4LGZ7	17;17	31.5	13032000	23839000	2502300	13032000	23839000	2502300	6342964.131	29487469.11	4156317.601	4.648846896	7.094614017
zormin	>tr|Q0E8J3|Q0E8J3	34;34;32;29;27;27	12.8	397850	710290	96230	397850	710290	96230	193642.4403	878587.7947	159837.9263	4.537165475	5.496741698
CG10359	>tr|B7Z0B3|B7Z0B3	2;2	9.2	155320	273250	0	155320	273250	1	75597.69731	337994.5021	1	4.470962928	337994.5021
CG13048	>tr|Q9VV17|Q9VV17	2	9.2	6904600	12019000	3907100	6904600	12019000	3907100	3360622.325	14866810.32	6489688.886	4.423826567	2.290835598
Ccp84Ag	>tr|O97064|O97064	8	73.8	18840000	32721000	12249000	18840000	32721000	12249000	9169846.856	40473991.23	20345575.79	4.413813214	1.989326409
Irk1	>tr|E1JIU2|E1JIU2	2;2;2;2;2	4.6	156560	265940	12369	156560	265940	12369	76201.23288	328952.4534	20544.89579	4.316891486	16.01139557
mge	>tr|Q9VZL1|Q9VZL1	4;2;1	40.5	1622900	2756300	564350	1622900	2756300	564350	789901.5109	3409384.249	937384.7415	4.316214366	3.637123689
Desat1;Desat2	>tr|Q7K4Y0|Q7K4Y0	2;1	11.5	380380	623610	113620	380380	623610	113620	185139.4029	771369.6302	188722.6976	4.166426045	4.087317742
Act57B	>sp|P53501|ACT3	6	8	60651000	97229000	19889000	60651000	97229000	19889000	29520190.11	120266669.5	33035607.55	4.074047933	3.640516353
Fas2	>tr|X2JCI0|X2JCI0	5;5;5;5;5	9.1	106710	169310	122730	106710	169310	122730	51938.1296	209426.7124	203854.3978	4.032234391	1.027334777
Mhc	>sp|P05661|MYSA	4	2.6	1813600	2813900	779610	1813600	2813900	779610	882719.4406	3480632.13	1294931.369	3.943078593	2.687889267
Lsp1beta	>tr|X2J8F5|X2J8F5	4;4	5.3	211540	326990	351640	211540	326990	351640	102961.2212	404467.785	584073.6609	3.928350696	0.692494478
CG9485	>tr|Q7KVP4|Q7KVP4	21;21;21;21	18.1	652180	993620	902570	652180	993620	902570	317430.5056	1229050.676	1499167.797	3.871873226	0.819821956
Nup154	>tr|Q9V463|Q9V463	3	2.3	15749	23863	5223.6	15749	23863	5223.6	7665.388632	29517.15576	8676.394097	3.850705707	3.402007265

full_dataset_V1

CRIF	>tr|Q9VP13|Q9VP13	4	28.4	1227600	1826100	983790	1227600	1826100	983790	597500.2125	2258780.458	1634074.129	3.78038436	1.382299871
Surf4	>sp|O18405|SURF4	2	7.4	730830	1081200	875340	730830	1081200	875340	355711.2092	1337382.088	1453938.796	3.7597412	0.919833828
Vinc	>tr|X2JAB9|X2JAB9	31;31	45	3420200	4979200	959920	3420200	4979200	959920	1664687.379	6158983.439	1594426.085	3.699783826	3.862821549
wupA	>tr|M9NFC0|M9NFC0	3	23.1	1544700	2243300	371140	1544700	2243300	371140	751839.8324	2774832.814	616463.1399	3.690723336	4.501214485
CG11309	>tr|Q9VP52|Q9VP52	2;2	7.2	703130	1002100	1439200	703130	1002100	1439200	342229.0034	1239539.947	2390509.648	3.621960544	0.51852539
Swim	>tr|Q7JWQ7|Q7JWQ7	22	46.9	28866000	41127000	9673200	28866000	41127000	9673200	14049723.96	50871728.77	16067174.77	3.620834753	3.166190043
CG13026	>tr|Q9VV95|Q9VV95	3	28.8	69174000	95469000	21228000	69174000	95469000	21228000	33668523.69	118089650.9	35259685.11	3.507419928	3.349140827
Cp19	>sp|P07186|CH19	4	42.2	1177800	1621800	223470	1177800	1621800	223470	573261.4453	2006073.133	371183.4291	3.499403542	5.40453311
CG13049	>tr|Q8SWS3|Q8SWS3	3	33.1	322050000	441070000	145550000	322050000	441070000	145550000	156748894.9	545578170.3	241758393	3.480587028	2.256708292
Treh	>tr|A4UZR3|A4UZR3	3;3	7	57835	77357	84285	57835	77357	84285	28149.5805	95686.15079	139997.2942	3.399203438	0.683485715
Ccp84Ae	>tr|O97062|O97062	6	41.8	5721800	7598900	2320200	5721800	7598900	2320200	2784927.269	9399401.361	3853849.698	3.375097607	2.438964178
Tret1-1;Tret1-2	>sp|A1Z8N1|TRE11	2;1	2.2	200730	264800	296190	200730	264800	296190	97699.75387	327542.3391	491971.2707	3.352540064	0.665775338
Msp300	>tr|M9PCM8|M9PCM8	30;30;30;30;30;30;19;0	3.2	183360	240640	58167	183360	240640	58167	89245.3887	297657.8115	96615.3244	3.335273854	3.080855065
CG5214	>tr|Q9VGQ1|Q9VGQ1	15	33.1	21129000	27515000	10671000	21129000	27515000	10671000	10283954.05	34034469.26	17724519.49	3.309473098	1.920191364
Hrb27C	>tr|E1JHA4|E1JHA4	2;2	6.9	71064	92043	111050	71064	92043	111050	34588.42891	113851.8864	184453.9304	3.291617746	0.617237519
rhea	>tr|M9PEJ8|M9PEJ8	38;38;38;32;2	19.3	819480	1060700	339190	819480	1060700	339190	398859.1351	1312024.77	563394.2243	3.289443953	2.328786333
Tsf2	>tr|Q9VTZ5|Q9VTZ5	4	7.2	57455	73988	106500	57455	73988	106500	27964.62605	91518.89196	176896.3853	3.272666396	0.517358745
CG18294	>tr|Q9VVZ6|Q9VVZ6	2;2	26	13587000	17440000	7553100	13587000	17440000	7553100	6613094.97	21572274.9	12545690.95	3.262054303	1.719496756
CG14095	>tr|Q9VVZ4|Q9VVZ4	4	56.8	253820000	319940000	116450000	253820000	319940000	116450000	123539837	395747341.3	193423324.4	3.203398603	2.046016645
Hexo2	>tr|Q9W3C4|Q9W3C4	3	5.1	132480	166890	79687	132480	166890	79687	64480.96152	206433.3118	132360.0212	3.201461439	1.559634926
CG7409	>tr|Q9VSA9|Q9VSA9	7	47.4	3990100	4988900	945390	3990100	4988900	945390	1942070.379	6170981.78	1570291.771	3.177527368	3.929831319
sls	>tr|M9PEA5|M9PEA5	2;132;131;131;131;131;130;129;128;113	11.5	1299200	1601500	254580	1299200	1601500	254580	632349.5243	1980963.203	422857.1056	3.132702922	4.684710689
Mcr	>tr|Q9VLT3|Q9VLT3	9	7.3	125070	152700	157800	125070	152700	157800	60874.34978	188881.0996	262105.6299	3.102802746	0.720629693
Ran	>tr|A4V4A5|A4V4A5	2;2	12	1269500	1549700	423520	1269500	1549700	423520	617893.874	1916889.588	703466.2634	3.102295828	2.724920423
Pdh	>tr|Q7KNR7|Q7KNR7	4;4;3;3	16.1	751650	914330	1133700	751650	914330	1133700	365844.7661	1130973.515	1883074.477	3.091402749	0.600599461
Rcc1	>sp|P25171|RCC1	3	7.3	297170	352960	123130	297170	352960	123130	144639.246	436591.1783	204518.7973	3.018483506	2.134723967
CAP	>tr|A1Z871|A1Z871	4;4;3;3;3;3;3;3;3;3;3;3;3;3;3;3	3.9	135800	161030	19143	135800	161030	19143	66096.87933	199184.8296	31796.50248	3.013528499	6.26436287
Ndg	>tr|A1Z877|A1Z877	7	7.1	339020	401390	124240	339020	401390	124240	165008.5714	496496.2972	206362.5061	3.008912162	2.40594237
Cyp4g1	>sp|Q9V3S0|CP4G1	16	24.1	21430000	25217000	11389000	21430000	25217000	11389000	10430457.44	31191975.7	18917116.72	2.990470541	1.648875786
Irp-1B	>tr|Q9VGZ3|Q9VGZ3	4;1	5.6	37769	44181	51749	37769	44181	51749	18383.01218	54649.35079	85955.03332	2.972818069	0.635790002
SPoCk	>tr|Q9VNR2|Q9VNR2	4;4;4;4;4;4	6.4	75297	86977	121490	75297	86977	121490	36648.72412	107585.5364	201794.7591	2.935587499	0.533143362
Inx2	>tr|E1JJF3|E1JJF3	4;4	12	1343300	1550000	7084900	1343300	1550000	7084900	653813.9748	1917260.671	11768011.26	2.932425345	0.162921383
CG13047	>tr|Q9VV18|Q9VV18	2	22.4	20475000	23332000	8776000	20475000	23332000	8776000	9965637.706	28860339.33	14576926.54	2.895985203	1.979864498
fau-RA	>tr|B9EQU5|B9EQU5	4	13.4	4046700	4568700	263710	4046700	4568700	263710	1969618.857	5651218.597	438022.0257	2.869193994	12.90167678
Cg25C	>sp|P08120|CO4A1	8	6.4	1740600	1936100	237800	1740600	1936100	237800	847188.7177	2394844.119	394985.5437	2.826813045	6.063118404
Ppat-Dpck	>tr|Q9VRP4|Q9VRP4	6	16.2	245840	268610	475830	245840	268610	475830	119655.7938	332255.0895	790353.1169	2.776757222	0.420388156
Mf	>tr|Q70VI1|Q70VI1	5;5;4;4;4;0;0;0;0;0	17	39674000	43251000	12466000	39674000	43251000	12466000	19310217.84	53498994.36	20706012.56	2.770501855	2.583742003
T-cp1	>tr|A4V391|A4V391	2;2	3.1	67069	73093	85509	67069	73093	85509	32643.97359	90411.82854	142030.3569	2.769633062	0.636566932
Cpr64Ad	>tr|Q9VZF9|Q9VZF9	10	49	68685000	73849000	36784000	68685000	73849000	36784000	33430516.52	91346956.94	61098184.33	2.732442285	1.49508464
CG3164	>tr|Q9VPJ9|Q9VPJ9	5;5	7.2	775590	829530	798330	775590	829530	798330	377496.8963	1026080.803	1326025.269	2.718117189	0.773801847
ade5	>sp|Q9I7S8|PUR6	6;5	14	645250	680520	339830	645250	680520	339830	314057.5206	841764.0204	564457.2636	2.680286143	1.491280341
CG14762;CG14762-RA	>tr|Q7K2X5|Q7K2X5	2;2	5.5	73685	77647	43204	73685	77647	43204	35864.12788	96044.86408	71761.79753	2.678020344	1.338384313
Glt	>tr|M9NCS8|M9NCS8	26;26	31.5	36594000	38329000	9069400	36594000	38329000	9069400	17811113.37	47410764.03	15064263.62	2.661864143	3.147234092
Nup205	>tr|Q9VWB8|Q9VWB8	3;3	1.6	10242	10554	0	10242	10554	1	4985.009301	13054.68978	1	2.618789453	13054.68978
NTPase	>tr|O76268|O76268	4;4;4;1	13.9	366880	371620	109750	366880	371620	109750	178568.6528	459672.5229	182294.6318	2.574206143	2.52159111
LanB2	>tr|X2JAW6|X2JAW6	40;40	32.3	2743700	2777900	834230	2743700	2777900	834230	1335419.789	3436102.204	1385655.13	2.573050237	2.479767244
if	>sp|P12080|ITA2	5	5.4	332230	335220	109110	332230	335220	109110	161703.7274	414647.8207	181231.5925	2.564244049	2.287944475
Jbug	>tr|Q9W204|Q9W204	5;5;5;5	3.7	541110	545280	26855	541110	545280	26855	263370.2673	674479.9345	44606.12617	2.560957019	15.12079153
mRpL17	>tr|Q9W0S6|Q9W0S6	7	34.1	24968000	25115000	14428000	24968000	25115000	14428000	12152480.7	31065807.57	23964892.44	2.556334657	1.296304903
nrv1	>tr|B5RIR1|B5RIR1	4;4	21.7	399750	401920	736810	399750	401920	736810	194567.2125	497151.8766	1223840.615	2.555167801	0.406222731
CG16885	>tr|Q8SZM2|Q8SZM2	4	21.1	4101400	4118100	1211500	4101400	4118100	1211500	1996242.564	5093852.366	2012300.194	2.551720146	2.531358086

full_dataset_V1

Prm	>tr|A4V1N8|A4V1N8	71;71	49.3	387000000	386140000	87852000	387000000	386140000	87852000	188361503.9	477632926	145922077.3	2.535724743	3.273205364
pain	>sp|Q9W0Y6|PAIN	2;1	2.5	81426	80572	34338	81426	80572	34338	39631.84468	99662.92051	57035.38109	2.514718185	1.747387649
goe	>tr|X2JFT2|X2JFT2	2;2	3.1	52156	51418	45666	52156	51418	45666	25385.48494	63601.10271	75851.17688	2.505412162	0.838498562
pug	>tr|A0A0B4K623|A0A0B4K623	7;7	9.6	173960	170990	244360	173960	170990	244360	84670.19972	211504.7755	405881.6966	2.497983662	0.521099565
Tm2	>tr|A0A0B4KHJ9|A0A0B4KHJ9	16;15	60.6	13576000	13217000	1859500	13576000	13217000	1859500	6607741.025	16348667.28	3088627.495	2.47416889	5.293181942
didum	>tr|A1Z700|A1Z700	2;2;2	2	1596000	1538200	460270	1596000	1538200	460270	776808.6829	1902664.751	764507.9737	2.449335071	2.488744154
Mlc2	>sp|P18432|MLR	6	40.5	3875800	3693800	1846900	3875800	3693800	1846900	1886438.028	4569017.719	3067698.908	2.422034359	1.489395751
LanB1	>sp|P11046|LAMB1	16	11.9	706760	673130	168840	706760	673130	168840	343995.8051	832623.0163	280443.058	2.420445261	2.968955702
Cont	>sp|Q9VN14|CONT	3	3.1	86356	82041	47573	86356	82041	47573	42031.38528	101479.9888	79018.70182	2.414386016	1.284252797
Vha100-2	>tr|Q9VE75|Q9VE75	11	17.5	2570600	2440200	1016000	2570600	2440200	1016000	1251168.17	3018386.767	1687574.904	2.412454887	1.788594248
CG6230-RA	>tr|Q9VKJ6|Q9VKJ6	9	9.6	274240	260290	88940	274240	260290	88940	133478.7052	321963.729	147729.2442	2.412098084	2.179417696
RyR	>tr|A0A0B4K715|A0A0B4K715	33;33;33;33;33;33;32	7.6	272260	256980	183580	272260	256980	183580	132514.9951	317869.4498	304926.1821	2.398743247	1.042447216
	>tr|M9PBJ2|M9PBJ2	4;4;4	4.9	279720	263890	149630	279720	263890	149630	136145.943	326416.7215	248535.2688	2.397550117	1.313361774
RpL35A	>tr|Q9VNB9|Q9VNB9	2	11.5	2684200	2529700	808350	2684200	2529700	808350	1306459.816	3129093.109	1342668.478	2.395093267	2.330503143
Ppn	>sp|Q868Z9|PPN	46	25.1	4153800	3897500	504810	4153800	3897500	504810	2021746.809	4820982.88	838488.8657	2.384563121	5.749608703
CG8067	>tr|Q7K1S1|Q7K1S1	3	10.8	910400	850700	1376100	910400	850700	1376100	443111.9204	1052266.873	2285700.616	2.3747203	0.46036951
CG10096;CG10097	>tr|Q9VG87|Q9VG87	5;4	7.6	1195500	1111600	376220	1195500	1111600	376220	581876.4289	1374985.136	624901.0144	2.363019136	2.200324699
CG2254	>tr|Q9W3K9|Q9W3K9	3	12.2	883160	799170	747190	883160	799170	747190	429853.6068	988527.2323	1241081.784	2.299683466	0.796504505
ppk14	>tr|Q9VME8|Q9VME8	2	4.8	2053100	1857600	389440	2053100	1857600	389440	999289.4152	2297744.143	646859.4201	2.299378046	3.552153793
CG8199	>tr|Q9VHB8|Q9VHB8	4	14.8	884220	784180	631500	884220	784180	631500	430369.5324	969985.4662	1048920.819	2.253843251	0.924746128
CG17083	>tr|Q9VCN4|Q9VCN4	2	5.6	88484	78469	16597	88484	78469	16597	43067.13019	97061.63071	27567.59923	2.253728778	3.520859031
tmod	>tr|O46231|O46231	3;3;3;3;3;3;3;3;3;3	13.1	815240	717180	89662	815240	717180	89662	396795.4328	887110.3276	148928.4854	2.235686841	5.956619548
CG4598	>tr|Q9VL68|Q9VL68	3	10	787250	682830	1085800	787250	682830	1085800	383172.0775	844621.3572	1803512.629	2.204287334	0.468320179
CG4461	>tr|Q9VSX2|Q9VSX2	3	19.5	760070	658160	124300	760070	658160	124300	369942.9673	814105.989	206462.1661	2.200625667	3.943124324
Cyp9f2	>sp|Q9VG82|CP9F2	2	3.9	14649000	12666000	14100000	14649000	12666000	14100000	7129993.981	15667112.03	23420084.79	2.197352772	0.668960517
stmA	>tr|A0A0B4LFU5|A0A0B4LFU5	5;5	8.2	211640	182320	127530	211640	182320	127530	103009.8934	225519.3326	211827.1926	2.189297795	1.064638255
Cp36	>sp|P07182|CH36	5	24.6	3690700	3173100	0	3690700	3173100	1	1796345.743	3924941.828	1	2.184959017	3924941.828
TRAM	>tr|Q9W5C2|Q9W5C2	2	4.9	640370	549580	141500	640370	549580	141500	311682.3161	679798.7867	235031.3475	2.181063062	2.89237497
Tim22	>sp|Q8IN78|TIM22_	3	22.1	1460000	1251800	1993400	1460000	1251800	1993400	710614.4593	1548404.456	3311035.25	2.178965593	0.467649644
Cpr64Ab	>tr|Q9VZG1|Q9VZG1	5	52.5	8318500	7091400	2548700	8318500	7091400	2548700	4048798.889	8771653.109	4233387.951	2.166482789	2.072017309
ocn	>tr|Q9Y170|Q9Y170	3	20.3	5057000	4260300	1919800	5057000	4260300	1919800	2461354.329	5269745.571	3188785.73	2.140994293	1.652586915
LanA	>sp|Q00174|LAMA	59	20.9	2387000	2010800	582960	2387000	2010800	582960	1161805.969	2487243.714	968295.9314	2.140842603	2.568681364
CG7627-RA	>tr|Q9VLN6|Q9VLN6_	3	2.8	152090	127920	39767	152090	127920	39767	74025.5845	158229.6678	66052.94424	2.137499742	2.395497575
ERp60	>tr|Q3YMU0|Q3YMU0	8	18.4	1601600	1346900	733550	1601600	1346900	733550	779534.3274	1666037.676	1218425.759	2.137221694	1.367369053
CG18003	>tr|A1Z8D3|A1Z8D3	10	36.6	4807400	4035100	3633300	4807400	4035100	3633300	2339868.46	4991186.15	6034907.382	2.133105444	0.827052651
CG42672	>tr|B7YZM7|B7YZM7	3;3;3;3;3;3;3;3;3	3.2	133520	111380	34004	133520	111380	34004	64987.15264	137770.641	56480.60746	2.119967338	2.439255652
CG2964	>tr|Q9VQH0|Q9VQH0	2	4	97333	81007	12070	97333	81007	12070	47374.13523	100200.9904	20048.25711	2.115099093	4.997990094
uex	>tr|A0A0B7P9G0|A0A0B7P9G0_DR	7	13.4	954940	793250	429660	954940	793250	429660	464790.5287	981204.5335	713664.7967	2.111068262	1.374881151
mesh	>tr|A0A0B4LHZ4|A0A0B4LHZ4_DRO	9;9	9.7	1415800	1153400	155990	1415800	1153400	155990	689101.3366	1426689.327	259099.2219	2.070362154	5.506343543
CG12338	>tr|Q7JZB1|Q7JZB1_DROME RE49	14	45.7	4677700	3798600	4773800	4677700	3798600	4773800	2276740.586	4698649.28	7929276.652	2.063761374	0.592569724
CG17221	>tr|Q9VQL4|Q9VQL4_DROME Unch	2;2	8.3	255030	206830	235890	255030	206830	235890	124128.7711	255836.79	391813.0357	2.061059558	0.6529563
CG32473-RB;CG32473	>tr|Q8INH5|Q8INH5_DROME RE431	4;4;4;1	5.8	228980	184900	142640	228980	184900	142640	111449.6569	228710.6439	236924.8863	2.052143095	0.965329761
CG7264	>tr|Q9VTP5|Q9VTP5_DROME CG72	2	5.2	257380	206790	48081	257380	206790	48081	125272.5683	255787.3123	79862.48927	2.041846158	3.202846726
Ncc69	>tr|Q9VTW8|Q9VTW8_DROME GH2	2;2;2	3.4	196340	157590	194360	196340	157590	194360	95563.04327	194929.7478	322831.7505	2.039802638	0.603812195
mfas	>tr|Q9VGF0|Q9VGF0_DROME Midli	19;19;18;18;18;18;18	29.7	3692600	2963500	909310	3692600	2963500	909310	1797270.515	3665678.708	1510362.929	2.039580952	2.427018458
CG5958-RA	>tr|Q9VM12|Q9VM12_DROME CG5	2	8.5	658050	528060	227130	658050	528060	227130	320287.5651	653179.7869	377262.6852	2.039354187	1.731366002
CG10924	>tr|Q7JXB5|Q7JXB5_DROME RE12	18;17	35.6	1125600	903250	1458900	1125600	903250	1458900	547854.5448	1117268.194	2423231.327	2.039351876	0.46106543
Cp16	>sp|P22977|CH16_DROME Chorion	2	26.1	1782700	1425000	0	1782700	1425000	1	867679.7236	1762642.875	1	2.031444122	1762642.875
	>tr|Q9V9A9|Q9V9A9_DROME L(2)0	16;16;15;7;7	13.4	4100600	3265800	668470	4100600	3265800	668470	1995853.186	4039606.386	1110327.949	2.023999768	3.638210124
Act88F	>sp|P83967|ACT6_DROME Actin, in	7	24.2	1764900000	1396800000	694990000	1764900000	1396800000	694990000	859016067.7	1727761100	1154377640	2.011325707	1.496703539
CG6484	>tr|Q7K3P6|Q7K3P6_DROME CG64	2	6.9	2642200	2089300	0	2642200	2089300	1	1286017.482	2584343.69	1	2.009571196	2584343.69

full_dataset_V1

Nrx-IV	>tr|Q8IQH0|Q8IQH0_DROME Fl128	2;2	1.6	83816	65412	33076	83816	65412	33076	40795.11081	80910.87421	54939.20046	1.983347332	1.472734833
CG5167	>tr|Q9VG81|Q9VG81_DROME CG5	7	23.9	1524400	1179600	1801300	1524400	1179600	1801300	741959.371	1459097.217	2991957.357	1.966545979	0.487673133
Nrg	>tr|E1JJF9|E1JJF9_DROME Neurog	18;18;18;18	21.1	1258900	971870	498820	1258900	971870	498820	612734.6184	1202147.179	828539.4822	1.961937751	1.450923227
Prm	>tr|A4V1N9|A4V1N9_DROME Param	16;16;14	20.3	46130000	35590000	10205000	46130000	35590000	10205000	22452496.57	44022778.88	16950493.99	1.96070752	2.597138402
PlexA	>tr|Q0KIF1|Q0KIF1_DROME Plexin A	2;2;2	1.9	37980	29227	0	37980	29227	1	18485.71058	36152.11462	1	1.955678927	36152.11462
CG13091	>tr|Q9VLJ7|Q9VLJ7_DROME GH27	5	13	1144900	879680	550010	1144900	879680	550010	557248.2839	1088113.462	913566.0169	1.952654667	1.191061666
mRpL11	>sp|Q9VFJ2|RM11_DROME 39S rib	3	22.4	2373800	1820800	1050900	2373800	1820800	1050900	1155381.235	2252224.664	1745543.767	1.94933464	1.290271093
T3dh	>sp|Q9W265|HOT_DROME Probabl	8	19.4	3742800	2856900	3322200	3742800	2856900	3322200	1821703.971	3533820.651	5518170.617	1.939843524	0.640397135
RpL13A	>sp|Q9VNE9|RL13A_DROME 60S ri	3;1	18	942130	714330	438430	942130	714330	438430	458555.6169	883585.0418	728231.7573	1.926887403	1.213329456
rept	>tr|M9PFN1|M9PFN1_DROME RuvB	2;2	4.6	142790	107960	0	142790	107960	1	69499.06774	133540.2981	1	1.921468912	133540.2981
Eaat1	>tr|O77062|O77062_DROME Amino	5	10.9	12985000	9805900	4424000	12985000	9805900	4424000	6320088.186	12129333.17	7348259.229	1.919171507	1.650640348
	>tr|E1JGY7|E1JGY7_DROME Letha	3;3;2;2	3.2	671520	506900	114740	671520	506900	114740	326843.7136	627006.0864	190583.0164	1.91836667	3.289936839
CG10914	>tr|Q8SZ15|Q8SZ15_DROME RE23	2	4.8	489180	366480	15929	489180	366480	15929	238094.7818	453314.6391	26458.05195	1.903925133	17.13333393
fon	>tr|Q8INW9|Q8INW9_DROME Fond	4;4;4	10.4	18395000	13730000	3115400	18395000	13730000	3115400	8953255.463	16983218.71	5174676.04	1.896876369	3.281986849
Act79B	>tr|M9PFZ6|M9PFZ6_DROME Actin	12;12	26.9	160540000	119130000	38755000	160540000	119130000	38755000	78138387.17	147356944.3	64372013.2	1.885845737	2.289146121
Galphas	>tr|A0A0B4LGI1|A0A0B4LGI1_DRO	2;2	7.6	533140	393320	376970	533140	393320	376970	259491.0911	486514.1722	626146.7636	1.874878132	0.776997025
PHGPx	>tr|Q9VZQ8|Q9VZQ8_DROME Gluta	2;2;2	14.8	785150	578780	477010	785150	578780	477010	382149.9608	715917.5038	792313.0957	1.873394157	0.903579037
Droj2	>tr|Q9VFV9|Q9VFV9_DROME DnaJ	8	27	5464100	4003400	784560	5464100	4003400	784560	2659498.949	4951975.076	1303153.314	1.8619955	3.799994232
CG9399	>tr|A0A0B4KFZ7|A0A0B4KFZ7_DRO	2;2	18.3	1868600	1363800	2377400	1868600	1363800	2377400	909489.1634	1686942.002	3948858.836	1.854823641	0.427197343
CG9911	>tr|Q9VXI3|Q9VXI3_DROME CG991	2;2	6.1	274460	200150	324390	274460	200150	324390	133585.7841	247574.015	538811.4403	1.853296118	0.459481734
Cyp12b2	>sp|Q9V8M2|C12B2_DROME Proba	11	19.1	3099700	2253100	1837300	3099700	2253100	1837300	1508692.904	2786954.85	3051753.319	1.847264505	0.91323071
Mhc	>tr|M9ND95|M9ND95_DROME Myos	4	1.4	2433900000	1754900000	464120000	2433900000	1754900000	464120000	1184633241	2170710162	770902819.4	1.832390048	2.815802598
SERCA;Ca-P60A	>tr|A0A0B4LGB7|A0A0B4LGB7_DR	48;48	40.6	34458000	24824000	19038000	34458000	24824000	19038000	16771474.68	30705857.35	31622097.47	1.83083825	0.971025321
CG33080	>tr|Q9W492|Q9W492_DROME Unch	2;2;2	3	85139	61164	14949	85139	61164	14949	41439.04433	75656.34303	24830.27301	1.825726058	3.046939637
Aats-glupro	>sp|P28668|SYEP_DROME Bifuncti	2	1.2	30466	21857	10752	30466	21857	10752	14828.47972	27035.84937	17859.06053	1.823238111	1.513844993
Myo10A	>tr|Q0KHU0|Q0KHU0_DROME Myos	3;2	1.2	79331	56695	188740	79331	56695	188740	38612.1616	70128.44758	313496.9366	1.816226926	0.223697394
RpL30	>tr|Q9VJ19|Q9VJ19_DROME RE252	5	53.2	19718000	14076000	14575000	19718000	14076000	14575000	9597188.976	17411200.77	24209059.28	1.814197972	0.719201873
Bsg	>tr|Q7KTJ7|Q7KTJ7_DROME Basigi	5;4;4	8.2	877810	621330	641300	877810	621330	641300	427249.6429	768549.4016	1065198.608	1.798829828	0.721508079
Ost48	>sp|Q24319|OST48_DROME Dolich	10	33.9	11825000	8362400	8978300	11825000	8362400	8978300	5755490.397	10343806.86	14912946.62	1.797206866	0.693612545
vkg	>tr|Q9VMV5|Q9VMV5_DROME Vikir	13	7.9	2084100	1463100	553370	2084100	1463100	553370	1014377.804	1809770.379	919146.9733	1.784118669	1.968967348
Cht5	>tr|Q9VFR3|Q9VFR3_DROME Cht5	4	7.6	22640	15881	176090	22640	15881	176090	11019.39153	19643.88177	292485.3002	1.782664834	0.067161945
CG12262	>sp|Q9VSA3|ACADM_DROME Prob	36	53	198330000	138600000	161770000	198330000	138600000	161770000	96531620.32	171440212.2	268699795.5	1.776000565	0.638036259
Tm1	>sp|P49455|TPM4_DROME Tropom	2;0;0	4.6	60530000	42298000	7985700	60530000	42298000	7985700	29461296.72	52320188.29	13264239.09	1.775895636	3.944454555
CG9572;CG9572-RB	>tr|M9MSF5|M9MSF5_DROME CG9	2;2;2	6.9	64219	44669	0	64219	44669	1	31256.81523	55252.97867	1	1.767709802	55252.97867
Cklalpha	>tr|E1JJI5|E1JJI5_DROME Casein ki	2;2	7.7	1306600	907370	271290	1306600	907370	271290	635951.2689	1122364.397	450612.3975	1.76485912	2.490753478
CG10399	>tr|Q9VM58|Q9VM58_DROME TA01	5	20.7	729100	503430	501440	729100	503430	501440	354869.1797	622713.8964	832891.2993	1.754770298	0.747653261
CG1358-RB	>tr|Q7K1D7|Q7K1D7_DROME CG13	2	3.1	266520	183600	161520	266520	183600	161520	129721.2095	227102.6188	268284.5459	1.750697666	0.84649071
CG5676	>tr|Q9VL16|Q9VL16_DROME CG56	3	25	1598800	1100200	483040	1598800	1100200	483040	778171.5051	1360883.993	802328.9192	1.748822701	1.696167196
Tapdelta	>tr|Q7KLX3|Q7KLX3_DROME GM12	5	28.3	12422000	8542000	9508600	12422000	8542000	9508600	6046063.569	10565961.71	15793774.35	1.747577012	0.668995357
Tg	>tr|Q8IPH0|Q8IPH0_DROME Transg	8;7	10.7	767690	527440	527580	767690	527440	527580	373651.7907	652412.8827	876309.8111	1.746045112	0.74450026
CG9527	>tr|Q9VMD7|Q9VMD7_DROME Acyl	9;9	19.8	595160	408500	434580	595160	408500	434580	289677.6039	505290.9574	721836.9114	1.744321793	0.700007092
CG1444	>tr|Q9W3N1|Q9W3N1_DROME CG1	4	16.8	2135400	1439000	689870	2135400	1439000	689870	1039346.655	1779960.068	1145873.326	1.712575933	1.553365479
Aldh-III	>tr|A1Z6Z3|A1Z6Z3_DROME Aldehy	3;3;3;3;3;2;2;2;2	6	751920	506290	611160	751920	506290	611160	365976.1811	626251.5516	1015136.101	1.711181175	0.616913881
RpII140	>tr|A0A0B4LI86|A0A0B4LI86_DROM	2;2	3.1	44214	29623	0	44214	29623	1	21519.93697	36641.9438	1	1.702697542	36641.9438
chp	>tr|A0A0B4KHG5|A0A0B4KHG5_DR	29;29;29;28;28	29.9	3771400	2524000	2388100	3771400	2524000	2388100	1835624.227	3122042.537	3966631.525	1.700807001	0.78707652
CG2118	>tr|Q9V9T5|Q9V9T5_DROME CG21	23;22	36.1	21825000	14599000	13459000	21825000	14599000	13459000	10622712.72	18058121.63	22355384.48	1.699953873	0.807775042
Mfe2	>tr|X2JFD6|X2JFD6_DROME Peroxi	10;10	24.1	1844900	1233400	1926700	1844900	1233400	1926700	897953.8465	1525644.717	3200246.622	1.699023533	0.476727233
Sec23	>tr|Q9VNF8|Q9VNF8_DROME Sec2	5;5;5	9.7	293770	195980	107010	293770	195980	107010	142984.3904	242415.9653	177743.4947	1.695401608	1.363852813
CG3862	>tr|Q9VPU0|Q9VPU0_DROME CG3	2	7	575620	383550	52541	575620	383550	52541	280167.0515	474429.2453	87270.54446	1.69337987	5.436304405
hts	>tr|A8DYJ2|A8DYJ2_DROME Hu li ta	11;10;10;10	7.7	1765100	1174800	1440800	1765100	1174800	1440800	859113.4123	1453159.894	2393167.246	1.691464565	0.60721201
Uro	>sp|P16163|URIC_DROME Uricase	14	55.7	13078000	8574600	1494500	13078000	8574600	1494500	6365353.354	10606286.03	2482362.888	1.666252514	4.272657346

full_dataset_V1

Cat	>sp|P17336|CATA_DROME Catalas	28	63.6	66587000	43460000	19795000	66587000	43460000	19795000	32409373.28	53757515.32	32879473.65	1.658702711	1.634987101
OstDelta	>tr|A0A0B4LFR4|A0A0B4LFR4_DR	14;14	25.4	3320700	2162800	2113900	3320700	2162800	2113900	1616258.517	2675258.954	3511185.62	1.655217235	0.761924672
CG1371	>tr|A1Z843|A1Z843_DROME CG137	18	21.3	440160	286000	355760	440160	286000	355760	214235.6579	353765.5173	590916.9764	1.651291483	0.598672117
sif	>tr|A8JNL5|A8JNL5_DROME Still life	3;3	1.3	39151	25356	34164	39151	25356	34164	19055.66231	31363.91071	56746.36728	1.645910292	0.55270341
CG17734	>tr|Q8INK7|Q8INK7_DROME Uncha	2;2;2	17.9	5367500	3470000	2260000	5367500	3470000	2260000	2612481.582	4292190.017	3753857.563	1.64295513	1.1434078
cype	>tr|Q9VMS1|Q9VMS1_DROME Cycl	3	36.4	26946000	17400000	4426000	26946000	17400000	4426000	13115217.27	21522797.21	7351581.227	1.64105533	2.927641897
26-29-p	>tr|Q9V3U6|Q9V3U6_DROME 26-29	5	11.3	1830100	1179000	2095000	1830100	1179000	2095000	890750.3574	1458355.052	3479792.741	1.637220844	0.419092504
Vha26	>tr|A0A0B4LGS4|A0A0B4LGS4_DR	4;4	19.5	670840	431700	2225000	670840	431700	2225000	326512.7425	533988.0203	3695722.6	1.635427813	0.144488123
CG3902-RA	>tr|Q9VVU1|Q9VVU1_DROME CG3	14	40.8	33329000	21337000	13626000	33329000	21337000	13626000	16221965.28	26392639.31	22632771.3	1.626969289	1.16612495
CG10086	>tr|Q8SYU5|Q8SYU5_DROME RE3	2	4.1	396810	253580	111300	396810	253580	111300	193136.2492	313663.8457	184869.1801	1.624054765	1.696680028
	>tr|Q9V3Z9|Q9V3Z9_DROME HL02	6	25.6	6393300	4059300	1302600	6393300	4059300	1302600	3111761.248	5021120.155	2163617.195	1.613594282	2.320706346
CG5599	>tr|Q9VXY3|Q9VXY3_DROME CG55	3	12.8	924160	586470	112130	924160	586470	112130	449809.2184	725429.5906	186247.8092	1.612749497	3.894969792
Cyp12c1	>tr|X2JB94|X2JB94_DROME Cyp12	6;6	11.6	1484300	934600	594580	1484300	934600	594580	722441.8095	1156046.337	987596.7389	1.60019015	1.170565163
mRpL55	>sp|Q9VE04|RM55_DROME 39S rib	2	27.1	1174000	738770	263310	1174000	738770	263310	571411.9009	913815.9133	437357.6261	1.599224503	2.089402033
Tudor-SN	>tr|Q9W0S7|Q9W0S7_DROME LD2	4	5.5	167150	105050	69090	167150	105050	69090	81355.62132	129940.7958	114758.4156	1.597195052	1.13229821
CG30268	>tr|Q9W206|Q9W206_DROME Unch	2	2.4	83907	52531	19046	83907	52531	19046	40839.40254	64977.81956	31635.38559	1.591057056	2.053960094
Unc-89	>tr|A8DYP0|A8DYP0_DROME Unc-8	59;58;58;58;57;57	18.7	1524100	953330	223100	1524100	953330	223100	741813.3544	1179214.268	370568.8595	1.589637421	3.182173131
Dip-B	>tr|Q9VFQ9|Q9VFQ9_DROME Dipe	7	21.9	3182100	1985600	1513100	3182100	1985600	1513100	1548798.815	2456072.766	2513257.468	1.585791997	0.977246779
CG17726	>sp|Q9VGR2|NDUF7_DROME NADI	2	7.8	346680	216300	279100	346680	216300	279100	168736.8637	267550.6342	463584.7991	1.585608672	0.577134183
CG8909-RB;CG8909	>tr|B5X533|B5X533_DROME CG890	2;2	1.5	14785	9187.2	9221.5	14785	9187.2	9221.5	7196.1884	11364.03695	15316.90168	1.579174463	0.741927916
Rtnl1	>tr|Q9VMV9|Q9VMV9_DROME Reti	2;2;1;1;1;1;1	4.4	649130	401990	372050	649130	401990	372050	315946.0028	497238.4626	617974.6489	1.573808366	0.804625988
EMC1	>tr|A0A0B4LGV1|A0A0B4LGV1_DR	10;9	13.9	706510	437370	202650	706510	437370	202650	343874.1245	541001.4836	336601.4316	1.573254412	1.607246532
ATPsynE	>tr|O77134|O77134_DROME 9 kD b	2	14.8	7070400	4376100	3446400	7070400	4376100	3446400	3441320.871	5412983.497	5724466.683	1.572937747	0.945587388
Gs1	>tr|E1JHQ1|E1JHQ1_DROME Gluta	11;11	26.1	10248000	6340900	5095400	10248000	6340900	5095400	4987929.436	7843327.862	8463453.905	1.572461672	0.926728963
Pfk	>sp|P52034|PFKA_DROME ATP-dej	10;9;9	17.1	2320100	1432300	709070	2320100	1432300	709070	1129244.251	1771672.554	1177764.505	1.568901105	1.504267233
Atpalpha	>sp|P13607|ATNA_DROME Sodium	2;1	2.9	99988000	61562000	65625000	99988000	61562000	65625000	48666382.56	76148646.07	109003054.2	1.564707341	0.698591857
cher	>tr|A0A0B4JCY6|A0A0B4JCY6_DR	7;7;7;7;7;3;3;3	5.3	149840	91661	49098	149840	91661	49098	72930.45947	113379.3744	81551.72518	1.554623065	1.39027561
Mhc	>tr|M9NEP1|M9NEP1_DROME Myos	2	1.3	12737000	7784900	1303400	12737000	7784900	1303400	6199381.072	9629472.641	2164945.994	1.55329581	4.44790432
FASN1	>tr|Q9VQL7|Q9VQL7_DROME Fatty	55;55	30.6	3341700	2041700	1418500	3341700	2041700	1418500	1626479.684	2525465.233	2356126.97	1.552718585	1.07187145
bdl	>sp|Q9U4G1|BDL_DROME Protein b	5	9.7	1419800	866360	390450	1419800	866360	390450	691048.2256	1071637.39	648537.029	1.55074183	1.652391987
mRpL27	>tr|Q86BM8|Q86BM8_DROME Mitoc	6	50.7	11615000	7083000	1388400	11615000	7083000	1388400	5653278.728	8761262.793	2306130.903	1.549766643	3.799117727
Gk1	>tr|Q9W0U0|Q9W0U0_DROME GH1	10;9	28.3	6828700	4144700	9273900	6828700	4144700	9273900	3323680.108	5126755.033	15403937.9	1.542493521	0.332821066
CG5065	>tr|E1JH83|E1JH83_DROME CG506	6;6	15.4	1033200	626270	398600	1033200	626270	398600	502881.4106	774659.8969	662074.1702	1.540442499	1.170050021
CG13504	>tr|Q9W287|Q9W287_DROME Unch	2	30.9	387330	234750	604970	387330	234750	604970	188522.1224	290372.2209	1004854.518	1.540255421	0.288969414
NLaz	>tr|Q8SXR1|Q8SXR1_DROME Neur	2;2	8.5	1390600	842410	477850	1390600	842410	477850	676835.9364	1042012.62	793708.3348	1.53953501	1.312840718
inaC	>sp|P13677|KPC2_DROME Protein	16;1	24.1	5364700	3230200	1650900	5364700	3230200	1650900	2611118.76	3995571.237	2742143.12	1.530214289	1.457097993
Gat	>tr|Q9V4E7|Q9V4E7_DROME Trans	7;3	8.8	1428600	857020	1732600	1428600	857020	1732600	695331.3812	1060084.348	2877846.732	1.524574292	0.368360252
Cyp12d1-p	>tr|A0A0B4LF45|A0A0B4LF45_DRO	3;3;2	8.8	482040	288830	0	482040	288830	1	234619.585	357266.0642	1	1.522746126	357266.0642
FASN2	>tr|Q9VQL6|Q9VQL6_DROME Fatty	15;15	8.4	409460	244430	225480	409460	244430	225480	199293.2854	302345.8231	374522.0369	1.517089863	0.807284467
CG14450	>tr|Q9VNR9|Q9VNR9_DROME RE6	2;1	10.2	851920	508420	105150	851920	508420	105150	414648.4043	628886.2388	174654.0367	1.516673481	3.6007541
dlu	>tr|A0A0B4KEX0|A0A0B4KEX0_DR	4;4	4.1	124440	74190	61020	124440	74190	61020	60567.71478	91768.75431	101354.1543	1.515143087	0.905426669
CG30491	>tr|Q7JUS1|Q7JUS1_DROME AT09	11;2;2;1	35.6	4461600	2658300	2165000	4461600	2658300	2165000	2171559.912	3288163.897	3596062.665	1.514194418	0.91437892
yip2	>tr|Q9VL70|Q9VL70_DROME HL081	9	29.6	3030100	1800700	1993100	3030100	1800700	1993100	1474817.036	2227362.122	3310536.951	1.510263353	0.672809926
Vps13	>tr|A1Z713|A1Z713_DROME Vacuol	6	2.7	103640	61521	36521	103640	61521	36521	50443.89234	76097.93145	60661.34174	1.508565813	1.254471617
Gbeta13F	>tr|A4V4I0|A4V4I0_DROME G prote	9;9	37.4	10153000	6022500	6923700	10153000	6022500	6923700	4941690.824	7449485.412	11500258.23	1.507477031	0.647766795
Eno	>tr|E1JHR5|E1JHR5_DROME Enola	5;5	18.2	2353000	1395700	1569800	2353000	1395700	1569800	1145257.413	1726400.463	2607436.107	1.507434437	0.662106526
prtp	>tr|M9PGX2|M9PGX2_DROME Prot	3;3	9.3	203340	120420	92630	203340	120420	92630	98970.0989	148952.6	153858.3302	1.505026282	0.968115277
alpha-Est7	>tr|Q9VIB5|Q9VIB5_DROME Carbox	7	21.9	553610	327670	664250	553610	327670	664250	269454.2952	405308.9058	1103318.534	1.504184246	0.367354389
Cyt-b5-r	>tr|M9PD26|M9PD26_DROME Cytoc	8;8	19	10607000	6276800	3452600	10607000	6276800	3452600	5162662.718	7764039.856	5734764.876	1.503882837	1.353854957
RpL12	>tr|Q9W1B9|Q9W1B9_DROME RE2	6	47.3	32558000	19240000	15098000	32558000	19240000	15098000	15846702.44	23798771.16	25077761.72	1.501812207	0.948999015
CG4706	>tr|Q8T4D6|Q8T4D6_DROME Aconi	3	5.1	579290	340850	73414	579290	340850	73414	281953.3221	421611.8062	121940.575	1.49532484	3.457518602

full_dataset_V1

His3	>tr|E2QCP0|E2QCP0_DROME Histo	8;8;8	27.2	199500000	117220000	58562000	199500000	117220000	58562000	97101085.34	144994384.4	97271418.84	1.493231346	1.490616526
ThrRS	>tr|Q8IP94|Q8IP94_DROME Threony	7;7	13.8	1051200	612150	428250	1051200	612150	428250	511642.4107	757194.2707	711322.7883	1.479928667	1.064487576
ND-B17	>tr|Q9V3W2|Q9V3W2_DROME GM1	7	59.3	12046000	6976000	5003800	12046000	6976000	5003800	5863056.01	8628909.96	8311306.404	1.471742713	1.038213434
CG5989	>tr|M9PF10|M9PF10_DROME CG59	3;3;3	7.5	2057200	1187400	407060	2057200	1187400	407060	1001284.976	1468745.368	676126.2211	1.466860487	2.172294643
CG3603	>tr|Q9W4U2|Q9W4U2_DROME CG3	6	29.7	5635600	3225500	3018700	5635600	3225500	3018700	2742971.812	3989757.608	5014057.444	1.454538319	0.79571438
Etf-QO	>tr|Q7JWF1|Q7JWF1_DROME Elect	19	38.6	30883000	17657000	16362000	30883000	17657000	16362000	15031442.7	21840691.39	27177264.35	1.453000343	0.803638332
gatA	>sp|Q9VE09|GATA_DROME Glutam	9	20.7	593770	339450	700200	593770	339450	700200	289001.06	419880.0869	1163031.445	1.452866944	0.361022128
ATPCL	>tr|E2QCF1|E2QCF1_DROME ATP-	8;8;8	11.1	570760	325970	422510	570760	325970	422510	277801.5815	403206.1038	701788.6545	1.451417597	0.574540642
COX5B	>tr|Q9VMB9|Q9VMB9_DROME Cyto	2	15	7711100	4380900	0	7711100	4380900	1	3753163.805	5418920.82	1	1.443827422	5418920.82
RpL22	>sp|P50887|RL22_DROME 60S ribo	6	27.1	20881000	11855000	9425100	20881000	11855000	9425100	10163246.93	14663951.77	15655080.94	1.442841237	0.936689618
CG9940-RA;CG9940	>tr|C5WLN1|C5WLN1_DROME CG9	2;2	2.5	56063	31829	33450	56063	31829	33450	27287.1087	39370.63866	55560.41405	1.442829253	0.708609526
wupA	>sp|P36188|TNNI_DROME Troponin	4;4;2	21.9	6586800	3717500	1410800	6586800	3717500	1410800	3205942	4598333.253	2343337.279	1.434315797	1.962301072
AcCoAS	>tr|Q59E09|Q59E09_DROME Acetyl	8;8	18.5	526760	297160	354970	526760	297160	354970	256385.8033	367569.7941	589604.7873	1.433658921	0.623417248
kcc	>tr|Q8MKK5|Q8MKK5_DROME GH0	4;4;4;4;4;4	4	611380	343430	221180	611380	343430	221180	297572.2386	424803.1175	367379.7416	1.427563	1.156305232
Hsp60	>sp|O02649|CH60_DROME 60 kDa	9	19.5	7409800	4155800	3279700	7409800	4155800	3279700	3606514.397	5140485.093	5447578.163	1.425333307	0.943627597
Mlc1	>tr|A0A0B4LHS1|A0A0B4LHS1_DR	5;5	18.1	51396000	28582000	10431000	51396000	28582000	10431000	25015575.85	35354286.77	17325879.75	1.413290942	2.040547855
Galphao	>sp|P16378|GNAO_DROME G prote	16;0;0	34.7	31132000	17285000	24272000	31132000	17285000	24272000	15152636.53	21380548.83	40315765.82	1.411011792	0.53032724
LamC	>sp|Q03427|LAMC_DROME Lamin-C	26;25	42	13655000	7557500	3268000	13655000	7557500	3268000	6646192.082	9348191.947	5428144.476	1.406548567	1.722170806
MRP	>tr|Q9I7N0|Q9I7N0_DROME FI2322	14;14;14;14;14;14;14;14;14;14;14;14;14;13	13.2	797750	440810	587670	797750	440810	587670	388282.661	545256.5653	976119.2363	1.404277399	0.558596271
Mtpalpha	>tr|Q8IPE8|Q8IPE8_DROME Mitoch	47;47	60.5	114010000	62965000	40117000	114010000	62965000	40117000	55491201.7	77884076.21	66634293.73	1.403539189	1.168828719
Gapdh1	>sp|P07486|G3P1_DROME Glycerat	2	5.4	1789400	986970	1148700	1789400	986970	1148700	870940.7626	1220825.009	1907989.461	1.401731394	0.639848927
RFeSP	>tr|Q9VQ29|Q9VQ29_DROME Cyto	11	34.3	366280000	202000000	131960000	366280000	202000000	131960000	178276619.2	249862358.4	219185417.7	1.40154306	1.139958858
Hsc70-3	>tr|F3YDH0|F3YDH0_DROME Heat	19;19	35.4	7310500	4025900	4743300	7310500	4025900	4743300	3558182.879	4979806.28	7878616.184	1.39953635	0.632066109
	>tr|Q9W2J4|Q9W2J4_DROME UDP	3	8.8	1932400	1063500	1176200	1932400	1063500	1176200	940542.0418	1315488.209	1953666.932	1.398649024	0.673343131
CG4928	>tr|X2JFT8|X2JFT8_DROME CG492	2;2;2	6.1	1041300	573060	533850	1041300	573060	533850	506823.8606	708842.1935	886724.2744	1.398596729	0.799394145
Ank	>tr|Q0KIE7|Q0KIE7_DROME Ankyrir	22	18.7	3306800	1817900	580480	3306800	1817900	580480	1609493.078	2248637.531	964176.6541	1.397109166	2.332184171
Flo2	>tr|A4V4F2|A4V4F2_DROME Flotillir	22;21;21;21;21;21;19;19	52	14163000	7776200	3368200	14163000	7776200	3368200	6893446.976	9618711.243	5594576.568	1.395341297	1.719292091
Hmu	>tr|Q9VB46|Q9VB46_DROME FI186	2	4.5	301090	165090	95602	301090	165090	95602	146547.1971	204206.8156	158794.819	1.393454256	1.285979082
Prat	>tr|A0A0B4K6L4|A0A0B4K6L4_DRC	2;2	7	477030	260890	0	477030	260890	1	232181.1066	322705.8944	1	1.389888691	322705.8944
vari	>tr|Q2PDR9|Q2PDR9_DROME Varic	2;2;2;2	7.7	1195700	653880	359980	1195700	653880	359980	581973.7733	808811.8757	597926.3919	1.389773754	1.352694724
Sc2	>tr|Q9VZL3|Q9VZL3_DROME Sc2 C	7	24.2	13056000	7137700	1838100	13056000	7137700	1838100	6354645.465	8828923.541	3053082.118	1.389365243	2.891806771
Hsc70-5	>tr|A0A0B4LFD2|A0A0B4LFD2_DRC	27;27	39.8	27721000	15148000	15428000	27721000	15148000	15428000	13492427	18737202.99	25625891.36	1.388719983	0.731182488
COX5A	>tr|A0A0B4KFT0|A0A0B4KFT0_DRC	3;3	28.9	8734100	4772700	3516300	8734100	4772700	3516300	4251080.649	5903554.84	5840570.508	1.388718617	1.010783935
betaTub56D	>sp|Q24560|TBB1_DROME Tubulin	9;6	35.8	28232000	15394000	16518000	28232000	15394000	16518000	13741142.06	19041490.81	27436380.19	1.385728401	0.694023435
CG4115	>tr|Q9VGA3|Q9VGA3_DROME CG4	4	25.5	1928700	1050400	1794800	1928700	1050400	1794800	938741.1695	1299284.263	2981160.864	1.384070823	0.435831652
Nc73EF	>tr|A8JNU6|A8JNU6_DROME Neura	2	4.3	102460000	55785000	32752000	102460000	55785000	32752000	49869559.92	69002830	54401036.68	1.383666311	1.268410204
Cyp12e1	>sp|Q9VGZ0|C12E1_DROME Proba	3	8.2	561170	305380	414610	561170	305380	414610	273133.9153	377737.4604	688666.763	1.382975307	0.548505432
Chc	>tr|X2JC31|X2JC31_DROME Clathri	41;41	29	4886200	2658700	2099700	4886200	2658700	2099700	2378222.171	3288658.674	3487599.436	1.382822309	0.94295768
Flo1	>sp|O61491|FLOT1_DROME Flotillir	17	39.2	23043000	12475000	5451900	23043000	12475000	5451900	11215540.4	15430856.04	9055600.02	1.375845969	1.704012546
CG8507	>tr|Q9VH64|Q9VH64_DROME CG85	3	8.4	488040	264090	122370	488040	264090	122370	237539.9184	326664.11	203256.4382	1.375196692	1.607152585
Sec24CD	>tr|Q9VQ94|Q9VQ94_DROME LP05	4;4	5.2	206820	111420	95059	206820	111420	95059	100663.8923	137820.1187	157892.8966	1.36911176	0.872870925
Strn-Mlck	>tr|A1ZA73|A1ZA73_DROME Stretch	47;11;11;11;11	31.5	4985100	2679300	771030	4985100	2679300	771030	2426359	3314139.687	1280679.999	1.365890079	2.587796866
Psa	>tr|Q9W0E4|Q9W0E4_DROME Purc	17;17;17	22.7	1049700	563620	778110	1049700	563620	778110	510912.3274	697165.4575	1292439.871	1.364550081	0.539418098
Hmt-1	>tr|Q9VF20|Q9VF20_DROME Heavy	4	6.8	143370	76914	101600	143370	76914	101600	69781.36663	95138.18533	168757.4906	1.363375209	0.563756815
Cp1	>tr|A0A0B4JD48|A0A0B4JD48_DRC	4;4	22.1	4425800	2372500	2307200	4425800	2372500	2307200	2154135.256	2934645.768	3832256.712	1.362331247	0.765774839
Hrd3	>tr|Q9V415|Q9V415_DROME BcDN	3	6.7	143310	76682	87674	143310	76682	87674	69752.1633	94851.2147	145626.4196	1.359831871	0.651332464
jar	>tr|A0A0B4LHV4|A0A0B4LHV4_DRC	4;4;4;4	4.1	148950	79622	13978	148950	79622	13978	72497.27669	98487.82526	23217.44305	1.358503792	4.241975528
CG1673	>tr|Q9VYD5|Q9VYD5_DROME Bran	5	18.5	1840000	981040	1113100	1840000	981040	1113100	895568.9075	1213489.941	1848857.9	1.35499338	0.656345705
CG17896	>sp|Q7KW39|MMSA_DROME Proba	31	60.8	114910000	60951000	68177000	114910000	60951000	68177000	55929251.71	75392874.28	113241923.5	1.348004344	0.665768224
Dhc36C	>tr|Q9VJC6|Q9VJC6_DROME Dynei	2	0.6	12146	6441.2	0	12146	6441.2	1	5911.72843	7967.393209	1	1.347726524	7967.393209
Rfabg	>tr|L0MPS3|L0MPS3_DROME Retin	66;66	25.6	3286100	1740200	939180	3286100	1740200	939180	1599417.928	2152527.109	1559976.967	1.345819046	1.379845443

full_dataset_V1

RpL36	>tr|X2JC35|X2JC35_DROME 60S rib	4;4	31.3	12225000	6472900	2208700	12225000	6472900	2208700	5950179.29	8006604.255	3668648.318	1.345607227	2.18239842
AspRS-m	>tr|Q9VJH2|Q9VJH2_DROME SD02	8	10.3	577640	305360	366510	577640	305360	366510	281150.2304	377712.7215	608772.7148	1.343455138	0.620449492
VhaAC39-1	>sp|Q9W4P5|VA0D1_DROME V-typ	2	6.3	999030	527560	517220	999030	527560	517220	486250.1119	652561.3157	859101.8623	1.342028104	0.759585498
CG3499	>tr|Q9W1Y0|Q9W1Y0_DROME CG3	20;20;20	36.4	10429000	5474500	2256600	10429000	5474500	2256600	5076026.16	6771640.994	3748210.166	1.334043754	1.806633218
mRpL38	>tr|Q9VY48|Q9VY48_DROME Mitoc	14	34.9	9413100	4928600	3780400	9413100	4928600	3780400	4581565.045	6096394.155	6279240.323	1.330635732	0.970880846
Rala	>tr|Q962I2|Q962I2_DROME RAL2 O	3;3	19.8	2222300	1162200	661760	2222300	1162200	661760	1081642.817	1437574.42	1099182.646	1.329065749	1.307857639
CG9531	>tr|Q9VMD3|Q9VMD3_DROME CG9	6	15.8	3021600	1579100	1358100	3021600	1579100	1358100	1470679.897	1953255.693	2255802.635	1.328131089	0.86588058
CD98hc	>tr|Q9VHX9|Q9VHX9_DROME CD9	5;5	13.3	1294700	674580	888890	1294700	674580	888890	630159.2743	834416.5827	1476445.331	1.324136003	0.565152373
CG3270-RA	>tr|A1Z6N5|A1Z6N5_DROME CG32	17	45.7	13831000	7185300	7373800	13831000	7185300	7373800	6731855.195	8887801.998	12247873.85	1.320260425	0.725660805
ACC	>tr|Q7JV23|Q7JV23_DROME Acetyl	22;22;22	11.8	768080	398580	353980	768080	398580	353980	373841.6123	493020.4891	587960.3984	1.318795107	0.838526694
CG31198	>tr|Q8IN25|Q8IN25_DROME LP0775	11	13.7	1159100	601190	712560	1159100	601190	712560	564159.7396	743637.3823	1183561.392	1.318132667	0.628304867
CG33791	>tr|Q0E8J6|Q0E8J6_DROME Uncha	6;6;6	8	554430	287530	86573	554430	287530	86573	269853.4074	355658.0391	143797.6598	1.317967568	2.47332286
fln	>tr|M9PD14|M9PD14_DROME Flight	8;8	50.5	10045000	5206400	2708500	10045000	5206400	2708500	4889124.823	6440016.745	4498815.579	1.317212585	1.431491608
Ef1gamma	>tr|A0A0B4JD11|A0A0B4JD11_DRO	8;8	18.3	1981500	1026700	437080	1981500	1026700	437080	964440.1034	1269968.729	725989.4087	1.31679378	1.749293742
Mdr65	>sp|Q00748|MDR65_DROME Multid	2	3	31168	16118	34708	31168	16118	34708	15170.15873	19937.03712	57649.9507	1.314227324	0.345829214
Gdh	>sp|P54385|DHE3_DROME Glutama	9;3	16.4	33473000	17303000	10199000	33473000	17303000	10199000	16292053.28	21402813.8	16940528	1.313696526	1.263408897
Arr2	>sp|P19107|ARRB_DROME Phosres	19	48.6	24931000	12883000	7736700	24931000	12883000	7736700	12134471.97	15935528.53	12850650.36	1.313244496	1.240056191
Gp210	>tr|A1Z6H7|A1Z6H7_DROME Gp210	14	9.7	653370	337170	127570	653370	337170	127570	318009.7051	417059.8583	211893.6325	1.311468963	1.968251019
Aldh	>tr|Q9VLC5|Q9VLC5_DROME Aldeh	32	62.7	345800000	177960000	191690000	345800000	177960000	191690000	168308547.9	220126263.8	318396883.3	1.307873347	0.691358099
gish	>tr|Q8IHB0|Q8IHB0_DROME AT186	3;3;3;3;3;3;3;3;3	10.9	601450	308600	146540	601450	308600	146540	292739.0868	381720.4148	243402.7821	1.303961213	1.568266441
Gp93	>tr|Q9VAY2|Q9VAY2_DROME Glyco	28	34.3	15951000	8181500	9544500	15951000	8181500	9544500	7763706.327	10120043.98	15853404.21	1.303506799	0.638351477
Sec24AB	>tr|A0A0B4LEK8|A0A0B4LEK8_DRO	5;5	6.5	404280	207280	158560	404280	207280	158560	196772.0643	256393.4141	263367.9891	1.302997024	0.973517757
CG10932	>tr|Q9W3N9|Q9W3N9_DROME LD2	16	44.9	66449000	34068000	33298000	66449000	34068000	33298000	32342205.61	42140152.6	55307942.09	1.30294616	0.76191865
ATPsynbeta	>tr|X2JH42|X2JH42_DROME ATP sy	38;38;38	80	1382900000	708080000	911780000	1382900000	708080000	911780000	673088175	875854152	1514465597	1.301247273	0.578325552
Dhc64C	>tr|M9PE73|M9PE73_DROME Dynei	26;26;26;26;26;26;26	7.1	293380	150040	81844	293380	150040	81844	142794.5687	185590.8329	135942.7959	1.299705126	1.365212711
LKRSDH	>tr|Q9VLX0|Q9VLX0_DROME Lysine	34	44.1	17651000	9022400	8623900	17651000	9022400	8623900	8591134.122	11160188.82	14324288.6	1.299035571	0.779109465
Gapdh2	>tr|M9PJN8|M9PJN8_DROME Glyce	5;5	16.9	32811000	16751000	21199000	32811000	16751000	21199000	15969843.16	20720021.61	35211516.14	1.297446781	0.58844446
alphaCOP	>tr|Q9W0B8|Q9W0B8_DROME Coat	4	3.4	195170	99436	59732	195170	99436	59732	94993.57826	122996.6013	99214.78771	1.294788591	1.239700292
Galphai	>sp|P20353|GNAI_DROME G protei	2	9.6	782940	398410	298310	782940	398410	298310	381074.3047	492810.2089	495492.5884	1.293212906	0.994586439
Arr1	>tr|X2J8V5|X2J8V5_DROME Arrestin	5;5;5	18.3	1659100	843860	438100	1659100	843860	438100	807520.8557	1043806.187	727683.6276	1.292605856	1.434423075
CG6178	>tr|Q9VCC6|Q9VCC6_DROME CG6	6	16.4	2263400	1151200	1272300	2263400	1151200	1272300	1101647.101	1423968.054	2113288.928	1.292580948	0.673816077
	>tr|Q9VQM2|Q9VQM2_DROME NAD	4	36.2	17858000	9058700	8730400	17858000	9058700	8730400	8691885.624	11205089.83	14501184.98	1.289143727	0.772701668
Lsp1gamma	>sp|P11997|LSP1G_DROME Larval	8	11	399030	202130	922620	399030	202130	922620	194216.7725	250023.1609	1532470.825	1.287340726	0.163150356
RpS5a	>tr|X2JKU5|X2JKU5_DROME Ribosc	4;4;1;1	16.7	7494700	3787800	3111900	7494700	3787800	3111900	3647837.114	4685290.302	5168862.544	1.284402279	0.906445134
	>tr|A0A023GQA5|A0A023GQA5_DR	25;25	88	334140000	168280000	153310000	334140000	168280000	153310000	162633366.7	208152661.7	254647744.7	1.279889029	0.817414118
CG1635	>tr|Q95TK5|Q95TK5_DROME CG16	16;1	40	23649000	11896000	12525000	23649000	11896000	12525000	11510494.07	14714666.41	20804011.49	1.278369662	0.707299475
CG1733	>tr|Q960J9|Q960J9_DROME LD475	2	18.6	1410400	708780	1402800	1410400	708780	1402800	686473.0366	876720.0117	2330049.287	1.27713685	0.376266724
CG8525	>tr|Q7K209|Q7K209_DROME CG85	3	8.4	496970	249470	0	496970	249470	1	241886.348	308580.0126	1	1.275723145	308580.0126
CG8778	>tr|A1Z934|A1Z934_DROME CG877	8	27.8	6984700	3494900	2773900	6984700	3494900	2773900	3399608.776	4322989.882	4607444.908	1.271613932	0.938261871
Vha55	>tr|E1JIJ5|E1JIJ5_DROME Vacuolar	10;10	25.1	3037600	1512200	1530700	3037600	1512200	1530700	1478467.453	1870504.249	2542491.049	1.265164306	0.735697477
	>sp|Q9V9A7|MCCB_DROME Probab	19	45.8	14203000	7064500	8637900	14203000	7064500	8637900	6912915.865	8738379.36	14347542.58	1.264065632	0.609050596
Sec61alpha	>tr|Q8STG9|Q8STG9_DROME DSec	4	6.9	2887300	1433400	663660	2887300	1433400	663660	1405313.101	1773033.19	1102338.544	1.261664172	1.608428916
Mtp	>tr|Q9VIH3|Q9VIH3_DROME Micros	9	11.9	216780	107490	270540	216780	107490	270540	105511.6457	132958.9352	449366.6484	1.260135166	0.295880737
pdgy	>tr|Q9VXZ8|Q9VXZ8_DROME BcDN	17	40.4	4700400	2323900	4766500	4700400	2323900	4766500	2287789.181	2874530.369	7917151.359	1.256466458	0.363076344
whd	>tr|Q7JQH9|Q7JQH9_DROME LD31	9;9	15	1343400	664030	1853000	1343400	664030	1853000	653862.647	821366.8407	3077831.002	1.256176422	0.266865478
Iva	>tr|X2JAF1|X2JAF1_DROME Lava la	6;6	3.1	72681	35865	34718	72681	35865	34718	35375.45876	44362.93806	57666.56068	1.254059724	0.769300918
Acsl	>tr|A1Z7H3|A1Z7H3_DROME Acyl-C	40;40;40;40	53.2	27606000	13567000	8495300	27606000	13567000	8495300	13436453.94	16781597.11	14110684.14	1.248960267	1.189283024
ND-75	>tr|A4V449|A4V449_DROME NADH	51;51	59.9	169910000	83437000	56528000	169910000	83437000	56528000	82698974.48	103206760.4	93892947.03	1.247981139	1.099196091
ND-30	>tr|Q9VZU4|Q9VZU4_DROME LD25	18	53.6	103960000	51033000	34847000	103960000	51033000	34847000	50599643.27	63124879.87	57880829.42	1.247536065	1.090600817
Rab1	>tr|O18332|O18332_DROME FI0154	2;0	11.2	2524700	1237200	1357600	2524700	1237200	1357600	1228827.62	1530345.098	2254972.136	1.245370036	0.678653662
Sec63	>tr|Q9VS57|Q9VS57_DROME RE14	7	13	4066800	1991100	1471700	4066800	1991100	1471700	1979401.974	2462875.949	2444492.113	1.244252548	1.007520514

full_dataset_V1

MetRS-m;Aats-met-m	>tr|A0A0B4KH54|A0A0B4KH54_DR(	8;8	21.3	5189800	2540400	1090700	5189800	2540400	1090700	2525991.041	3142328.392	1811651.524	1.243998233	1.73451039
CG16935-RA;CG16935	>tr|H8F4T6|H8F4T6_DROME FI199	14;14	51.8	32907000	16082000	18902000	32907000	16082000	18902000	16016568.5	19892507.16	31396201.61	1.241995573	0.63359981
cathD	>tr|Q7K485|Q7K485_DROME CathD	7	22.7	6295300	3068300	5514100	6295300	3068300	5514100	3064062.469	3795310.268	9158914.153	1.238653032	0.414384304
schlank	>tr|Q9W423|Q9W423_DROME LD1	2	5.2	272250	132300	51651	272250	132300	51651	132510.1279	163647.4753	85792.25542	1.234980887	1.907485408
Rab2	>tr|O18333|O18333_DROME GH01	5	29.1	1939400	940490	1050900	1939400	940490	1050900	943949.0974	1163331.928	1745543.767	1.232409598	0.666458183
ttm50	>tr|A0A0S0X8K7|A0A0S0X8K7_DRO	11;11;1	26.9	4080600	1977900	3914000	4080600	1977900	3914000	1986118.741	2446548.31	6501149.779	1.231823787	0.37632548
CG10639-RA	>tr|Q9VJ28|Q9VJ28_DROME FI052	17	44.6	35518000	17210000	26650000	35518000	17210000	26650000	17287400.25	21287778.16	44265621.26	1.231404251	0.48090996
Fbp1	>sp|Q04691|FBP1_DROME Fat-body	23;22	27.7	5479000	2653200	2500800	5479000	2653200	2500800	2666751.111	3281855.491	4153826.103	1.230656839	0.790080136
Tim23	>tr|Q8MRW1|Q8MRW1_DROME SD	4	19.4	6428800	3112000	2599500	6428800	3112000	2599500	3129039.887	3849364.65	4317766.697	1.230206322	0.891517518
Acp36DE	>tr|X2J8Y6|X2J8Y6_DROME Access	15;15	27.4	2972900	1438000	133550	2972900	1438000	133550	1446976.524	1778723.125	221826.4061	1.22926882	8.018536461
Idh	>tr|Q7KUB0|Q7KUB0_DROME Isocit	25;25;25;25;25	51.2	60312000	29160000	41807000	60312000	29160000	41807000	29355191.27	36069239.45	69441381.91	1.228717576	0.519419955
Dp1	>tr|Q7KN75|Q7KN75_DROME Dode	6	6	283960	137110	111910	283960	137110	111910	138209.6453	169597.1681	185882.3894	1.227100813	0.912389649
CG5482	>tr|Q7K3D4|Q7K3D4_DROME CG54	4	12.1	1897700	916270	855740	1897700	916270	855740	923652.7803	1133373.184	1421383.217	1.227055456	0.797373411
	>tr|Q9VXP5|Q9VXP5_DROME EFH(	14	22.7	4143000	1999100	310880	4143000	1999100	310880	2016490.208	2472771.488	516371.3448	1.226274979	4.788746534
Gs2	>tr|X2JJG8|X2JJG8_DROME Glutam	10;10;10	24.7	13306000	6420200	6577100	13306000	6420200	6577100	6476326.023	7941417.392	10924556.01	1.226222609	0.726932736
TER94	>sp|Q7KN62|TERA_DROME Transit	10;9	17.2	416060	200610	381700	416060	200610	381700	202505.6521	248143.0085	634003.2885	1.225363371	0.391390728
mtTFB2	>sp|Q9VH38|TFB2M_DROME Dimet	7	21.2	1727000	831440	380210	1727000	831440	380210	840569.2953	1028443.363	631528.4001	1.223508125	1.628498991
Rac1	>tr|M9PBH7|M9PBH7_DROME Rac1	4;4	24	6908600	3317900	2291800	6908600	3317900	2291800	3362569.214	4104051.083	3806677.328	1.220510515	1.078118981
Cpr	>tr|M9PCQ1|M9PCQ1_DROME NAD	13;13;11	22.4	1856600	891580	699700	1856600	891580	699700	903648.4966	1102833.077	1162200.946	1.220422632	0.948917724
nrv3	>tr|Q7JS69|Q7JS69_DROME FI046	7;6	23.2	11721000	5625700	7704200	11721000	5625700	7704200	5704871.284	6958666.68	12796667.89	1.219776281	0.543787394
RpL34b;RpL34a	>tr|Q9VHE5|Q9VHE5_DROME RH4	6;4	31.5	76054000	36446000	14951000	76054000	36446000	14951000	37017172.65	45081601.55	24833594.88	1.217856425	1.815347386
CG30415	>tr|Q0E8X7|Q0E8X7_DROME Uncha	3	37.8	10233000	4871300	4885100	10233000	4871300	4885100	4980628.603	6025517.358	8114145.832	1.209790538	0.742594166
mRpL45	>sp|Q9VCX3|RM45_DROME Probab	7	23.8	3935400	1868100	1227800	3935400	1868100	1227800	1915446.673	2310732.038	2039374.476	1.206367199	1.133059213
CG11473	>tr|Q9W4A6|Q9W4A6_DROME RE5	2	4	4122300	1955800	997680	4122300	1955800	997680	2006415.058	2419211.884	1657145.404	1.2057385	1.459866996
CG11999	>tr|Q9VNA3|Q9VNA3_DROME GH2	3	19	1138000	539850	607080	1138000	539850	607080	553889.9005	667763.3374	1008359.225	1.205588578	0.662227627
CG3999	>tr|Q9VH09|Q9VH09_DROME CG39	32	40.8	14111000	6693900	8420500	14111000	6693900	8420500	6868137.42	8279968.518	13986441.42	1.205562442	0.591999657
ico	>sp|Q9VM33|EFGM_DROME Elonga	4	6.4	442690	209840	132160	442690	209840	132160	215467.0652	259559.9865	219517.6176	1.204638799	1.18241073
CG8036	>tr|Q9VHN7|Q9VHN7_DROME CG8	15;14	27.2	4657800	2207000	2036200	4657800	2207000	2036200	2267054.814	2729931.806	3382126.004	1.204175475	0.807164429
CG6812-RA	>tr|Q9VVW3|Q9VVW3_DROME Side	7	30	9016100	4268800	4349900	9016100	4268800	4349900	4388336.318	5280259.581	7225179.209	1.203248611	0.730813649
CG4587	>tr|A8DZ06|A8DZ06_DROME CG45	8;8	8.9	671860	317910	349440	671860	317910	349440	327009.1992	393236.3483	580419.4633	1.202523811	0.677503725
CG10672	>tr|Q9VRJ4|Q9VRJ4_DROME SD02	4	16.1	2118100	1001500	954420	2118100	1001500	954420	1030926.36	1238797.782	1585290.591	1.201635567	0.781432621
CG7639	>sp|Q9V784|SAM50_DROME SAM5	7	18.3	2382400	1126300	1000600	2382400	1126300	1000600	1159567.046	1393168.189	1661995.521	1.201455486	0.838250267
Top2	>sp|P15348|TOP2_DROME DNA top	25	20.3	2924500	1382100	466850	2924500	1382100	466850	1423419.168	1709578.047	775437.3466	1.201036269	2.204663026
beta-Spec	>sp|Q00963|SPTCB_DROME Spectr	3	0.8	22206000	10478000	3269500	22206000	10478000	3269500	10808153.89	12960682.13	5430635.974	1.199157809	2.386586432
PCB	>tr|Q0E9E2|Q0E9E2_DROME Pyruv	85;84	67.1	148210000	69812000	92666000	148210000	69812000	92666000	72137102.04	86353420.6	153918126.1	1.197073602	0.561034771
RpS27A;RpL40	>sp|P15357|RS27A_DROME Ubiquit	12;11;11;11;11;11;9	50.6	173260000	81418000	57694000	173260000	81418000	57694000	84329493.96	100709373.7	95829671.78	1.194236666	1.050920575
Hsc70-4	>tr|C7LA75|C7LA75_DROME Heat s	24;24;2;2	41	31475000	14737000	9939100	31475000	14737000	9939100	15319582.26	18228819.68	16508834.38	1.189903182	1.10418575
Tspo	>tr|Q9VPR1|Q9VPR1_DROME GH0	3	16.8	6816600	3191300	2485300	6816600	3191300	2485300	3317790.769	3947454.179	4128080.62	1.189783942	0.956244449
Nc73EF	>tr|Q8IQQ0|Q8IQQ0_DROME Neura	2	2.9	3676000	1714800	849630	3676000	1714800	849630	1789190.926	2121108.773	1411234.514	1.185512816	1.503016509
CG9629	>tr|Q8SXQ1|Q8SXQ1_DROME CG9	3	8.5	285380	133030	204560	285380	133030	204560	138900.7908	164550.4433	339773.9395	1.184661673	0.484293891
EF2	>sp|P13060|EF2_DROME Elongatio	14	19.4	4355000	2028000	1499800	4355000	2028000	1499800	2119675.322	2508519.123	2491166.183	1.183444982	1.00696579
RpL8	>sp|Q9V3G1|RL8_DROME 60S ribo	12	45.3	53881000	25061000	10888000	53881000	25061000	10888000	26225080.6	30999012.69	18084956.26	1.182036889	1.714077283
P5cr-2	>tr|Q8IN96|Q8IN96_DROME Pyrrolin	2;2;2	12.1	2921800	1357300	1040400	2921800	1357300	1040400	1422105.018	1678901.876	1728103.278	1.180575172	0.971528668
CG33303	>tr|Q76NQ0|Q76NQ0_DROME Dolic	14	41.5	8604400	3985700	6287100	8604400	3985700	6287100	4187952.775	4930081.197	10442866.32	1.177205537	0.472100384
RpL21	>tr|Q9V9M7|Q9V9M7_DROME RE62	7	41.5	37332000	17253000	7388400	37332000	17253000	7388400	18170314.37	21340966.68	12272124.43	1.174496282	1.738979
CG6638	>tr|Q9VSL9|Q9VSL9_DROME CG66	10	30.2	9463700	4373100	4579600	9463700	4373100	4579600	4606193.19	5409272.67	7606710.661	1.174347763	0.711118499
blw	>sp|P35381|ATPA_DROME ATP syr	71	70.3	1316700000	607620000	750090000	1316700000	607620000	750090000	640867163.2	751590921.7	124589681	1.172771777	0.603252041
Rack1	>tr|M9PCC1|M9PCC1_DROME Rece	10;10;4;1	34	7174900	3308300	6493700	7174900	3308300	6493700	3492183.344	4092176.436	10786028.7	1.171810307	0.379396027
Unc-115b	>tr|Q8INN5|Q8INN5_DROME Unc-1	2;2;2;2;2;2;2;2;2;2;2;2	5.1	200650	92319	7760.5	200650	92319	7760.5	97660.8161	114193.2825	12890.18226	1.169284541	8.858934668
Rho1	>sp|P48148|RHO1_DROME Ras-like	8	36.5	25785000	11847000	10273000	25785000	11847000	10273000	12550132.76	14654056.23	17063441.92	1.167641531	0.858798377
Surf1	>sp|Q9U4F3|SURF1_DROME SURF	3	24.3	5537900	2544200	1873900	5537900	2544200	1873900	2695419.05	3147028.773	3112545.879	1.167547129	1.011078678

full_dataset_V1

CG6984	>tr|Q7K1C3|Q7K1C3_DROME CG6	3	16.5	4028800	1847600	43973	4028800	1847600	43973	1960906.53	2285374.719	73039.1057	1.165468463	31.28974126
CG11771	>tr|Q9VC06|Q9VC06_DROME LD37	25	37.5	11724000	5374900	4429000	11724000	5374900	4429000	5706331.451	6648441.534	7356564.223	1.165099082	0.903742744
PNPase	>tr|Q9V9X7|Q9V9X7_DROME FI188	8	13.7	1716800	786880	580910	1716800	786880	580910	835604.7285	973325.2106	964890.8836	1.164815346	1.008741224
Aph4	>sp|Q24238|APH4_DROME Alkaline	4	6.5	203620	93205	258800	203620	93205	258800	99106.38113	115289.2134	429866.521	1.163287491	0.268197703
ND-B22	>tr|Q9VJZ4|Q9VJZ4_DROME AT12	6	39.6	10449000	4782100	6099100	10449000	4782100	6099100	5085760.605	5915182.099	10130598.52	1.163087011	0.583892658
alpha-Spec	>tr|M9PBI5|M9PBI5_DROME Alpha	170;170;169;169	65.5	38494000	17616000	4322400	38494000	17616000	4322400	18735885.61	21789976.76	7179501.738	1.163007568	3.035026322
mRpS14	>tr|Q9VWI3|Q9VWI3_DROME IP02	2	19.5	2407000	1101000	782680	2407000	1101000	782680	1171540.413	1361873.547	1300030.636	1.162463993	1.047570349
mRpL41	>sp|Q7JZM8|RM41_DROME 39S rib	3	22.9	2094000	956390	883400	2094000	956390	883400	1019196.355	1182999.311	1467326.447	1.160717762	0.806227758
CG7920	>tr|Q9VAC1|Q9VAC1_DROME CG7	17	46.1	31032000	14172000	6608200	31032000	14172000	6608200	15103964.31	17529947.24	10976213.07	1.160618953	1.597085181
RpL5	>tr|R9Q794|R9Q794_DROME Ribos	16;16	51.8	85026000	38728000	28397000	85026000	38728000	28397000	41384044.52	47904304.03	47167386.37	1.157554912	1.015623458
beg	>sp|Q8T3L6|FABD_DROME Probabl	2	7.4	852180	387580	270820	852180	387580	270820	414774.9521	479414.1231	449831.728	1.155841549	1.065763247
CG4538-RA;CG4538	>tr|Q9VDS7|Q9VDS7_DROME CG4	5;5	12.8	592360	268810	301550	592360	268810	301550	288314.7817	332502.478	500874.2249	1.153261987	0.663844258
UQCR-Q	>tr|Q9VVH5|Q9VVH5_DROME AT13	2	20.2	6921300	3126100	3111300	6921300	3126100	3111300	3368750.586	3866805.537	5167865.945	1.1478456	0.748240295
CG17597	>tr|Q9VJ44|Q9VJ44_DROME SD06	4	21.4	26868000	12132000	9798000	26868000	12132000	9798000	13077252.94	15006584.81	16274467.43	1.147533422	0.922093756
Mul1	>tr|Q9VZJ9|Q9VZJ9_DROME AT15	4	14.8	1442800	650730	1067100	1442800	650730	1067100	702242.8369	804915.5072	1772451.949	1.146206789	0.454125432
Fatp	>tr|Q9VKU1|Q9VKU1_DROME Fatty	7;7;1;1	14.2	1335000	601600	771370	1335000	601600	771370	649774.1803	744144.5287	1281244.738	1.145235608	0.580798115
sta	>tr|X2JC80|X2JC80_DROME 40S rib	7;6	36.7	13152000	5903800	7350300	13152000	5903800	7350300	6401370.799	7302660.353	12208840.37	1.140796336	0.598145289
CG8613	>tr|Q5BIA9|Q5BIA9_DROME CG861	3	5.2	248460	111480	57673	248460	111480	57673	120931.006	137894.3352	95794.79093	1.140272787	1.439476342
bgm	>tr|B5RIV0|B5RIV0_DROME Bubble	9;9	15	5775400	2588300	2265700	5775400	2588300	2265700	2811015.58	3201577.931	3763325.257	1.138939945	0.850731126
mRpS17	>tr|Q9W199|Q9W199_DROME Mitoc	5	35.5	5069900	2271500	1069000	5069900	2271500	1069000	2467633.046	2809714.589	1775607.847	1.138627396	1.582395907
	>tr|Q9W4H6|Q9W4H6_DROME Pyru	25;25;19	57.1	44886000	20096000	39836000	44886000	20096000	39836000	21847014.12	24857593.83	66167553.04	1.1378028	0.375676486
ND-MLRQ	>tr|Q8SYJ2|Q8SYJ2_DROME NADH	3	30.1	33149000	14828000	6805700	33149000	14828000	6805700	16134355.28	18341381.43	11304260.36	1.136790477	1.622519373
cpa	>sp|Q9W2N0|CAPZA_DROME F-act	5	24.8	5348400	2391400	1108800	5348400	2391400	1108800	2603185.187	2958023.979	1841715.604	1.13630947	1.606124188
mfrn	>sp|Q9VAY3|MFRN_DROME Mitofer	3	6.1	1226900	545940	623410	1226900	545940	623410	597159.5069	675296.3165	1035483.338	1.130847468	0.652155657
RpL3	>sp|O16797|RL3_DROME 60S ribos	11	25.5	10484000	4663100	2603300	10484000	4663100	2603300	5102795.883	5767985.957	4324078.492	1.130357962	1.333922584
CG31548	>tr|Q8IPP8|Q8IPP8_DROME Unchar	5	27	6431500	2854100	3304100	6431500	2854100	3304100	3130354.037	3530357.213	5488106.537	1.127782088	0.643274176
cora	>tr|A0A0B4LFX4|A0A0B4LFX4_DRO	12;12;12	12.2	1982900	875640	582910	1982900	875640	582910	965121.5145	1083116.215	968212.8815	1.122258906	1.118675692
Rab5	>tr|Q9V3I2|Q9V3I2_DROME Drab5	6	35.6	6025500	2657600	3455200	6025500	2657600	3455200	2932744.811	3287298.038	5739083.474	1.120894674	0.572791466
SsRbeta	>tr|Q9VUZ0|Q9VUZ0_DROME Trans	4	36.3	25645000	11298000	12897000	25645000	11298000	12897000	12481991.65	13974974.87	21421903.09	1.119610978	0.652368504
ND-51	>tr|Q9VMI3|Q9VMI3_DROME GM14	32;2	76.2	117260000	51532000	42271000	117260000	51532000	42271000	57073048.95	63742114.11	70212085.41	1.116851391	0.907851031
Adh	>sp|P00334|ADH_DROME Alcohol d	5	33.2	8239100	3620300	5557900	8239100	3620300	5557900	4010153.144	4478102.455	9231665.906	1.116691132	0.485080645
CG6094	>tr|Q9VKU3|Q9VKU3_DROME CG6	3	20.2	1076100	471480	261180	1076100	471480	261180	523761.7943	583193.5877	433819.6984	1.113471036	1.344322514
mRpS28	>tr|A1ZBA5|A1ZBA5_DROME FI072	2	18	4077100	1786100	1753500	4077100	1786100	1753500	1984415.213	2209302.764	2912561.609	1.113326863	0.758542843
CG8531	>tr|Q7K0W1|Q7K0W1_DROME CG8	5	8.6	1247100	546080	304180	1247100	546080	304180	606991.296	675469.4884	505242.6521	1.112815773	1.336920954
ND-20	>tr|Q9VXK7|Q9VXK7_DROME LD31	4	13.6	29433000	12871000	14802000	29433000	12871000	14802000	14325695.46	15920685.22	24586106.04	1.111337684	0.647548058
Spp	>tr|Q9VPQ7|Q9VPQ7_DROME SD07	5	9.3	6855100	2992600	1773700	6855100	2992600	1773700	3336529.575	3701673.731	2946113.787	1.10943831	1.256459865
nmd	>tr|Q9VL02|Q9VL02_DROME GH08	9;6	22.2	8052100	3511200	1520300	8052100	3511200	1520300	3919136.087	4343152.043	2525216.66	1.10819118	1.719912636
CG8323	>tr|Q7JZE8|Q7JZE8_DROME CG83	2	8.3	2582700	1125100	652320	2582700	1125100	652320	1257057.509	1391683.858	1083502.817	1.107096412	1.28443031
Arc42	>tr|Q9VDT1|Q9VDT1_DROME Arc42	14	33.8	13296000	5774000	14819000	13296000	5774000	14819000	6471458.8	7142105.233	24614343.02	1.103631415	0.290160303
Pdk	>tr|A0A0B4K7V5|A0A0B4K7V5_DRO	7;7;6;6	22.5	1991500	864620	1066500	1991500	864620	1066500	969307.3257	1069485.11	1771455.35	1.103349868	0.603732468
Tor	>tr|M9PFS0|M9PFS0_DROME Targe	4;4	2.5	66883	28997	18968	66883	28997	18968	32553.44325	35867.61787	31505.82767	1.101807191	1.138443917
RpL31	>sp|Q9V597|RL31_DROME 60S ribo	5	46	14778000	6375000	4119500	14778000	6375000	4119500	7192781.148	7885507.597	6842485.057	1.096308567	1.152433294
CG6412	>sp|Q9VJC7|EFTS_DROME Elongat	7	26.4	2467600	1063800	1599200	2467600	1063800	1599200	1201035.781	1315859.291	2656269.475	1.095603739	0.495378689
levy	>tr|Q9W1N3|Q9W1N3_DROME Levy	5	34.9	93654000	40359000	25280000	93654000	40359000	25280000	45583483.94	49921757.03	41990052.74	1.095172039	1.18889484
CG31272	>tr|Q9VGX6|Q9VGX6_DROME FI03	2	3.9	491250	211490	84509	491250	211490	84509	239102.2968	261600.9415	140369.358	1.094096313	1.863661309
AP-2sigma	>tr|Q9VDC3|Q9VDC3_DROME Adap	2	11.3	3756800	1616700	1241900	3756800	1616700	1241900	1828518.082	1999764.727	2062794.561	1.093653241	0.969444444
CG31803	>tr|Q8T3V7|Q8T3V7_DROME AT29	4	17.4	1421000	609860	204690	1421000	609860	204690	691632.2922	754361.6726	339989.8694	1.090697588	2.218776912
CG6406	>tr|Q7K1C5|Q7K1C5_DROME CG64	2	4.8	1090400	467040	91294	1090400	467040	91294	530721.9222	577701.5636	151639.2357	1.088520258	3.809710337
ninaC	>sp|P10676|NINAC_DROME Neither	60;52	44.2	17283000	7399300	6008500	17283000	7399300	6008500	8412020.34	9152507.664	9980112.02	1.088027286	0.917074643
bsf	>tr|Q9VJ86|Q9VJ86_DROME Bicoid	70	52.5	26688000	11358000	5543200	26688000	11358000	5543200	12989642.93	14049191.42	9207249.222	1.081568715	1.52588369
CG32103;CG4392	>tr|M9PF04|M9PF04_DROME Unchs	4;4;4	11.4	743720	316480	353500	743720	316480	353500	361985.0588	391467.5207	587163.1189	1.081446627	0.666709996

full_dataset_V1

CG17691	>tr|Q7PLE6|Q7PLE6_DROME Uncha	6	26.1	25934000	11017000	7023300	25934000	11017000	7023300	12622654.37	13627394.07	11665693.73	1.079598131	1.168159767
CG4972-RA	>tr|Q9VKZ7|Q9VKZ7_DROME Nicali	2	4.8	271630	114990	0	271630	114990	1	132208.3601	142236.0029	1	1.075847267	142236.0029
ScpX	>tr|Q9VJ43|Q9VJ43_DROME LD107	3	10.7	2573100	1087100	1005800	2573100	1087100	1005800	1252384.976	1344680.048	1670632.715	1.073695448	0.804892683
CG17593-RA	>tr|Q9VQR9|Q9VQR9_DROME FI04	7	21.6	3078700	1300200	1204600	3078700	1300200	1204600	1498471.737	1608272.467	2000839.301	1.073275143	0.803798919
RpL35	>tr|Q9W499|Q9W499_DROME FI02	2	17.1	18516000	7789500	3124400	18516000	7789500	3124400	9012148.853	9635162.576	5189625.03	1.06913043	1.856620184
PI4KIIIalpha	>tr|Q9W4X4|Q9W4X4_DROME Phos	17;17	11.8	540090	226950	147510	540090	226950	147510	262873.8106	280724.0705	245013.951	1.067904291	1.14574729
scu	>sp|O18404|HCD2_DROME 3-hydro	19;5	85.1	138210000	58035000	59703000	138210000	58035000	59703000	67269879.72	71785950.33	99166618.61	1.067133621	0.723892287
RpL37A	>tr|M9MRF2|M9MRF2_DROME Ribo	2;2	30.4	3513400	1475200	167100	3513400	1475200	167100	1710049.891	1824737.381	277552.9199	1.067066751	6.574376454
	>tr|Q9VPX3|Q9VPX3_DROME CG47	3	8	557740	234070	93997	557740	234070	93997	271464.458	289531.1001	156128.9158	1.066552514	1.854436116
CG5839	>tr|Q8SWX4|Q8SWX4_DROME GH2	6	7.9	215080	90195	263110	215080	90195	263110	104684.2179	111566.0169	437025.4264	1.065738649	0.255284956
CG1907	>tr|Q9VAJ9|Q9VAJ9_DROME CG19	18	58	48932000	20496000	15501000	48932000	20496000	15501000	23816292.27	25352370.78	25747144.28	1.064496962	0.98466729
COX4	>tr|Q9VIQ8|Q9VIQ8_DROME Cytoch	6	38.5	174060000	72852000	86744000	174060000	72852000	86744000	84718871.75	90113725.4	144081690.4	1.063679479	0.625434954
CG10252	>tr|Q9VCJ6|Q9VCJ6_DROME AT18	8	48	4075200	1704500	453870	4075200	1704500	453870	1983490.441	2108368.266	753877.5806	1.062958622	2.796698457
Mpc1	>tr|A0A0B4KHD3|A0A0B4KHD3_DR	2;2	12.1	9142100	3822900	2950500	9142100	3822900	2950500	4449663.32	4728706.979	4900777.318	1.062711185	0.964889174
CG3842-RA	>tr|Q9W404|Q9W404_DROME CG3	2	4.4	543400	226300	159190	543400	226300	159190	264484.8612	279920.0579	264414.4184	1.058359472	1.05864143
QIL1	>sp|Q9VVH3|MIC13_DROME MICO	6	68.9	7405300	3081800	3693100	7405300	3081800	3693100	3604324.147	3812008.99	6134235.117	1.057621023	0.621431836
tzn	>tr|Q9I7P8|Q9I7P8_DROME CG436	6;6;6	23.2	2673700	1111500	1169700	2673700	1111500	1169700	1301349.233	1374861.442	1942870.439	1.056489225	0.707644429
RpL28	>tr|D1Z3A1|D1Z3A1_DROME MIP15	10;10;1	59	27043000	11224000	5848300	27043000	11224000	5848300	13162429.33	13883441.14	9714019.993	1.05477802	1.429216859
mRpS18C	>tr|Q9VA81|Q9VA81_DROME IP027	2	16.4	1485300	616210	609500	1485300	616210	609500	722928.5318	762216.2567	1012378.843	1.05434524	0.752896272
Rap1;R	>tr|M9MRT6|M9MRT6_DROME Rap	4;4	22.3	7053200	2925600	3666400	7053200	2925600	3666400	3432949.249	3618798.592	6089886.446	1.054136933	0.594230882
CG9090-RA	>tr|Q7JUS9|Q7JUS9_DROME CG90	19	37.2	259790000	107300000	114080000	259790000	107300000	114080000	126445568.7	132723916.1	189486757	1.049652569	0.700439008
Cyp12a4	>sp|Q9VE00|C12A4_DROME Probal	20	40.3	52416000	21640000	18602000	52416000	21640000	18602000	25512032.53	26767432.85	30897901.94	1.049208166	0.86631784
CG7131	>tr|Q9VE97|Q9VE97_DROME CG71	3	7.1	533750	220300	172030	533750	220300	172030	259787.9917	272498.4037	285741.6446	1.048926095	0.953653095
ND-39	>tr|Q9VPE2|Q9VPE2_DROME NADI	31	70.2	134900000	55669000	38895000	134900000	55669000	38895000	656588.29.13	68859344.69	64604553.05	1.048744633	1.065859006
Ald	>tr|C8VV14|C8VV14_DROME Fructo	2;2;2;2	8.6	337740	139320	69013	337740	139320	69013	164385.5669	172330.8107	114630.5187	1.048332977	1.503358902
mRpL3	>tr|Q9VXQ0|Q9VXQ0_DROME Mitoc	13	37.3	21734000	8936600	6389300	21734000	8936600	6389300	10578421	11054059.17	10612620.41	1.044963059	1.041595642
RpL6	>tr|Q9V9W2|Q9V9W2_DROME Ribo	10;10	31.7	17684000	7264000	2315800	17684000	7264000	2315800	8607195.955	8985149.362	3846541.303	1.043911328	2.335903518
CG7461	>tr|A1ZBJ2|A1ZBJ2_DROME CG746	37	58.1	59042000	24208000	22094000	59042000	24208000	22094000	28737054.04	29943900.85	36698110.17	1.041996191	0.815952121
Adck	>tr|Q9W133|Q9W133_DROME AarF	8	19.9	2439300	999710	654800	2439300	999710	654800	1187261.541	1236583.655	1087622.094	1.041542753	1.136960771
RpLP1	>tr|M9PBK5|M9PBK5_DROME Ribos	3;3	50	10325000	4231300	633570	10325000	4231300	633570	5025407.048	5233874.242	1052359.087	1.041482648	4.973467999
mRpL43	>tr|Q9W1L1|Q9W1L1_DROME Mitoc	4	30.7	10802000	4421300	2297100	10802000	4421300	2297100	5257573.553	5468893.292	3815480.623	1.040193397	1.433343223
porin	>tr|M9PD75|M9PD75_DROME Porin	26;26	78.4	71932000	29402000	43672000	71932000	29402000	43672000	35010903.61	36368579.51	72539144.9	1.038778659	0.501364878
Incenp	>tr|A0A0B4LFQ2|A0A0B4LFQ2_DR	2;2	1.2	310700	126810	32128	310700	126810	32128	151224.5978	156856.6617	53364.57348	1.037243041	2.939340681
Acon	>tr|Q9VIE8|Q9VIE8_DROME Aconita	30	42.4	19380000	7902700	5338600	19380000	7902700	5338600	9432676.861	9775184.452	8867408.842	1.036310752	1.102372139
CG4860	>tr|Q9VGC2|Q9VGC2_DROME CG4	4	12	617550	251800	607700	617550	251800	607700	300575.3147	311462.0883	1009389.045	1.036219786	0.308564958
mRpL15	>tr|Q9VPF6|Q9VPF6_DROME FI068	10	45.8	8957700	3646600	1968900	8957700	3646600	1968900	4359911.74	4510634.04	3270340.777	1.034570035	1.379255052
CG15096	>tr|Q7JRA7|Q7JRA7_DROME RH60	2;2	5.3	884920	360110	567080	884920	360110	567080	430710.238	445435.3162	941919.2685	1.034187899	0.472901799
CG34417	>tr|M9PDW3|M9PDW3_DROME Unc	3;3;3;3;3;3;3;3;3;3;3;3;3;3;2;1	2.5	54542	22092	7913.1	54542	22092	7913.1	26546.80419	27326.53082	13143.6507	1.02937177	2.079067031
RpL4	>sp|P09180|RL4_DROME 60S ribos	20	51.6	19551000	7918000	2944000	19551000	7918000	2944000	9515906.363	9794109.671	4889980.825	1.029235608	2.002893267
Coprox	>tr|X2J9R2|X2J9R2_DROME Coprog	4;4	12.3	2532400	1025300	1092700	2532400	1025300	1092700	1232575.381	1268237.01	1814973.522	1.028932615	0.698763368
mRpS34	>tr|Q9VV39|Q9VV39_DROME Mitoc	8	47.9	9160900	3700500	3978000	9160900	3700500	3978000	4458813.698	4577305.233	6607453.71	1.026574677	0.69274874
CG4692	>sp|Q9W141|ATPK_DROME Putativ	9	62.6	96308000	38874000	40680000	96308000	38874000	40680000	46875244.74	48084897.62	67569436.13	1.025805793	0.711636805
SdhB	>sp|P21914|SDHB_DROME Succina	15	43.4	63722000	25717000	17935000	63722000	25717000	17935000	31014914.08	31810446.88	29790015.66	1.025650008	1.067822429
Kr-h2	>tr|X2J4W8|X2J4W8_DROME Krupp	2;2	14.1	391090	157640	177150	391090	157640	177150	190352.198	194991.5949	294245.9591	1.0243727	0.66268232
Argk	>tr|A8JNP1|A8JNP1_DROME Arginit	15;15;15	40.2	11876000	4774100	5017300	11876000	4774100	5017300	5780313.23	5905286.56	8333729.889	1.021620512	0.708600667
CG9314	>tr|Q9VLI6|Q9VLI6_DROME CG931	12	29.1	8801500	3537700	965490	8801500	3537700	965490	4283885.727	4375931.016	1603677.849	1.021486401	2.728684579
CG15908	>tr|Q4QPU3|Q4QPU3_DROME IP04	2	9.6	208260	83674	199450	208260	83674	199450	101364.7723	103499.9157	331286.235	1.021063959	0.312418401
RpS3	>tr|G3M3A2|G3M3A2_DROME Ribos	12;12	48	8413900	3379800	2040600	8413900	3379800	2040600	4095232.19	4180617.816	3389434.399	1.020850008	1.233426384
Myo61F	>sp|Q23979|MY61F_DROME Myosin	35	36.2	8402100	3369000	1623100	8402100	3369000	1623100	4089488.868	4167258.838	2695967.35	1.019017039	1.545737874
Ef1alpha48D	>tr|C6TP87|C6TP87_DROME Elong	8;8	28.5	86670000	34619000	22786000	86670000	34619000	22786000	42184215.87	42821707.84	37847521.43	1.015112097	1.131427006
dre4	>sp|Q8IRG6|SPT16_DROME FACT	4	4.6	304400	121490	34816	304400	121490	34816	148158.2477	150276.1283	57829.33858	1.01429472	2.598613991

full_dataset_V1

CG11897	>tr|Q961D3|Q961D3_DROME LD17(	2	2	35576	14195	66834	35576	14195	66834	17315.63033	17558.39694	111011.202	1.014020085	0.158167794
CG4627	>tr|Q059A4|Q059A4_DROME CG46	2	11.3	1167500	465690	538460	1167500	465690	538460	568248.2064	576031.6914	894381.4794	1.013697333	0.644055925
Myo31DF	>tr|M9MRS7|M9MRS7_DROME Myo	26;26	33.6	4921300	1960500	308130	4921300	1960500	308130	2395306.122	2425025.513	511803.5978	1.012407346	4.738195517
Hcs	>tr|Q9VNC3|Q9VNC3_DROME Holo	2;2;1;1	2.7	118920	47198	57449	118920	47198	57449	57881.00805	58381.20592	95422.72717	1.008641831	0.611816573
mRpL24	>sp|Q9VMY1|RM24_DROME Probat	10	34	5519500	2173800	1854500	5519500	2173800	1854500	2686463.361	2688865.32	3080322.5	1.000894097	0.87291682
Gk2	>tr|Q9W095|Q9W095_DROME FI03	14	24.8	12360000	4867700	8501200	12360000	4867700	8501200	6015886.791	6021064.365	14120484.03	1.00086065	0.426406372
betaTub85D	>sp|P61857|TBB2_DROME Tubulin	14	45.3	294170000	115810000	58189000	294170000	115810000	58189000	143179079.1	143250295.7	96651866.24	1.000497395	1.482126535
CG1213	>tr|Q7JVN6|Q7JVN6_DROME CG12	2	6.7	0	0	784660	1	1	784660	1	1	1303319.414	1	7.67272E-07
CG14997	>tr|Q9VZF6|Q9VZF6_DROME GH04	11	24.9	6736500	2649800	2095300	6736500	2649800	2095300	3278804.318	3277649.887	3480291.04	0.999647911	0.941774653
EF-G2	>sp|Q9VCX4|RRF2M_DROME Ribos	5;3	7.3	619030	242670	405140	619030	242670	405140	301295.6636	300168.8045	672937.1032	0.996259956	0.446057742
CG4467	>tr|Q9VCP4|Q9VCP4_DROME CG4	2;2	3.7	117290	45853	13983	117290	45853	13983	57087.65082	56717.51843	23225.74805	0.993516419	2.442010406
UQCR-C2	>tr|Q9VV75|Q9VV75_DROME AT02	37	88.2	802250000	313530000	323470000	802250000	313530000	323470000	390472910.8	387818540.7	537283321.1	0.993202166	0.721813846
CG14231	>tr|M9NHD5|M9NHD5_DROME Uncl	2;2	8.8	955000	372570	256590	955000	372570	256590	464819.732	460847.6181	426195.7134	0.991454507	1.081305146
Tom40	>tr|M9PGL7|M9PGL7_DROME Trans	11;11;1	45.1	10373000	4040800	6753300	10373000	4040800	6753300	5048769.715	4998236.721	11217224.02	0.989991028	0.445585888
CG5131	>tr|Q9VJD0|Q9VJD0_DROME CG51	4	17.7	2648100	1031100	855440	2648100	1031100	855440	1288889.143	1275411.276	1420884.918	0.989543036	0.897617576
CG12163	>sp|Q9VN93|CPR1_DROME Putativ	7	12.7	1866200	724880	958200	1866200	724880	958200	908321.03	896634.7838	1591569.167	0.987134234	0.563365264
Pdp	>tr|Q9W3Q1|Q9W3Q1_DROME GM	3	9.1	526170	204330	190310	526170	204330	190310	256098.6371	252744.4341	316104.7049	0.986902691	0.799559229
mRpL21	>tr|Q9VVX4|Q9VVX4_DROME Mitoc	3	24.4	2497700	968580	1337300	2497700	968580	1337300	1215686.12	1198077.639	2221253.858	0.985515603	0.539369976
arg	>tr|O76895|O76895_DROME Argina	8	25.9	2978400	1152900	2321000	2978400	1152900	2321000	1449653.497	1426070.856	3855178.497	0.983732223	0.369910461
cpb	>tr|M9PBN7|M9PBN7_DROME Capp	3;3	15.6	4069000	1569300	564730	4069000	1569300	564730	1980472.763	1941133.658	938015.9211	0.980136508	2.069403743
RpL9	>tr|X2JDU0|X2JDU0_DROME Ribos	7;7	37.4	9906600	3819700	3331700	9906600	3819700	3331700	4821762.466	4724748.763	5533950.107	0.979880033	0.853775092
mRpS29	>tr|Q9W253|Q9W253_DROME LD47	8	25.5	4916700	1891500	1572600	4916700	1891500	1572600	2393067.2	2339676.489	2612086.904	0.977689423	0.895711581
RpL7A	>tr|X2JCS6|X2JCS6_DROME Ribos	10;10	29.2	29301000	11270000	5583800	29301000	11270000	5583800	14261448.13	13940340.49	9274685.778	0.977484219	1.503052591
sea	>tr|Q7KSQ0|Q7KSQ0_DROME LD46	27	53.6	101250000	38853000	37103000	101250000	38853000	37103000	49280626.02	48058921.83	61628042.98	0.97520924	0.779822294
CG13126	>tr|Q9VL60|Q9VL60_DROME RE01	14	31.7	6737200	2577200	1224700	6737200	2577200	1224700	3279145.023	3187847.871	2034225.379	0.972158245	1.567106528
ninaE	>sp|P06002|OPS1_DROME Opsin R	12	23.9	59420000	22730000	24270000	59420000	22730000	24270000	28921035.04	28115700.03	40312443.82	0.972154004	0.697444693
Karybeta3	>tr|Q9VN44|Q9VN44_DROME FI07	5	6.2	277740	106230	53443	277740	106230	53443	135182.233	131400.3878	88768.76549	0.972024096	1.480254761
CG9231	>tr|X2JGV8|X2JGV8_DROME CG92	3;3	24	3578700	1368000	1307100	3578700	1368000	1307100	1741832.853	1692137.16	2171091.69	0.97146931	0.779394609
aralar1	>tr|A0A0B4K6V1|A0A0B4K6V1_DRO	2;2;0;0;0;0;0;0;0;0	2.3	106270000	40575000	37557000	106270000	40575000	37557000	51723971.62	50188936.59	62382136.49	0.970322561	0.8045402
CG8602	>tr|Q9VS47|Q9VS47_DROME CG86	2	4.8	1175600	448830	613940	1175600	448830	613940	572190.6564	555176.8431	1019753.678	0.970265482	0.544422496
mRpL39	>sp|Q9VUJ0|RM39_DROME 39S rib	12	46.8	20692000	7898600	5997700	20692000	7898600	5997700	10071256.43	9770112.989	9962173.232	0.970098722	0.98072105
CG11876	>tr|Q7K5K3|Q7K5K3_DROME GH08	19	58.4	146250000	55717000	72026000	146250000	55717000	72026000	71183126.47	68918717.92	119635108.3	0.96818897	0.576074356
Nipsnap	>tr|M9PJP0|M9PJP0_DROME Nipsn	13;13	45.4	28532000	10863000	11117000	28532000	10863000	11117000	13887158.73	13436904.94	18465325.01	0.967577689	0.7276831
beta-Spec	>tr|M9PF16|M9PF16_DROME Beta	2;0	1.2	233950	89030	32251	233950	89030	32251	113868.6664	110124.9791	53568.87635	0.967122761	2.055764216
CPT2	>tr|Q9VZW7|Q9VZW7_DROME CG2	21	41.2	6066200	2303400	2661500	6066200	2303400	2661500	2952554.406	2849173.051	4420748.63	0.964985792	0.644500126
RpL24	>tr|X2JE06|X2JE06_DROME Riboso	4;4	20	8504400	3228600	1319500	8504400	3228600	1319500	4139280.552	3993592.13	2191688.077	0.964803443	1.822153513
His1	>tr|Q4ABD8|Q4ABD8_DROME Histo	8;8;8;6;6	25	31730000	12028000	4328000	31730000	12028000	4328000	15443696.43	14877942.8	7188803.332	0.963366696	2.069599364
mRpL44	>tr|Q9VNC1|Q9VNC1_DROME Mitoc	5	13.4	4541400	1716600	1955700	4541400	1716600	1955700	2210400.346	2123335.269	3248415.591	0.960611173	0.653652591
CG1640	>tr|Q7KV27|Q7KV27_DROME CG16	9;9	16.4	2474100	935130	1159600	2474100	935130	1159600	1204199.475	1156701.917	1926094.349	0.960556736	0.600542708
Tango7	>tr|A0A0B4LFB3|A0A0B4LFB3_DRO	2;2	9	845360	318980	192590	845360	318980	192590	411455.5065	394559.8766	319891.7824	0.958936921	1.233416731
RpL15	>tr|A8Y560|A8Y560_DROME Ribosc	2;2	7.8	7739800	2918800	1134200	7739800	2918800	1134200	3767132.733	3610387.384	1883904.977	0.958391339	1.916438158
LeuRS-m	>tr|Q9VZ82|Q9VZ82_DROME LD44	20	28	2302300	867760	674430	2302300	867760	674430	1120580.596	1073369.109	1120227.503	0.957868728	0.958170645
CG18335	>sp|Q7JRP4|U605_DROME UPF060	2	6.8	543970	204620	100140	543970	204620	100140	264762.2929	253103.1474	166332.4321	0.955963724	1.521670453
CG5839	>tr|Q8MRN5|Q8MRN5_DROME GH1	5	6.5	310380	116720	159580	310380	116720	159580	151068.8466	144375.9132	265062.208	0.955696137	0.544686903
CG30022	>tr|Q86PD3|Q86PD3_DROME RE56	2	8.2	548440	205830	42714	548440	205830	42714	266937.9413	254599.8477	70947.90806	0.953779169	3.588546225
CG33506-RA	>tr|A1Z9W2|A1Z9W2_DROME RH47	4	13.8	2292200	859490	1317100	2292200	859490	1317100	1115664.701	1063139.596	2187701.68	0.952920349	0.485961869
Ssadh	>tr|Q9VBP6|Q9VBP6_DROME GH21	11	27.1	3883400	1453200	2528000	3883400	1453200	2528000	1890137.117	1797524.649	4199005.274	0.951002249	0.428083446
CG41128	>tr|Q8SY69|Q8SY69_DROME MICO	2	23.6	5147700	1922400	1360400	5147700	1922400	1360400	2505500.035	2377898.008	2259622.933	0.949071233	1.052342837
CG3262	>tr|Q9V9M8|Q9V9M8_DROME CG32	6;4	25.6	3538100	1321200	1118500	3538100	1321200	1118500	1722071.93	1634248.257	1857827.294	0.949001159	0.87965564
ATPsyngamma	>sp|O01666|ATPG_DROME ATP sy	35	63	525090000	195970000	238700000	525090000	195970000	238700000	255572976.9	242403595.9	396480442.6	0.948471152	0.611388532
CG11779-RB	>tr|Q9VDZ8|Q9VDZ8_DROME Mitoc	2;2	4.9	367790	137130	139050	367790	137130	139050	179011.57	169621.907	230961.9002	0.947547172	0.7344151

full_dataset_V1

Rab32	>tr|A0A0B4LEY0|A0A0B4LEY0_DRO	6;6;6;6;6	29.4	3572600	1331800	1454700	3572600	1331800	1454700	1738863.847	1647359.846	2416255.131	0.947377133	0.681782244
kl-5	>tr|Q5LJN5|Q5LJN5_DROME Male f	17	4.7	216220	80498	19796	216220	80498	19796	105239.0813	99571.38677	32881.13478	0.946144584	3.028222336
His2Av	>tr|A0A0B4KH25|A0A0B4KH25_DRO	5;5;2;2	39	29257000	10886000	5137500	29257000	10886000	5137500	14240032.35	13465354.62	8533381.959	0.945598598	1.577962253
Ebp	>tr|A0A0B4KGF3|A0A0B4KGF3_DR	8;8	18.6	72388000	26885000	15108000	72388000	26885000	15108000	35232848.95	33255195.57	25094371.71	0.943869047	1.325205347
RhoGAP100F	>tr|A0A0B4K813|A0A0B4K813_DRO	7;7;7;7;7;7	7.9	493650	182720	35343	493650	182720	35343	240270.4301	226014.1095	58704.68501	0.940665522	3.850018265
mRpL4	>tr|Q9V3D0|Q9V3D0_DROME LD33	7	24.7	14379000	5311000	4749200	14379000	5311000	4749200	6998578.978	6569400.917	7888416.078	0.9386764	0.832790874
Got2	>tr|Q9VQ61|Q9VQ61_DROME Aspa	14;14	38.2	11579000	4269700	10548000	11579000	4269700	10548000	5635756.727	5281372.829	17520216.62	0.937118666	0.301444494
CG4611	>tr|Q9VRJ7|Q9VRJ7_DROME CG46	4	6.7	714260	263200	57646	714260	263200	57646	347646.2218	325563.2313	95749.94396	0.936478555	3.400140176
Hem	>sp|P55162|HEM_DROME Membran	17	15.5	2210600	813430	318590	2210600	813430	318590	1075948.167	1006166.031	529177.6465	0.935143589	1.901376668
CG9547	>tr|Q9VMC6|Q9VMC6_DROME CG9	12	34.6	11535000	4243100	4846100	11535000	4243100	4846100	5614340.949	5248470.162	8049366.874	0.934832816	0.652035153
CG3107	>tr|A0A0B4LES3|A0A0B4LES3_DRO	9;9	10.3	749890	275680	269800	749890	275680	269800	364988.1349	341000.2721	448137.5091	0.934277691	0.760927762
Thiolase	>tr|Q9W1H8|Q9W1H8_DROME GH1	26	53.5	105650000	38813000	33342000	105650000	38813000	33342000	51422203.84	48009444.13	55381026.04	0.933632566	0.866893367
RpL7	>tr|X2J5G6|X2J5G6_DROME Ribosc	12;12	45.2	13246000	4862600	1883700	13246000	4862600	1883700	6447122.689	6014755.959	3128823.669	0.932936482	1.922369745
ND-18	>tr|Q9VWI0|Q9VWI0_DROME NADH	6	43.7	73545000	26973000	19833000	73545000	26973000	19833000	35795986.57	33364046.49	32942591.61	0.932061097	1.012793617
COII	>tr|C6KI54|C6KI54_DROME Cytochr	6;6	26.3	411660000	150890000	120220000	411660000	150890000	120220000	200364074.1	186642233.9	199685290.3	0.931515466	0.934681937
colt	>sp|Q9VQG4|COLT_DROME Conge	12	29.7	32579000	11939000	14710000	32579000	11939000	14710000	15856923.6	14767854.93	24433294.14	0.931319044	0.604415223
ND-24	>tr|Q9VX36|Q9VX36_DROME NADH	20	50.8	64239000	23506000	17396000	64239000	23506000	17396000	31266549.48	29075567.3	28894737.24	0.929925681	1.006258235
CG5028-RC;CG5028	>tr|A8JRB8|A8JRB8_DROME CG50	22;22;22	61.2	297290000	108470000	110040000	297290000	108470000	110040000	144697652.4	134171138.7	182776321.3	0.927251662	0.734072869
pAbp	>sp|P21187|PABP_DROME Polyade	7	14.7	2727700	994860	990020	2727700	994860	990020	1327632.233	1230584.484	1644422.152	0.926901633	0.748338547
P5CDh1	>tr|Q9VNX4|Q9VNX4_DROME Delta	9	20.4	1472000	535670	404530	1472000	535670	404530	716455.1261	662592.9183	671923.8938	0.92482124	0.986113047
UQCR-C1	>tr|Q9VFF0|Q9VFF0_DROME GH01	31	67.2	1027100000	37342000	43350000	1027100000	37342000	43350000	49991240.48	46189901.91	72004303.25	0.923959907	0.641488075
CG2970	>tr|Q9W1F7|Q9W1F7_DROME CG2	17	56.6	77849000	28292000	14862000	77849000	28292000	14862000	37890839.06	34995573.48	24685765.97	0.923589299	1.417641791
tko	>tr|D3DMP8|D3DMP8_DROME MIP	2;2	11.7	5279900	1918600	1325000	5279900	1918600	1325000	2569844.714	2373197.627	2200823.571	0.923479	1.078322524
mRpL49	>tr|F3YDM8|F3YDM8_DROME MIP2	2;2	23.5	2240700	813180	836280	2240700	813180	836280	1090598.506	1005856.795	1389060.178	0.922297976	0.724127587
RpL10	>tr|M9PIM0|M9PIM0_DROME Ribos	12;12	61.5	58350000	21150000	9896700	58350000	21150000	9896700	28400242.25	26161331.09	16438408.03	0.921165772	1.591475953
CG5554	>tr|Q9W1I7|Q9W1I7_DROME CG55	2;2	7.4	714590	258940	400970	714590	258940	400970	347806.8401	320293.8568	666010.7377	0.920895796	0.480913953
	>tr|Q8MR63|Q8MR63_DROME Aldo	5	14.2	3792700	1373500	591360	3792700	1373500	591360	1845991.41	1698940.343	982248.3223	0.920340329	1.729644433
ND-49	>tr|Q9V4E0|Q9V4E0_DROME LD47	29	59.8	119520000	43273000	39182000	119520000	43273000	39182000	58173041.2	53526207.1	65081259.74	0.920120489	0.822451921
Prx5	>tr|Q960M4|Q960M4_DROME LD45	3	22.6	3433300	1240600	1015500	3433300	1240600	1015500	1671063.44	1534550.702	1686744.405	0.918307866	0.909770738
CG6329	>tr|Q7K188|Q7K188_DROME CG63	3	20	3228500	1166100	1912600	3228500	1166100	1912600	1571382.727	1442398.495	3176826.537	0.917916731	0.454037537
Syt1	>tr|X2J4C1|X2J4C1_DROME Synapt	7;7;7	14.6	4227100	1525500	569400	4227100	1525500	569400	2057423.548	1886955.583	945772.786	0.917144933	1.995146837
SdhA	>sp|Q94523|SDHA_DROME Succina	38	63.5	125080000	45035000	54857000	125080000	45035000	54857000	60879216.81	55705699.55	91117417.84	0.915019977	0.611361701
Rab3	>sp|P25228|RAB3_DROME Ras-rela	5	27.3	1950700	701990	1165100	1950700	701990	1165100	949449.0587	868321.173	1935229.844	0.914552671	0.448691496
Ucp4A	>tr|X2JL00|X2JL00_DROME Ucp4A,	3;3	30.5	6070300	2183100	2641300	6070300	2183100	2641300	2954549.967	2700368.884	4387196.451	0.913969611	0.615511276
CG12512-RA	>tr|Q9VMR6|Q9VMR6_DROME MIP	23	41.7	13070000	4699700	2197500	13070000	4699700	2197500	6361459.576	5813258.047	3650045.13	0.913824568	1.592653745
	>tr|Q9VQD7|Q9VQD7_DROME NAD	3	23.9	5022500	1805700	2004800	5022500	1805700	2004800	2444562.412	2233546.834	3329970.638	0.913679611	0.670740699
Cisd2	>sp|Q9VAM6|CISD2_DROME CDGS	3	20.3	11651000	4187100	2888600	11651000	4187100	2888600	5670800.728	5179201.39	4797961.485	0.913310419	1.079458726
	>tr|O46102|O46102_DROME EG:8D	7;2	15	1342800	482530	407130	1342800	482530	407130	653570.6137	596861.8009	676242.491	0.913232309	0.882615051
AP-2alpha	>sp|P91926|AP2A_DROME AP-2 co	22	24.5	9194200	3301700	1542100	9194200	3301700	1542100	4475021.548	4084012.617	2561426.437	0.912624123	1.594429009
	>sp|Q27237|TID_DROME Protein tu	20;18;16;16	44	14825000	5317000	3002900	14825000	5317000	3002900	7215657.093	6576822.571	4987813.662	0.91146551	1.318578242
eIF-4a	>tr|C9QP42|C9QP42_DROME Eukar	5;5	14.9	2323400	832480	828950	2323400	832480	828950	1130850.435	1029729.783	1376885.056	0.910579995	0.747869096
Yp2	>tr|X2JB25|X2JB25_DROME Yolk pr	3;3	11.3	735040	263210	0	735040	263210	1	357760.3098	325575.6007	1	0.910038346	325575.6007
Nmdar1	>sp|Q24418|NMDA1_DROME Glutar	4	4.4	418240	149750	20176	418240	149750	20176	203566.7066	185232.1196	33512.31437	0.909933273	5.527285213
CG3803	>tr|Q9W1F5|Q9W1F5_DROME CG3	3	12.2	1705700	609730	583430	1705700	609730	583430	830202.1118	754200.8701	969076.6009	0.908454531	0.778267548
mRpS35	>tr|Q9VZX6|Q9VZX6_DROME LD06	11;1	39.6	7620500	2724000	2614000	7620500	2724000	2614000	3709066.771	3369431.011	4341851.181	0.908430939	0.776035583
mRpL28	>tr|A8E702|A8E702_DROME IP199	10;10	39.4	6772300	2420500	2047700	6772300	2420500	2047700	3296228.974	2994019.002	3401227.492	0.908316451	0.880276021
Glg1	>tr|Q9VP27|Q9VP27_DROME Golgi	3;3	2.4	133250	47561	14971	133250	47561	14971	64855.73764	58830.21599	24866.81498	0.907093468	2.36581227
CG8520	>tr|Q7K4T8|Q7K4T8_DROME CG85	11	27.1	9022900	3210500	2450400	9022900	3210500	2450400	4391646.03	3971203.473	4070111.757	0.904263105	0.975698877
Vha68-2	>tr|A4V0N4|A4V0N4_DROME MIP16	17;17;2	31.3	8640900	3069500	3487900	8640900	3069500	3487900	4205718.137	3796794.599	5793398.138	0.902769628	0.65536573
CG5919	>tr|Q9VDC2|Q9VDC2_DROME CG5	3	19.5	2513300	892590	1347700	2513300	892590	1347700	1223278.987	1104082.388	2238528.247	0.90255976	0.493217984
TrpRS-m	>tr|Q9VVL8|Q9VVL8_DROME CG74	11	25.4	5971700	2120400	1051700	5971700	2120400	1051700	2906559.155	2622812.597	1746872.566	0.902377161	1.501433275

full_dataset_V1

CG42613	>tr|A0A0B4K686|A0A0B4K686_DRO	6;6;6;6	9.5	427520	151500	141630	427520	151500	141630	208083.4889	187396.7688	235247.2774	0.900584519	0.796594846
alphaTub84D;alphaTub84B	>sp|P06605|TBA3_DROME Tubulin	12;12	28.7	202600000	71771000	51606000	202600000	71771000	51606000	98609924.26	88776590.7	85717510.34	0.900280488	1.035687928
Fas1	>tr|B7Z0L1|B7Z0L1_DROME Fascic	11;11;11;11;11;11;11	22.8	1181400	415460	669450	1181400	415460	669450	575013.6454	513900.0763	1111955.728	0.893718054	0.462158756
CG42540	>tr|M9PEM4|M9PEM4_DROME Unc	6;6;6;6;6;6;6	15.8	1862800	655080	270090	1862800	655080	270090	906666.1744	810296.2065	448619.1988	0.893709537	1.806200467
CG14683	>sp|Q9VGY5|MET15_DROME Prob	2	9.3	499880	175480	0	499880	175480	1	243302.7097	217058.6468	1	0.892134112	217058.6468
ATPsynB	>sp|Q94516|AT5F1_DROME ATP sy	12	39.1	35882000	12543000	6963800	35882000	12543000	6963800	17464567.14	15514968.12	11566864.29	0.888368317	1.341328794
Dhod	>sp|P32748|PYRD_DROME Dihydro	5	18.8	4414400	1542400	1210100	4414400	1542400	1210100	2148586.622	1907859.909	2009974.795	0.887960434	0.949195937
CG11241	>tr|Q9VNR7|Q9VNR7_DROME FI06	9;9	20.3	2407600	839880	417460	2407600	839880	417460	1171832.447	1038883.156	693400.6099	0.886545819	1.498243788
Vps16A	>tr|Q9VHG1|Q9VHG1_DROME RE6	4	5.3	149430	51989	42444	149430	51989	42444	72730.90336	64307.3968	70499.43835	0.884182567	0.91216924
CG3884;CG3884-RB	>tr|Q8SZ28|Q8SZ28_DROME RE21	4;4	16.1	6729900	2338100	3037200	6729900	2338100	3037200	3275591.951	2892094.951	5044785.925	0.882922841	0.57328398
CG3961-RD;CG3961	>tr|E2QCY2|E2QCY2_DROME CG3	11;11;11	23.4	2857700	989800	1105700	2857700	989800	1105700	1390906.123	1224325.556	1836566.508	0.880235938	0.66663829
Liprin-alpha	>tr|M9PC73|M9PC73_DROME Liprin	2;2;2;2	2.1	446530	154490	138170	446530	154490	138170	217336.0786	191095.2265	229500.2211	0.879261408	0.832658137
mRpL47	>tr|Q8T3V6|Q8T3V6_DROME AT29	6	17.7	3415900	1180300	1071400	3415900	1180300	1071400	1662594.473	1459963.077	1779594.245	0.878123379	0.820390986
CG4546	>tr|Q9VF23|Q9VF23_DROME CG45	14	30.4	14249000	4917500	1789800	14249000	4917500	1789800	6935305.088	6082664.095	2972855.87	0.877057897	2.046067607
Tektin-A	>tr|Q9V3M9|Q9V3M9_DROME GH1	7	14.9	1867800	643860	214170	1867800	643860	214170	909099.7856	796417.7132	355736.1391	0.876050931	2.238787757
Rac2	>tr|M9PBU2|M9PBU2_DROME Rac2	2;2	10.4	3313200	1142100	1290200	3313200	1142100	1290200	1612608.1	1412711.879	2143020.809	0.876041661	0.659215194
CG12264	>sp|Q9VKD3|NFS1_DROME Probab	22;2	52.6	36499000	12565000	12448000	36499000	12565000	12448000	17764874.76	15542180.86	20676114.57	0.874882659	0.751697366
Hsp83	>tr|M9PBL3|M9PBL3_DROME Heat	18;18	25.7	7523700	2589300	3927800	7523700	2589300	3927800	3661952.059	3202814.874	6524071.564	0.874619553	0.490922707
His2B	>sp|P02283|H2B_DROME Histone H	7	64.2	89388000	30717000	12622000	89388000	30717000	12622000	43507126.9	37995158.72	20965128.39	0.873308845	1.812302697
inaD	>tr|D3DMF9|D3DMF9_DROME Inact	11;11	17.2	2551700	876430	565130	2551700	876430	565130	1241969.12	1084093.4	938680.3206	0.872882733	1.154912248
Tim17b	>tr|Q7PLT4|Q7PLT4_DROME Tim17	6	45.1	10676000	3660400	5507500	10676000	3660400	5507500	5196246.552	4527703.844	9147951.56	0.871341227	0.494941825
Torsin	>tr|F6JQA6|F6JQA6_DROME CG30	3;3	7.9	1843800	631720	346660	1843800	631720	346660	897418.452	781401.2328	575801.8863	0.870721157	1.357066122
RpL11	>tr|A0A0B4LGZ5|A0A0B4LGZ5_DRO	6;6	30.4	50596000	17299000	10288000	50596000	17299000	10288000	24626198.06	21397866.03	17088356.9	0.8689066	1.252189789
sicily	>tr|X2JJK8|X2JJK8_DROME Severe	9;9	32.6	7333600	2502600	1566600	7333600	2502600	1566600	3569426.163	3095571.97	2602120.911	0.867246395	1.189634178
CG8004	>tr|Q9VW58|Q9VW58_DROME CG8	2	10	3049800	1040400	1083700	3049800	1040400	1083700	1484405.464	1286914.84	1800024.531	0.866956415	0.714942945
FASN3	>tr|Q7PLB8|Q7PLB8_DROME Fatty	3	1.9	25685	8749.9	8861.5	25685	8749.9	8861.5	12501.46073	10823.12205	14718.94207	0.865748594	0.735319291
Fpps	>tr|Q7KN61|Q7KN61_DROME Farne	4	11.5	1921500	654230	402790	1921500	654230	402790	935236.7695	809244.8055	669033.7557	0.865283351	1.20957246
CG30438	>tr|Q7K142|Q7K142_DROME UDP-g	2;2	4.6	401110	136490	70323	401110	136490	70323	195229.1548	168830.2638	116806.4273	0.864779976	1.445385051
CG15116	>tr|Q4V6H2|Q4V6H2_DROME Gluta	3	16.6	1696800	577040	132050	1696800	577040	132050	825870.2839	713765.2241	219334.9077	0.864258272	3.254225383
CG4329	>tr|Q9W235|Q9W235_DROME CG4	3	2.9	292350	99408	40650	292350	99408	40650	142293.2448	122961.967	67519.60629	0.864144796	1.821129798
yellow-g	>tr|Q9W029|Q9W029_DROME FI16	3	9.7	2031700	690080	594850	2031700	690080	594850	988873.5595	853589.1894	988045.2086	0.86319346	0.863917139
PyK	>sp|O62619|KPYK_DROME Pyruvat	14	36	6109400	2067200	2883100	6109400	2067200	2883100	2973580.806	2557007.263	4788825.991	0.859908451	0.533952845
Opa1	>tr|A0A0B4LGF5|A0A0B4LGF5_DRO	64;64;62;62;34	52.8	32898000	11111000	7537700	32898000	11111000	7537700	16012188	13743666.65	12520111.57	0.858325337	1.097727171
Pdi	>tr|X2JGP4|X2JGP4_DROME Protei	18;18	50.4	6134800	2071900	1752700	6134800	2071900	1752700	2985943.551	2562820.893	2911232.81	0.858295158	0.88032152
mRpL20	>tr|Q9VU36|Q9VU36_DROME LP04	5	36.7	5294900	1780700	1478600	5294900	1780700	1478600	2577145.548	2202623.275	2455953.005	0.854675545	0.896850742
Pka-R2	>sp|P81900|KAPR2_DROME cAMP-	2	6.4	245180	81737	85286	245180	81737	85286	119334.5571	101103.9584	141659.9541	0.847231186	0.713708818
CG5903	>tr|Q9VEY5|Q9VEY5_DROME MICO	5	39.4	10387000	3456100	3833900	10387000	3456100	3833900	5055583.827	4274996.518	6368103.765	0.845598978	0.671313891
CG18769	>tr|Q7KU70|Q7KU70_DROME Unch	9;9;9;9;9	31.2	6991600	2326200	2166700	6991600	2326200	2166700	3402967.159	2877375.337	3598886.363	0.845548958	0.799518253
CG34120	>tr|E2QD66|E2QD66_DROME Unch	3;3;3	1.7	33557	11155	26356	33557	11155	26356	16332.93814	13798.09214	43777.2877	0.844801592	0.315188374
mRpS9	>tr|Q8SXF0|Q8SXF0_DROME Mitoc	8	18.7	8160800	2705900	1918700	8160800	2705900	1918700	3972042.793	3347042.354	3186958.631	0.842650124	1.050230876
RpL10Ab	>sp|Q9VTP4|R10AB_DROME 60S r	10	44.7	60438000	20012000	9142000	60438000	20012000	9142000	29416518.27	24753690.67	15184852.14	0.84148948	1.630156846
Sply	>sp|Q9V7Y2|SGPL_DROME Sphing	24	49	41250000	13653000	10842000	41250000	13653000	10842000	20077292.08	16887974.15	18008550.31	0.841148004	0.937775327
mRpL1	>tr|Q9VHT5|Q9VHT5_DROME LD31	7	21.2	2400400	794100	910950	2400400	794100	910950	1168328.047	982255.9345	1513086.968	0.840736416	0.649173481
Mpcp	>tr|Q0E8E8|Q0E8E8_DROME MIP0	17	46.6	86589000	28622000	30718000	86589000	28622000	30718000	42144791.37	35403764.46	51022564.87	0.84005077	0.693884452
Syt7	>tr|Q59DP7|Q59DP7_DROME Synap	2;2;2;2	8.5	2063800	681680	228720	2063800	681680	228720	1004497.343	843198.8735	379903.6735	0.839423697	2.219507029
14-3-3zeta	>tr|A0A0B4KEH0|A0A0B4KEH0_DR	9;9	45.2	19123000	6298100	5705400	19123000	6298100	5705400	9307589.248	7790386.729	9476663.247	0.836992966	0.822060099
Pex1	>tr|Q9VUC7|Q9VUC7_DROME LD43	2	2.2	108270	35523	17186	108270	35523	17186	52697.41628	43939.90377	28545.92759	0.833815144	1.539270483
CG16985	>tr|Q9VZZ6|Q9VZZ6_DROME CG16	2	16.8	6276900	2057600	4342400	6276900	2057600	4342400	3055106.78	2545132.617	7212721.717	0.833074848	0.352867158
Ppox	>tr|Q9VC52|Q9VC52_DROME LD41	18	32.8	10249000	3349500	1254000	10249000	3349500	1254000	4988416.159	4143138.462	2082892.648	0.830551889	1.98912722
Scsalpha	>tr|M9MRQ9|M9MRQ9_DROME Suc	22;22	49.1	348000000	113730000	83631000	348000000	113730000	83631000	169379336.8	140677455.5	138911000.8	0.830546737	1.012716449
mRpL53	>tr|A1Z9J6|A1Z9J6_DROME Mitoch	8	63.2	10037000	3278300	3884400	10037000	3278300	3884400	4885231.045	4055068.165	6451984.211	0.830066813	0.628499394

full_dataset_V1

CG6255	>tr|Q9VDW7|Q9VDW7_DROME CG	4	17.8	3088000	1007800	293750	3088000	1007800	293750	1502998.253	1246590.519	487918.4333	0.829402506	2.554915809
CG32819-RB;CG17450	>tr|Q8I044|Q8I044_DROME GH1100	8;8;8	17.3	3210700	1045500	153420	3210700	1045500	153420	1562719.071	1293223.246	254830.4547	0.827546851	5.074837886
COX6B	>tr|Q8IQW2|Q8IQW2_DROME Cytoc	5;5	42.9	20242000	6589600	4121600	20242000	6589600	4121600	9852231.426	8150955.429	6845973.155	0.827320744	1.190620419
Mlp60A	>tr|B7YZP9|B7YZP9_DROME Muscl	5;1;1	21.2	822850	267440	47673	822850	267440	47673	400499.389	330807.867	79184.80171	0.825988444	4.177668691
Cnx99A	>tr|Q0KHZ9|Q0KHZ9_DROME Calne	5;5;2;1	10.9	727640	236100	281080	727640	236100	281080	354158.5653	292042.0931	466873.577	0.824608302	0.62552714
CG3011	>tr|B7ZDX1|B7ZDX1_DROME Serine	5;5	17.1	587620	190200	334020	587620	190200	334020	286007.7183	235266.4384	554806.8599	0.822587725	0.424051063
CG4619	>tr|Q7KTG0|Q7KTG0_DROME CG4	5	13	2496600	807830	762460	2496600	807830	762460	1215150.725	999239.1533	1266445.238	0.822317045	0.789010945
CG5590	>tr|Q9VB10|Q9VB10_DROME CG55	10	26.2	2209900	714830	1209500	2209900	714830	1209500	1075607.461	884203.513	2008978.196	0.822050371	0.440125988
RpS20	>sp|P55828|RS20_DROME 40S ribo	3	23.3	8692700	2809600	1881100	8692700	2809600	1881100	4230930.349	3475313.277	3124505.071	0.821406403	1.112276408
dare	>sp|Q9V3T9|ADRO_DROME NADPH	8	22.3	3712200	1197800	1604200	3712200	1197800	1604200	1806810.271	1481609.569	2664574.47	0.820013918	0.556039842
CG7470	>tr|Q9VNW6|Q9VNW6_DROME CG	41	52.4	190180000	61335000	45154000	190180000	61335000	45154000	92564834.13	75867860.15	75000745.3	0.819618604	1.011561416
ValRS-m	>tr|Q9VSR7|Q9VSR7_DROME CG5	15	19	1467400	472980	560390	1467400	472980	560390	714216.2038	585049.0013	930807.1857	0.819148317	0.628539412
CG4882	>tr|O77477|O77477_DROME CG488	9	24.1	7832200	2522300	2298200	7832200	2522300	2298200	3812105.868	3119939.735	3817307.722	0.818429457	0.817314181
Scox	>tr|Q9VMX4|Q9VMX4_DROME AT1	3	15.9	2342700	752970	669610	2342700	752970	669610	1140244.174	931380.4949	1112221.488	0.81682548	0.837405593
CG9281	>tr|Q9VXR5|Q9VXR5_DROME CG9	4	7	854040	274240	173550	854040	274240	173550	415680.2554	339219.0751	288266.363	0.816057705	1.176755663
AP-2mu	>tr|O62530|O62530_DROME Adapto	6	19.2	4813700	1545100	1083100	4813700	1545100	1083100	2342934.81	1911199.653	1799027.932	0.815728908	1.062351295
Miro	>tr|A0A0B4J3Z9|A0A0B4J3Z9_DRO	4;4;4	9.5	521930	167390	126680	521930	167390	126680	254034.9349	207051.783	210415.3435	0.815052399	0.984014662
RpS14b;RpS14a	>tr|X2JCX8|X2JCX8_DROME Ribosc	5;5	35.1	10613000	3399300	3964700	10613000	3399300	3964700	5165583.051	4204738.192	6585362.424	0.813991015	0.638497614
ProRS-m	>tr|Q9VZY9|Q9VZY9_DROME FI227	5	10.9	1003500	321330	505470	1003500	321330	505470	488425.7603	397466.6912	839585.125	0.813770942	0.473408448
His4r;His4	>tr|A0A0B4KFZ9|A0A0B4KFZ9_DRO	10;10	65	139540000	44476000	19237000	139540000	44476000	19237000	67917220.29	55014248.76	31952636.25	0.810019146	1.721743656
	>tr|Q9W347|Q9W347_DROME C12	14;14	11.3	618470	196930	283110	618470	196930	283110	301023.0992	243591.0606	470245.4048	0.809210527	0.518008381
CG5805	>tr|Q9VC40|Q9VC40_DROME CG58	2	5.9	661790	210010	104320	661790	210010	104320	322107.9063	259770.2668	173275.4076	0.806469701	1.499175621
RpS6	>sp|P29327|RS6_DROME 40S ribos	5;3	27.4	6561500	2080400	1225400	6561500	2080400	1225400	3193627.927	2573334.903	2035388.079	0.805771668	1.264296932
CG6332	>tr|Q9VD59|Q9VD59_DROME CG63	6	21.8	1406600	445010	91260	1406600	445010	91260	684623.4921	550451.7233	151582.7617	0.804021085	3.631360961
CG11739	>tr|Q9VN13|Q9VN13_DROME Sider	15	35.8	37074000	11720000	15120000	37074000	11720000	15120000	18044740.04	14496964.55	25114303.69	0.803390047	0.577239359
Cyt-c1	>tr|Q9VRL0|Q9VRL0_DROME Cytoc	13	40.4	35424000	11181000	12062000	35424000	11181000	12062000	17241648.36	13830252.62	20034968.99	0.802142135	0.690305666
mRpL48	>tr|Q9VQ35|Q9VQ35_DROME Mitoc	6	55.8	4900400	1545600	584280	4900400	1545600	584280	2385133.627	1911818.124	970488.45	0.801555981	1.969954536
Plip	>sp|Q86BN8|PTPM1_DROME Phosp	2	14	282000	88899	291530	282000	88899	291530	137255.6697	109962.9396	484231.0157	0.801154079	0.227087766
Pgam5	>tr|X2JC94|X2JC94_DROME Phospl	6;6	29.5	5049700	1589100	1199300	5049700	1589100	1199300	2457801.256	1965625.117	1992036.007	0.799749415	0.986741761
Cdc42	>tr|M9NFF8|M9NFF8_DROME Cdc4	2;2	16.2	2774500	873010	1121500	2774500	873010	1121500	1350410.834	1079863.057	1862810.291	0.799655209	0.579695669
	>tr|Q9V3L7|Q9V3L7_DROME GH05	3	30	17806000	5600900	9083700	17806000	5600900	9083700	8666576.068	6927990.51	15088015.9	0.799391877	0.45917174
Marf	>sp|Q7YU24|MARF_DROME Transn	17	24.6	3667600	1153000	1149000	3667600	1153000	1149000	1785102.459	1426194.55	1908487.761	0.798942684	0.747290383
mRpS30	>tr|Q9VXP3|Q9VXP3_DROME GH0	31	58.2	28728000	9029300	7686500	28728000	9029300	7686500	13982556.29	11168723.72	12767268.21	0.79876122	0.874793538
	>tr|Q7JYH3|Q7JYH3_DROME NADH	2	14.1	4061200	1270500	2402700	4061200	1270500	2402700	1976676.33	1571535.279	3990882.109	0.795039256	0.393781434
Sra-1	>sp|Q9VF87|CYFIP_DROME Cytopl	15	13.3	2725200	851810	250130	2725200	851810	250130	1326415.428	1053639.879	415465.6604	0.794351345	2.536045645
CG6439	>tr|Q9VD58|Q9VD58_DROME CG64	22	60.5	254710000	79498000	72627000	254710000	79498000	72627000	123973019.8	98334444.38	120633368.7	0.793192297	0.815151276
CG32432;CG3116	>tr|M9PG87|M9PG87_DROME Unch	11;11	9.6	1321000	411230	152280	1321000	411230	152280	642960.069	508667.8101	252936.9159	0.791134371	2.011046147
mRpS25	>sp|Q9VY28|RT25_DROME Probabl	5	32.3	9106100	2830300	3915900	9106100	2830300	3915900	4432141.319	3500917.984	6504305.677	0.789893131	0.538246226
mtSSB	>sp|P54622|SSBP_DROME Single-s	7	45.9	71770000	22279000	11427000	71770000	22279000	11427000	34932054.61	27557839.02	18980234.68	0.788898315	1.451922987
EfTuM	>tr|A1Z9E3|A1Z9E3_DROME Elonga	29	63.8	138660000	43039000	36581000	138660000	43039000	36581000	67488904.72	53236762.58	60761001.55	0.788822441	0.87616664
Lam	>tr|M9NE89|M9NE89_DROME Lamir	15;15	29.1	6395700	1983700	887420	6395700	1983700	887420	3112929.381	2453722.576	1474003.663	0.788235863	1.664665182
GlyP	>tr|A4UZZ4|A4UZZ4_DROME Alpha-	19;19	27.8	1565700	484730	916530	1565700	484730	916530	762060.9992	599583.0741	1522355.342	0.786791444	0.393852248
GstT1	>tr|Q7K0B6|Q7K0B6_DROME Gluta	3	19.3	617060	190680	40047	617060	190680	40047	300336.8208	235860.1708	66518.02394	0.785318863	3.545808441
ATPsynD	>tr|A0A0B4LHL7|A0A0B4LHL7_DRO	12;12	62.9	29565000	9129800	13442000	29565000	9129800	13442000	14389942.8	11293036.43	22327147.5	0.784786749	0.505794442
nrv2	>tr|A4V0B5|A4V0B5_DROME Nerva	9;9;8	46.4	6640500	2050600	2385600	6640500	2050600	2385600	3232078.983	2536474.02	3962479.027	0.784780952	0.640123015
kl-3	>tr|A8Y5B7|A8Y5B7_DROME Male f	22	5.9	374390	115180	22726	374390	115180	22726	182223.9367	142471.022	37747.86162	0.781845813	3.774280605
Spn77Bb;Spn77Bc	>tr|Q9VWB4|Q9VWB4_DROME Ser	3;3	9.7	888850	273330	166720	888850	273330	166720	432623.0563	338093.4575	276921.7403	0.781496623	1.220898934
Adgf-D	>tr|Q9VFS1|Q9VFS1_DROME Aden	5	13.7	1777500	545740	369340	1777500	545740	369340	865148.768	675048.928	613473.3418	0.780269189	1.100372065
Moe	>tr|M9NG50|M9NG50_DROME Moes	11;11;11;11	18.5	2371700	727460	440200	2371700	727460	440200	1154359.118	899826.0951	731171.7254	0.779502739	1.230663145
Tom70	>tr|Q9VKC8|Q9VKC8_DROME FI03	23	41.4	16490000	5043200	6624400	16490000	5043200	6624400	8026049.61	6238147.751	11003121.26	0.777237627	0.56694347
RpL27A	>tr|M9MRC9|M9MRC9_DROME Ribo	4;4	28.2	18295000	5593600	2126600	18295000	5593600	2126600	8904583.239	6918960.83	3532280.307	0.777011191	1.95878023

full_dataset_V1

ZnT35C	>tr|Q8IP48|Q8IP48_DROME Zinc tra	2;2	7	535850	152560	76735	535850	152560	76735	260810.1083	188707.9277	127456.7524	0.723545299	1.480564381
unc-13	>tr|Q8IM86|Q8IM86_DROME Unc-13	2;2;1;1;1;1	0.7	16509	4687.4	5280.8	16509	4687.4	5280.8	8035.297529	5798.043685	8771.403235	0.721571748	0.661016662
ND-ASHI	>tr|Q9W3X7|Q9W3X7_DROME NAD	5	34.9	6976400	1980500	1935900	6976400	1980500	1935900	3395568.981	2449764.36	3215527.812	0.721459164	0.761854508
CG4042-RA	>tr|Q9VPC1|Q9VPC1_DROME CG4	4	12	3888200	1102600	1324000	3888200	1102600	1324000	1892473.384	1363852.655	2199162.572	0.720672041	0.620169092
bonsai	>sp|Q8WTC1|RT15_DROME 28S rib	8	33.2	9181300	2599700	2736200	9181300	2599700	2736200	4468742.831	3215679.074	4544825.249	0.719593675	0.707547353
mRpL14	>tr|Q9W4Z2|Q9W4Z2_DROME EG:E	4	32.3	4236400	1198300	945340	4236400	1198300	945340	2061950.065	1482228.04	1570208.721	0.718847689	0.943968799
Rbcn-3A	>tr|Q9W425|Q9W425_DROME Rabc	7	3	152640	43045	28925	152640	43045	28925	74293.28173	53244.18426	48044.39393	0.716675627	1.108228867
Rab39	>tr|Q9W3Q0|Q9W3Q0_DROME FI07	4;1;1	14.7	1569400	442110	853100	1569400	442110	853100	763861.8715	546864.5904	1416998.18	0.715920785	0.385931752
CG1774	>tr|Q9V9W4|Q9V9W4_DROME CG1	3	10.2	1320000	371590	298930	1320000	371590	298930	642473.3468	459635.4146	496522.4077	0.715415537	0.925709308
ATPsyndelta	>tr|Q9W2X6|Q9W2X6_DROME ATP	2	18.5	9743500	2740000	3134700	9743500	2740000	3134700	4742378.07	3389222.089	5206733.319	0.714667207	0.650930609
Ect4	>tr|M9NFP2|M9NFP2_DROME Ectoc	4;4;4;4;4;4;4	5.1	177010	49744	10894	177010	49744	10894	86154.70253	61530.46118	18094.92238	0.714185754	3.40042692
CG2124	>tr|Q9W2T3|Q9W2T3_DROME CG2	2	4.9	209230	58585	59765	209230	58585	59765	101836.8928	72466.26866	99269.60067	0.711591513	0.729994562
CG3626-RA	>tr|Q9W4K8|Q9W4K8_DROME CG3	19	24.2	3312900	927100	613360	3312900	927100	613360	1612462.083	1146769.269	1018790.299	0.711191464	1.125618561
RpS19a	>tr|E2QD65|E2QD65_DROME Ribos	4;4	26.9	2403600	671350	552150	2403600	671350	552150	1169885.558	830421.2589	917120.5546	0.709831191	0.905465759
CASK	>tr|E1JIS7|E1JIS7_DROME CASK o	12;12;12	16.2	4233000	1180100	653410	4233000	1180100	653410	2060295.209	1459715.689	1085313.305	0.708498317	1.344971707
Mal-A1	>sp|P07190|MAL1_DROME Maltase	9	24.1	2546400	705530	348920	2546400	705530	348920	1239389.492	872699.949	579555.7438	0.70413696	1.505808472
CG10194	>tr|Q9VIV6|Q9VIV6_DROME GH049	5	16.2	1538900	426200	362270	1538900	426200	362270	749016.8434	527184.8373	601730.0794	0.703835757	0.876115148
CG7632	>tr|Q9VP50|Q9VP50_DROME CG76	10;9	29.4	10634000	2944000	2159300	10634000	2944000	2159300	5175804.218	3641558.332	3586594.971	0.703573431	1.015324663
Lar	>tr|M9NCY3|M9NCY3_DROME Leuk	4;4;4;4;4;4;4	2.9	133160	36743	36632	133160	36743	36632	64811.93264	45448.97346	60845.71262	0.701243916	0.746954411
Fit1	>sp|Q9VZI3|UN112_DROME Unc-11	2	3	88526	24367	13977	88526	24367	13977	43087.57253	30140.57471	23215.78205	0.699518978	1.298279534
muc	>tr|Q9VM14|Q9VM14_DROME AT21	27;26;25;25;24	36.7	168070000	46105000	30094000	168070000	46105000	30094000	81803405.58	57029227.88	49986101.54	0.697149801	1.140901693
CG5946;zetaCOP	>tr|E1JHY0|E1JHY0_DROME NADH	4;4;4;4;4;4	23.2	1801300	493880	571560	1801300	493880	571560	876732.7572	610901.0968	949360.5437	0.696792827	0.643486925
	>tr|A0A0B4K7H0|A0A0B4K7H0_DR	3;3	4	443630	121570	80275	443630	121570	80275	215924.5841	150375.0837	133336.6886	0.696424098	1.127784748
Rpn1	>tr|Q9VW54|Q9VW54_DROME 26S	2	2.6	122680	33591	42169	122680	33591	42169	59711.08365	41550.13111	70042.66365	0.695852907	0.59321175
CG6543	>tr|Q7JR58|Q7JR58_DROME CG65	6	29.5	9110800	2490500	1682800	9110800	2490500	1682800	4434428.914	3080604.968	2795128.985	0.694701624	1.102133384
CG13293	>tr|M9PEA7|M9PEA7_DROME Unch	2;2;2	3.5	174970	47800	0	174970	47800	1	85161.78917	59125.84522	1	0.694276691	59125.84522
CG13321	>tr|Q7JZZ3|Q7JZZ3_DROME RE038	3	15.4	11636000	3167800	975300	11636000	3167800	975300	5663499.895	3918386.034	1619972.248	0.691866532	2.418798247
Ostgamma	>tr|Q8SY53|Q8SY53_DROME GH11	2	6.7	952640	259300	491540	952640	259300	491540	463671.0675	320739.1561	816447.41	0.691738559	0.392847294
	>tr|Q9W591|Q9W591_DROME EG:E	2	8.5	519490	141080	326960	519490	141080	326960	252847.3326	174507.8293	543080.2075	0.690170735	0.321329754
GABA-B-R2	>tr|Q8IN24|Q8IN24_DROME Metabc	3;3;3	2.5	318970	86537	75350	318970	86537	75350	155249.7906	107041.2817	125156.2689	0.689477785	0.855261048
mRpL37	>tr|Q9VGW9|Q9VGW9_DROME LD1	14	39.5	16703000	4531400	4134600	16703000	4531400	4134600	8129721.446	5605080.647	6867566.141	0.689455436	0.81616697
Pglym78	>tr|Q9VAN7|Q9VAN7_DROME GH1	3	14.9	1268800	343850	689140	1268800	343850	689140	617553.1685	425322.6333	1144660.797	0.688722291	0.371570892
CG32436-RA	>tr|Q9VP43|Q9VP43_DROME MIP0	7	5	497930	134890	17825	497930	134890	17825	242353.6013	166851.1561	29607.3059	0.688461633	5.635472427
CG7382	>tr|Q9VMR0|Q9VMR0_DROME CG7	6	25.4	10186000	2752000	2683200	10186000	2752000	2683200	4957752.658	3404065.397	4456792.306	0.686614608	0.763792693
mRpS6	>tr|M9NDH8|M9NDH8_DROME Mito	3;3	27.2	1995400	538640	475000	1995400	538640	475000	971205.5424	666266.6372	788974.4878	0.686020217	0.844471713
ATPsynO	>sp|Q24439|ATPO_DROME ATP sy	8	47.4	31615000	8521300	8688000	31615000	8521300	8688000	15387723.37	10540357	14430758.63	0.684984825	0.730409071
CG10602	>tr|Q9VJ39|Q9VJ39_DROME Leuko	3;3	6.9	2094500	562840	596540	2094500	562840	596540	1019439.716	696200.6425	990852.2968	0.682924779	0.702628076
RpLP0	>tr|M9PG76|M9PG76_DROME 60S	15;15	47.3	22875000	6145000	5935800	22875000	6145000	5935800	11133771.06	7601010.852	9859357.398	0.682698684	0.77094384
RpS13	>tr|X2J950|X2J950_DROME Riboso	3;3	14.6	8807600	2358900	1484400	8807600	2358900	1484400	4286854.733	2917823.352	2465586.799	0.680644326	1.183419441
Sucb	>tr|Q9V470|Q9V470_DROME Succir	11	29.6	8757500	2339500	3207200	8757500	2339500	3207200	4262469.949	2893826.67	5327155.741	0.678908404	0.543221714
	>tr|A0A0B4LGC6|A0A0B4LGC6_DR	8;8;8;8	34.7	25464000	6796500	7469100	25464000	6796500	7469100	12393894.92	8406878.805	12406167.04	0.678308059	0.67763708
GstT4	>tr|Q8MRM0|Q8MRM0_DROME GH	4	20.7	2568900	684910	921630	2568900	684910	921630	1250340.743	847194.1974	1530826.436	0.677570656	0.553422764
CG13601	>tr|A0A0B4KGV7|A0A0B4KGV7_DR	3;3	11.9	1569000	418260	318190	1569000	418260	318190	763667.1826	517363.5149	528513.247	0.677472499	0.97890359
CG6084	>tr|Q9VTK9|Q9VTK9_DROME CG60	3;3;3;3	12	565020	150320	130630	565020	150320	130630	275007.7959	185937.1768	216976.2892	0.676116021	0.856946985
mRpL18	>tr|Q7JVK1|Q7JVK1_DROME HL07	2	15.1	2711000	719940	80268	2711000	719940	80268	1319503.972	890524.2885	133325.0616	0.674893223	6.679346539
CG4562	>tr|Q9VDT3|Q9VDT3_DROME CG45	12;12;8;0;0;1;1;0;0;0	12.3	2335900	619710	901050	2335900	619710	901050	1136934.463	766545.555	1496643.078	0.674221409	0.512176594
RpL19	>sp|P36241|RL19_DROME 60S ribo	7	30	17267000	4578600	1158900	17267000	4578600	1158900	8404232.785	5663464.327	1924931.65	0.673882372	2.942163856
CG7834	>tr|Q0KHZ6|Q0KHZ6_DROME CG7	8	45.8	4967700	1306500	2648600	4967700	1306500	2648600	2417890.033	1616065.204	4399321.744	0.668378289	0.367344172
mRpL30	>tr|Q9W4I3|Q9W4I3	8	43.3	6835600	1794800	1615100	6835600	1794800	1615100	3327038.491	2220064.162	2682679.358	0.667279374	0.827554793
lig3	>tr|Q9VG84|Q9VG84	3	5	261670	68700	17276	261670	68700	17276	127360.6067	84977.94071	28695.4175	0.667223115	2.961376698
mRpL16	>tr|Q9W547|Q9W547	6	21.4	4383100	1148900	949850	4383100	1148900	949850	2133352.216	1421123.087	1577699.826	0.666145551	0.900756319

full_dataset_V1

CG9240	>tr|D5A7R5|D5A7R5	2;2	21.9	1245100	325520	310930	1245100	325520	310930	606017.8516	402649.4797	516454.3948	0.664418513	0.779641889
Ckllalpha	>tr|A4V2B8|A4V2B8	4;4	20.8	6579400	1718600	695480	6579400	1718600	695480	3202340.255	2125809.154	1155191.53	0.663829882	1.840222248
bor	>tr|Q9VEX6|Q9VEX6	33	47.7	56194000	14616000	9740600	56194000	14616000	9740600	27350869.12	18079149.65	16179126.09	0.661008232	1.117436723
mRpS23	>tr|Q8IP62|Q8IP62	3	23.8	2350200	610710	444150	2350200	610710	444150	1143894.59	755413.0737	737732.6711	0.660386962	1.023965866
CG7433	>tr|Q9VW68|Q9VW68	20	46.9	7636800	1983900	3101500	7636800	1983900	3101500	3717000.343	2453969.964	5151588.155	0.660201705	0.476352125
CG15891	>tr|Q9W412|Q9W412	3	14.1	2025300	525050	140050	2025300	525050	140050	985758.5372	649456.5904	232622.8991	0.658839428	2.791885893
RpL18	>tr|M9PHM6|M9PHM6	10;10	50.5	44804000	11585000	4880600	44804000	11585000	4880600	21807102.89	14329977.33	8106671.336	0.657124305	1.767677107
rdgA	>tr|A0A023GPM5|A0A023GPM5	20;20;19;19;19;18;16;16	22.8	8132300	2099200	1109200	8132300	2099200	1109200	3958171.21	2596589.419	1842380.004	0.656007353	1.409366913
CG1814-RB;CG1814	>tr|Q7K3S2|Q7K3S2	17;17;17	41.1	18507000	4770700	3703200	18507000	4770700	3703200	9007768.353	5901080.956	6151011.206	0.655110203	0.959367616
Top1	>tr|Q8IR39|Q8IR39	9;9;9;9;9	18.2	1185600	305590	265190	1185600	305590	265190	577057.8788	377997.2183	440480.3041	0.655042124	0.858147833
CG8728-RA	>tr|Q7K3W2|Q7K3W2	4	12.1	847180	218330	242700	847180	218330	242700	412341.3409	270061.6273	403124.4384	0.654946765	0.669921249
ABCB7	>tr|Q7KVB1|Q7KVB1	10;10	20.2	5029500	1293500	948220	5029500	1293500	948220	2447969.467	1599984.953	1574992.397	0.653596777	1.015868366
Gpdh	>tr|M9PET0|M9PET0	3;3;3;3	10.6	473590	121760	263360	473590	121760	263360	230506.7822	150610.1028	437440.6761	0.653386861	0.344298349
RpL23	>sp|P48159|RL23	4	34.3	9600600	2464000	1054000	9600600	2464000	1054000	4672825.463	3047825.995	1750692.863	0.652244775	1.740925584
kst	>tr|Q9VZQ3|Q9VZQ3	57;57;57;57;57	18.5	1539900	394830	185220	1539900	394830	185220	749503.5656	488381.9552	307650.2204	0.651607247	1.587458493
CG4586	>tr|Q9W3U0|Q9W3U0	13	24.1	1675600	427350	1472500	1675600	427350	1472500	815551.7726	528607.321	2445820.912	0.648159122	0.216126748
spg	>tr|B7Z0R2|B7Z0R2	10;10;10	5.5	289870	73922	12573	289870	73922	12573	141086.1737	91437.25376	20883.73957	0.648095071	4.378394658
alpha-Cat	>sp|P35220|CTNA	8;3	11.7	612230	155830	108070	612230	155830	108070	297985.9524	192752.7292	179504.1536	0.646851731	1.073806513
comt	>tr|M9PH10|M9PH10	29;29;7;7	40.5	10885000	2768800	2030800	10885000	2768800	2030800	5297971.498	3424846.029	3373156.61	0.646444782	1.015323753
CG15896-RA	>tr|Q9W413|Q9W413	3	6.8	1231300	312910	61326	1231300	312910	61326	599301.0848	387051.6364	101862.42	0.645838371	3.799749078
GC1	>tr|Q9VGF7|Q9VGF7	15;1;1	39.9	26766000	6798100	8121500	26766000	6798100	8121500	13027607.27	8408857.913	13489802.74	0.645464492	0.623349212
RpS16	>tr|A0A0B4LG52|A0A0B4LG52_DRO	5;5	31.8	1614200	409740	863140	1614200	409740	863140	785667.0275	506824.7659	1433674.609	0.645088502	0.353514502
CG5045	>tr|Q9VKY3|Q9VKY3	2	15	1067800	270730	87823	1067800	270730	87823	519721.9998	334877.4073	145873.9084	0.644339488	2.295663501
CG4434	>tr|Q9VCN3|Q9VCN3	15	28.4	7562800	1912400	725910	7562800	1912400	725910	3680982.898	2365528.585	1205735.727	0.642635038	1.961896402
mRpS10	>sp|Q9VFB2|RT10	5	35.3	12537000	3163400	3519800	12537000	3163400	3519800	6102036.626	3912943.487	5846384.004	0.641252049	0.669292931
SdhC	>tr|Q9VGS3|Q9VGS3	2	15.8	5046100	1269300	2200900	5046100	1269300	2200900	2456049.056	1570050.948	3655692.526	0.63925879	0.429481127
	>tr|Q9VJ10|Q9VJ10	11	23.3	9136100	2290900	4308900	9136100	2290900	4308900	4446742.986	2833711.271	7157078.253	0.637255465	0.395931296
mRpS5	>tr|Q8SYP9|Q8SYP9	11	35.6	7142900	1787400	1666000	7142900	1787400	1666000	3476608.233	2210910.789	2767224.203	0.635939007	0.798963375
DNApol-gamma35	>tr|Q9VJV8|Q9VJV8	3	8	728000	181790	64405	728000	181790	64405	354333.7853	224863.7531	106976.6357	0.634609971	2.10198939
CG34370	>tr|A8DYL2|A8DYL2	21	25.6	7859000	1960200	887780	7859000	1960200	887780	3825150.023	2424654.43	1474601.623	0.633871721	1.644277609
RpL23A	>tr|Q9W0A8|Q9W0A8	7	26	9288300	2316600	1368100	9288300	2316600	1368100	4520822.11	2865500.69	2272412.625	0.633845044	1.260994882
Rab7	>tr|O76742|O76742	6	36.7	2847800	709580	1574800	2847800	709580	1574800	1386087.573	877709.5656	2615741.102	0.633228075	0.335549097
sesB	>tr|X2JB48|X2JB48	44;42;6	83.9	1439000000	358250000	252260000	1439000000	358250000	252260000	700393292.2	443134603.4	419003587.9	0.632693957	1.057591429
CG6512	>tr|Q8T4G5|Q8T4G5	25;24	37.2	14833000	3670900	4905000	14833000	3670900	4905000	7219550.871	4540691.739	8147199.71	0.628943797	0.557331586
sgg	>tr|A4V3W2|A4V3W2	3;3;3;3;3;3;3;1;1	10.3	866630	214030	52871	866630	214030	52871	421808.0883	264742.7751	87818.67411	0.627637977	3.014652382
zip	>tr|A0A0B4JD95|A0A0B4JD95	2;2;2;1;1	1.4	17164000	4237100	830840	17164000	4237100	830840	8354100.395	5241048.508	1380024.344	0.627362404	3.797794242
CG6028	>tr|Q95SI7|Q95SI7	8	42.7	4987400	1228600	2733100	4987400	1228600	2733100	2427478.461	1519707.393	4539676.152	0.626043616	0.334761191
sigA	>tr|A4V4U5|A4V4U5	2;2	3.3	123490000	30381000	31844000	123490000	30381000	31844000	60105328.46	37579546.09	52892849.66	0.625228196	0.710484429
CG4095-RA	>tr|Q9W3X5|Q9W3X5	5	12.9	1480800	364110	140140	1480800	364110	140140	720738.2817	450383.0857	232772.389	0.624891305	1.93486473
RpL27	>tr|Q9VBN5|Q9VBN5	8	52.6	55261000	13587000	8536600	55261000	13587000	8536600	26896757.28	16806335.96	14179283.39	0.624846177	1.185274001
	>sp|Q9VWH4|IDH3A	34;1	66.8	233480000	57108000	54828000	233480000	57108000	54828000	113639906.8	70639304.76	91069248.87	0.6216065	0.775665833
Rbcn-3B	>tr|Q9W543|Q9W543	5	3.9	166730	40764	44267	166730	40764	44267	81151.19798	50422.71872	73527.43939	0.621342876	0.68576737
Trap1	>tr|A1Z6L9|A1Z6L9	24	40.2	5429800	1327400	2664100	5429800	1327400	2664100	2642804.377	1641917.299	4425067.227	0.621278409	0.37104912
CG5254	>tr|Q9V3T2|Q9V3T2	5;3	22.5	9755500	2379800	2319900	9755500	2379800	2319900	4748218.737	2943675.448	3853351.398	0.619953631	0.763926033
CG2258	>tr|Q9W3K6|Q9W3K6	4	6	737900	179940	145710	737900	179940	145710	359152.3354	222575.4097	242024.153	0.619724245	0.919641313
Nmdar2	>tr|Q6IWN7|Q6IWN7	5;5;5;3;3	5.9	373290	91028	58140	373290	91028	58140	181688.5423	112596.3899	96570.47742	0.619722017	1.165950432
Cyp312a1	>tr|M9PI92|M9PI92	6;6	15.9	1805000	438760	347600	1805000	438760	347600	878533.6294	542720.8335	577363.2252	0.617757608	0.93998964
ND-B14	>tr|Q7JZK1|Q7JZK1	5	33.9	18888000	4535800	3971300	18888000	4535800	3971300	9193209.523	5610523.193	6596325.017	0.61028993	0.850552873
CG5991	>tr|Q9VCE0|Q9VCE0	7	22.1	2476700	594440	1056000	2476700	594440	1056000	1205464.953	735288.0213	1754014.861	0.609962172	0.419202846
mRpL19	>sp|Q9VHN6|RM19	7	23.2	5347400	1277500	1817900	5347400	1277500	1817900	2602698.465	1580193.875	3019529.94	0.607136745	0.52332446
CG7488	>tr|Q9VG07|Q9VG07	3	11.8	728010	173920	104250	728010	173920	104250	354338.6525	215129.0167	173159.1377	0.60712828	1.242377501

full_dataset_V1

Rm62	>tr|E1JJ68|E1JJ68	24;24;24;20;20;20;20;1;1	47.1	16978000	4051000	2086400	16978000	4051000	2086400	8263570.059	5010853.533	3465508.15	0.60637878	1.445921728
mRpL2	>tr|Q9VTF8|Q9VTF8	4	20.1	7106900	1695200	1306400	7106900	1695200	1306400	3459086.233	2096864.702	2169928.991	0.606190352	0.966328719
RpL26	>tr|Q9VVU2|Q9VVU2	4;1	14.8	11054000	2636200	1902600	11054000	2636200	1902600	5380227.556	3260827.471	3160216.548	0.606076125	1.031836718
GLS	>tr|A1Z942|A1Z942	10;10;10;10;10;10;10;10;10;10	20.2	4319200	1029100	578560	4319200	1029100	578560	2102250.666	1272937.391	960987.5362	0.605511708	1.324613841
CG9393	>sp|Q9VHB6|MTX1	6;5	20.2	3443900	819570	1123800	3443900	819570	1123800	1676222.696	1013760.857	1866630.588	0.604788886	0.54309667
mRpS11	>tr|Q9VEN6|Q9VEN6	2	12.5	7603800	1808100	821540	7603800	1808100	821540	3700938.51	2236515.496	1364577.054	0.604310363	1.63898073
Acp26Aa	>sp|P10333|MS2A	5	26.5	4609800	1096000	0	4609800	1096000	1	2243692.146	1355688.835	1	0.604222303	1355688.835
GluClalpha	>tr|E1JIQ1|E1JIQ1	6;6;6;6;6;6;4;3	10.3	1803900	427790	169920	1803900	427790	169920	877998.235	529151.5757	282236.9369	0.602679544	1.874848776
CG2604	>tr|Q9VN86|Q9VN86	3	6.3	421200	99865	53760	421200	99865	53760	205007.4044	123527.2496	89295.30215	0.602550186	1.383356645
ND-23	>tr|Q9VF27|Q9VF27	3	18.9	4664200	1105500	564000	4664200	1105500	564000	2270169.836	1367439.788	936803.3919	0.602351316	1.459687059
PGRP-LD-RB;Pmi	>tr|G4LTX1|G4LTX1	3;3	21.4	3401400	803090	1379500	3401400	803090	1379500	1655537.001	993376.0464	2291348.012	0.600032525	0.433533466
CG13850	>tr|Q9VD14|Q9VD14	14	27.3	10440000	2464900	2246400	10440000	2464900	2246400	5081380.105	3048939.243	3731267.977	0.60002188	0.817132209
Nrx-1	>tr|A0A0B4KH61|A0A0B4KH61	11;11;11;11;10	11.2	843240	199010	131170	843240	199010	131170	410423.6553	246163.9007	217873.2287	0.599780002	1.129849235
CG2233	>tr|Q9W3L4|Q9W3L4	6	21.5	4839000	1136400	1329000	4839000	1136400	1329000	2355248.882	1405661.307	2207467.567	0.596820709	0.63677552
RpS15Aa	>tr|E1JJM9|E1JJM9	4;4;2	23.1	5807800	1363700	1670600	5807800	1363700	1670600	2826785.381	1686818.307	2774864.798	0.596726698	0.60789207
RpS3A	>sp|P55830|RS3A	14	42.2	13381000	3128600	2450000	13381000	3128600	2450000	6512830.19	3869897.893	4069447.358	0.594196038	0.950963989
CG1537	>tr|Q9VZ38|Q9VZ3	2	11.1	2776200	645530	354070	2776200	645530	354070	1351238.261	798483.4069	588109.8883	0.590927174	1.357711242
ND-SGDH	>tr|Q9VTU2|Q9VTU2	3	22.6	1438600	333120	474800	1438600	333120	474800	700198.6035	412050.2417	788642.2881	0.58847624	0.522480531
CG2658	>tr|Q9W4W8|Q9W4W8	13	15	2125500	491990	410050	2125500	491990	410050	1034528.105	608563.2757	681092.6079	0.588252047	0.893510322
CaMKII	>tr|D1YSG7|D1YSG7	8;8;7;7;6;6;6;5	22.6	2072500	479550	305060	2072500	479550	305060	1008731.827	593175.7126	506704.3311	0.58804104	1.170654514
CG11236	>tr|M9NDG8|M9NDG8	2;2	7.7	619700	142860	266740	619700	142860	266740	301621.7675	176709.5867	443054.8524	0.585864834	0.398843587
CG7718	>tr|Q8SYL0|Q8SYL0	2	5.9	737060	169830	119740	737060	169830	119740	358743.4887	210069.9224	198888.011	0.585571387	1.056222149
waw	>sp|Q9VRH6|GUF1	3	7.3	608490	140100	80779	608490	140100	80779	296165.6113	173295.6258	134173.832	0.585130816	1.291575438
CG4669	>tr|Q9VRK6|Q9VRK6	8	16	2339200	537550	222810	2339200	537550	222810	1138540.646	664918.37	370087.1698	0.584009339	1.796653395
GlyS	>tr|A0A0B4KHJ5|A0A0B4KHJ5	7;7	12.9	958590	219120	359590	958590	219120	359590	466567.0648	271038.8117	597278.6023	0.580921441	0.453789589
mTerf5	>tr|Q9VEB4|Q9VEB4	8	19.5	3642900	829430	167080	3642900	829430	167080	1773080.42	1025957.108	277519.6999	0.578629766	3.696880289
CG5463	>sp|Q9VCD0|GATB	3	6.4	629400	143170	233400	629400	143170	233400	306342.9732	177093.0389	387677.1484	0.578087485	0.456805462
CG8080	>tr|A0A0B4KF27|A0A0B4KF27	2;2;2;2;2	6.6	775510	176370	234220	775510	176370	234220	377457.9585	218159.5255	389039.1675	0.577970395	0.56076494
trp	>sp|P19334|TRP	3;1	3.4	260400	59113	22337	260400	59113	22337	126742.4695	73119.37423	37101.73304	0.576912968	1.97078056
CG8043	>tr|Q9VHN4|Q9VHN4	10	42	12926000	2930800	1174700	12926000	2930800	1174700	6291371.574	3625230.692	1951175.433	0.576222633	1.857972702
140up	>tr|A0A0B4KFZ0|A0A0B4KFZ0	2;2	10.7	530040	119660	137470	530040	119660	137470	257982.2522	148012.5238	228337.5219	0.57373142	0.64821814
RpS4	>tr|X2JGM9|X2JGM9	9;9	33	9111000	2047900	1317400	9111000	2047900	1317400	4434526.258	2533134.276	2188199.979	0.571229964	1.157633808
RpS9	>tr|Q95RG1|Q95RG1	2;2;2	12.4	3403600	763010	588880	3403600	763010	588880	1656607.79	943799.3963	978129.045	0.569718072	0.964902741
Tps1	>tr|Q9Y119|Q9Y119	30	40.5	7942800	1774000	2633700	7942800	1774000	2633700	3865937.347	2194335.761	4374572.86	0.567607688	0.501611433
CG8298	>tr|Q7JY99|Q7JY99	6	13.6	1327300	296130	387410	1327300	296130	387410	646026.4191	366295.7435	643487.5923	0.566998087	0.56923513
S-Lap5	>tr|A1Z9G3|A1Z9G3	13	38.4	21078000	4687100	1086900	21078000	4687100	1086900	10259131.21	5797672.574	1805339.728	0.565123153	3.211402532
HtrA2	>tr|A0A0B4KG52|A0A0B4KG52	5;5	16.6	2645200	587900	347030	2645200	587900	347030	1287477.649	727198.4182	576416.4559	0.564824111	1.261585111
ND-13A	>tr|Q9VMU0|Q9VMU0	5	46.8	7215500	1602200	796200	7215500	1602200	796200	3511944.267	1981829.062	1322487.341	0.56431108	1.498561839
Mulk	>tr|Q9VL10|Q9VL10	9	18.9	4981900	1096400	643780	4981900	1096400	643780	2424801.489	1356183.612	1069317.886	0.559296758	1.268269829
	>tr|Q500Y7|Q500Y7	2	38.6	13775000	3024200	2957100	13775000	3024200	2957100	6704598.75	3740761.11	4911739.911	0.557939595	0.761595927
RpL14	>sp|P55841|RL14	9	42.2	32928000	7196100	3868600	32928000	7196100	3868600	16026789.66	8901160.975	6425740.428	0.555392637	1.385235067
Lrpprc2	>tr|Q9W592|Q9W592	26	30	8250900	1790400	1265900	8250900	1790400	1265900	4015896.466	2214621.616	2102658.535	0.551463822	1.053248342
Tom20	>tr|Q95RF6|Q95RF6	5	52	27337000	5930600	4201000	27337000	5930600	4201000	13305525.66	7335810.408	6977856.469	0.551335633	1.051298553
FK506-bp1	>sp|P54397|FKB39	5	19.3	4314800	927940	377240	4314800	927940	377240	2100109.088	1147808.301	626595.2333	0.54654699	1.831817799
kdn	>sp|Q9W401|CISY	3	8	718520	152490	132360	718520	152490	132360	349719.6585	188621.3417	219849.8174	0.539350126	0.857955417
Acox57D-d	>tr|Q9W2G8|Q9W2G8	8	18.6	2102900	444680	819280	2102900	444680	819280	1023528.182	550043.5323	1360823.197	0.537399499	0.404199115
CG5705	>tr|Q9VK20|Q9VK20	2	6.9	535310	112830	45100	535310	112830	45100	260547.2783	139564.2074	74911.05149	0.535657898	1.863065658
EndoG	>tr|Q7JXB9|Q7JXB9	8	31.3	8985600	1877400	983440	8985600	1877400	983440	4373491.29	2322235.602	1633492.779	0.530979816	1.421638119
Lon	>sp|Q7KUT2|LONM	27	28.3	12193000	2545600	1418800	12193000	2545600	1418800	5934604.178	3148760.492	2356625.27	0.530576328	1.336131176
S-Lap3	>tr|Q961W5|Q961W5	19	34.8	197680000	41080000	13404000	197680000	41080000	13404000	96215250.87	50813592.48	22264029.54	0.528124097	2.28231787
Dic1	>tr|Q9Y166|Q9Y166	8	33.9	12138000	2502900	2631000	12138000	2502900	2631000	5907834.455	3095943.053	4370088.163	0.524040251	0.708439495

full_dataset_V1

Mitofilin	>tr|A0A0B4KHL7|A0A0B4KHL7	36;36;34	48.8	27173000	5602400	5186200	27173000	5602400	5186200	13225703.22	6929845.923	8614272.607	0.52396805	0.80446095
RpL17	>tr|X2JIQ5|X2JIQ5	7;7	33.9	22061000	4547800	2956800	22061000	4547800	2956800	10737579.17	5625366.502	4911241.611	0.52389523	1.145406182
CG6767	>tr|Q9VT32|Q9VT32	2;2;2;2;2;2	7.1	1083800	222740	307920	1083800	222740	307920	527509.5555	275516.5431	511454.788	0.52229678	2	0.538691884
UQCR-14;UQCR-14L	>tr|Q9VXI6|Q9VXI6	2;1	17.1	9259300	1901800	2461400	9259300	1901800	2461400	4506707.165	2352416.996	4088382.746	0.521981329	0.575390599
CG3364	>tr|Q7K332|Q7K332	14	55.6	49583000	10102000	7967200	49583000	10102000	7967200	24133148.44	12495591.8	13233510.61	0.517777108	0.944238621
CG4679	>sp|A1Z9A8|PTCD3	24	44.9	18342000	3719800	3209200	18342000	3719800	3209200	8927459.184	4601178.221	5330477.739	0.515396164	0.863183085
mRpL50	>tr|Q9V3E3|Q9V3E3	4	25.4	2051100	414530	115960	2051100	414530	115960	998315.9708	512749.7199	192609.4351	0.513614662	2.662121509
Cdep	>tr|A8JQT5|A8JQT5	7;5;5;5	2.6	227640	45926	26983	227640	45926	26983	110797.4491	56807.81522	44818.73403	0.512717717	1.267501558
CG9791-RC;CG9791	>tr|H1UUI2|H1UUI2	8;8	11.4	1095100	218180	171680	1095100	218180	171680	533009.5167	269876.0859	285160.295	0.506325079	0.946401342
mRpL46	>tr|Q9W086|Q9W086	12	44.6	12062000	2402200	1051900	12062000	2402200	1051900	5870843.566	2971382.957	1747204.766	0.506125384	1.700649526
mRpS16	>sp|Q9V6Y3|RT16	5	59.7	14670000	2900600	1697300	14670000	2900600	1697300	7140215.147	3587875.033	2819213.47	0.502488365	1.272651068
CG2858	>tr|Q9W0Y5|Q9W0Y5	3;1;1	4.8	808060	159440	141870	808060	159440	141870	393300.7672	197218.0912	235645.9171	0.501443444	0.83692556
Acox57D-p	>tr|Q9W2G9|Q9W2G9	7	15.1	145780	28710	426350	145780	28710	426350	70954.36721	35512.61541	708166.8903	0.50049936	0.050147241
Pmp70	>tr|M9PF96|M9PF96	8;8	16.1	6399200	1257900	872980	6399200	1257900	872980	3114632.909	1555949.805	1450018.839	0.499561216	1.07305489
ZnT49B	>tr|A1Z936|A1Z936	2;2	3.5	683580	134200	24396	683580	134200	24396	332713.5837	165997.6658	40521.72982	0.498920615	4.096509862
ND-13B	>tr|Q9VTB4|Q9VTB4	8	89.5	43294000	8472900	8275300	43294000	8472900	8275300	21072152.32	10480488.99	13745264.38	0.497362055	0.762479986
S-Lap2	>tr|Q9VSM7|Q9VSM7	13	33.5	150580000	29358000	8655400	150580000	29358000	8655400	73290633.73	36314154.04	14376610.07	0.495481512	2.525919106
Ank2	>tr|Q7KU95|Q7KU95	11;11;11;11;11;11;11;11;11;11;11;11;6;6;4;4	5.6	425550	82829	70160	425550	82829	70160	207124.6461	102454.6994	116535.6845	0.494652381	0.879170186
Gel	>tr|A0A0C4DHG6|A0A0C4DHG6	3;3;3	5	952840	183900	61967	952840	183900	61967	463768.412	227473.7015	102927.1203	0.490489856	2.210046301
Sod2	>tr|A0A0B4LGQ1|A0A0B4LGQ1	6;6	34.6	38892000	7486500	5257300	38892000	7486500	5257300	18929601.06	9260369.039	8732369.63	0.489200433	1.06046462
RpL18A	>sp|P41093|RL18A	13	63.3	62726000	12060000	4134200	62726000	12060000	4134200	30530138.74	14917524.96	6866901.741	0.48861635	2.172380721
prom	>tr|Q8MLN9|Q8MLN9	6;6;6;6	8.2	891540	170610	94786	891540	170610	94786	433932.3391	211034.7374	157439.4439	0.486330975	1.340418463
UGP	>tr|E1JI91|E1JI91	6;6;5;5	15.1	2666600	509740	335930	2666600	509740	335930	1297893.505	630519.0027	557979.3678	0.485801801	1.130004153
	>tr|O97418|O97418	4	45.6	6746200	1282400	355850	6746200	1282400	355850	3283525.523	1586254.893	591066.4663	0.48309504	2.683716609
CG3517	>tr|Q9VDW9|Q9VDW9	4	17.5	787980	149070	89505	787980	149070	89505	383527.3848	184390.9988	148667.7086	0.480776618	1.240289506
CG17544-RA	>tr|Q9VIX4|Q9VIX4	6	14.1	73372	13864	166040	73372	13864	166040	35711.78382	17148.96902	275792.2611	0.480204772	0.062180748
CG17097	>tr|E2QCS7|E2QCS7	9	9.3	6442400	1216000	647290	6442400	1216000	647290	3135659.309	1504121.92	1075147.992	0.479682826	1.398990586
CG8654-RA	>tr|Q7K3M6|Q7K3M6	2	7.2	566260	106790	312330	566260	106790	312330	275611.3314	132093.0755	518779.7933	0.479273021	0.25462263
TM4SF	>tr|O76137|O76137	9;9	27.6	42831000	8063200	3292200	42831000	8063200	3292200	20846799.93	9973713.703	5468340.649	0.478429003	1.823901315
CysRS-m	>tr|Q7K3P0|Q7K3P0	10	26.3	1356300	255280	173400	1356300	255280	173400	660141.3638	315766.6478	288017.2131	0.478331862	1.096346445
CG12935	>tr|Q7JW07|Q7JW07	4	20.3	2326400	437610	450100	2326400	437610	450100	1132310.601	541298.3497	747615.6147	0.478047586	0.724032964
Ctr1B	>tr|Q9VHS6|Q9VHS6	2	12.1	2896600	543570	130640	2896600	543570	130640	1409839.618	672364.7631	216992.8992	0.476908688	3.098556522
Mtch	>tr|Q9V3Y4|Q9V3Y4	4	16.8	2101100	390990	655440	2101100	390990	655440	1022652.082	483632.0965	1088685.133	0.472919485	0.444235052
AsnRS-m	>tr|Q7JZR5|Q7JZR5	3	7.8	1244300	231270	291220	1244300	231270	291220	605628.4738	286067.6615	483716.106	0.472348435	0.591395775
RpS17	>sp|P17704|RS17	5	43.5	15807000	2920700	2556500	15807000	2920700	2556500	7693618.325	3612737.575	4246343.743	0.469575877	0.850787829
regucalcin	>tr|Q9VYR1|Q9VYR1	2;1	12.5	459980	84732	191580	459980	84732	191580	223882.4926	104808.6008	318214.1735	0.46814112	0.329364967
Ced-12	>tr|Q9VKB2|Q9VKB2	6	9.5	473940	86962	70618	473940	86962	70618	230677.1349	107566.9822	117296.422	0.466309685	0.917052545
CG32206-RB;CG32206	>tr|Q9VVY7|Q9VVY7	4;4	2.5	371010	67989	44568	371010	67989	44568	180578.8156	84098.47469	74027.40006	0.465716172	1.136045229
Adk3	>tr|Q9VGU6|Q9VGU6	4;1;1	17.1	2620300	480100	408000	2620300	480100	408000	1275358.265	593856.031	677687.5601	0.465638595	0.876297672
Rme-8	>tr|A0A0B4LFW6|A0A0B4LFW6	2;2	1.1	52016	9373.5	5256.4	52016	9373.5	5256.4	25317.34383	11594.47931	8730.874862	0.457965867	1.327985969
mRpL9	>sp|Q9VF89|RM09	5	29	5135900	915080	1164200	5135900	915080	1164200	2499756.713	1131901.222	1933734.945	0.452804554	0.585344556
RpS10b	>tr|M9NEQ9|M9NEQ9	2;2;1	14.4	1079700	191990	401890	1079700	191990	401890	525513.9944	237480.5653	667538.8567	0.451901506	0.355755418
loopin-1	>tr|Q7K2S9|Q7K2S9	26	51.7	176090000	31148000	10092000	176090000	31148000	10092000	85706917.88	38528280.88	16762801.12	0.449535251	2.298439301
CG8701	>tr|Q7K2U6|Q7K2U6	5	32.9	4942200	871980	0	4942200	871980	1	2405478.616	1078589.006	1	0.448388524	1078589.006
mRpL23	>tr|M9PE14|M9PE14	3;3	20	3688900	645250	943090	3688900	645250	943090	1795469.643	798137.063	1566471.473	0.444528297	0.50951267
CG2794	>tr|Q9VPR3|Q9VPR3	4	6.1	591890	103380	53805	591890	103380	53805	288086.0222	127875.102	89370.0471	0.44387819	1.430849666
mmd	>tr|M9NDY9|M9NDY9	27;27;27;27;27;27;27;21	31.3	6783800	1180300	632710	6783800	1180300	632710	3301826.279	1459963.077	1050930.628	0.44216835	1.389209752
CG4662	>tr|E1JIQ4|E1JIQ4	7;7;7;5;5;5	16.4	3449300	599920	440860	3449300	599920	440860	1678850.996	742066.4655	732267.9847	0.442008533	1.013381004
mRpL22	>sp|Q9VXB5|RM22	3	11.6	2326000	403420	635380	2326000	403420	635380	1132115.912	499007.2902	1055365.495	0.440774027	0.472828885
FeCh	>sp|Q9V9S8|HEMH	20	62.2	109890000	19046000	12923000	109890000	19046000	12923000	53485906.1	23558804.34	21465089.06	0.440467519	1.097540489
CG5844	>tr|Q9VG69|Q9VG69	3	15.9	4378400	752390	1171500	4378400	752390	1171500	2131064.622	930663.0684	1945860.237	0.436712739	0.478278476

full_dataset_V1

S-Lap7	>tr|Q500X4|Q500X4	27	49.9	140760000	24175000	8923000	140760000	24175000	8923000	68511021.41	29903081.75	14821093.38	0.436471113	2.017602952
Prx3	>tr|Q9VEJ0|Q9VEJ0	6	29.5	10833000	1846000	1712200	10833000	1846000	1712200	5272661.942	2283395.612	2843962.354	0.433063154	0.802892348
mRpL12	>tr|Q9VSR5|Q9VSR5	2	18.1	2107600	356730	222970	2107600	356730	222970	1025815.777	441254.451	370352.9297	0.4301498	1.191443123
CG9577	>tr|Q9W5W8|Q9W5W8	13	61.2	63986000	10806000	7032000	63986000	10806000	7032000	31143408.75	13366399.23	11680144.42	0.429188704	1.144369346
CG6891	>tr|Q9VWQ7|Q9VWQ7	2;1	17.2	653600	109850	151970	653600	109850	151970	318121.6512	135878.1192	252422.0062	0.427126285	0.538297438
Cyp6g1	>tr|B6IDY5|B6IDY5	2;2	3.8	209550	35082	86617	209550	35082	86617	101992.644	43394.41218	143870.7437	0.425466097	0.301620823
RpS2	>tr|M9PB84|M9PB84	6;6	29.2	7304800	1211800	571790	7304800	1211800	571790	3555408.562	1498926.762	949742.5735	0.421590581	1.578245309
CG32500	>sp|Q8SY96|NFU1	2	11.7	2113600	350450	468150	2113600	350450	468150	1028736.11	433486.4529	777596.6452	0.421377697	0.557469551
CG1665-RA	>tr|A1Z803|A1Z803	2	5.6	690530	113180	77403	690530	113180	77403	336096.3032	139997.1372	128566.2996	0.41653876	1.088910061
CG3121	>tr|Q9W1D3|Q9W1D3	6	10.9	3570500	583260	174750	3570500	583260	174750	1737841.73	721459.0056	290259.5617	0.415146554	2.485564994
sif	>tr|Q8IQ62|Q8IQ62	12;12;12;12;12;12;12;11;12;0	6.7	4859700	791340	294900	4859700	791340	294900	2365324.032	978841.9736	489828.5821	0.41382997	1.998335764
GstS1	>tr|A4UZL5|A4UZL5	2;2;1	11.6	2331500	379030	335520	2331500	379030	335520	1134792.885	468838.2658	557298.3583	0.413148754	0.841269777
NitFhit	>sp|O76464|NFT1	3	7	232820	37414	61713	232820	37414	61713	113318.6703	46278.96179	102505.2266	0.408396619	0.451479045
tutl	>tr|E1JHT0|E1JHT0	5;5;5;5;5;5	6.9	586190	93956	70257	586190	93956	70257	285311.7055	116218.1572	116696.8014	0.407337501	0.995898395
trmt10c	>sp|Q7JUX9|MRRP1	4	10.8	986310	156580	71519	986310	156580	71519	480059.0051	193680.436	118792.982	0.403451313	1.630403015
CanA-14F	>tr|M9NEL1|M9NEL1	3;3;1;1	9.1	457730	72464	398850	457730	72464	398850	222787.3676	89633.79179	662489.42	0.402328879	0.13529845
lost	>tr|Q9VN21|Q9VN21	6	15.2	918040	145090	89124	918040	145090	89124	446830.4783	179467.9682	148034.868	0.401646658	1.212335787
Khc	>sp|P17210|KINH	2	2.2	31996	5048.6	10343	31996	5048.6	10343	15573.16474	6244.827268	17179.71197	0.400999243	0.363500114
TFAM	>tr|Q9VDL2|Q9VDL2	21;21	57.6	138260000	21618000	8091500	138260000	21618000	8091500	67294215.83	26740220.11	13439972.77	0.397362831	1.989603741
GABA-B-R1	>tr|Q9V3Q9|Q9V3Q9	6	10.2	1041400	160970	213860	1041400	160970	213860	506872.5329	199110.613	355221.2295	0.392821864	0.560525657
RpL36A	>tr|Q9VLT7|Q9VLT7	2	13.5	2261800	343350	278790	2261800	343350	278790	1100868.345	424704.1621	463069.8895	0.385790148	0.917149164
CG18324	>tr|Q7K2Y2|Q7K2Y2	2;2	14.1	698000	104630	46851	698000	104630	46851	339732.1183	129421.28	77819.4606	0.38095097	1.663096596
S-Lap4	>tr|Q95R35|Q95R35	27	44.1	58729000	8689700	2996200	58729000	8689700	2996200	28584709.98	10748658.1	4976684.969	0.376028237	2.159802793
Hasp	>tr|Q9VIU9|Q9VIU9	4;4;4;1	4.3	404920	59650	124920	404920	59650	124920	197083.5665	73783.61228	207491.9854	0.374377294	0.355597408
IleRS-m	>tr|Q9VUY4|Q9VUY4	12	16.2	1228000	180440	215310	1228000	180440	215310	597694.9014	223193.8809	357629.6779	0.373424435	0.624092168
strB	>tr|X2JCY4|X2JCY4	2;2;2	2.7	99580	14433	0	99580	14433	1	48467.80008	17852.78922	1	0.368343296	17852.78922
CG4495	>sp|A2VEI2|MICU1	5	9	2589100	375210	305420	2589100	375210	305420	1260172.532	464113.146	507302.2907	0.368293336	0.91486507
mTTF	>tr|Q9V3F3|Q9V3F3	7	14.9	2141700	305850	256430	2141700	305850	256430	1042413.005	378318.8233	425929.9536	0.362926039	0.888218403
Letm1	>sp|P91927|A60DA	6	7.4	943040	134360	77199	943040	134360	77199	458998.5341	166195.5766	128227.4559	0.362083023	1.296099774
CG3213-RA	>tr|Q9VQS0|Q9VQS0	7	13.5	441140	62242	278590	441140	62242	278590	214712.6457	76989.7669	462737.6897	0.358571181	0.166378855
fax	>tr|Q59E30|Q59E30	2;2;1;1;1;1	5.8	395160	55454	272780	395160	55454	272780	192333.1575	68593.40211	453087.2859	0.356638465	0.151391143
Dap160	>tr|M9PDC7|M9PDC7	3;3;3;3;3;3	3.9	462980	63451	119620	462980	63451	119620	225342.6593	78485.23022	198688.6911	0.34829282	0.395016092
Vha68-1	>tr|M9PD18|M9PD18	4;4	10.9	356330	48258	172970	356330	48258	172970	173433.7332	59692.36483	287302.9836	0.344179669	0.207767995
CG11200	>tr|Q7K0F7|Q7K0F7	4	12.7	1608800	212010	1749900	1608800	212010	1749900	783038.7274	262244.1515	290658.2.013	0.334905723	0.090224239
CG5762	>tr|Q9VC86|Q9VC86	3	24	755140	98142	0	755140	98142	1	367543.4267	121395.9979	1	0.330290216	121395.9979
CG10628	>sp|Q9I7M2|GTPBA	4	16.7	1021200	131630	17403	1021200	131630	17403	497040.7438	162818.7239	28906.36436	0.327576212	5.632625463
tobi	>tr|Q9VBR6|Q9VBR6	3	5.6	577950	74413	122080	577950	74413	122080	281301.1143	92044.59246	202774.7485	0.327210195	0.453925319
CG5089	>tr|Q8T0U2|Q8T0U2	5	13.1	3605800	458700	82394	3605800	458700	82394	1755023.025	567385.4643	136856.3453	0.323292319	4.145846969
	>tr|Q9Y171|Q9Y171	2	5.2	2380500	295580	60603	2380500	295580	60603	1158642.274	365615.4252	100661.5178	0.315555054	3.632127086
GCS2beta	>tr|Q9VJD1|Q9VJD1	2	3.8	1098000	135910	210430	1098000	135910	210430	534421.0112	168112.8373	349524.0032	0.314570037	0.480976516
Drep2	>tr|Q7K304|Q7K304	11;11;11	31.1	8330700	1027400	121110	8330700	1027400	121110	4054736.9	1270834.589	201163.5795	0.313419741	6.317418849
	>tr|Q8IMW8|Q8IMW8	12	44.1	29880000	3647200	188760	29880000	3647200	188760	14543260.3	4511376.205	313530.1566	0.31020391	14.3889706
CG7430	>tr|Q9VVL7|Q9VVL7	10	23.6	5407700	650430	1127100	5407700	650430	1127100	2632047.816	804544.4245	1872111.885	0.30567242	0.429752319
ome	>tr|M9PCH6|M9PCH6	3;3;3;3	6	157450	18798	19834	157450	18798	19834	76634.41566	23252.04266	32944.25274	0.303415149	0.705799669
Syn	>tr|E2QCZ0|E2QCZ0	5;5;5	7.9	955160	112140	1176400	955160	112140	1176400	464897.6076	138710.7172	1953999.131	0.298368318	0.070988116
CG31538	>tr|Q8I0F1|Q8I0F1	12	33.7	8706700	1014400	117910	8706700	1014400	117910	4237744.46	1254754.338	195848.383	0.296090137	6.406763841
ND-PDSW	>tr|Q9VQR2|Q9VQR2	3	21.4	2723200	316960	686510	2723200	316960	686510	1325441.983	392061.253	1140292.37	0.295796616	0.343825201
Mhcl	>tr|Q0KI66|Q0KI66	5;5;5;5;3;2;2;1	3	196570	22835	15140	196570	22835	15140	95674.98939	28245.579	25147.5238	0.295224271	1.123195239
CG7616	>tr|Q9VTG5|Q9VTG5	8	16	2025200	226690	258920	2025200	226690	258920	985709.865	280402.4655	430065.8409	0.284467545	0.651998924
CG12360	>tr|Q9VG01|Q9VG01	2	3	246620	26931	75878	246620	26931	75878	120035.4371	33312.09494	126033.2763	0.277518837	0.264311902
CG32332	>tr|Q86BK2|Q86BK2	3;3	12.6	1242800	134110	82236	1242800	134110	82236	604898.3904	165886.341	136593.9074	0.274238357	1.214449049

Acknowledgments

I would like to say thanks to Prof. Rodolfo Costa, for giving me the opportunity to pursue my PhD on an extremely interesting and innovative topic of the Biomedical research field. I am very thankful to Dr. Cristiano DePittà for his supervision and advices. I am also grateful to all the Costa's lab members for sharing their expertise and funny moments working in the lab.

I want to say thanks also to my collaborators: Dr. Joy Chakraborty for mitochondrial network images, Dr. Katia Cortese and Dr.Cristina Gagliani for electron microscopy analysis, Patrizio Castagnola for membrane potential and ROS measurments, the technicians of the Microscopy facility of the Department of Biology (University of Padova) for correlative microscopy images, Emanuela Bottani for the blue native analysis, Vanessa Checchetto for electrophysiological recordings and the Mass spectrometry facility of the European Molecular Biology Laboratories (EMBL) in Heidelberg for mass spec analysis.

Finally, I want also to thank Prof. Massimo Zeviani and Prof.Claudia Donnini for their suggestions as members of my thesis advisatory committee.